An Investigation into the Nature of Field Electron Emission Sites on Broad-area Metallic Electrodes.

Chamkour Singh Athwal B.Sc., M.Sc.

A Thesis submitted for the Degree of Doctor of Philosophy.

The University of Aston in Birmingham.

October, 1981.

An Investigation into the Nature of Field Electron Emission Sites on Broad-area Metallic Electrodes

Chamkour Singh Athwal B.Sc., M.Sc.

A Thesis submitted for the Degree of Doctor of Philosophy, 1981.

SUMMARY

A wide ranging investigation has been carried out into the nature of the localised electron emission sites that give rise to the prebreakdown conduction between extended area electrodes separated by a small (< 5mm) high vacuum gap. A high resolution electron spectrometer has been used to measure the energy distribution of the electrons arising from sites on copper, stainless steel, titanium and gold specimens. At low currents these distributions are shifted 100-500meV below the metal Fermi level and have half-widths of between 300 and 500meV. An extensive series of measurements on copper electrodes has shown that the energy distributions shift to lower energies and become wider as the gap field and the associated site current increases; several sites have displayed multi-peaked spectra, where the relative magnitudes of the peaks is also found to be a function of the gap field. The effect of two forms of in situ surface treatment are reported: outgassing of the specimen is found to increase the stability of the spectrum, whilst ion etching firstly destabilises the emission and then for sufficient depths can eliminate emission sites. A further facility has been developed to obtain complementary optical spectra from electron emission sites. Finally a micropoint anode probe technique has been established to directly locate emission sites in a scanning electron microscope; insulating particles of micron dimensions have been observed within the identified areas at a resolution of $\sim$ 4 microns. The findings of these experiments are interpreted in terms of a model in which the electrons are emitted through a typically micron sized insulating impurity; it is assumed that at a certain critical penetrating field the insulator switches to a high conductivity state with associated electron and optical emission.

Key words: Prebreakdown conduction.
Field emission spectroscopy.

CONTENTS

LIST OF FIGURES

CHAPTER 1

INTRODUCTION

Although, from a dielectric viewpoint, ultra high vacuum should behave as a perfect electrical insulator, it is found that measurable currents flow between vacuum-insulated high voltage electrodes. These are known as prebreakdown currents and are strongly dependent upon the voltage applied across the electrode gap. If, however, this voltage is increased beyond a certain point, an arc will be struck between the two electrodes, when the gap resistance effectively falls to zero. This is termed "electrical breakdown" and is a catastrophic irreversible process which clearly has profound implications for the design of commercial devices that use high-voltage vacuum insulation (e.g. high-energy particle accelerators, x-ray tubes, electron microscopes, transmitting valves, etc.) since the occurrence of a breakdown represents a disaster both from the performance and financial points of view. The problem is conventionally tackled by such empirical means as maximising the dimensions of vacuum gaps, using special materials and surface finishes for the electrodes, and the incorporation of sophisticated electronic protection circuitry. However, in the long term the problem is probably best solved by discovering the fundamental physical processes which give rise to the electrical breakdown.

For electrodes separated by gaps of < 5mm, the prebreakdown currents are believed to be responsible for initiating electrical breakdown. For larger gaps, loosely adhering microparticles are assumed to be electrostatically pulled off the electrode surfaces and because of their

charge are accelerated by the gap field to gain sufficient energy to trigger a breakdown; a process that occurs before the field attains a value high enough to allow the flow of continuous prebreakdown currents. An analysis of the actual breakdown mechanism, whether electron beam or microparticle initiated, is outside the scope of this thesis. Instead it concentrates on the nature of the prebreakdown currents, since it is clear that a thorough understanding of this phenomenon must be a prerequisite of giving informed prescriptions to improve the insulating characteristic of vacuum gaps. Thus, the aim of this investigation was to review and extend the present knowledge of the processes occurring on the surface of extended area electrodes which give rise to electron emission under the action of an electrostatic field.

The traditionally accepted explanation of prebreakdown conduction is a metallic type electron field emission from features such as protrusions or whiskers, where the field becomes geometrically enhanced. Such a model is supported by three main observations. The first of these is that the electron emission has been observed to arise from a small number of extremely localised sites. Secondly, the current voltage characteristics of conditioned electrode gaps appear to follow the predictions of "metallic" field emission theory. Finally microscopic pro sions have been observed on electrodes which were previously exposed to high electric fields. However, doubts as to the validity of the microprotrusion model have been raised by the unrealistically high geometrical field enhancement factors that are usually assumed, and the fact that the prebreakdown conduction is frequently

more complicated than can be accounted for by a straightforward application of "metallic" field emission theory. An alternative viewpoint to prebreakdown conduction is hinted at when one considers the insulator type inclusions and impurities which are invariably present on nominally clean metallic surfaces. There have been several reports of the involvement of such impurities in electrical breakdown in low pressure systems and more recently, in high vacuum systems. Furthermore a number of recent experiments have led to the conclusion that semiconducting or insulating impurities probably play an important role in prebreakdown conduction.

One of the aforementioned techniques, which also forms the major experimental effort in the present study, is the measurement of the energy distribution of the electrons emitted from the localised sites on broad area electrodes. An electron spectrum in principle contains more basic information than the commonly measured total current, which in mathematical terms is an integration of the energy distribution over all energies. Thus electron spectrometry is a sensitive test of any electron emission mechanism and has been very widely and successfully applied to study field emission from metals, semiconductors and through adsorbed atoms and molecules. In these experiments the specimen has invariably been in the form of an isolated micropoint at which the field can become sufficiently enhanced for true field emission to occur.

The heart of the electron spectrometer system employed in this work is a hemispherical electrostatic deflection analyser, an instrument which is capable of providing the

energy distribution directly with a resolution determined to be ~30 meV. The spectrometer was originally established to measure the emission from conventional micropoint specimens, and has been considerably modified to interface with a broad area electrode gap. A large number of measurements have been taken using this facility, mainly with copper disc specimens. In particular, the variation of the electron spectra with the gap field has been found to be an interesting and informative characteristic.

A number of additional techniques have been developed in this investigation, either to be used in conjunction with the spectrometer or in subsidiary experiments. The former, which involved instrumental developments within the spectrometer vacuum chamber, include facilities for surface treatment, namely electron bombardment and ion bombardment, and a technique for measuring the intensity and spectrum of the light which is also found to be emitted from electron emission sites. An important subsidiary experiment has been the identification of emission sites in situ in a conventional scanning electron microscope, where a resolution of ~ 4μm has been realised. Thus the identified area can be directly viewed at high magnification, and its elemental composition discovered by means of a standard x-ray spectrometer facility.

The results of the experiments carried out in this investigation cannot be satisfactorily explained on the basis of the microprotrusion field emission hypothesis, and an explanation based on electron emission through an insulating or semiconducting impurity is thought to be more suitable. Two models have been recently proposed for electron emission in such a regime. However, although each of these have many

attractive features, they are also recognised to have some evident limitations. Therefore a new model has been evolved which includes many of the concepts of the earlier models. In essence this assumes that the external field penetrates into the insulator-type impurity and at a certain value causes it to switch from a low to a high conductivity state. Then electrons are able to cross the typically micron-sized impurity and are accelerated or "heated" near the vacuum interface so that they escape over the work function barrier. Since the exact composition and dimensions of the impurity involved in the emission mechanism will in general be unknown, it is not possible to make quantitative comparisons between theory and experiment. However, the general trends in the exerpimental results will be shown to be satisfactorily explained by this new model.

CHAPTER 2

A REVIEW OF PREBREAKDOWN CONDUCTION BETWEEN VACUUM INSULATED HIGH VOLTAGE ELECTRODES

2.1 Fowler Nordheim Theory

The first theory to satisfactorily describe the field emission of electrons from metals was formulated by Fowler and Nordheim in 1928.[1,2] They consider the quantum mechanical tunnelling of electrons through the modified potential barrier, illustrated in Figure 2.1, that results from the presence of a high external field acting on an atomically clean surface. According to the Fowler-Nordheim model, electrons arrive at the surface of a metal according to Fermi-Dirac statistics and penetrate the potential hump in front of the surface with a probability which is predicted by a solution of the Schrodinger equation. The general steps and definitions of their derivation are as follows:

1) $N(W)\,dW$ = Supply function, equal to the number of electrons with the z part of their energy within the range W to W + d W incident on the surface per second per unit area.

2) $D(W)$ = Probability that an electron with energy W will penetrate the barrier.

3) $P(W)\,dW$ = $N(W)\,D(W)\,dW$

= number of electrons in the range W to W + d W penetrating the barrier

= normal-energy distribution

4) J = $e\int_W P(W)\,dW$

= electric current per unit area

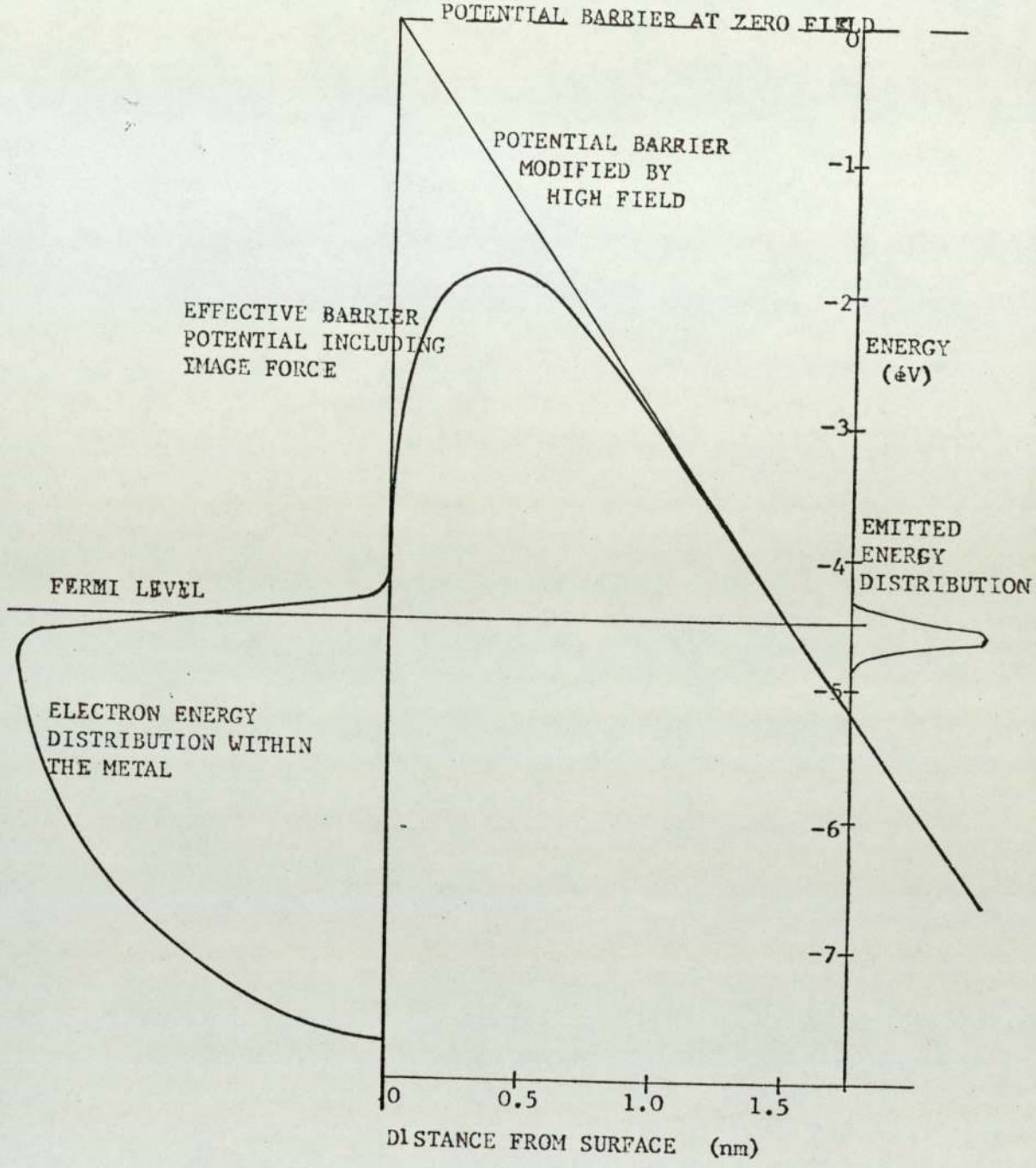

Fig. 2.1: A schematic representation of metallic field electron emission.

The detailed evaluation of N (W), D (W) and the integration of P (W) d W is an extended and largely mathematical exercise, of which there are comprehensive modern treatments in reviews by Good and Muller[3] and Van Oostrom.[4] At low temperatures ($T < 300^{o}K$) when few electron states above the Fermi level are occupied, the Fowler-Nordheim equation is usually expressed in the form

$$J = \frac{1.54 \times 10^{-6} E^2}{\phi\, t^2(y)} \exp\left(- \frac{6.83 \times 10^9\, \phi^{3/2} v(y)}{E} \right) \qquad 1.$$

where J is the current density ($A\ m^{-2}$),

E is the surface electric field (Vm^{-1}),

and ϕ the work function of the emitting surface (eV);

t(y) and v(y) are tabulated dimensionless elliptic functions [3-6] of the parameter y, which is given by

$$y = 3.79 \times 10^{-5} \frac{E^{1/2}}{\phi} \qquad 2.$$

For the field range of stable field emission,

$$2 \times 10^9 < E < 6 \times 10^9 V\ m^{-1}$$

$$t(y) \simeq 1 \qquad 3.$$

$$v(y) \simeq 0.956 - 1.062y^2 \qquad 4.$$

The F-N equation may be expressed in a form convenient for comparison with experiment by substituting from equations (2), (3) and (4) into equation (1) and then taking logarithms.

$$\log\left(\frac{J}{E^2}\right) = \log\left(\frac{1.54 \times 10^{-6} \times 10^{4.54\phi^{-1/2}}}{\phi}\right) - \frac{2.84 \times 10^9\, \phi^{3/2}}{E} \qquad 5.$$

Then if the field is locally enhanced by a factor β over an emitting area A, the emission current I from this region is given by

$$I = J A \qquad 6.$$

(assuming uniform field over the whole of the emitting area) and the enhancement factor β can be defined by

E microsocopic = E macroscropic x β

For the plane parallel gaps which are commonly encountered E mac. = $\frac{V}{d}$, where V is the applied potential difference and d the gap separation. Then the enhanced field at the region of emission is expressed as

$$E_{mic} = \beta \frac{V}{d} \qquad 7.$$

Finally substituting equations (6) and (7) into (5) the F-N equation can be expressed in terms of the most commonly measured parameters, viz. applied potential difference and emission current:

$$\log \left(\frac{I}{V^2} \right) = \log \left(\frac{1.54 \times 10^{-6} \, A \, \beta^2 \, 10^{4.52 \, \phi^{-1/2}}}{\phi \, d^2} \right) - \left(\frac{2.84 \times 10^9 \, \phi^{3/2} d}{\beta V} \right)$$

It follows, therefore, that if the current-voltage characteristic of a gap having a single emitter if presented in the form of log (I/V^2) versus 1/V (F-N plot) it will give a straight line with a slope.

$$m = \frac{2.84 \times 10^9 \, \phi^{3/2} \, d}{\beta}$$

and an intercept

$$c = \log \left(\frac{1.54 \times 10^{-6} \, A \, \beta^2 \, 10^{4.54 \, \phi^{-1/2}}}{\phi \, d^2} \right)$$

Thus if d is known and the work function ϕ of the emitter is assumed to have the same value as the bulk electrode material, the slope of such a F-N plot provides an indirect measure of the β-factor of the emitter; it follows that this value may then be used to determine the emitting area from the intercept of the plot. For the more complicated

regime of a number of emitters distributed over the cathode surface, the F-N plot may well be expected not to produce a straight line. In fact, however, a computer simulation study by Tomasche and Alpert[7] has shown that the pre-breakdown regime will always be dominated by one emitter whose enhancement factor and area will accordingly be reflected in the associated F-N plot.

The Fowler-Nordheim theory was first tested for a point cathode and plane anode geometry by Haefer[8] and subsequently and more extensively by Dyke and his co-workers[9, 10] using micro-point emitters whose geometry was accurately known so that the microscopic cathode field could be well determined. They found good agreement with theory over several orders of magnitude of current density, and departures from the Fowler-Nordheim predictions at high current densities could be satisfactorily explained by taking space charge into account. However, the field at which they obtained a given current was one or two orders of magnitude higher than that required when using a broad-area parallel plate configuration.

2.2. Evidence for the Metallic Microprotusion Hypothesis

Experiments employing an extended area parallel plate geometry have a long history, which can be conveniently separated into two eras, viz. before and after the introduction of ultra-high vacuum techniques. In the earlier period some useful work was reported by Millikan and his co-workers.[11-14] Their most important results may be summarised as follows:

1) Field emission from tungsten is normally observed in

the field range of 1 to 5 x 10^7 Vm^{-1}. However, if the tungsten is annealed at 2700°K and subsequently recooled, it could withstand a field of 4 x 10^8 Vm^{-1} before emission.

2) Spots of light are observed on the anode, suggesting that the emission does not occur from the whole of the cathode but from a few localised sites.

3) The emission current at a given field is independent of temperature up to 1000°K.

4) A plot of the logarithm of the current versus the inverse of the field, in all cases produces a straight line.

Since this work was carried out before the theory of Fowler and Nordheim had been formulated, the conclusion drawn by Millikan was that the emission occurred from regions where the work function had been reduced by surface roughness, or chemical impurities.

The introduction of ultra-high vacuum techniques made it possible to carry out experiments in which contamination from the vacuum system and the effects of residual gases could be eliminated or controlled, and the nature of the cathode surface better defined. Thus Boyle, Kisliuk and Germer[15] carried out an investigation to discover if the results of Dyke et.al. for point-plane geometries could be repeated in a broad-area geometry using U.H.V. techniques. They also used pulsed fields to prevent undue heating of their electrodes, which were in the shape of crossed tungsten wires of small (0.75 mm) diameter. Nevertheless, these are considered "broad area" in the sense that the gap spacings used were smaller than or comparable to the dimensions of the electrodes. (In fact they are so close to being plane parallel electrodes that the average field is

given by V/d to a good approximation). The current-voltage data followed a dependence close to that predicted by the Fowler-Nordheim expression including localised field enhancement. As was the case for Dyke's results, there is some departure, attributed to space-charge saturation, from a straight line F-N plot at higher values of current. However Boyle et.al. discovered that the currents varied in an anomalous way as a function of gap spacing, i.e. the average field (V/d) required to draw a given current varied strongly with the gap separation d. They explained these effects and brought their results into agreement with the Fowler-Nordheim theory by postulating that the current was drawn from an emission site which was very minute in area ($\sim 10^{-15} m^2$), and that the electric field at the emission site exceeded the average electric field by an enhancement factor β, which ranged from unity at gap spacings of a few angstroms up to values as high as 30 at 10 microns. They explained the observed variation of β with gap spacing as due to the enhancement of the electric field at small projections on the surface of the cathode.

The work of Boyle et.al. was extended to more practical regimes by Alpert et.al.[16] using electrodes consisting of 35mm diameter discs cut from single crystal tungsten and gap spacings of .005mm to 4mm. Again, their results obeyed the Fowler-Nordheim equation if local field enhancement at the point of emission of 50-200 times was assumed. They, also, found a variation of β with gap spacing, which they considered to be due to two contributions to β, a microscopic one caused by protusions on the cathode and a macroscopic one from the changes of electric field in large gaps

due to end effects. Another observation they reported, which is of interest in retrospect is that "when a pair of freshly baked-out electrodes are initially exposed to high voltage (in U.H.V.), the pre-breakdown current is found to fluctuate sharply. For the first few seconds, sharp spikes appear on the current waveform, corresponding to virtual shorting of the electrodes; these are typically accompanied by gas bursts. The current pulses rapidly diminish in amplitude and increase in frequency becoming indetectably small within 30 seconds after application of the voltage." No explanation was offered for this observation.

Further evidence for the microprotusion model for electron emission from broad-area cathodes was obtained from electron microscope studies by Little and Smith[17], and Tomasche and Alpert[18]. The latter workers observed the blunt end of a 70 micron tungsten wire, by means of shadow electron microscopy. Electrode projections of micron dimensions, capable of producing the necessary field enhancement, were observed on previously smooth regions of the cathode after electrical breakdown. Moreover very small gaps showed extremely large fluctuations in current at higher currents, and when the cathode was observed after several minutes of operation in the unstable mode a large proliferation of whiskerlike projections (approximately 0.1 micron in height) were discovered. However, when both (and only when both) the cathode and the anode were heated to 2000°K, and subsequently recooled, the fluctuations disappeared and the current followed a Fowler-Nordheim relationship right up to breakdown of the gap.

Similar results were reported by Little and co-workers[17,19] using 13mm diameter buttons of aluminium, stainless steel, Kovar, nickel, silver and copper. They also established a vacuum gap using a fluorescent anode and a gap of 0.1mm and observed that as the current flows one or more fluorescent spots (diameter < 0.2mm) appear on the anode; further it was usually noted that the spots appeared suddendly, i.e. with a risetime less than a millisecond. The cathode could be repositioned in the same vacuum system for shadow electron microscope investigation, when it was found that every cathode surface included one or more protrusions, which could possibly give rise to sufficient field enhancement for Fowler Nordheim type emission. The surfaces had been examined prior to the application of electric field and no protrusions were observed, therefore Little et.al. concluded that the protrusions had grown in the field. Another important observation for stainless steel and tungsten cathodes was that the emission current was independent of temperature (within 30%) until 1000^{o}K, when the current began to rise exponentially indicating the onset of thermionic emission. This verified that pre-breakdown emission does not originate from extremely low work-function areas, as is further confirmed by their observation that visible light illuminating the cathode has no effect on the pre-breakdown emission.

Another investigation into the properties of electron emitting sites was carried out by Brodie[20,21] using a nickel wire of diameter 0.125mm surrounded by 76mm cylinderical phosphorescent anode. When current was drawn the anode displayed elliptical spots of millimetre dimensions

which could be correlated with the assumption of the emission arising from whiskers of heights between 70 and 10000nm and base diameters of 7 to 1000nm. However, the structure within the larger ellipses could not be related to the field-emission images obtained from single-crystal nickel surfaces by Gomer.[22] At very high fields (> 5 x $10^{7}Vm^{-1}$) new extremely intense emission centres capable of delivering up to several milliamps without blowing up suddenly appeared. The images of these new spots were usually extremely large; the ellipses having minor axes up to 2cm and major axes up to 6cm. Brodie[21] also reported that emission from ordinary sites could be enhanced by the presence in the same vacuum system of an operating thermionic cathode, presumably by the evaporation of barium onto the emitting sites and so lowering their work function.

Measurements of the pre-breakdown current flowing between copper electrodes in ultra-high vacuum have been reported by Davies and Biondi.[23] Electrodes of OFHC copper were first metallographically polished and then electrolytically polished before assembly in the vacuum system. For bakeout, which lasted 20hours the electrodes were maintained at a temperature of 850°C by means of in situ tungsten filaments. Such high voltage gaps produced F-N type I-V characteristics with β values in the range of 140 to 240, for electrode separations of 0.3mm to 2mm. No significant correlation was found between β and electrode gap. In a further report Davies and Biondi[24] observed that the I-V characteristic is independent of cathode temperature in the investigated range of 313K to 913K.

2.3 Departures of the Pre-breakdown Current from Fowler-Nordheim Theory

From the preceding selection of reports it is clear that a considerable body of experimental work was established which favoured the microprotusion hypothesis for the source of electron emission on broad-area cathodes; however, certain effects such as the suddeness of the onset of emission from virgin electrodes and the large fluctuations in currents frequently reported imply that the emission process is not altogether straightforward. The richness of phenomena in pre-breakdown conduction is well illustrated by the investigations of current/voltage characteristics reported by Powell and Chatterton,[25] Hackam and Salman,[26] and more recently by Cox[27] and Hurley.[28] Amongst the phenomena discussed by these authors are curved FN plots, current noise, temporal variation of emission current, ignition-hysterisis phenomena, negative resistance and high current sites. Also of interest are the bursts of charge, termed microdischarges. Although some of these effects were reported earlier (for a review see Hawley and Zaky[29]) in poor vacuum ($> 10^{-7}$ torr), the later experiments show that though they are indeed more common in these conditions, many of the phenomena still manifest themselves in ultra-high vacuum ($\leq 10^{-9}$ torr) in baked systems.

In particular the work of Powell and Chatterton[25] serves well to illustrate that the frequently reported straight line FN plots are not necessarily typical of the conduction between unconditioned electrodes. These authors carried out an investigation into the pre-breakdown conduction between stainless steel, copper, aluminium, and

tungsten electrodes at small gaps (< 1cm) and in both poor vacuum (10^{-7} - 10^{-6} torr unbaked) and clean vacuum (3×10^{-9} torr, baked). The electrodes consisted of a hemisphere in conjunction with a planar disc, with rounded edges, and were machined from the solid and buffed to a mirror finish.

In general their results are remarkable for the similarity in the behaviour of the different materials. In a vacuum of 3×10^{-7} torr, the field dependent currents were marked by their variability with time and general non-reproducibility, making the plotting of I-V characteristics obviously difficult, and the use of them to determine the emission mechanism of dubious value, see, for example, Fig. 2.2. Therefore a fast response current measuring system was constructed using a storage oscilloscope, enabling a plot of the I-V relationship to be made from currents of 10^{-9}A to 10^{-3}A in five steps of amplifier sensitivity in a time of less than 15s, a single plot over one order of magnitude taking about half a second.

The application of this faster time constant measuring system revealed the presence of irregular bursts of charge termed microdischarges and previously observed by Pivovar and Gordienko.[30, 31]. These occurred for all electrode materials and appeared at a sharp gap-dependent voltage, and were encountered mainly during the early stage of the examination of the conduction between a pair of electrodes freshly installed in the vacuum system. They generally occurred in bursts rather than singly, and were variable in magnitude from less than a μA to several tens of mA, and in duration from tens of μs to tens of ms. In a clean,

baked system microdischarges were observed with tungsten electrodes, but not with stainless steel. The microdischarges could be conditioned away; the rate of conditioning being a function of the electrode material.

The continuous currents did not condition away, but rather in the early stages tended to increase in magnitude at a given voltage after the passage of microdischarges. Application of the oscilloscope fast current measuring system revealed the traces of Fig. 2.3 where the variation of current with time at a fixed voltage was termed rectangular pulse conduction. The size of the pulses ranged from 5% to 30% of the time average current, and they lasted from a few tenths of a ms to several s, with a risetime of less than 5 μs.

A further effect observed when making oscillograms of the I-V relationship for currents in the region of a few μA is shown in Figs. 2.4 and 2.5. As the applied voltage was increased the current at first increased steadily then, with no change in the rate of rise of the voltage, rose dramatically. This effect was a regular feature of the conduction at these current levels and the term "ignition" was used to describe it. On reducing the voltage an hysterisis was always observed, the emission tending to remain in the higher state.

The ignition-hysterisis effect was reproducible as long as the current was limited to below 10^{-4}A. The passage of currents in the mA range completely removed the ignition-hysterisis, and led to a considerable reduction in the frequency and magnitude of the rectangular pulses. This effect was referred to as ageing, and was

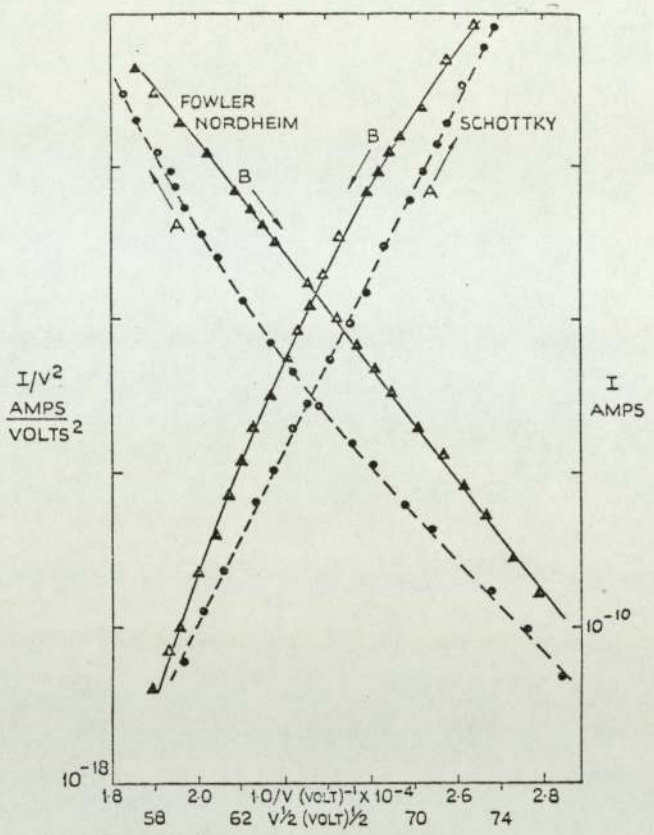

Fig 2.2 Typical current/voltage data plotted according to the FN and Schottky equations showing the dependence of the fit on the mode of accumulating the data. Curves 'A' are for increasing voltages; curves 'B' are for decreasing voltages. Stainless Steel electrodes in unbaked vacuum system 10^{-6} torr. From Powell & Chatterton. (25)

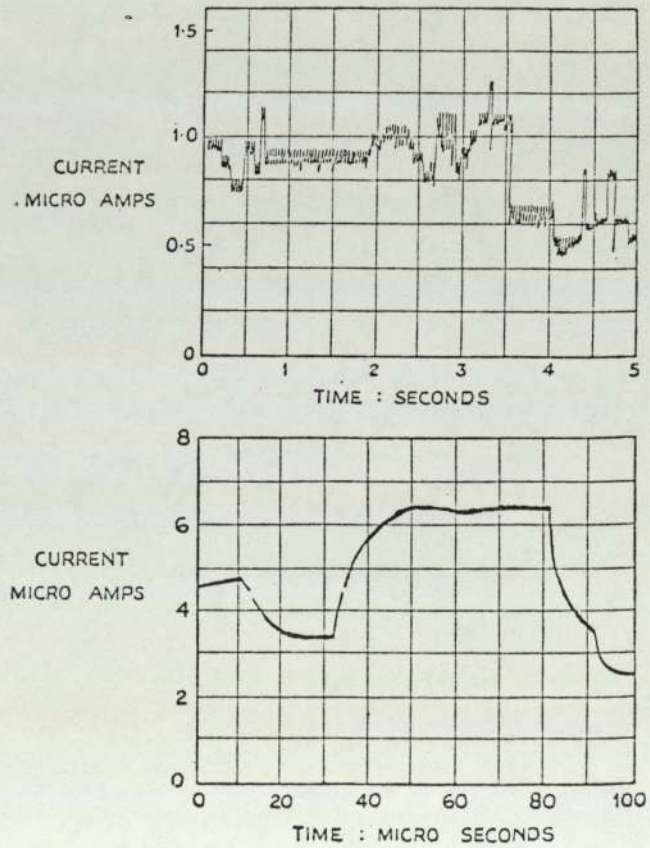

Fig 2.3 The 'rectangular pulse conduction', the discrete steps which comprised the observed variations in the gap current at constant applied voltage. From Powell & Chatterton (25).

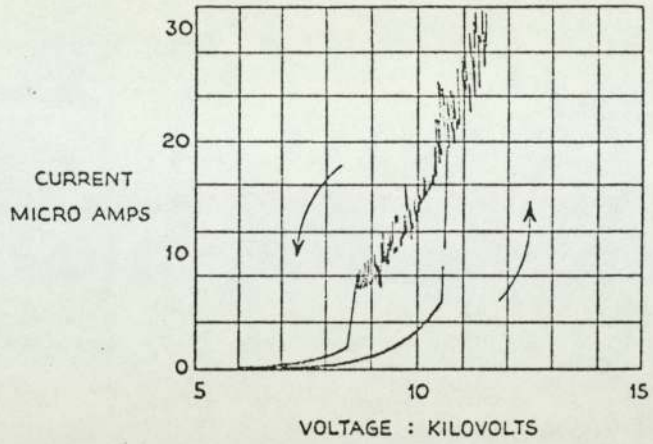

The 'ignition-hysterysis' effect. The arrows show the direction in which the plot was made. The sharp rise of current on the upgoing trace has been termed the ignition.

Figure 2.4 From Powell & Chatterton[25]

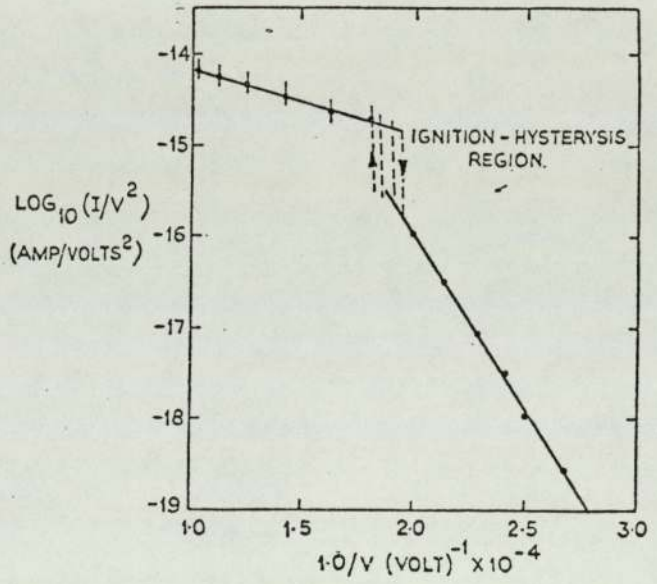

Fowler-Nordheim plot of the region about the ignition-hysterysis showing the 'bend' associated with it.

Figure 2.5 From Powell & Chatterton[25]

a function only of current, occurring at the same value for all gaps. However, the pre-breakdown current was still not free from variation with time at constant voltage, taking the form of a continuous decrease in the emission. Further de-ageing, i.e. when the electrodes were not subject to high currents (< μA), resulted in a return to rectangular pulse conduction. This took about 20 minutes at zero current for stainless steel electrodes in a vacuum of 3×10^{-7} torr, although the ignition - hysterisis effect only returned after several days of de-ageing or after deliberate contamination of the vacuum system such as by warming the liquid nitrogen traps. When stainless steel electrodes were aged in a clean baked system of 3×10^{-9} torr, and then allowed to de-age for 30 minutes no change in the emission characteristics was observed. However, if air was now admitted into the system at a pressure of 2×10^{-6} torr for a few minutes the electrodes completely de-aged - with a return to the rectangular pulse conduction. (The return to this mode had taken several hours when the system pressure was 3×10^{-9} torr).

Powell and Chatterton explained the various temporal instabilities in terms of gas coverage of an emitting protusion. They assumed that the equilibrium surface coverage σ of adsorbed gases would vary with the current as follows:

1) At low currents the most important contribution would be the arrival of molecules at the tip due to surface migration, so that an increase in electric field will lead to an increase in σ.

2) At intermediate currents the temperature of the tip will rise and sputtering of the tip due to positive ions increase. Thus in general the level of coverage will decrease.

3) At high values of current the tip may become very hot and σ will tend to reduce drastically.

If it is further assumed that adsorbed gases generally suppress the emission, then many of the pre-breakdown observations described can be explained using the above model. Thus, when increases in current lower σ, the current will increase more rapidly than allowed by the FN equation, leading to the kind of bending of the FN plot shown in Fig. 2.2. A plausible explanation of the ignition-hysterisis effect was given by comparison with the observation of molecular images in the field emission microscope.[3] It was suggested that the ignition occurs on an adsorbate covered field emitter when empty electron energy levels in the adsorbate dip below the Fermi level of the bulk emitter due to the high electric field, at which point sudden enhanced emission will occur. Desorption may be expected to accompany the enhanced emission, leading to a change in the slope of the FN plot. The ageing process is considered as a complete or nearly complete removal of adsorbed gas from an emitting protusion, de-ageing corresponds to re-contamination, and the rectangular pulse conduction is attributed to the migration of small groups of atoms across the emission region.

Hackam and Salman[26] studied the pre-breakdown currents from aluminium electrodes in a baked system at 10^{-9} torr. In order to obtain reproducible data the electrodes were first conditioned at a gap of 0.25mm using currents in the

range 50-100 μA. Two distinct behaviours of the FN plots was observed. At short gaps ($\leq$ 0.76 mm) a single straight line was observed over several orders of magnitude of current and no ignition type phenomenon was found. As the gap separation was increased ($\geq$ 0.89 mm) ignition-hysterisis effects appeared at a particular voltage depending on the gap separation and at current within 2.4 and 6.6 x 10^{-9}A. The current during the ignition rose in two stages, increasing slowly to 6-10 x 10^{-9}A (in a matter of 30s) and when this intermediate value is reached, it jumps suddenly to a value in the range 0.26 - 6.5 x 10^{-7}A. After the ignition the gap remains in a higher β state and the FN plot is seen to exhibit a distinct convex curvature, the onset of emission now occurring at a considerably reduced voltage (sometimes by a factor of two). The ignition-hysterisis effect observed by Hackam and Salman, differs from that reported by Powell and Chatterton, in two respects: firstly the former never observed a discontinuity in the downward cycle of voltage application as shown in Fig. 2.4, secondly they found the ignition to occur at currents in the nA rather than in μA range. Hackam and Salman also studied ageing and deageing effects using a fast current monitoring technique which revealed that after an elapse of 5 minutes with no field applied to the surface an ignition was not observed, after 6 minutes a much diminished ignition reappears, returning to its maximum value after a delay of 10 minutes. When using the slow measuring method (with a digital voltmeter) the ignition effect reappears after at least 2 hours are allowed at zero current and zero voltage. If, however, during the deageing

time, the gap is subjected (say for 30 minutes) to a high electric field (at negligibly small currents < 10^{-11}A) a longer period (∿ 4 hours) is necessary for the reappearance of the ignition.

More recently Cox[27] and Hurley[28] have also reported current - voltage relationships for pre-breakdown conduction, which do not appear to obey the Fowler Nordheim Law expected for emission from metallic protusions. Cox observed some unusual I-V characteristics during a large number of tests on commercial vacuum switch electrodes. In these experiments 14mm discs of the copper-chromium alloy were set in a plane parallel gap of 6mm in a vacuum which reached 0.1 μPa after baking at 250°C. A deconditioning pulse was applied before each test by passing a ringing discharge of 14kHz frequency with a current of 16kA at the first peak. The majority of the tests revealed I-V relationships fitting the FN equation with βs from 300-500. However, other runs produced unstable emission and I-V plots exhibiting large hysterisis-like, but irreversible, current decreases between increasing and decreasing currents, see Fig. 2.6 and 2.7. A third type of site, termed "switch on", occurred in only about 1% of the total tests, for which the current increased from zero or at most 10^{-7}A to usually more than 10^{-5}A, with virtually no change in the applied voltage. They differed from ignition sites[25] in that the switch-on only occurred once even if the maximum current was limited. A further type of site, which appeared similarly infrequently was one which passed the maximum current (500 μA) available without causing breakdown, and exhibited unusually high β values (in

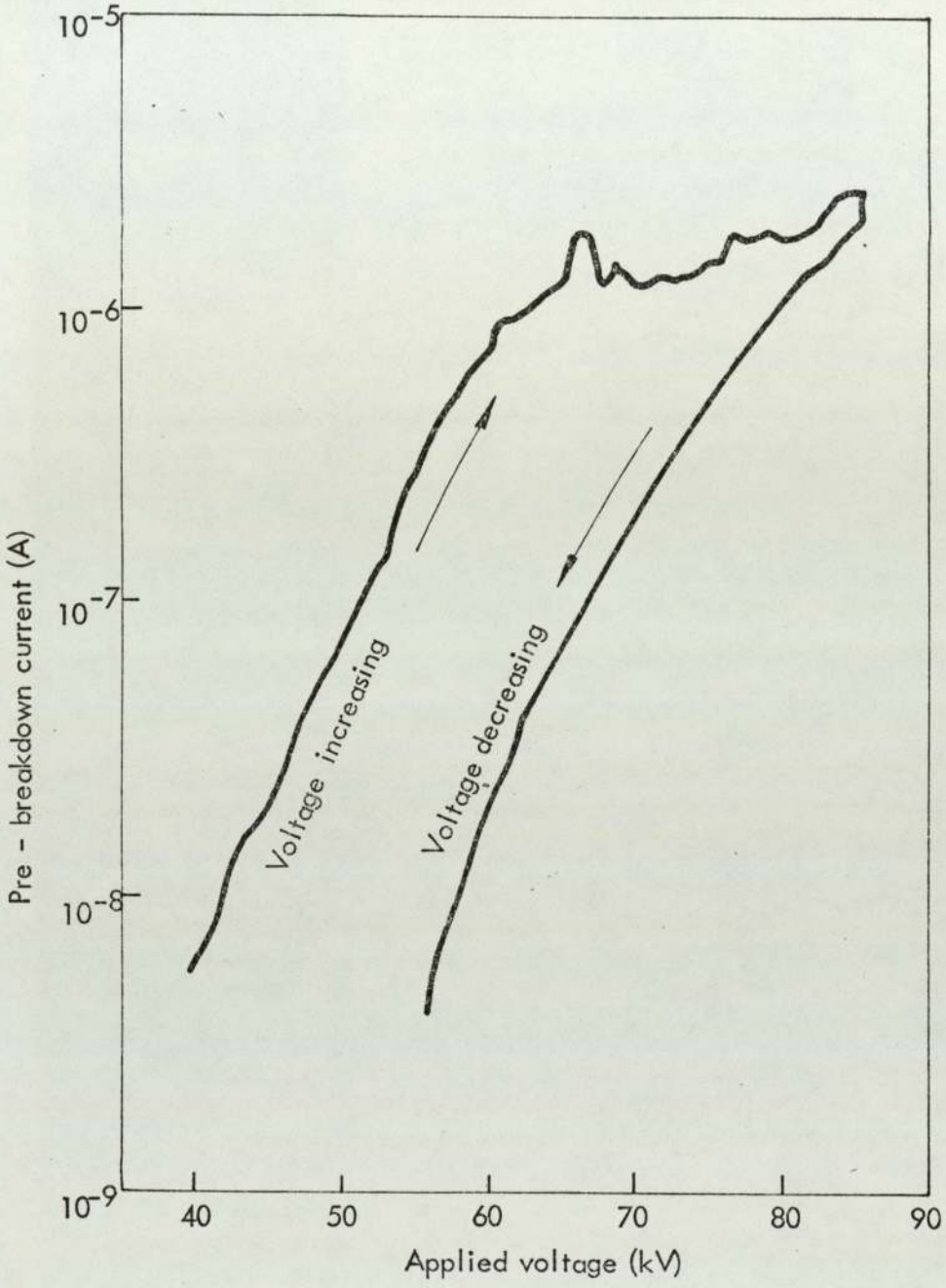

FIG. 2.6 VOLTAGE vs CURRENT PLOT SHOWING HYSTERESIS-LIKE BEHAVIOUR. FROM COX[27].

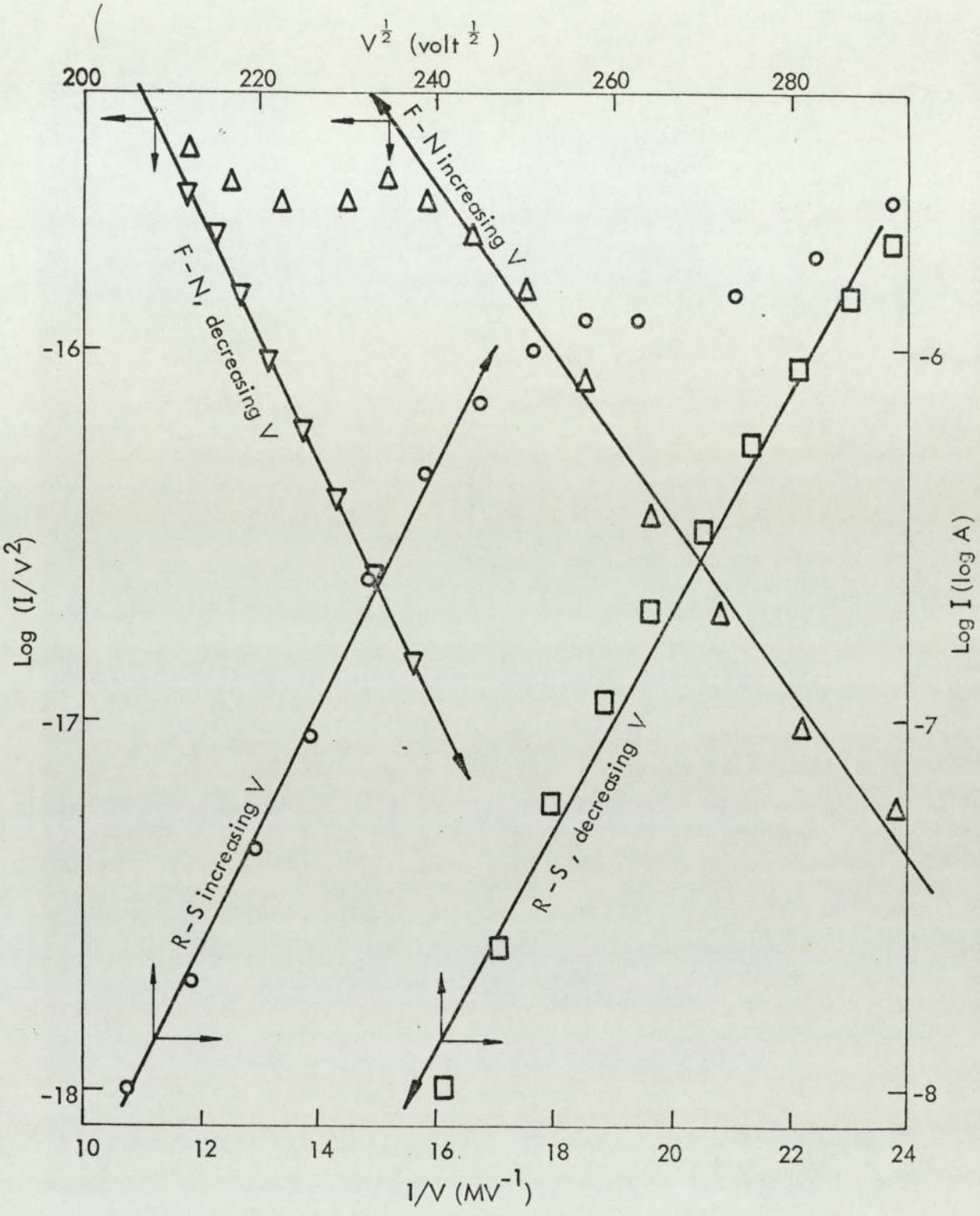

FIG. 2.7 FOWLER-NORDHEIM (F-N) AND RICHARDSON - SHOTTKY (R-S) GRAPHS OF V-I DATA IN FIG. 2.6. FROM COX[27].

the region of 1000).

Hurley,[28] using a pointed anode probe to locate and measure the emission from individual electron emitting sites found that two types of emitters (which he termed "a" and "b") could be distinguished on OFHC copper. Each type of site produced fairly straight FN plots for currents up to 10^{-5}A, the "a" sites being characterised by β in the range 150 to 300 and calculated emitting areas in the range 10^{-14} to $10^{-16}m^2$, whilst the "b" sites had β in the range 10 to 150 and calculated emitting areas in the range 10^{-13} to $10m^2$!! Whilst for "a" sites breakdown and destruction of the site occurred when the current reached a value of the order of 5 ($\pm$ 2) x 10^{-5}A, for b sites and I > 10^{-5}A, the current would adjust itself to an equilibrium value partly determined by the voltage drop across a 23 MΩ series resistor. I-V characteristics taken in this region revealed a current controlled negative resistance region, Fig. 2.8. The total current that could be drawn from a "b" site was limited by the power supply. If the series safety resistor was removed, breakdowns occurred randomly at currents between 10^{-5} to 10^{-3}A, but without destruction of the emitting site.

2.4 The Role of Insulating Impurities

The assumption of electron emission from broad area electrodes occurring purely from microprotusions was chiefly based upon two observations: the I-V characteristics producing straight line FN plots, and the observation of field-enhancing features on electrodes. However, it has been shown that in many cases the pre-breakdown conduction is much more complicated than can be explained by a straight-

forward application of Fowler-Nordheim theory; and also none of the observations of field enhancing features have been correlated with an actual individual emission site. A number of recent experiments have led to the alternative hypothesis that insulating impurity particles and inclusions, which are invariably present on nominally pure or clean surfaces, may be involved in the emission process. Before discussing these investigations it is informative to collate some of the earlier reports which have alluded to the role of impurities in the phenomenon of electrical breakdown in vacuum.

The role of insulating particles in the initiation of breakdown in low-pressure devices has been suggested many times. For example insulating inclusions were identified as unwanted arc initiation sites in low pressure plasma by Pfeil and Griffiths,[32] Hancox[33] and Maskrey and Dugdale.[34] They hypothesised that the initial event in arc formation is the dielectric breakdown of insulating cathodic inclusions previously charged to breakdown potential by incoming gas ions. In order to determine their precise role Maskrey and Dugdale,[35] carried out an experiment which enabled in situ optical microscopy of stainless steel and copper surfaces in a vacuum of $\sim 5 \times 10^{-6}$ torr. They employed a 0.5mm diameter anode probe, which could be located over any chosen area of the cathode, and a test gap of 0.05mm established. Breakdowns occurred at fields of around $3 \times 10^{8} Vm^{-1}$, with considerable scatter down to $1 \times 10^{8} Vm^{-1}$. Comparison of photomicrographs taken before and after the breakdown revealed that the spark damage pits coincided with the position of typically

micron diameter dark inclusions. These authors suggested that positive ions produced by field emission electrons could lead to charging and subsequent breakdown of the insulating inclusions.

Donaldson and Rabinowitz [36] found that the thermal decomposition of glass (for example in glass-blowing for closing vacuum chambers) generates particles of diameters between 10^{-2} and 0.5 μm , containing a variety of elements including sodium, potassium and boron. These particles are not removed by bakeout at 450°C and when present on electrode surfaces can reduce breakdown voltages by as much as 50%, independently of system pressure in the range 10^{-5} to 10^{-9} torr. They also noted that the breakdown field varied from $2 \times 10^{8} Vm^{-1}$ at a gap of 0.1 mm to $10^{7} Vm^{-1}$ at a gap of 0.3mm, which could explain why the macroscopic breakdown field was so high in the results of Maskrey and Dugdale.[35] Pokrovskaya-Soboleva et.al.[37] have demonstrated that insulating inclusions (FeS, Al_2O_3, SiO_2 and alumina silicate glass) added to pure iron cathodes produced a significant degradation (20-30%) of the breakdown voltage, larger particles (50 to 500 μm) producing a greater and more sustained effect. Using a method similar to that of Maskrey and Dugdale,[35] they confirmed that breakdowns are localised in the region of the inclusions. In the case of SiO_2 the breakdown results in fusing the iron near the inclusion, whereas on cathodes with FeS the inclusion material melts; an effect which is determined by the melting temperature ratios of the cathode and the included material.

Farrall, et.al.[38,39] have used a novel technique

for locating the electron emission sites on broad area electrodes. The approximate positions of the emitting sites are found by using a phosphor screen as the anode, whence their individual I-V relationships are determined by monitoring the intensity of the phosphorescent spots. In general the emission is found to follow the FN Law reasonably well with β factors in the region 150 to 250, although one site was found which produced two straight lines of differing slope. Next the phosphor screen was replaced by an anode coated with lead. When steady currents are drawn for several minutes the electron beams vaporise some of the lead, which is dispersed throughout the gap volume. It is believed that a part of this vapour arrives in the vicinity of the cathode and is ionised by electron emission close to the cathode emitter, and is drawn by the emitting field to the emitting region. This in effect "tags" the emitter but does not destroy it. Subsequently this lead can be detected in the scanning electron microscope using solid state x-ray analysis.

On every specimen studied lead deposits were found to be concentrated on isolated insulating particles (typically 1 to 10 μm diameter), no lead being found on many other similar particles or on the substrate metal. No specific elements were identified as always being present in the tagged particles. In one experiment the specimen was deliberately contaminated by touching with a particulate zinc sulphide screen. Subsequently the surface was incapable of withstanding a fraction of the voltage withstood prior to contamination; even low voltages maintained for a few minutes would ultimately result in breakdown. More

stable emission was generated by rubbing the sample electrode firmly against the particulate screen, after which tagging of one of the emitting sites identified a 5 to 10μm sized zinc sulphide particle.

More recently Farrall, et.al.[40] have reported the effect on breakdown and emission properties of copper electrodes which have been intentionally contaminated by adding ½% by weight of alumina powder having average sizes of 500, 50, and 5 μm . Prior to the occurrence of any breakdown events electron emission currents of $\sim 10^{-5}$A were obtained at voltages of 30% and 60% compared to those required from an uncontaminated surface, for the 50μm and 5μm contaminated surfaces respectively. High current pulsed breakdowns led to a rapid convergence of the emission properties for all surfaces, although the 500μm surface did not condition as quickly as the others. Subsequent scanning electron microscopy confirmed that breakdowns on the contaminated surfaces were clearly associated with metal-insulator boundaries. All the particles showed signs of smoothing, probably due to melting, and on the 5μm surface (and less commonly on the 50μm surface) cavities were found which appeared to be the remnants of particles which had been ejected from the surface. The authors concluded that the principal effect of inclusions is the formation of sharp metallic edges and protrusions, which greatly enhance the surface electric field at inclusion boundaries with the metallic matrix.

2.5 Recent Experimental Observations Disputing the Metallic Microprotrusion Hypothesis

The assertion that pre-breakdown currents arise from

field enhancing microprotusions has been strongly challenged in recent years by the results of the experiments of Cox,[41] Hurley and Dooley,[42] and Allen and Latham.[43] These authors have used vastly different techniques to study pre-breakdown currents, but have each concluded that insulating or semiconducting impurities at the metallic surface are involved in the emission process.

Initially Cox and Wort[44] reported an improved method for locating and mapping field emission sites on broad area electrodes using a probe hole of 0.5mm diameter in the anode, behind which was mounted a secondary probe anode. With this system, the position of each site could be determined to $\sim$ 0.1mm, by moving the anode assembly relative to the specimen. In addition this technique allowed the measurement of the voltage/current characteristics of an individual site, and the mapping of constant current contours. An interesting experiment was carried out with this apparatus by artificially inserting a tungsten tip into a planar copper surface and then measuring any emission from this "site". When this was done emission was obtained at a position close to but quite separate from this artificial protusion. This result showed that the feature on the cathode surface which appears on microscopic examination to be the most likely source of emission is not necessarily the one which actually emits.

In the next stage of his work, Cox[41] improved the probe hole facility and incorporated it into an ultra high vacuum scanning electron microscope. Thus, referring to Fig. 2.9, all the emitting sites could be initially located by scanning the specimen below the large aperture, before

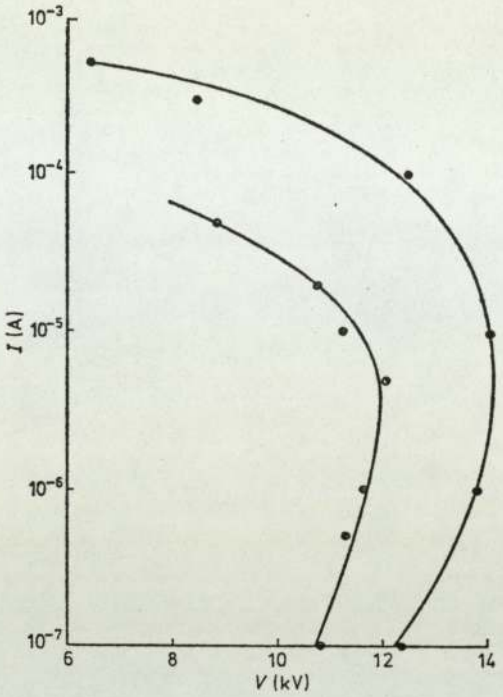

Current–voltage characteristics of typical b-sites. ●, d=0·16 mm; ⊙, d=0·32 mm. d=distance between the tip of the positive probe and the negative broad area electrode.

Fig. 2.8 From Hurley[28]

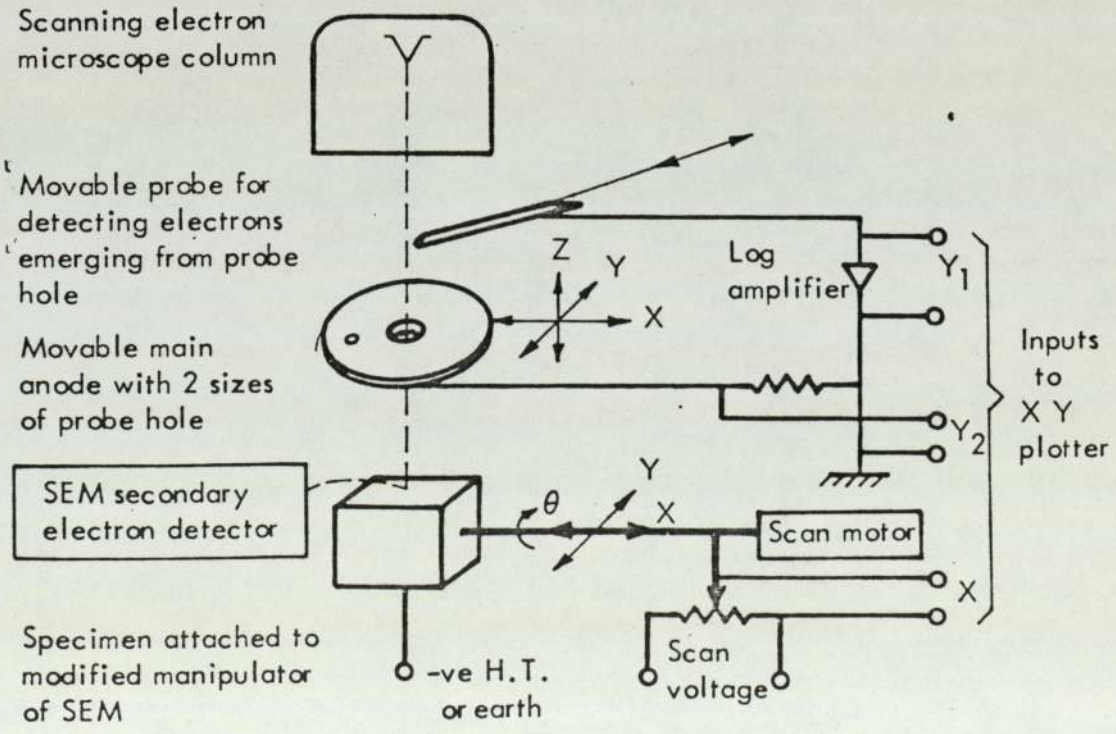

Fig. 2.9 A schematic representation of the probe hole facility for identifying electron emission sites in situ in a S.E.M.. From Cox[41]

being selected for detailed examination with the smaller probe hole. The specimen is then positioned such that the current collected by the probe is a maximum. This process is repeated at gradually reducing separation of specimen and anode; a process which effectively gives the trajectory of the electron beam's centre. By reducing the gap to 50μm and then extrapolating to zero the co-ordinates of the emitter were determined to a resolution of $\pm$10 μm . The probe and anode may then be pulled clear and the predicted area examined.

The results of this technique showed that whilst the Fowler-Nordheim plots of many individual emission sites predicted field enhancement factors of $\geq$ 100 times, no complementary surface features were found which could give enhancement of this order. On high-purity vacuum-arced copper samples, dust particles were found to be responsible for many observed emission sites. Subsequently the installation of the SEM and specimen cleaning bath in a clean room dramatically reduced the incidence of such particles. Then many of the more strongly emitting sites were found near the edges of the specimen despite attempts to eliminate non-uniformity of the field in these regions. In the central regions of the specimen cracks and grain boundaries featured prominently in site predictions. The same technique was used by Cox and Williams[45] to identify field emission sites on unpolished stainless steel. An insulating particle of $\sim$ 5μm diameter was found to be the source of an exceedingly strongly emitting site (β = 735), and as the applied field was further increased the current suddenly dropped. Examination of the previous emitting area revealed

that the particle had disappeared.

Another observation that is not consistent with the microprotusion hypothesis of electron emission was reported by Hurley and Dooley,[42] who carried out an investigation into the spots of light which appear on the surface of the cathode during pre-breakdown current emission, a phenomenon earlier briefly noted by Klyarfeld and Pokrovskaya-Soboleva.[46] The technique used broad area copper electrodes and it was observed that these cathode (or K) spots were sometimes unambiguously associated with subsequent discharge flares and tracks. The procedure was to observe the cathode spots using an image intensifier and then to measure their spectral content by interposing optical filters and using a photomultiplier. The same technique was used in part of the investigation reported in this thesis, and is more fully described in another chapter. The observed spectrum corresponded neither to a black body curve nor to any obvious discharge spectra. The shape of the spectrum suggested rather that the luminosity is caused by electroluminescence produced by the action of the electric field on semiconducting inclusions on the cathode surface. Further measurement of the applied voltage/light intensity relationship of the cathode spots confirmed that they obeyed the Alfrey-Taylor[47] expression characteristic of electroluminescent cells. In a subsequent experiment, when he located electron emitting sites using a pointed anode probe, Hurley[48] demonstrated that on copper electrodes such sites are also invariably the source of electroluminescence.

Hurley and Dooley[49] also observed discharges to occur from within the light emitting regions; a positive

correlation being found to exist between the occurrence of a discharge flare and breakdown of the gap, for electrodes of OFHC and high-purity copper, molybdenum, stainless steel and duraluminium. In the case of copper, straight tracks were sometimes observed originating from the cathode light emitting regions. They are believed to be caused by the emission of an uncharged particle ejected from the electrode once the applied voltage has collapsed.

Concurrently with the work of Hurley and Dooley, Allen and Latham[43] reported the results of measurements of the energy distribution of the electrons emitted from broad area copper electrodes. Electron spectrometry forms the major part of the work in this thesis and is considered in detail in the next chapter. However, at this point it suffices to say that the energy distribution they measured was not consistent with emission from a metallic micro-protusion, but more characteristic of a semiconducting emitter.

CHAPTER 3

THE ENERGY DISTRIBUTION OF FIELD EMITTED ELECTRONS

3.1 Introduction

Most of the experiments described in the previous chapter have involved the measurement of the total current as a function of the field or surface condition. However, it is clear from the derivation of the Fowler Nordheim equation that this current is an integration of the probability of emission of electrons over all energies. Therefore a more basic quantity is the electron energy distribution after emission, i.e. the product of the energy distribution inside the emitter and the transmission probability for each energy. The external electron energy distribution is measurable and should be a sensitive test of the validity of any model for the field emission process. Information about the origin of the emitted electrons and the energy dependence of the electron emission probability can be expected from this source.

3.2 Field Emission from Metals

Henderson and co-workers[50,51] were the first to apply a retarding-potential analyser to study the field emission of electrons. They used a platinum wire cathode to show that the electrons originate from energy levels at or below the Fermi energy. However, field distortions in their cylinderical tube resulted in poor resolution. Muller,[52, 53] employing a spherical retarding-potential device using a tungsten tip as an emitter with a concentric anode and collector obtained good agreement with the energy distribution predicted in the derivation of the Fowler Nordheim equation as discussed in Chapter 2.1. A similar

distribution was later verified by Muller and Bahadur.[54]

However, Young and Muller,[55] using an improved retarding potential analyser, subsequently recorded a much narrower energy distribution than predicted by the Fowler Nordheim derivation. They indicated that the good agreement previously reported between experimental and theory was brought about by the limited resolution of the retarding potential tubes employed. In the Fowler-Nordheim derivation discussed in Chapter 2.1, the parameter which determines the tunnelling probability is "the normal component" of energy, i.e. that which is directed towards the surface. Thus the measured energy distribution might be expected to be the distribution of the normal energies of the electrons.

This is true for a perfectly plane parallel case, but in the spherical geometry of the more usual field emission cathode situation "the transverse component" of the energy, which is conserved in the tunnelling process, is rapidly transferred to the direction of motion once the electron has left the tip; hence the *total energy* of the electron is measured and not its *normal energy*. In fact, Gadzuk and Plummer[56] have shown that only when the distance (r) of the probe hole of an anlyser from the emitter approaches the radius (ro) of the emitter can the normal energy distribution be measured; when r > 10ro the total energy distribution is obtained.

In order to derive the total energy distribution of electrons field-emitted from a metal obeying free electron theory, Young[57] reformulated the Fowler Nordheim equation by defining the new parameters:-

$N(W, E)\, dW dE$ = number of electrons with total energy within the range E to E + dE whose Z part of the energy lies in the range W to W + dW incident upon the surface per second per unit area.

$P(W, E)\, dW dE = N(W, E)\, D(W)\, dW dE$

= number of electrons in the given energy ranges penetrating the barrier.

$P(E)\, dE = \int w\, P(W, E)\, dW dE$

= total energy distribution

$J = e \int P(E)\, dE$

= electric current per unit area

= Fowler Nordheim equation

Using these new parameters, Young showed that

$$P(E)\, dE = \frac{4\pi\ md}{h^3} \exp\left(-C - \frac{E_F}{d} \right) x \frac{\exp\ (E/d)\ \ dE}{\exp\ \ (E - E_F)/KT + 1} \qquad 3.1$$

where $C = \frac{4\ (2m\ \emptyset^3)^{1/2}}{3\ \hbar\ e\ F}\ v\ (y)$

$$d = \frac{\hbar\ e\ F}{2\ (2m\ \emptyset)^{1/2}\ t\ (y)}$$

$E_F = -\emptyset$ = the Fermi energy, with the other parameter having been previously defined in Chapter 2.1. The total energy distribution of equation (3.1) may be compared with the normal energy distribution using the parameters defined in Chapter 2.1:

$$P(W)\, dW = \frac{4\pi\ m\ k\ T}{h^3} \exp \frac{-4\pi\sqrt{2m}\,|W|^2}{3\ h\ e\ F}\ V\ (y) \log \left[1 + \exp - \left(\frac{W - E_F}{k\ T} \right) \right] d$$

The value of E when P (E) is a maximum can be found by

differentiating the exponential part of equation (3.1) with respect to E. This leads to

$$E_{max} = E_F - k T \ln ({}^{d}/_{k T} - 1)$$

so that when $T = 0$, $E_{max} = E_F$.

The full-width at half maximum (FWHM) of the total energy distribution at zero temperature is found to be

$$\sigma = 0.693\ d$$

Fig. 3.1 shows the normal and total energy distribution curves obtained by Young[57] at three different temperatures. Henceforth we shall only be interested in the directly measurable total energy distribution, and call it the field emission energy distribution or F.E.E.D.

It was first established by Swanson and Crouser[58] that equation (3.1) is not always valid. In particular, they found that in experiments on tungsten micro-tip emitters the energy distribution from the (100) direction contained a low energy hump 0.35eV below the Fermi energy (now often referred to as the "Swanson hump"). This was attributed to the non-free electron behaviour for this direction caused by band structure effects. Similar effects for tungsten were studied by Plummer and Bell[59] who suggested that non-free electron contributions are present in nearly all spectra but their influence on the energy distribution of field emitted electrons is so small that they can only be revealed by plotting the current axis of the distribution in logarithmic form; the Swanson hump being one of the few effects noticeable without such a procedure.

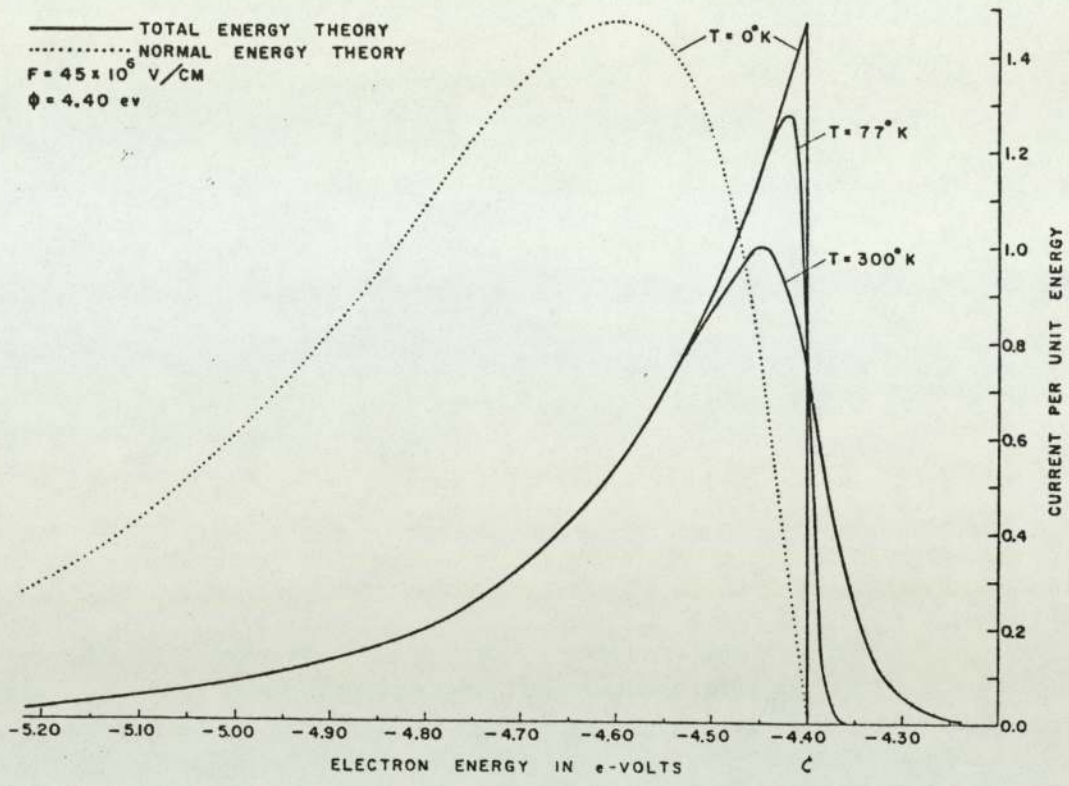

(a) Total- and normal-energy distributions for field emitted electrons. The 300°K curve is arbitrarily normalized.

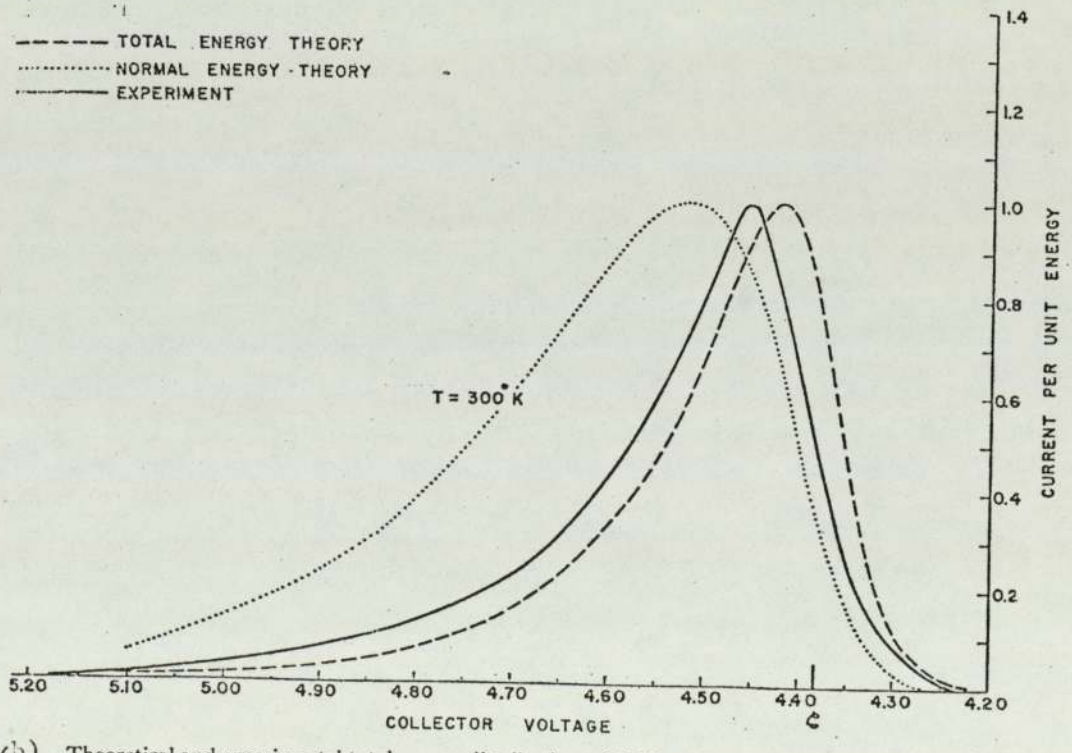

(b) Theoretical and experimental total-energy distributions of field-emitted electrons at room temperature. The theoretical normal-energy distribution is shown for comparison. All three curves are arbitrarily normalized.

Fig. 3.1 Metallic Total and Normal Energy Distributions ; (a) from Young&Muller[55], (b) from Young[57].

Nicolaou and Modinos[60, 61] have developed a systematic theory of field emission from transition metals, based on the use of the "Muffin tin approximation", whereby the potential seen by an electron inside the metal is represented by a superposition of non-overlapping spherical potentials centred on each of the ions of the crystal; outside these spheres the potential is approximated by a constant. It is assumed that the bulk potential is terminated abruptly at the surface and outside the metal an electron sees only the applied field. Low energy electron diffraction (LEED) data has shown that the "Muffin tin approximation" is reasonable for transition metals, but for other metals it may not be valid and for semiconductors it is certainly incorrect since re-arrangement occurs at the surface. Modinos[62] has calculated an expression for the total emitted current, from which calculations of the energy distribution are possible and have shown to give excellent agreement with experimental results (Fig. 3.2).

Whitcutt and Blott[63] first measured the energy distribution of electrons field emitted from a copper crystal grown by vacuum evaporation on the end of a tungsten field emission tip. Emission was obtained from the (111) plane of the copper and found to have the expected peak at the Fermi level. However, when a crystal was grown having a particularly large (111) region ($\sim$ 1000 A), it was found that the spectrum at the edge of the region occupied the expected energy range but that from the centre was displaced to lower energies by about 400 meV. Kar and Soven[64] have applied the method of Modinos to the (111) plane of copper to explain this result. More recently Jones and

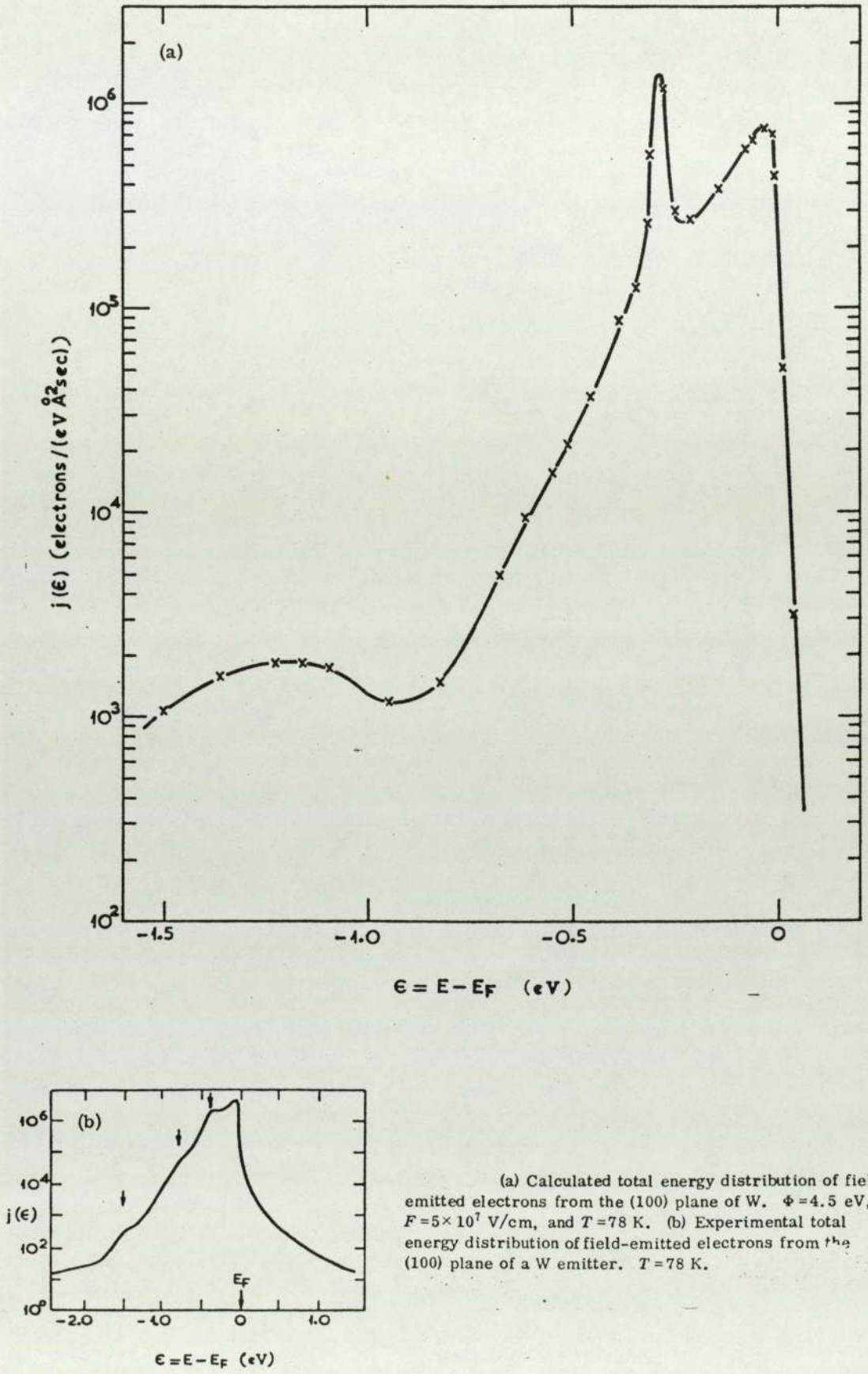

(a) Calculated total energy distribution of field-emitted electrons from the (100) plane of W. $\Phi = 4.5$ eV, $F = 5 \times 10^7$ V/cm, and $T = 78$ K. (b) Experimental total energy distribution of field-emitted electrons from the (100) plane of a W emitter. $T = 78$ K.

Fig. 3.2 From Modinos & Nicolaou[61]

Roberts[65] have observed an additional peak at about 750 meV below the Fermi level for what they believed was emission from the (110) plane of a copper crystal grown on a tungsten micro-tip. Again they suggest it is caused by a virtual surface state existing due to band structure effects.

FEEDs have also been obtained from molybedenum [66] platinum, iridium, rhodium, palladium[67] and nickel.[68] In every case the deviations from free electron theory have been explained in terms of band structure and the local density of states at the metal-vacuum interface. Other effects which have been considered to cause deviations from the FN theory are relaxation processes involving electron scattering in the bulk (e.g. the mechanism for replacement of the emitted electrons),[69, 70, 71] and energy broadening due to tunnelling lifetimes.[72] For the most part the phenomena referred to above lead to relatively small perturbations in the FEED that require sensitive electron spectrometers for their detection, have no detectable effect on the FN plots, and have little effect on the full width at half maximum (FWHM) of the energy distribution.

More recently, however, Bell and Swanson[73] have measured an anomalously wide FEED from tungsten at extremely high current densities (10^{10} to 10^{12} A m^{-2}). They employed a special built-up tungsten emitter, which is sharpened in situ in the vacuum system by heating to 1800K and applying a positive field of 5 to 6 x 10^{9} Vm^{-1}; and is then found to be capable of stable high current density operation and also confines the emission to a small (8^{o}) half angle. It was discovered that the FWHM of the energy distribution appreciably exceeds the value predicted by

FN theory; the dependence of the FWHM on applied field and current is shown in Fig. 3.3 for two extreme temperatures of operation (84K and 1685K). By noting the dependence of the FWHM on the beam angular intensity (in m A/sr), the authors concluded that the anomalous broadening was most likely due to coulomb (space charge) interactions in the vacuum space in front of the emitter, although internal electron energy-broadening mechanisms could not be ruled out. It should be noted, however, that no anomalous shift was found in the position of the FEED with respect to the Fermi level.

3.3 Field Emission through Adsorbates

Any field emitting tip, such as a microprotusion on a broad area cathode, which has not been specifically cleaned, may be reasonably expected to be covered by adsorbed gas atoms. Duke and Alferieff,[74] have shown theoretically that such a coverage can have a dramatic effect on the energy distribution of electrons obtained from the tip. They pointed out the role of elastic resonance tunnelling through virtual energy levels of atoms or molecules adsorbed on metal surfaces, by realizing that adsorption can not only vary the surface barrier, resulting in a real work function change but also vary the shape or effective "thickness" of the barrier due to the presence of the attractive potential well of the adatom. Thus although the thermodynamically defined work function could remain constant the field emission tunnelling probability could drastically change; in turn affecting the energy spectrum and FN plots.

A substantial body of knowledge was previously deve-

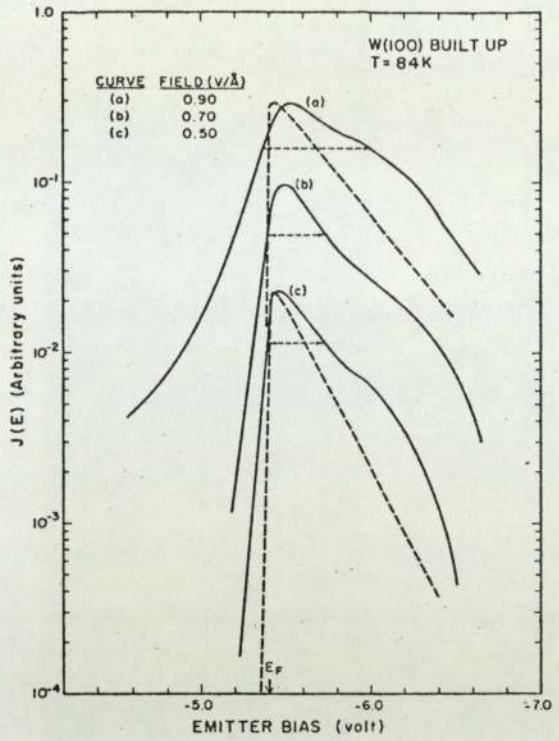

(a) Solid lines are the experimental TED curves for a W(100) builtup emitter taken at the indicated electric fields and temperature; dashed lines are the corresponding theoretical curves using $\phi = 4.5$ eV, and normalized to the peak heights and Fermi-level E_F of the respective experimental curves. Horizontal dashed lines indicate the experimental FWHM values. Crossover analyzer with $\Omega = 0.14$ msr used for these results.

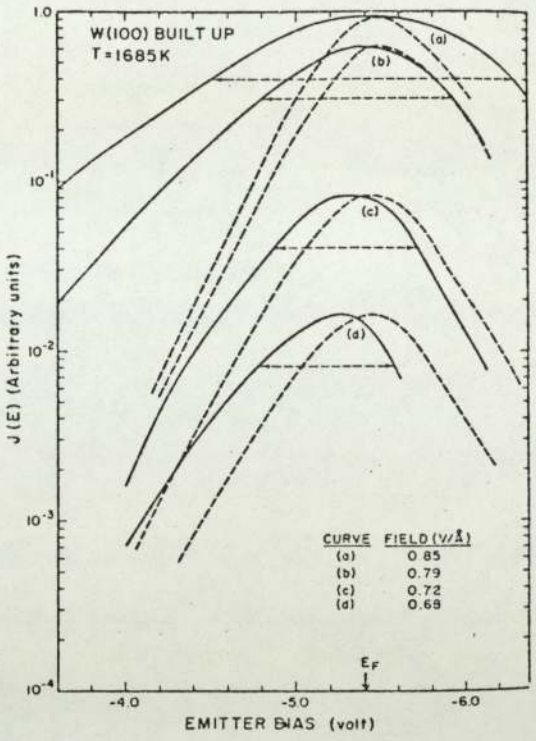

(b) Solid lines are the experimental TED curves for a W(100) built-up emitter taken at the indicated electric fields and temperature; dashed lines are the corresponding theoretical curves using $\phi = 4.5$ eV and normalized to the peak heights and Fermi-level E_F of the respective experimental curves. Horizontal dashed lines indicate the experimental FWHM values. Crossover analyzer with $\Omega = 0.14$ msr used for these results.

Fig. 3.3 The dependence of the FWHM of the electron spectra on field for a high current density emitter at (a) 84 K and (b) 1685 K ; from Bell & Swanson[73].

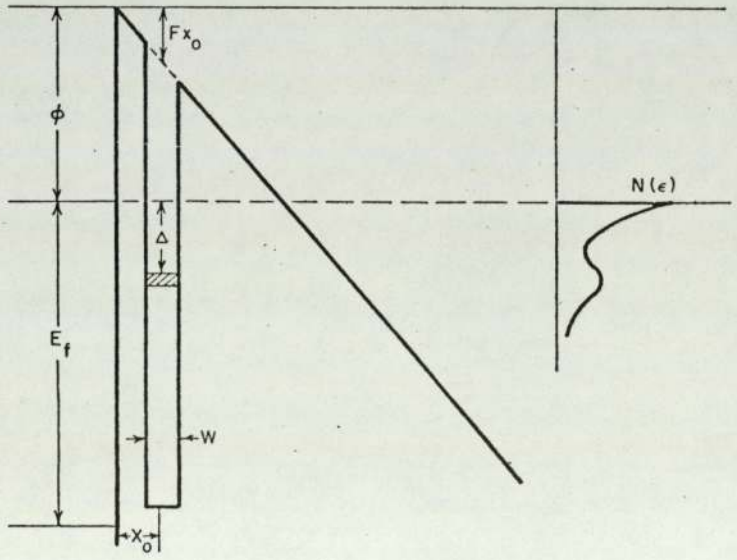

Fig. 3.4 Electric potential diagram and energy distribution , $N(\varepsilon)$, for tunnel resonance enhanced field emission.

loped dealing with the problem of double barrier potentials (see, for example, (75)). The most pertinent conclusion is that if the energy of the tunnelling electron is the same as the energy of an allowed level for the potential well between the two barriers, then barrier penetration is much easier. In Fig. 3.4 a schematic potential diagram is shown in which the adatom potential is taken to be a square well. If the adatom has a virtual energy level near the Fermi level, then an electron tunnelling from a metal state to a vacuum state can go either directly or via the intermediate resonance atomic state. The latter case is particularly advantageous because the atomic potential cuts a hole in the barrier which should reduce the WKB phase integral used to evaluate the transmission probability, and thus increase the transmission function. Then an energy distribution of electrons field emitted through an adatom would tend to display structure which could be related to the energy states of this atom.

Duke and Alferieff illustrated this point by performing an exact wave matching calculation for the triangular barrier with various combinations of square well and delta function model potentials representing the atom core. With these model calculations they were able to show that neutral adsorbates could lead to reductions in the total current, even with no change in the work function. However, metallic adsorbates should generally lead to wide ($\sim$ 1eV) resonances in the transmission probability, which can cause an additional peak or shoulder in the field emitted energy distribution and a large (10^2 - 10^4) enhancement in the emission current. Further, the extra peak, which may often totally dominate

the distribution, is expected to shift linearly with applied field towards low energies, due to the lowering of the energy levels of the adatom with increasing fields.

The predictions of Duke and Alferieff have been tested for various adsorbates on tungsten microtips. Measurement of the energy distributions for adsorbates including monolayer coverage of alkaline earth metals, hydrogen, oxygen, krypton and germanium has been reviewed by Gadzuk and Plummer[56] and agreement between theory and experiment is generally good. The results of these measurements are often presented in terms of an enhanced resonance factor R, defined as the ratio of the tunnelling probability of an electron through the barrier with atomic potential present with respect to the tunnelling probability with the atomic potential missing. Fig. 3.5, reported by Plummer and Young,[76] shows the experimental enhancement factor for single barium atoms adsorbed on the (111) plane of tungsten, where the shift of the 3D peak is induced by changing the field, such that the shift with field is given by $E/e\Delta F = 1.3 \pm 0.3A^{o}$.

The effect of polyatomic adsorbates on the F.E.E.D. has been investigated by Plummer and Bell[59] and by Swanson and Crouser,[77] who demonstrated that molecules are capable of inelastically scattering tunnelling electrons. The former authors used the high signal-to-noise ratio of an electrostatic deflection spectrometer/multichannel analyser combination to discover a set of very weak energy losses in the region of 0.55 eV, which were attributed to the field emission electron excitation of $W-H_2$ vibrational modes. In contrast, Swanson and Crouser[77] reported dramatic effects in the F.E.E.D. due to the adsorbtion of the large aromatic

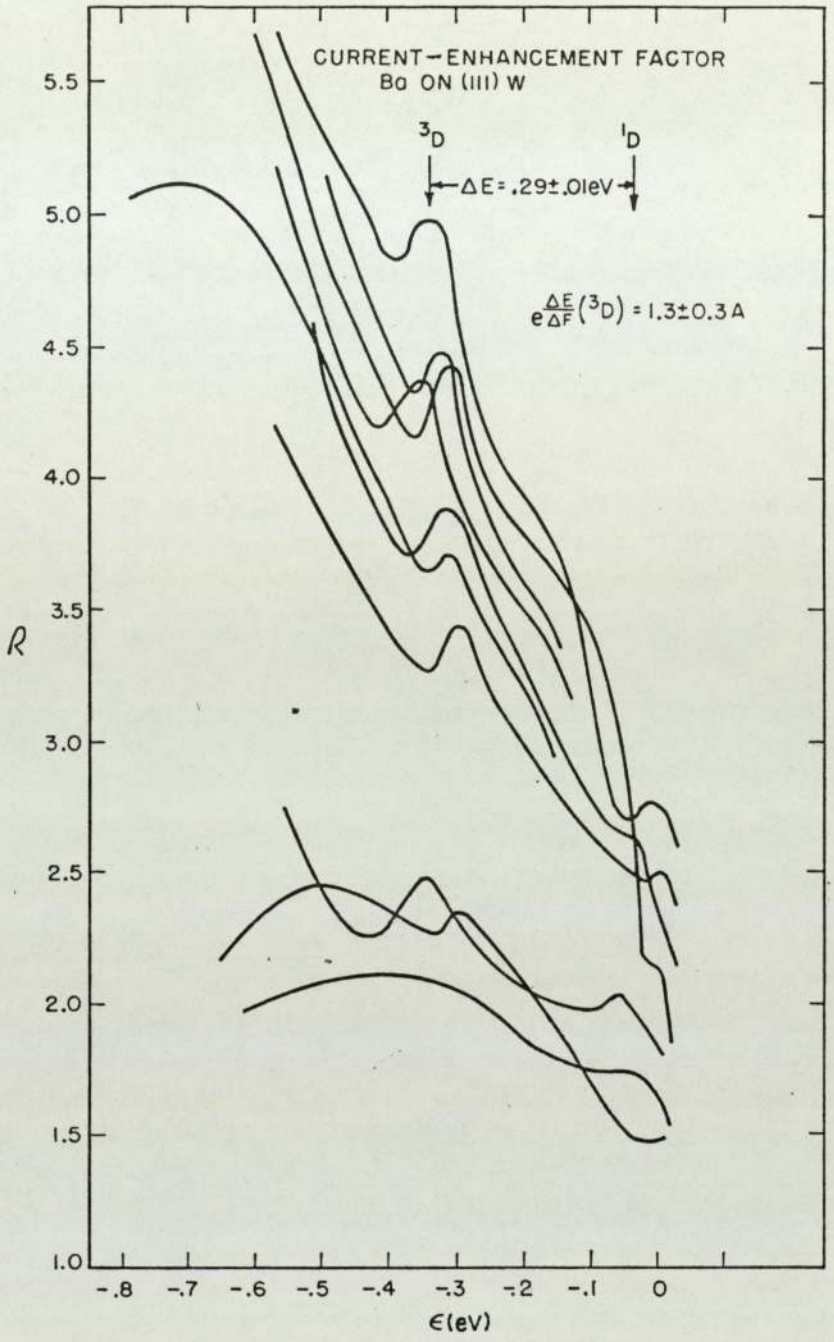

Fig. 3.5 Experimental enhancement factor for single Ba atoms on the (111) plane of tungsten. The three lower curves represent cases where adsorption of electronegative gases was observed before the Ba atom arrived. The shift in the narrow peaks with field was $\Delta E/e\Delta F$=1.3±0.3Å, while the peak separation was 0.29± 0.01eV .From Plummer & Young[76].

molecules, phthalocyanine, pentacene and anthracene on various faces of tungsten and molybedenum. Their hope was to interpret structure in the energy distributions as being due to either resonance tunnelling, inelastic vibrational excitation or inelastic electron excitation within the molecule. The criteria for placing a given peak in one of these categories was taken to be the degree of field dependence of the peak position. Since electron levels at an energy Ea shift with field, from their unperturbed level Eo, as $Ea = Eo - eFx$, $\Delta Ea/-e\,\Delta F = x$ should be of the order of the molecule-substrate separation if resonance tunnelling is the predominant mechanism. On the other hand vibrational levels shift very little with field, and no "a priori' rule can be given for electron excitation of a molecule.

In their investigation, Swanson and Crouser confined their interest to the F.E.E.D. obtained from those parts of the field emission pattern on the anode which are known to result from the adsorption of the molecule. The energy distributions for the molecules exhibited marked structure down to as much as 3eV below the Fermi level. Occasionally peaks above the Fermi level were seen, as in Fig. 3.6, in which a large peak is observed at 950meV above the Fermi level. The authors suggest an explanation for this result in terms of an Auger type mechanism in which the excited electronic state of the molecule is sufficiently long-lived (compared to the inter-electron tunnelling time) that a subsequent tunnelling electron stimulates the de-excitation energy in the process and appears above the Fermi level. A typical set of distributions for phthalocyanine on the (110) plane of molybedenum are shown in Fig. 3.7, with the inset

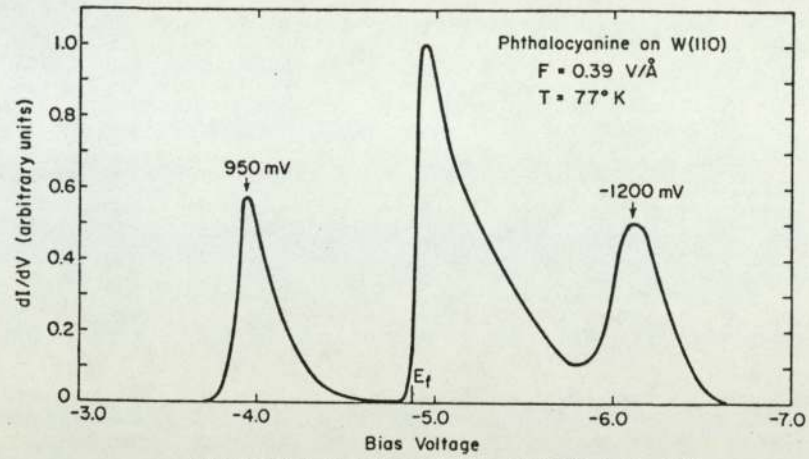

TED spectra phthalocyanine on W (110); $I_a/I_e = 540$.
Note the peak 950 mV above the Fermi level.

Fig. 3.6 From Swanson & Crouser[77]

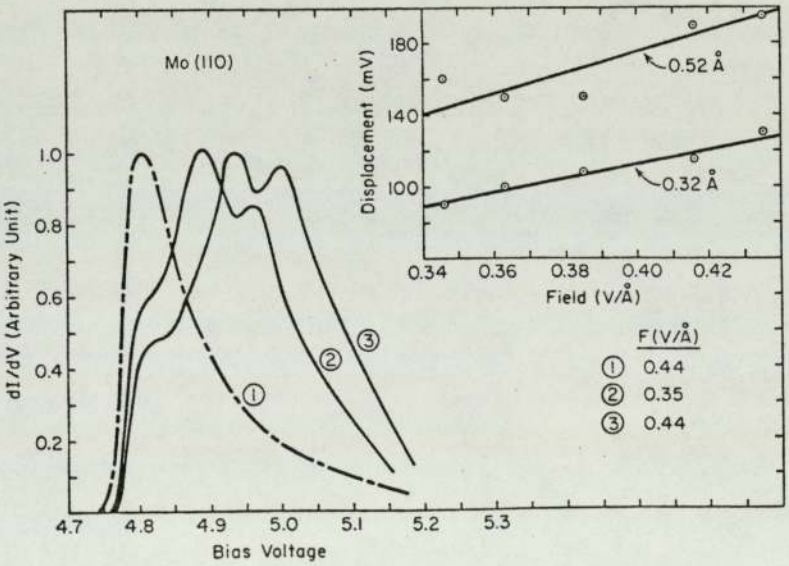

TED spectra for phthalocyanine on Mo (110); $I_a/I_e = 27$; curve 1 is clean TED.

Fig. 3.7 From Swanson & Crouser[77]

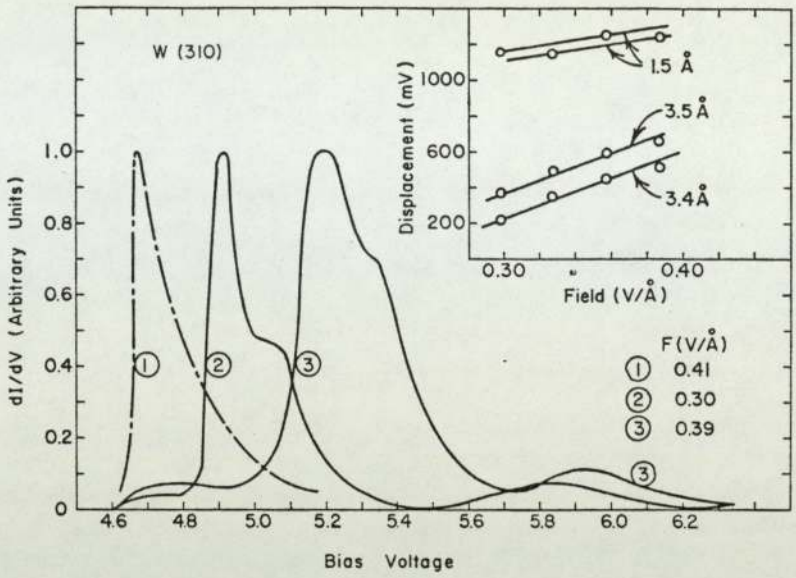

TED spectra pentacene on W (310); curve 1 is clean, $\Delta\phi = -1.7$ eV, $B = 2.0$; $I_a/I_e = 680$.

Fig. 3.8 From Swanson & Crouser[77]

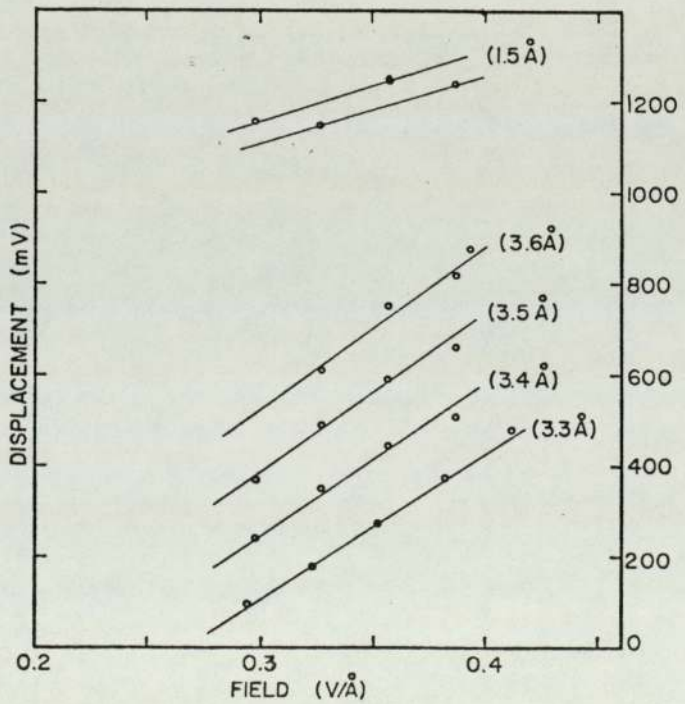

Summary of peak displacements versus field strength for pentacene on W (310); numbers in parenthesis are the slopes.

Fig. 3.9 From Swanson & Crouser[77]

showing the shifts of the peaks with field. Since a phthalocyanine molecule measures approximately 10A° by 10A°, the slope of the field effect is too small to be due to elastic resonance tunnelling, but is not inconsistent with a phonon excitation in the molecule. Typical results for pentacene molecules, which measure 4A° by 12A°, are reproduced in Fig. 3.8, and suggest that elastic resonance tunnelling plays a strong part, although energy losses due to electron-electron scattering are also believed to be important.

Swanson and Crouser report many F.E.E.D.s, such as those of Fig. 3.7 and 3.8, which are reproducible in the sense that all have dramatic structure, but are not reproducible in the sense that the position, relative peak heights and field shifts vary from run to run. A number of reasons are pointed out for this problem. The current in the probe hole of their analyser was very noisy and erratic due to thermally or field induced random steric changes in the adsorbate-substrate configuration which would also alter the energy distribution. Furthermore it was difficult to position the probe hole over a single molecular spot; thus two or more molecules with different steric configurations may have been contributing to the energy distribution. Also, the large number of combinations of inelastic and elastic tunnelling possibilities could interfere and couple in manners difficult to appreciate theoretically. However, it is worthy of note that all the measurements of the shift of the peaks in the energy distribution show a linear effect with field, as illustrated in Fig. 3.9.

3.4 Field Emission from Semiconductors

As discussed in Chapter 2.4 and 2.5 it appears that

insulating or semiconducting impurities may be involved in the electron emission process from broad area electrodes. Therefore, in order to fully discuss the electron energy distributions obtained from such electrodes, it is appropriate to first review the properties of field emission from semiconductors and, in particular, the aspects which are illustrated in the energy distributions. The theoretical treatment of the emission process is more complex than for metals due to a number of factors, in particular:

1) the more complicated energy band structure,
2) the presence of additional interband surface states,
3) the penetration of the external field into the semiconductor surface layer,
4) the potential dropped within the emitter due to its higher electrical resistance.

Stratton,[78, 79, 80] in a series of theoretical papers has considered the field emission of electrons from semiconductors. He assumed a FN type of barrier at the surface and modified the image force correction to allow for the dielectric constant of the material. Although he considered the effect of surface states on field penetration he did not allow for emission from these states. The general conclusions of Stratton's theory as pertaining to the F.E.E.D. can be realized by considering a model for the semiconductor surface and then discussing the effect of a gradually increasing externally applied field. At the surface of semiconductor there will generally exist a density of surface states within or overlapping with the bulk energy bands. These surface states are a consequence of the fact that the periodic lattice conditions which give

rise to the well defined energy bands will no longer be satisfied at the surface due to the termination of the crystal and re-arrangement of the lattice atoms. Then, since excess charge may be stored in these states, the resulting field gives rise to band bending which, in principle, may be in either direction depending on the exact nature and purity of the semiconductor and its surface.[81] As the external field is applied and increased, the behaviour of the F.E.E.D. will display a number of distinct phases, as illustrated in the series of Fig. 3.10:

Fig. 3.10(a) - When an external field is applied, charge will be induced into unoccupied surface states and if there is a sufficient density of these to accommodate the induced charge without significantly altering the position of the Fermi level, the external field will be effectively shielded. At this stage therefore field emission, if any, is expected to occur from the Boltzmann tail of electrons in the conduction band, or from the valence band, depending on such factors as the position of the Fermi level, the width of the band gap, and the density of states in the vanence band. In general, therefore, two peaks may be observed in the F.E.E.D., with the separation of the appropriate cut-off energies being equal to the forbidden energy gap of the semiconductor.

When the empty surface states density is no longer great enough to effectively peg the Fermi level at the surface, field penetration will occur, and the situations illustrated in Fig. 3.10(b), (c) and (d) may be considered:

Fig. 3.10(b) - If the field penetration is insufficient to lower the conduction band edge at the surface below the

Fermi-level, the F.E.E.D. will not be qualitatively different from the case of Fig. 3.10(a), however both peaks may be expected to move to lower energies with respect to the Fermi-level as the applied field is increased.

Fig. 3.10(c) - If the field penetration is sufficient for the conduction band edge to dip below the Fermi level, the conduction band will become degernate (i.e. electrons inside it will obey Fermi-Dirac statistics as opposed to Boltzmann statistics). The electron emission may be expected to become enhanced at this stage, with the F.E.E.D. yielding two peaks - one at the Fermi level and the other (possibly unobservably small) at just below the valence band edge. The peak at the Fermi level should be metallic-like and not shift with increasing applied field, although the valence band peak may move slightly to lower energies.

Fig. 3.10(d) - In general, when a field emission current flows through a semiconductor a voltage drop will occur within it with a consequent variation of the Fermi level. This is an ohmic effect and the voltage drop is directly proportional to the bulk resistance of the semiconductor. Therefore, in order to determine the position of the Fermi-level at the surface compared to the Fermi level of the contacting metal, which is amenable to experimental measurement, it is necessary to refer back to the contact. The additional band bending at the metal-semiconductor contact is defined by surface states in the semiconductor and work function differences between the two interfaces. Then the F.E.E.D. obtained for any of the cases illustrated in Fig. 3.10 (b), (c) (d) will include additional contributions to the shift from the measurable Fermi-level (that of the

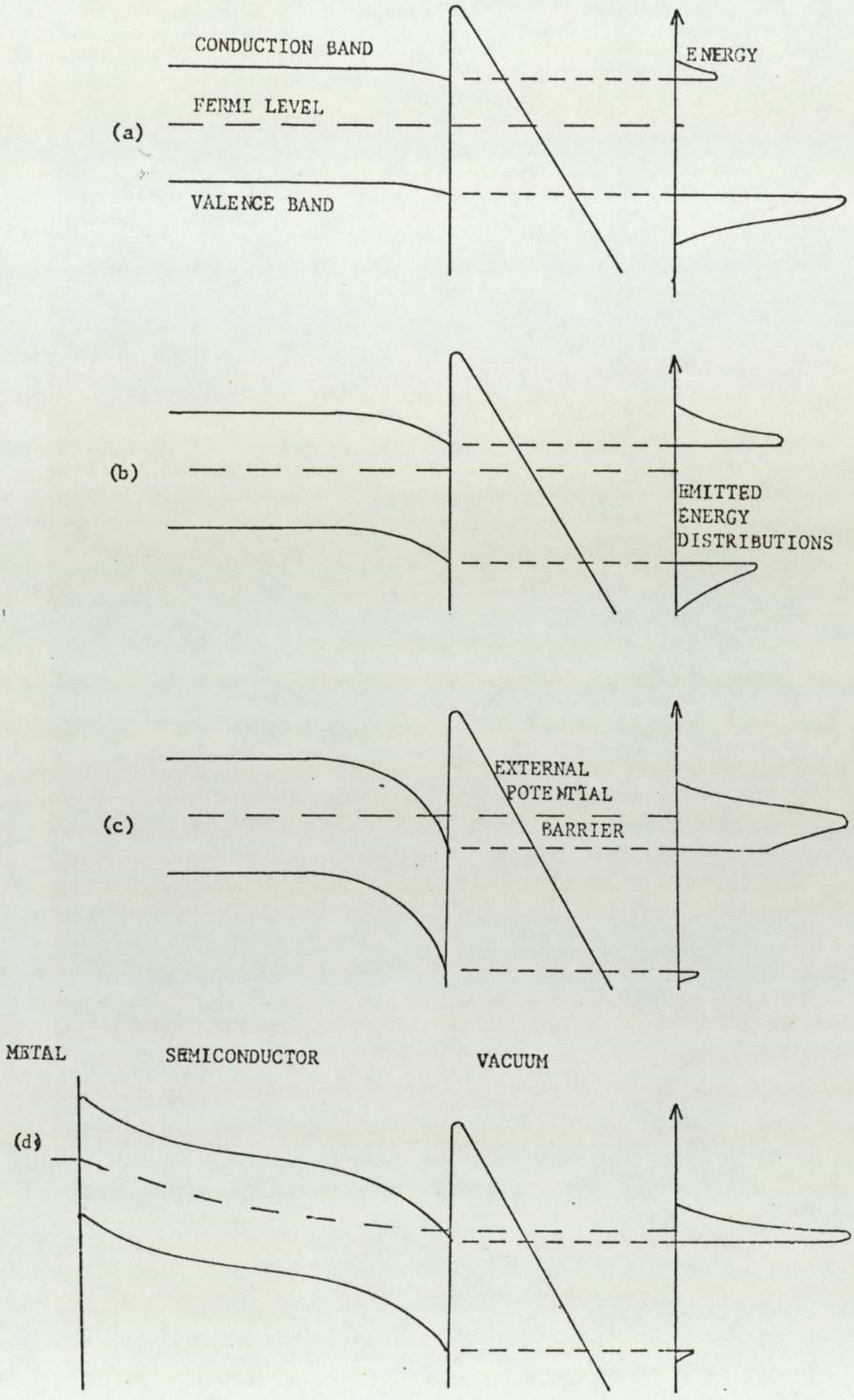

Fig. 3.10: Stages in the FEED from an idealised semiconductor as the applied field is gradually increased.

contacting metal) due to the bulk resistivity and the metal-semiconductor barrier.

It must, however, be borne in mind that every semiconductor should not be expected to exhibit all the phenomena illustrated in Fig. 3.10(b) to (d), since, for instance, the applied field may be high enough to saturate the surface states before reaching the value required for field emission.

Stratton[78, 79] has also deduced the form of the current-voltage characteristics to be expected from his model. In general the theory predicts that at low fields the emission will predominantly occur from the valence band (Fig. 3.10(a)) and at high fields from the conduction band (Fig. 3.10(c)), both situations producing essentially linear FN plots. In the transition region (Fig. 3.10(b)), the current will increase more rapidly with field as the conduction band population increases. Agreement between Stratton's theory and experimental measurements of the current-voltage characteristics was poor a feature which led Baskin et.al.[82] to consider the problem in more detail and explain the saturation region observed in the mid-current range where Stratton had predicted a pronounced increase in the current. By considering the electron flow within the semiconductor they showed that the emission current could be restricted by the inability of sufficient carriers to arrive at the surface, either due to a weakly conducting depletion region just within the surface for p-type semiconductors, or because an n-type specimen would be unable to generate enough carriers in the bulk. However, they did not discuss the effects of electron injection at the metal-

semiconductor junction. Numerical calculations based on their expressions showed qualitative agreement with observed effects, although the saturation currents were smaller than experimental values.

Experimental studies of the F.E.E.D. from semiconductors, such as the work of Arthur[83] on germanium, Hughes and White[84] on gallium arsenide, Salmon and Braun[85] on cadmium sulphide and Lewis and Fischer[86] on silicon, have shown that the observed distributions are wider and different in shape from the predictions of Stratton's theory for valence band and conduction band emission. This led Modinos[87] to propose a theory which includes emission from surface states. His model (see Fig. 3.11) was primarily concerned with germanium, but he suggests that in a qualitative way his results could provide a basis for understanding the observed F.E.E.D. from semiconductors in general. The basis of the theory is a model for the semiconductor surface originally put forward by Handler,[88] in which it is assumed that a uniformly dense band of surface states exists which ranges in energy from within the valence band to above the conduction band edge. By applying a FN barrier to the resulting density of states function, expressions for the emission current density, and hence the energy distribution, are derived. However, these expressions include two unknown parameters, viz the shift (Vs) of the electrostatic potential at the surface relative to its bulk value, and the quasi-Fermi level (Fq) at the surface appropriate to a given applied field. Since Vs and Fq can be related by solving the electrostatic Poisson equation at the surface, and an additional equation obtained by

considering the replenishment of the surface states from the conduction and valence bands, the unknown parameters can be eliminated and the energy distribution calculated from known (and assumed) properties of the bulk semiconductor and its surface.

Modinos calculated the F.E.E.D. corresponding to p-type, intrinsic and n-type germanium at 300K for three different values of external field. The distributions for the intrinsic material are shown in Fig. 3.12; the F.E.E.D. from the two types of extrinsic material are practically the same as this case, with respect to the Fermi-level, although the valence band edge is at different position for each of them. The theory predicts that at low current densities ($< 10^{6} Am^{-2}$) most of the electrons are emitted from surface states and the valence band. As a consequence of variations of Vs and Fq with applied field, the energy distribution shifts away from the Fermi level towards lower energies for increasing field; at the same time the relative amplitude of the emission from the valence band increases. The contribution to the emission current from the conduction band also increases with field, but it is not expected to be observable in a linear F.E.E.D. for current densities of $\sim 10^{7} Am^{-2}$. At even higher currents the conduction band becomes degenerate and the theory in its present form is no longer applicable.

Modinos compared his theory with the experimental work of Arthur[83] and Shepherd and Peria[89] on germanium, and found reasonable agreement. Subsequently his theory has been successfully applied to explain the F.E.E.D. from lead telluride by Sykes and Braun[90] and zinc oxide by Rihon.[91]

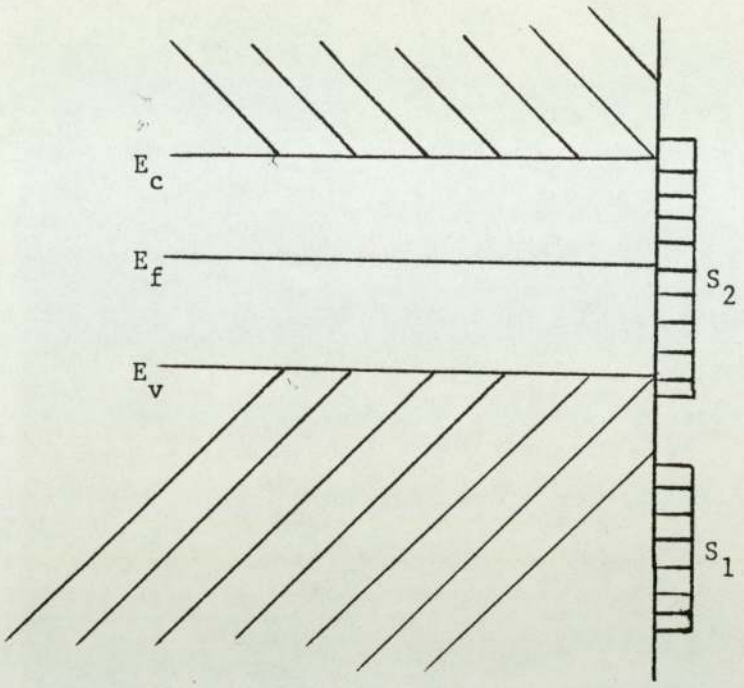

Fig. 3.11 Surface states of Ge according to Handler's model[88]

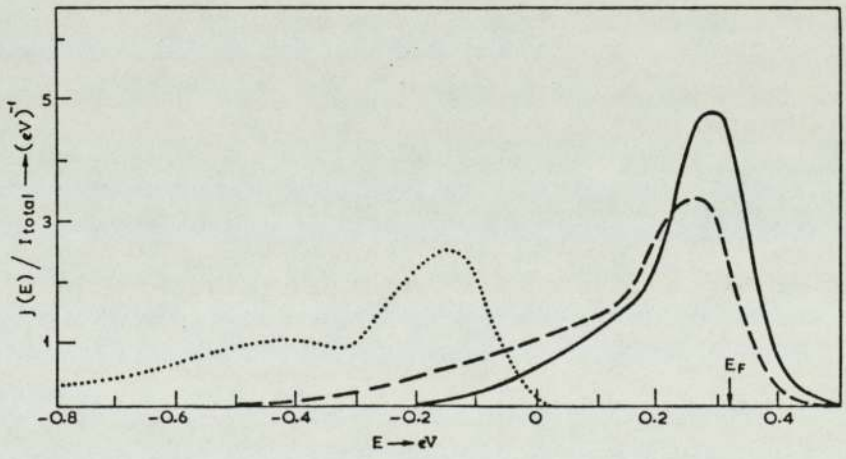

Total energy distributions for $u_b = 0$. The parameters are those of table 2.
Solid line: $F = 0.2$ V/Å, $V_s = -10\,kT$, $E_F - F_t < kT$, $I_c = 1.9 \times 10^{-12}$ A cm^{-2}, $I_s = 1.75 \times$ $\times 10^{-3}$ A cm^{-2}, $I_v = 9.98 \times 10^{-4}$ A cm^{-2}, log $I_{total} = -2.56$.

Broken line: $F = 0.3$ V/Å, $V_s = -7.5\,kT$, $E_F - F_t < kT$, $I_c = 1.36 \times 10^{-8}$ A cm^{-2}, $I_s =$ $= 9.14$ A cm^{-2}, $I_v = 7.04$ A cm^{-2}. log $I_{total} = 1.21$.

Dotted line: $F = 0.4$ V/Å, $V_s = 10\,kT$, $E_F - F_t = 16.25\,kT$, $I_c = 13.15$ A cm^{-2}, $I_s = 6.98 \times$ $\times 10^2$ A cm^{-2}, $I_v = 6.98 \times 10^2$ A cm^{-2}, log $I_{total} = 3.15$.

Fig. 3.12 The theoretical F.E.E.D. from intrinsic Ge for three values of applied field. From Modinos[87]

However, these authors did not measure significant increases of the shift of the distribution from the Fermi level with applied field. This is possibly because they did not attain sufficiently high current densities.

3.5 Emission from Broad Area Electrodes

The first measurement of the F.E.E.D. from a broad area electrode under ultra high vacuum conditions was made by Allen and Latham,[43] using a copper cathode and the high resolution electron spectrometer to be described in the next chapter. Their basic finding is illustrated in Fig. 3.13, and from this they were able to identify three important differences in the typical spectra obtained from sites on a broad area copper electrode compared to that from a reference tungsten microtip emitter: (i) all the electrons are emitted from states well below the Fermi level, (ii) the half-width is greater, and (iii) the shape of the spectrum is more symmetrical, i.e. lacking the characteristic sharp high energy edge of metallic F.E.E.D.s. In fact, the energy distribution from sites on the broad area electrode resembles that from semiconducting tips. In subsequent reports Latham and co-workers,[92, 93] measured a similar energy distribution from sites on stainless steel and a double-peaked spectrum from a titanium electrode. Furthermore they developed a model to explain their results, based on the concept of a very localised semiconducting impurity embedded in the electrode surface. This model and others are considered in detail in Chapter 7.

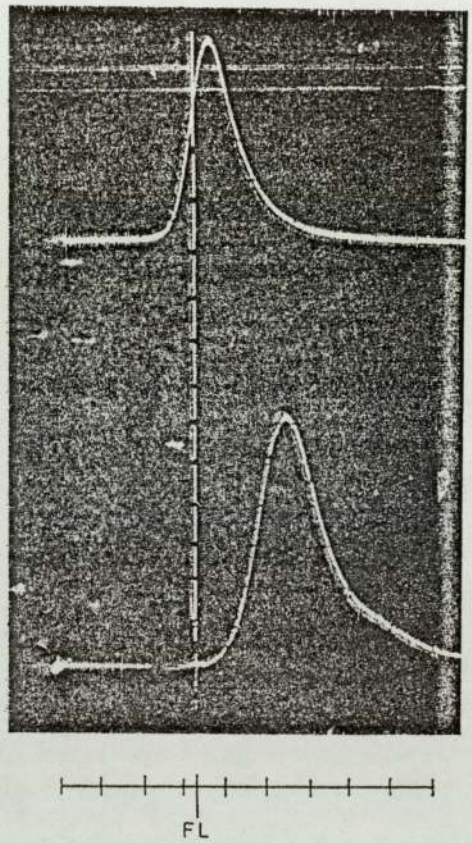

Fig 3.13 Electron energy spectrum obtained from (i) a reference tungsten emitter and (ii) a site on a broad-area copper cathode. The position of the Fermi level (FL) of each emitter is also shown. Electron energy in eV, 0·2 eV/div, is x axis (going from high energy to low energy left to right). Electron current per unit energy is y axis.

From Allen & Latham[43].

CHAPTER 4

AN ELECTRON SPECTROMETER FOR STUDYING THE EMISSION FROM BROAD-AREA ELECTRODES

4.1 Choice of Spectrometer

There have been two main types of spectrometer used to study field emission electron energy distributions; viz. the retarding potential analyser and the electrostatic deflection analyser. For this investigation the latter type was chosen as being the most suitable; however, in order to appreciate the reasons for this choice it is necessary to briefly consider the operating principles of the retarding potential analyser and the reasons why it has been largely superseded.

The most popular design for the retarding potential analyser is that due to van Oostrom;[94] where for the purposes of this discussion a simplified version of which is illustrated in Fig. 4.1. In order to create the necessary high field ($\gtrsim 10^{9} Vm^{-1}$) for field emission, whilst using a reasonable accelerating potential (0.5 - 4kV), the emitter is normally in the form of a thin wire with a sharply etched tip having an end radius $\sim$100nm. The emitted electrons are then retarded, by the lens L, to an energy of a few eV. If a slowly increasing voltage is now applied at the collector C, the electrons will be collected, the most energtic at the lower voltage. Fig. 4.2 shows a typical plot of the collector current versus the collector voltage, and this curve may be differentiated either manually or electronically to obtain the distribution of energies in the electron current.

The detection system of a retarding potential analyser suffers from a number of drawbacks. Firstly, reference

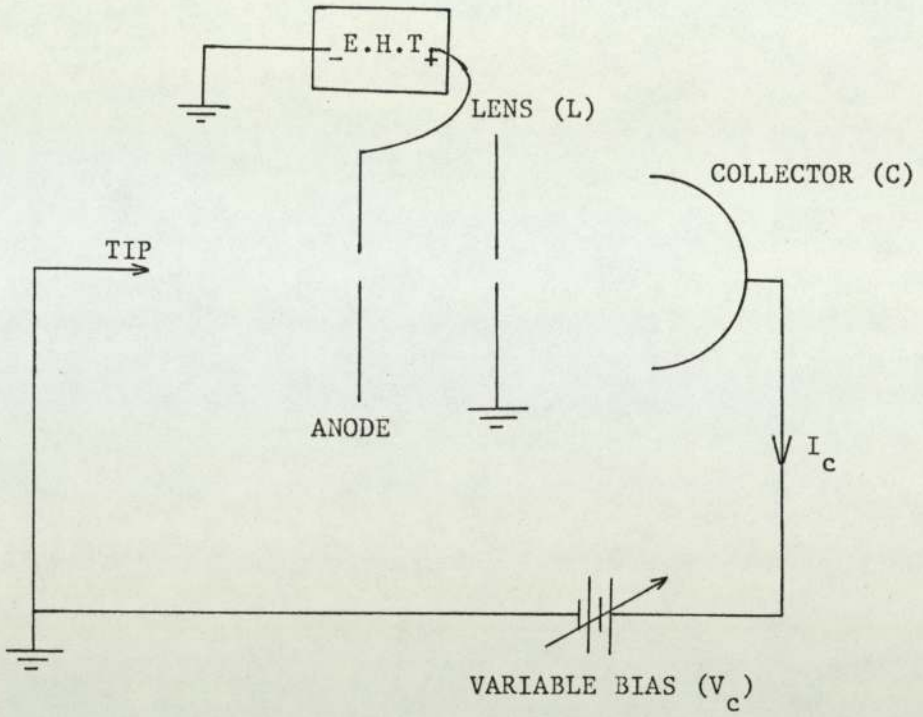

Fig. 4.1 Schematic representation of the essential features of a retarding potential analyser.

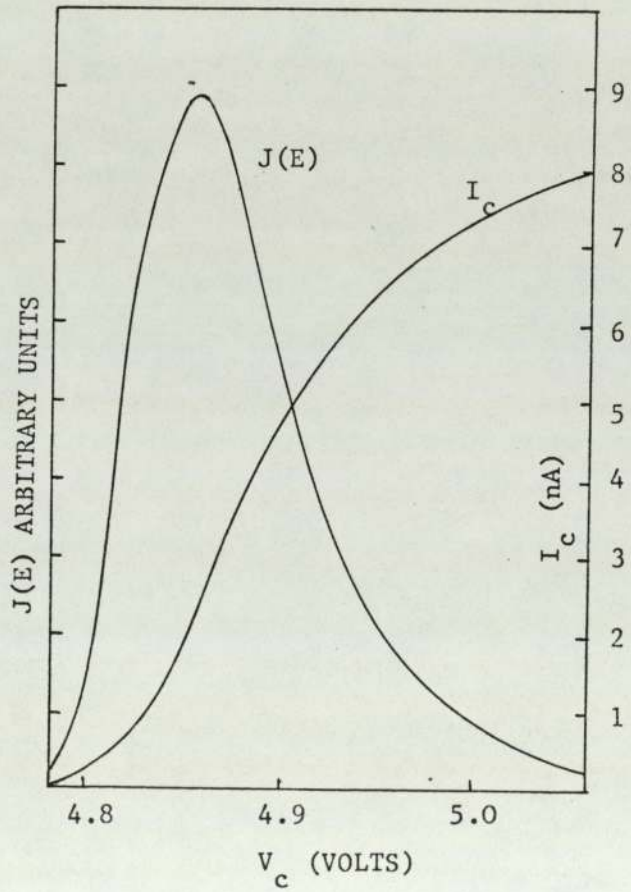

Fig. 4.2 Plot of integral current curve, I_c, obtained from a retarding potential analyser, and corresponding differential curve J(E) both plotted as a function of retarding voltage V_c.

to Fig. 4.2 shows that at the low energy end of the integral curve (higher values of V_c) there is only a relatively small increase in Ic, which results in a poor signal to noise ratio. In addition this shallow slope makes differentiation of the curve subject to greater error. Further, current detection at the collector is usually by means of an electrometer which gives rather limited sensitivity. For measuring energy distributions having typically $\sim$ 200meV half-widths, an instrumental resolution of $\sim$ 20meV is desirable, which means that for an electron beam arriving at the anode with an average energy of 2keV, the overall resolving power requirement is $\sim 10^5$. The retarding potential spectrometer can achieve this resolution near the peak of the distribution, but it cannot give a comparable resolution at the low energy tail. Since this part of the spectrum is very important in the study of many field emission phenomena, the retarding potential analyser is limited in its application.

In contrast the deflection analyser to be described below has a resolution of 30meV throughout the energy range, a direct energy distribution output from an electron multiplier which greatly increases sensitivity, as well as comprehensive output facilities in terms of gain, filtering and spectrum scan speed. For these reasons a hemispherical deflection analyser was chosen for the measurements described in this investigation.

The first electrostatic deflection spectrometer adapted for measuring F.E.E.D. was reported by Kuyatt and Plummer[95] who designed an instrument based on a 135^o deflection analyser formed from concentric spheroids of 25mm mean

radius. The instrument established in the Aston Field Emission Laboratory follows the general principles of the system developed by these authors, but exploits both the theoretical and operational advantages of using an analysing element consisting of hemispheres having a larger mean radius of 50mm with a 180^{o} deflection element. Such a system also requires a less complicated electron optical design for its input and output lenses, with a much simplified but more versatile electronic drive system. The design of this instrument and its performance for measuring the F.E.E.D. from tungsten microtips has been reported by Braun et. al.[96] Subsequently the spectrometer was modified by Allen and Latham[43] to enable the measurement of the energy spectra of electrons field emitted from broad area electrodes. Since the bulk of the results reported in this thesis were obtained from this apparatus, the principles of the spectrometer and its adaption to the particular case of broad area electrodes are discussed in some detail in the following sections.

4.2 The Principle of the Deflection Analyser

The actual analysing element consists of two concentric hemispheres as illustrated in Fig. 4.3, with a voltage difference ΔV across them. Incoming electrons have to be focussed onto the entrance aperture B; then by choosing a given value of ΔV the analyser is set to pass electrons with a kinetic energy very close to some specified value E, which traverse the analyser paraxially to be focussed onto the exit aperture C. The analyser has a certain pass-width ΔE so that electrons with kinetic energy outside the range $E \pm \Delta E$ collide with the hemispheres and are

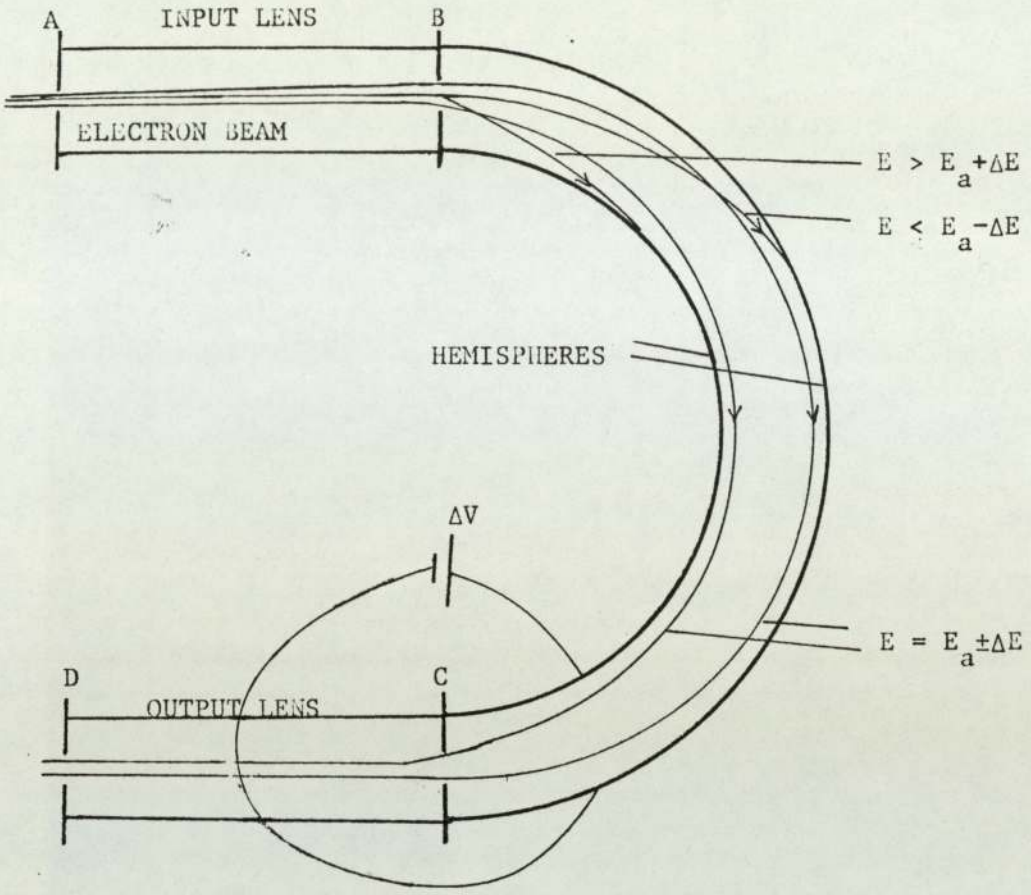

Fig. 4.3 The Principle of the Hemispherical Deflection Analyser.

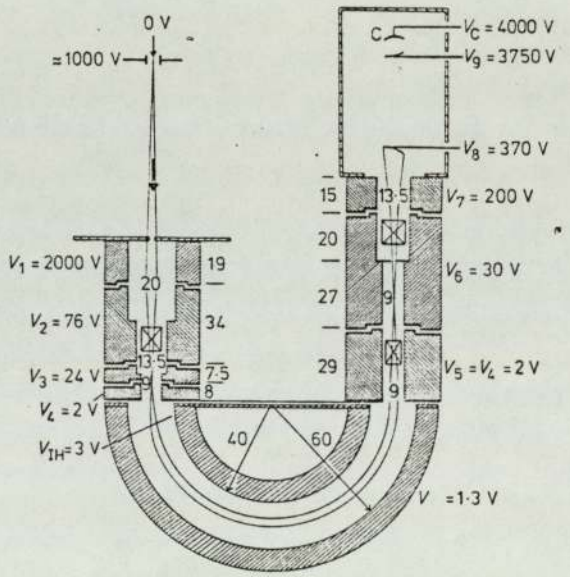

Essential features of the electron optical system. Lengths and internal diameters are shown to the nearest 0·5 mm. Deflector plates are contained in elements 2, 5 and 6. Also shown is a set of experimental operating voltages appropriate to an analysing energy of 2 eV; the voltages are given relative to a hypothetical stainless steel electrode outside whose surface the transmitted electrons would just come to rest. V_8 and V_9 are the voltages on the first and last dynodes of the electron multiplier and V_C is the voltage on its collector C.

Fig. 4.4 The design features of the unmodified electron spectrometer; from Braun et al.[96].

either trapped by them or emerge diffusly from aperture C. Now by varying (ramping) the voltage at B, the part of the energy distribution having the correct energy E for transmission will, in turn, vary; in effect, an energy window (ΔE) will scan the distribution. If this ramp voltage is simultaneously applied to the X axis of a graph plotter or oscilloscope, and the current emerging from the analyser to the Y axis, the electron energy distribution is obtained directly.

For faithful reproduction of the distribution, one requires a small pass-width (ΔE). Since this is linearly related to the pass energy E, it follows that for good resolution ($\Delta E \leqslant$ 20meV), the kinetic energy of the electrons entering aperture B must be relatively small ($\sim$ 2eV). However, to extract electrons from a fabricated microtip emitter a potential difference of $\sim$2kV is generally necessary whilst for small gaps with plane-parallel broad area electrodes the required potential difference may be as high as 10kV. Therefore, an input lens system is required firstly to retard the electrons near to the analysing energy and secondly to focus an image of aperture A onto B (see Fig. 4.3). The function of the output lens assembly is to accelerate the beam emerging from aperture C and to focus it onto a further aperture D, thus scattered electrons emerging from C should not get through D in any significant numbers. Finally, electrons passing through D are accelerated into the collector, which is usually an electron multiplier.

4.3 Design Considerations for the Analysing Element

The hemispherical deflection element forms the heart

of the spectrometer and the theory for this type of deflector was first given by Purcell.[97] He showed that electrons which are focussed on the entrance aperture and have the correct energy will travel in great circles between the spheres and be focussed at an exit aperture which makes an angle of 180° with the entrance aperture. The design considerations for a practical hemispherical analyser have been given by Kuyatt and Plummer[95] and are as follows:

1) An electron will be confined to execute circular motion in the mid-plane (radius Ro) if:

$$\frac{m\,v^2}{Ro} = (-e)\,(-Fo)$$

where m = electron mass

v = electron velocity

Fo = the radial electric field at Ro

By considering the electrostatic potentials immediately outside the heimspheres and at the mid-point, the potential difference ΔV across the hemispheres and the voltage at each hemisphere, V_1 and V_2, can be derived in terms of the analysing energy E and the radii, R_1 and R_2, of the internal and external hemispheres respectively.

$$\Delta V = \frac{E}{e}\left[\frac{R_2}{R_1} - \frac{R_1}{R_2}\right] \qquad 4.1$$

$$V_1 = \frac{E}{e}\left[\frac{R_2}{R_1} - 1\right] \qquad 4.2$$

$$V_2 = \frac{E}{e}\left[\frac{R_1}{R_2} - 1\right] \qquad 4.3$$

2) The resolution of the hemispherical analysing element is given by

$$\frac{\Delta E}{E} = \frac{Z}{2Ro} + \frac{1}{2}\alpha^2 \qquad 4.4$$

where Z is the input and output slit width (assumed equal) and α is the angular spread of the beam. In order to minimise broadening of the hemisphere transmission function, it is usual to design the input lens so that $\alpha^2 = \frac{Z}{4Ro}$ and then equation 4.4 becomes,

$$\frac{\Delta E}{E} = \frac{5}{8}\frac{Z}{Ro} \qquad 4.5$$

3) The maximum deviation Zm of a transmitted beam, from the central path of radius Ro is given by

$$\frac{Zm}{Ro} = \frac{\Delta E}{E} + \left[\alpha^2 + \left(\frac{Z}{Ro} + \frac{E}{E}\right)^2\right]^{\frac{1}{2}} \qquad 4.6$$

It is clear that to obtain the best resolution requires the smallest pass-width at a given analysing energy. Thus from equation 4.4 it is necessary for E, Z and α to be small and Ro large. There is a limitation on the minimum value of E, since very low energy electrons can be difficult to control due to the increasing importance of stray magnetic fields and the variation in the surface potential of the hemispheres.(98) Decreasing the size of the apertues improves resolution, but, on the other hand, reduces transmission and so consideration of the minimum detectable current puts a lower limit on this factor.

In the instrument used for the present experiments an analysing energy of 2eV was chosen as a reasonable compromise of the factors discussed. Then in order to obtain a resolution of $\sim$ 25meV for a 2eV analysing energy, and using equation 4.5, apertures (Z) of 1mm and a mean radius (Ro) of 50mm were found to be appropriate. Substituting these

values into equation 4.6, the maximum deviation of the beam (Zm) is found to be ∿ 5mm. Hence in order to accommodate this and allow some flexibility in the input conditions, R_1 and R_2 were set to 40mm and 60mm respectively. Now the voltages for the hemispheres are obtained by substitution into equations 4.1, 4.2 and 4.3 which leads to

$$\Delta V = 1.67 \text{ volts}$$

$$V_1 = 1.0 \text{ volt}$$

$$V_2 = -0.67 \text{ volts}$$

To eliminate the effects of stray magnetic fields a mu-metal shield surrounds the analyser and it has been shown by Pearson[99] that no detectable change in the energy spectrum is obtained by adding further shielding by means of Helmholtz coils.

4.4 The Input and Output Lenses

The input lens system of the spectrometer has to fulfil the following criteria:

1) To decelerate the electrons from an energy of ∿ 2keV at the anode to 2eV at L_4,

2) To focus the beam of electrons onto the entrance apperture of the analyser with a small angular divergence,

3) To be capable of operating over a range of input energies (1 to 4keV) and a range of analysing energies (1 to 18eV).

To satisfy these criteria a system was adopted that comprised a three element lens designed in accordance with the method described by Heddle et. al.[100] followed by a fixed ratio lens. The component lenses have different diameters so that the lens elements are of reasonable length, varying between 9 and 20mm, the total length being 70mm. X-y deflector plates are also contained within one of the lens

elements for fine beam steering.

The function of the output lens system is to re-accelerate the electron beam leaving the hemispheres and at the same time to collimate it into the electron multiplier. The electrons impinge diffusely at 200eV onto the first dynode of the electron multiplier, which is a Twentieth Century EP25 model with a quoted gain of 2.5×10^5.

Thus the complete design of the electron optical system of the spectrometer is as illustrated in Fig. 4.4.

4.5 The Electrical and Electronic Systems

The electronic control system for the analyser comprises two E.H.T. supplies (one for the lenses and the other for the electron multiplier) a battery supply for the hemisphere voltages, a ramp generator for scanning, and amplifiers to handle the output from the multiplier. Spectra are usually displayed on a storage oscilloscope, but there is also provision for the use of a X-Y recorder. The layout of the various units is shown in Fig. 4.5. The lens voltages (except L7) are supplied from a single power unit by means of a 2M Ω dropping resistor chain. This arrangement has the advantage that the lens voltage ratios are independent of the magnitude of the anode voltage V_1 , so that the focussing properties of the lenses are largely unaffected by changes in V_1 over the operating range of the instrument from 1-4kV. A wide range of individual voltage adjustments is available for all the lens elements and for the internal deflector plates. In-line jack plugs are also provided on the resistor chain for measurement of lens voltages and currents. The voltage

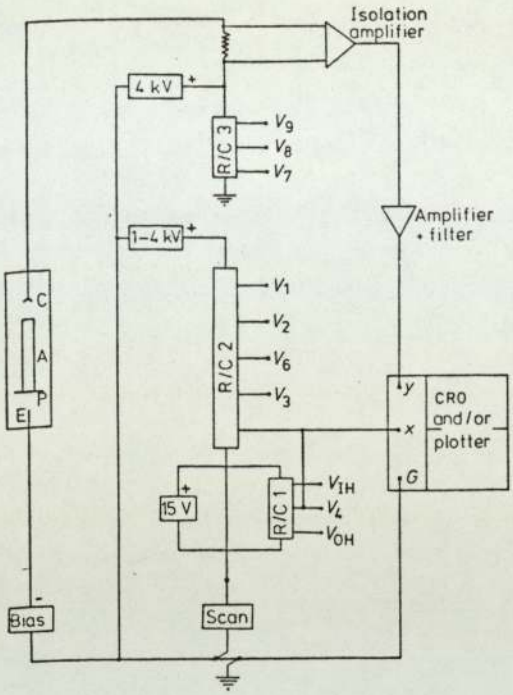

Fig 4.5 Voltage supply arrangements. Supplies for the beam deflector plates (not shown) are taken from a separate resistor chain.

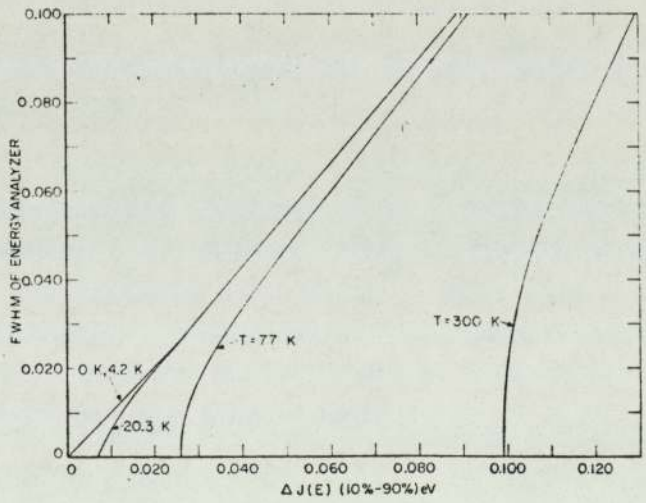

FWHM of energy analyzer as determined from the high energy edge of its measured E.D. at various temperatures: FWHM vs measured energy difference between the 10 and the 90% points on the E.D. leading edge. φ and F—same as above. Note that temperatures considerably below 300 K are needed for meaningful resolution determination.

Fig. 4.6 From Young & Kuyatt[101].

applied between the hemispheres can be varied to accommodate a range of analysing energies from 2 to 18eV. The former is required for high resolution (as discussed earlier) whereas the latter offers a greater output signal at low resolution for the initial beam alignment procedure. Separate adjustments are also provided for setting each hemisphere voltage relative to the hemisphere "mid-potential" V_4.

A versatile, purpose-built ramp generator is used for energy scanning. It provides a switched energy scan of 1, 2, 5 or 10V, the starting voltage of the scan is adjustable such that V_4 may be scanned through any of these ranges between 0 and 20V. The scan time is continuously adjustable between 10ms and 100s, and there is also a facility for manual scan.

4.6 Energy Scanning

The method adopted for energy scanning is to sweep the voltage V_4, applied to the input and output lens elements at either end of the hemispherical deflector, by applying the output from the ramp generator to the lower end of the input lens supply resistor chain. This sweeps the hemisphere "mid-potential" whilst leaving the voltage difference between the hemispheres (and hence the resolution) unchanged throughout the scan. The anode voltage V_1 is also unaffected so there is no interference with the emission process. Although the other lens voltages vary slightly this has negligible effect on the lens focussing properties, especially when the scan width is reduced for high resolution work.

In terms of electron energy, this scanning method amounts to a simultaneous adjustment of the potential energy of every electron entering the hemispheres. At different points in the scan, electrons from each part of the initial kinetic energy distribution will have their kinetic energies adjusted by this process to be equal to the fixed anlysing energy of the spectrometer (determined solely by the dimensions and voltages of the hemispheres as in equations 4.1 to 4.3). A representative number of electrons from all parts of the distribution will thus pass through the hemispherical deflector at the appropriate values of V_4.

The output signal from the electron multiplier is floating at 4kV and is brought to ground potential by an isolation amplifier (Analog Devices type 273K). The signal is then fed to a variable gain (5 to 5000) purpose-built amplifier, and then through a low-pass filter (time constant variable between 10ms and 100ms) which is used on slow scanning to reduce mains hum and spurious noise, to the Y axis of a storage oscilloscope; the X input being derived directly from the ramp generator.

4.7 Spectrometer Performance

1) Resolution: A criterion for determining the resolution of field emission energy spectra has been established by Young and Kuyatt.[101] They assume that an energy analyser has a Gaussian transmission function given by

$$G(E) = \frac{0.939438}{\Delta E} \exp\left\{-\frac{2.772588}{(\Delta E)^2} E^2\right\}$$

where ΔE is the full width at half maximum of the transmission function. Then the effect of the analyser on the field-emission energy distribution $P(E)dE$ (equation 3.1)

is given by the convolution

$$J(E) = \int P(E_1)\, G\,(E_1 - E)\, d\, E_1$$

Since the high energy edge of a F.E.E.D. is particularly sensitive to variation in the FWHM (ΔE) of the spectrometer transmission function, the difference in energy ($\Delta J(E)$) between the 10% and 90% of this edge was chosen as a pertinent parameter in defining the resolution of the spectrometer. Fig. 4.6 shows the calculated variation of $\Delta J(E)$ with ΔE, at different temperatures.

The method of Young and Kuyatt presupposes that a tungsten emitter can be regarded as an ideal metallic field emission electron source having a well calibrated and readily reproducible energy distribution. In fact, Braun et.al.[96] showed that the high-energy slope is critically dependent on the surface contamination of the emitter, and they only obtained an energy distribution close to the theoretical value after extensive cleaning of their specimen by field desorption. They report a high energy slope width of 0.11eV, compared with the theoretical value of 0.10eV, which using Fig. 4.6 leads to an upper limit of 50meV for the analyser FWHM. However from other considerations, such as the displacement of the peak (15meV) they concluded that the actual resolution of the unmodified analyser is probably better than 30meV.

2) Calibration: When a metal is earthed an electron at the Fermi level is taken to have zero potential energy. Therefore an electron at rest outside a metal surface will have an energy equal to the work function of the metal, and an electron having the analysing kinetic energy (Ea) will have a total energy of Ea + ϕ, where ϕ is the work

function of the material of the hemispheres. Then the condition for an electron field emitted at the Fermi level to be transmitted by the analysing element becomes

$$e V_4 = Ea + \emptyset$$

where V_4 is the scan voltage and also the mid-potential of the hemispheres. Thus if the position of the Fermi level can be identified on an energy distribution, the corresponding value of V_4 may be used in the above equation to find $\emptyset$, For the case of a room temperature tungsten distribution, Young[57] has calculated that the Fermi level occurs at a point 73% up the high energy slope. Accordingly $\emptyset$ has been measured to be 4.26 ± 0.03 eV.[96]

For any other earthed emitter, the position of the Fermi level on its resulting energy distribution, obtained with identical analysing conditions (i.e. $\Delta VH = 1.67V$) will occur at the same value of V_4 used to calculate $\emptyset$. This is because V_4 is only a function of the analyser parameters and not of the emitter.

4.8 Modifications for Broad Area Measurements

The spectrometer was originally developed by Braun et.al.[96] for fundamental field electron emission studies using laboratory fabricated micropoint emitters. The experimental arrangement for this type of measurement is illustrated in Fig. 4.7(a), where C_1 is the micropoint cathode situated a distance d (typically 4-5cm) in front of a phosphor-coated planar anode A_1 which has a 1mm diameter central probe hole L_1. In contrast, to obtain electron emission from localised sites on broad area electrodes it is generally necessary to have macroscopic gap fields in the range 1-2 x 10^7 Vm^{-1}, corresponding, for

example, to 5 - 10kV applied across a 0.5mm plane-parallel electrode gap. Accordingly in applying this basic spectrometer module to the analysis of the emission from this type of specimen, it is not sufficient to simply substitute a planar cathode for the micropoint cathode in Fig. 4.7(a) since firstly, the electric field distribution is quite different in each case and secondly the maximum voltage of 5kV that can be applied to A_1 (i.e. the maximum analysing energy of the complete instrument) will be too low to provide the required gap field. In addition the electron site has to be first located opposite a probe hole. Allen and Latham[43] approached these problems by a) designing a suitable interfacing lens to establish the "test gap" and b) constructing a manipulator stage to permit the necessary alignment and movement of the broad area specimen when initially locating an emission site on the surface.

1) The interfacing lens: The two functions of this lens are (i) to decelerate the electrons leaving L_2 from a typical energy of ~8keV to ~2keV at A_1, and (ii) to focus them in an approximately parallel beam at L_1. A suitable lens was designed using an empirical trial-and-error approach based on a graphical field plotting procedure. The constructional details are shown in Fig. 4.7(b), whilst Fig. 4.7(c) is an enlarged section showing the geometry of the planar specimen cathode, the anode aperture and the interfacing lens element. The associated equipotentials and electron tragectories are also shown in this Fig., which illustrates how paraxial emission is formed into an approximately parallel beam for injection into the spectrometer at L_1; it is also worthy of note that the equipotent-

ials show that the field at the surface of the specimen opposite the probe hole is not significantly perturbed from its value elsewhere in the gap. To accommodate a range of electron energies between say 5 - 10keV emerging from L_2, some adjustment to the focus of the interfacing lens is provided by varying the voltage on the second lens element L_2 (connected to A_1) within the range 1 - 3 kV which corresponds to the acceptable input requirements of the spectrometer.

A photograph of the spectrometer with the interfacing lens fitted is presented in Fig. 4.8.

2) Precision manipulator and scan facility: For systematically examining all regions of the planar specimen cathode C_2 for emission sites, it is necessary to incorporate an external specimen manipulating stage capable of scanning C_2 in a rastor pattern in a plane that is accurately parallel to that of the planar anode. The design criteria for this unit were:

(i) horizontal and vertical movement of at least 14mm to accommodate the full dimensions of the specimen

(ii) manipulation for aligning the specimen surface parallel to the anode and ensuring it remains so orientated during scanning

(iii) manipulation to vary the interelectrode gap.

The general layout of the complete experimental facility, showing the physical relation of this unit to the spectrometer, is illustrated schematically in Fig. 4.9. As will be seen, the mechanical manipulating system is mounted outside the vacuum chamber and has a single control rod R passing through a stainless steel bellows

with the specimen holder assembly attached to its lower end. The manipulator itself is built up from "Microcontrol" type MR translation stages having 25mm of travel in each direction, whilst the bellows is a Vacuum Generator (VG) type of UMDI which was specially chosen to accommodate the required translational motion. To provide specimen rotation through 360^{o}, the control rod R is attached to a V.G. rotary drive type RDI.

For accurately aligning the plane of the specimen to be parallel with that of the fixed anode, the split-beam auto-collimating optical system shown in Fig. 4.10 was employed. The two beams from the telescope mounted immediately behind the large viewing port shown in Fig. 4.9 fall respectively on the polished surface of the anode S_A and the polished surface of the specimen mounting S_C that is parallel to the plane of the specimen. When S_A and S_C are mutually parallel and thus perpendicular to the direction of the incident beams, the two images seen through the eyepiece of the telescope will appear superimposed: if however there is any misalignment of S_A and S_C, the images will be displaced. To correct for this, there are two independent mechanical adjustments of the manipulating stage:

(i) the orientation of the specimen about the y-axis via the RDI rod R,

(ii) the angle between the x-y and x-z planes by means of the 45^{o} micrometer-adjustable tie bar B_M.

In fact, with the autocollimating telescope being capable of detecting a misalignment of 1' of arc, it was possible in practice to apply the above two manipulations for obtaining the surfaces that are parallel to within 1% for a

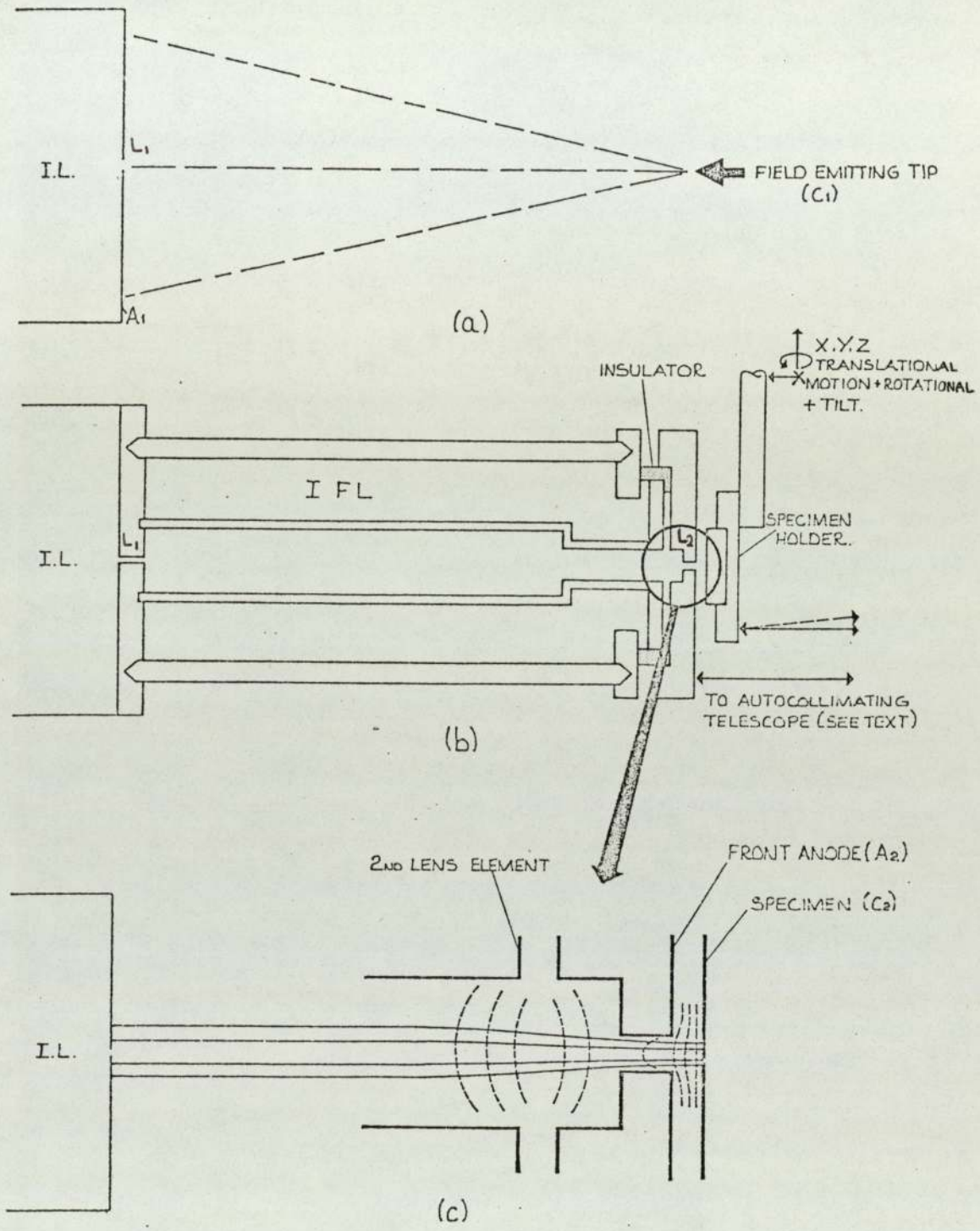

Fig. 4.7: Operation of the spectrometer with (a) field emission tip and (b) broad area electrodes, (c) shows the typical potential distribution and electron path in the interfacing lens.

Fig. 4.8: The hemispherical deflection analyser, with attached interfacing lens, input lenses, output lenses, and electron multiplier.

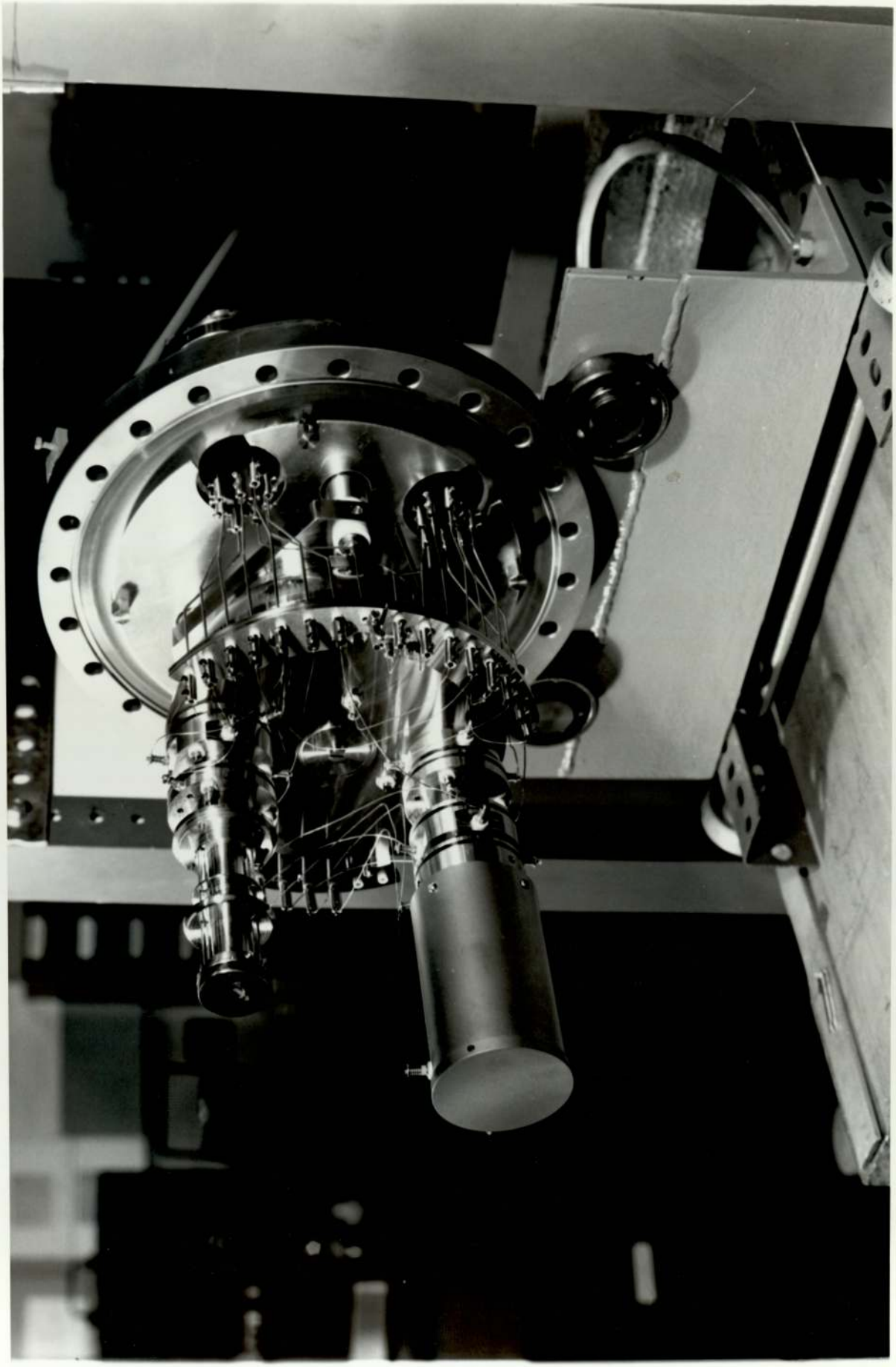

Fig. 4.9 The general layout of the complete spectrometer facility showing the vacuum chamber, electron optical system and mechanical manipulator for scanning the specimen.

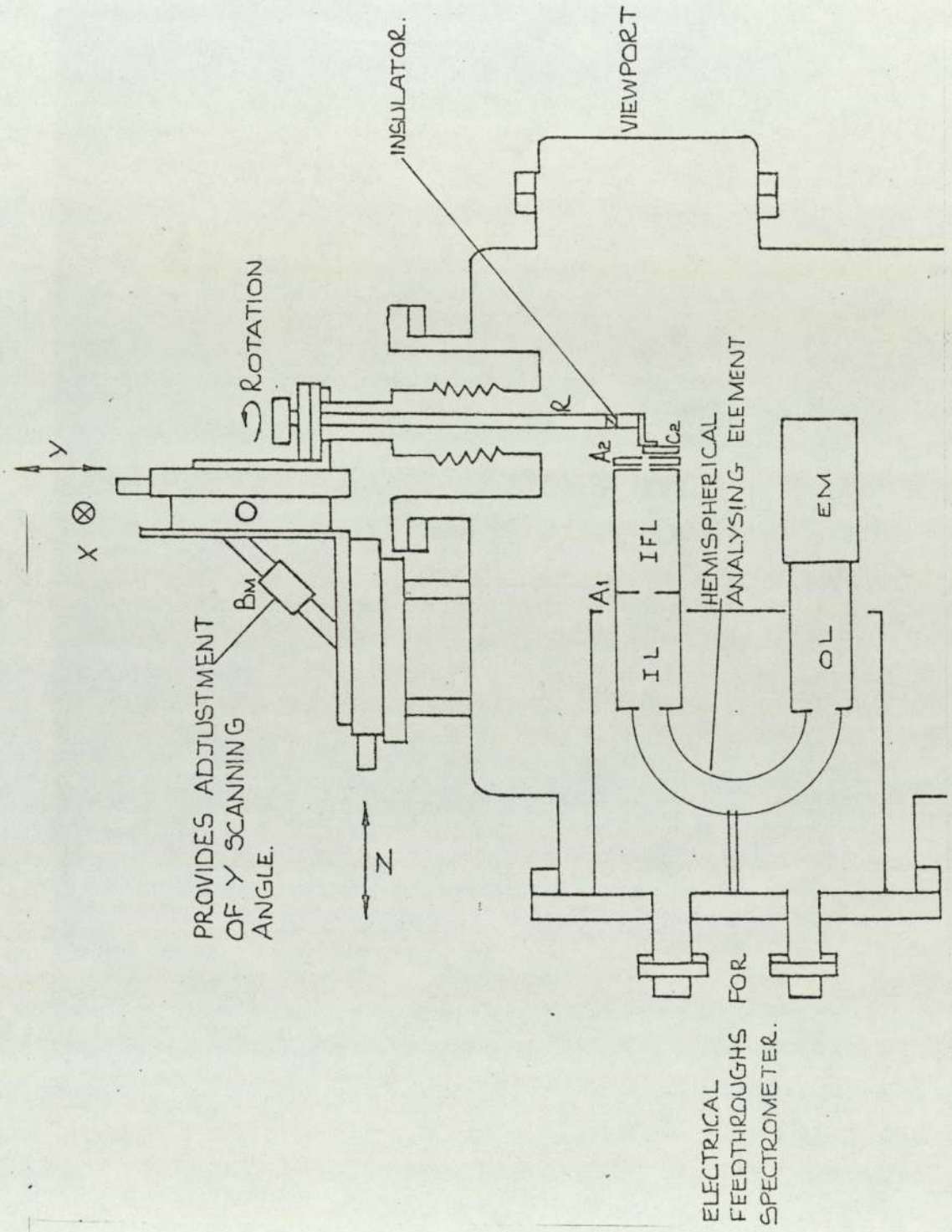

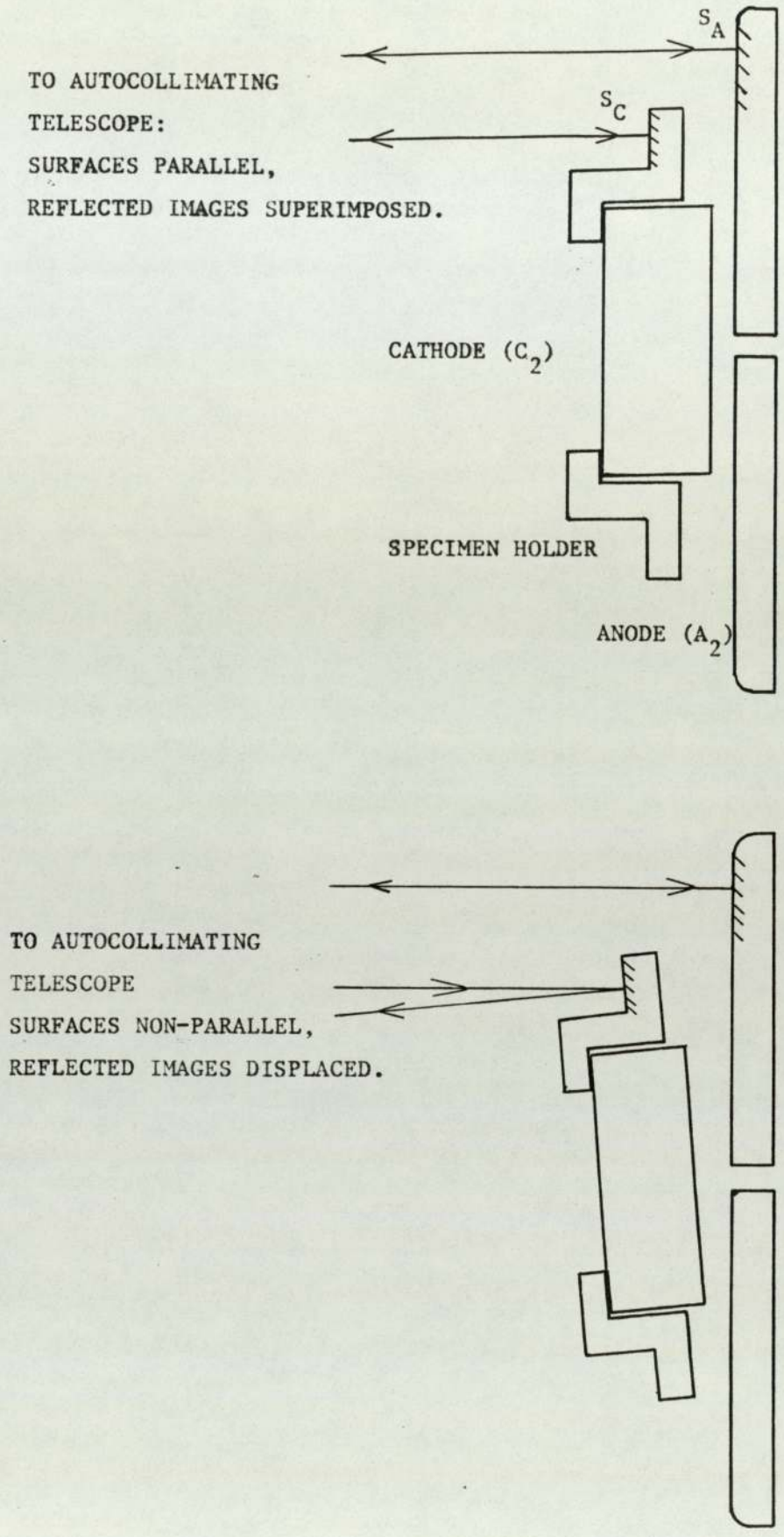

Fig. 4.10 Illustration of the optical alignment procedure for ensuring that the electrode surfaces of the "test" gap are accurately parallel.

Fig. 4.11: A general exterior view of the spectrometer and associated equipment.

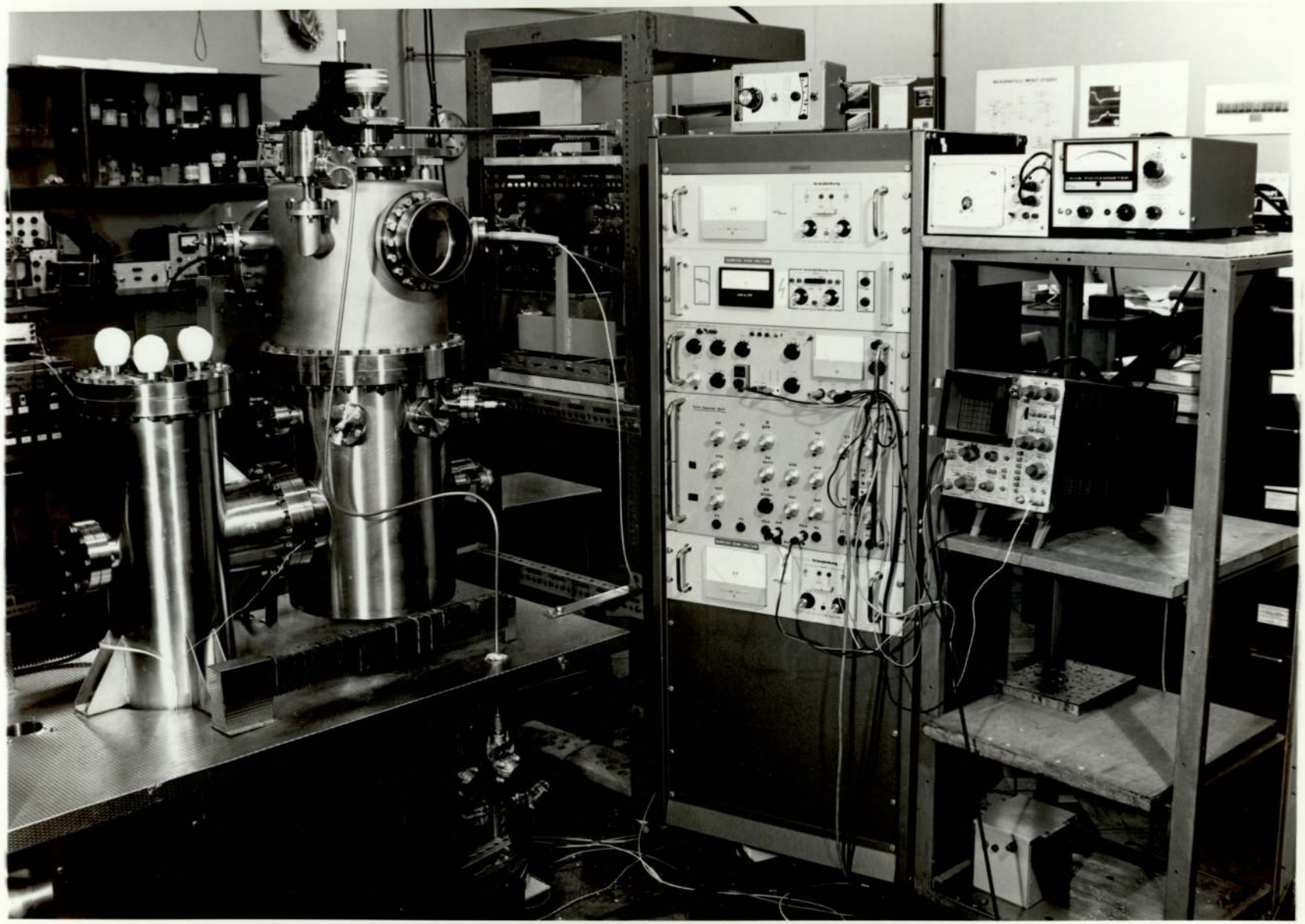

0.5mm gap.

Although not shown in Fig. 4.9, there is finally an adjustment to the angle of scan which is made by orbiting the whole of the manipulator assembly about its seating. This facility is for ensuring that the specimen is scanned in its own plane; i.e. that the inter-electrode gap remains constant during an x-scan. A check on this may be carried out by observing whether the total prebreakdown current flowing in the gap remains constant during a full scan of the specimen. The spacing of the test gap d (Fig. 4.7) is monitored in terms of the previously calibrated interelectrode capacitance using a direct-reading ECD 100 digitalised meter that has accuracy of 1% at 0.1pF. The accurancy of the gap setting using this technique is estimated to be within 20μm.

The mechanical layout of the complete facility in its stainless steel vacuum vessel is shown in Fig. 4.9, whilst the photograph of Fig. 4.11 also shows the electronic apparatus and part of the vacuum pumping system. The hemispherical analysing element with its associated input and output lens assembly and electron multiplier is mounted horizontally on a 250mm demountable flange, whilst the specimen stage is mounted vertically from the top flange. The chamber is pumped by a standard Vacuum Generator ultra-high vacuum pumping system, using an oil diffusion pump, a 24 hour liquid nitrogen cold trap and a titanium sublimation pump, where the ultimate pressure of the system is in the 10^{-11} torr range.

4.9 Performance of the Modified Spectrometer

The calibration and resolution of the basic spectro-

meter module have already been determined as discussed in section 4.7. However, it is necessary to check that the modifications for broad-area operation have not affected these properties. Since it is impractical to repeat the earlier type of calibration using an atomically clean isolated micropoint tungsten emitter whilst maintaining the electrode potentials appropriate to broad area operation, an equivalent emitting regime was fabricated by embedding a tungsten micropoint emitter in a re-entrant divot machined in the face of a standard broad area electrode (Fig. 4.12) Although this partially shielded arrangement of the emitter would not permit it to be effectively field-desorbed, so that it gave the broad spectrum of Fig. 4.13 that is characteristic of a contaminated tip, it is equally apparent that there is no spurious shift of the spectrum with respect to the Fermi level, other than that to be expected for a contaminated emitter (Braun et. al.[96]). From this observation it can be concluded that the original calibration of the instrumental Fermi level still holds with this modified electron optical regime.

However, due to the inability of obtaining a clean emitter the spectrum of Fig. 4.13 cannot be used to determine the resolution, and it is only possible to adopt an indirect approach based on measuring the steepness of the high energy slopes of experimentally obtained spectra and assuming the Young-Kuatt[101] criterion to apply. Thus referring to the energy spectrum of Fig.5.4(c) which was obtained from a site on a broad-area stainless steel electrode at $300^{o}K$ and which has a particularly steep high-energy slope width of 0.12eV, the Young-Kuyatt criteria

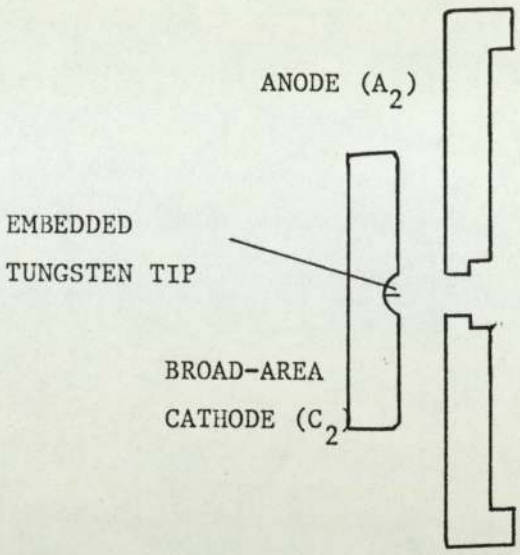

Fig. 4.12 A "control" cathode consisting of a standard micro-point tungsten emitter embedded in a broad-area copper electrode.

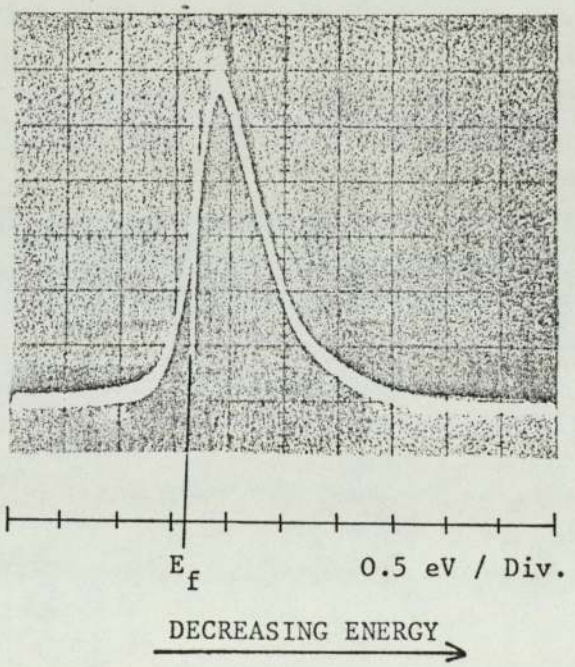

Fig. 4.13 The electron spectrum obtained from the embedded tungsten emitter.

predicts a resolution of $\lesssim$ 80meV. Although this value is rather higher than that originally obtained by Braun et.al.[96] it is most likely that this effect is non-instrumental since the Young-Kuyatt criterion is based on the assumption that the spectrum is from a clean metallic emitter, whereas evidence presented elsewhere in this thesis and independent of a resolution 80meV suggests that the present spectra are probably derived from a more complex insulating or semiconducting type of regime. For such emitters, it is well known that even atomically clean semiconducting field emitters exhibit a shallower slope, e.g.[89]. For this reason it is concluded that the apparently poorer performance of the spectrometer when using the interfacing lens is due to the nature of the emission source studied, rather than an effect of the lens itself: accordingly, it can reasonably be assumed that the resolution of this new instrumental development is also likely to be $\lesssim$ 30meV.

CHAPTER 5

EXPERIMENTAL TECHNIQUES AND RESULTS

5.1 Introduction

The modified spectrometer described in the previous chapter was first used by Allen and Latham[43] to measure the energy distribution of electrons emitted from localised sites on a broad area OFHC copper specimen. In the present investigation these measurements were extended to include stainless steel and titanium specimens,[92] and then gold evaporated on aluminuim. Later a detailed study was carried out of the electron spectra from sites on copper electrodes of varying purity and surface finish; in particular, the effect of the gap field and site current on the emission spectra has been determined for several such sites. Several other interesting effects have been noted including multiple peaked spectra, switching between two different spectra, a "switch on" phenomenon and non-linear FN plots. To extend the range of experimental observations a number of instrumental developments have also been incorporated into the spectrometer vacuum chamber including an electron bombardment facility for the in situ heating and outgassing of electrodes, an ion source for sputtering specimen sufaces, and a complementary optical spectrometry facility for studying electroluminescent effects.

5.2 The Experimental Technique for Recording Electron Spectra

The standard specimen geometry used throughout these investigations consisted of 14mm diameter discs, 4mm thick with radiused edges to prevent field enhancement. Three types of surface finish were employed: a) freshly turned

b) highly polished by a sequence of diamond paste and alumina powder to a surface roughness of 0.25μm, and c) a surface formed from the molten state. All samples were cleaned in an ultrasonic spirit bath before assembly in the spectrometer vacuum system (see Figs. 4.7 and 4.9 from Chapter 4). To achieve its optimum operating pressure the latter is baked for 18 hours at 250°C; subsequent cooling and filling of the liquid nitrogen trap realizes an ultimate pressure of 2×10^{-10}torr. Then, prior to applying any high voltage, the specimen is accurately aligned parallel to the anode and set to a known gap (usually of 0.5mm) as discussed in the previous chapter.

The circuit for detecting an emission site is shown in Fig. 5.1(a). With this, a negative voltage is applied to the specimen and slowly increased until a current of $\sim 10^{-6}$A is recorded at the anode. The specimen is then scanned in a raster fashion in front of the anode probe hole: a manipulation that is achieved by displacing the specimen by 0.5mm in the vertical direction between successive motorised horizontal scans. The speed of the chart xy recorder which records the output of the picoammeter is initially calibrated in accordance with the scan time so that the position of a site and the magnitude of its current can be read off directly from the recording (see Fig. 5.2.). Once the positions of all the sites have been determined, micro-adjustments can be made to both the horizontal and vertical positions to maximise the current entering the first lens from a particular site.

When measuring the spectrum of the electrons emitted

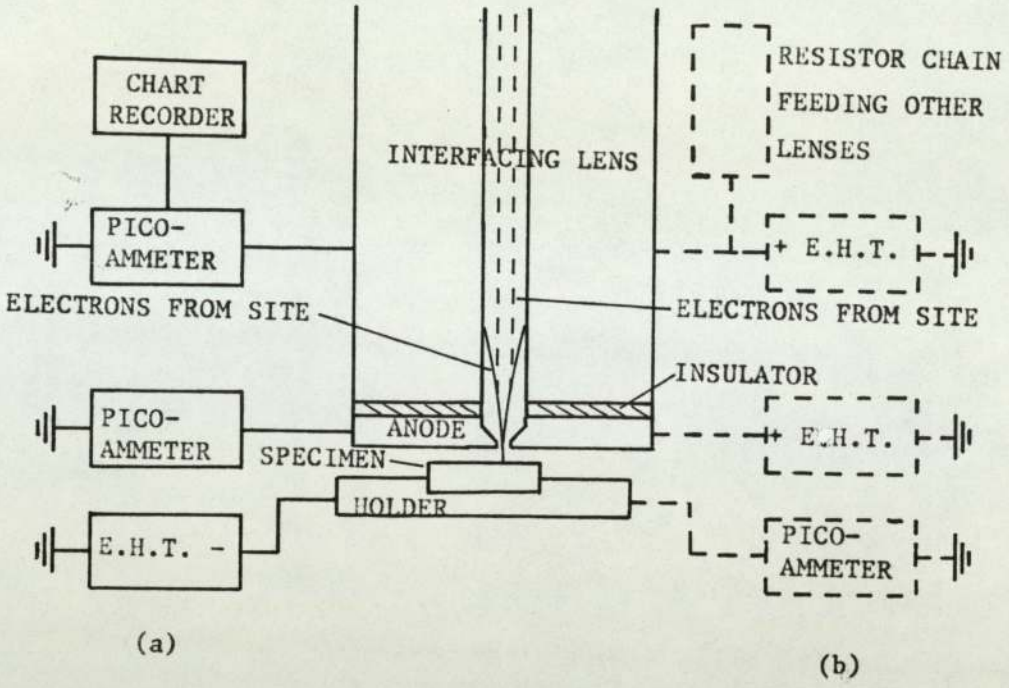

Fig. 5.1 The electrical connections for (a) detecting a site and measuring its I/V charactertistic, and (b) focussing the electronbeam onto the entrance aperture of the spectrometer.

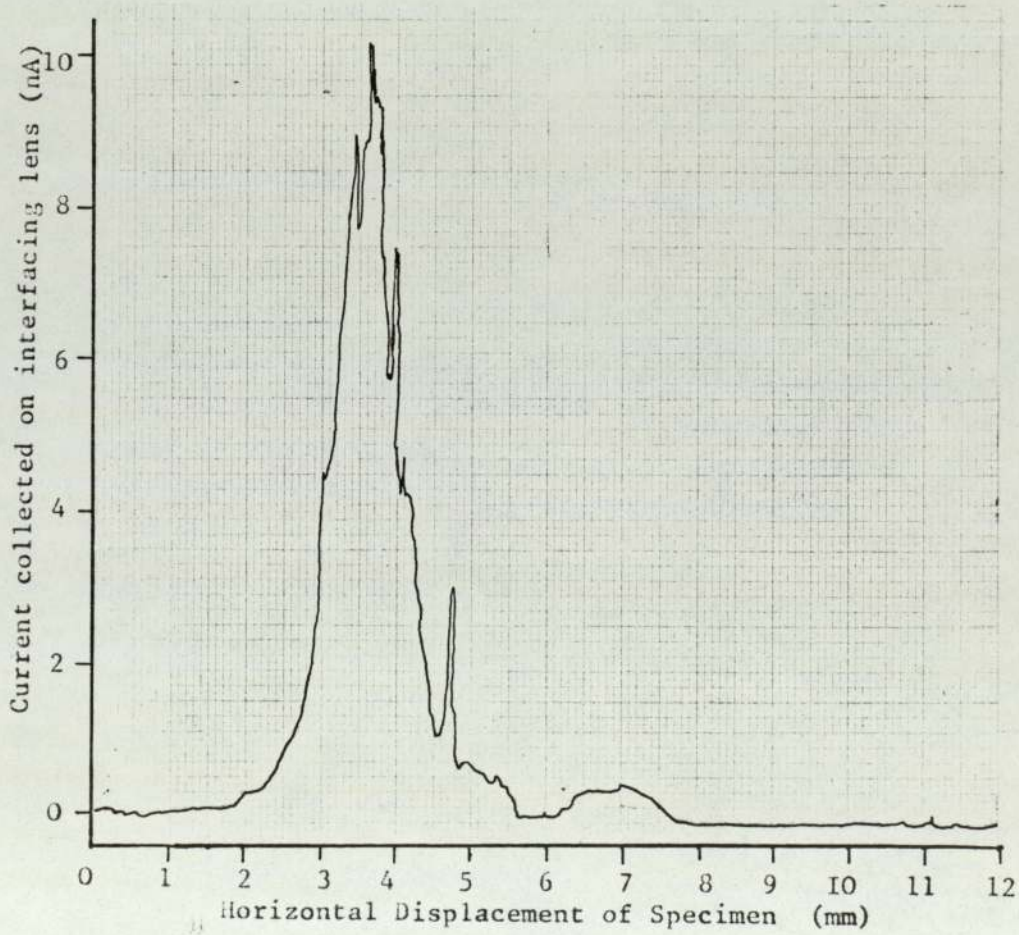

Fig. 5.2 A typical chart recorder output showing the location of two electron emitting sites.

from a site, the test gap is electrically connected as shown in Fig.5.1(b). Here it should be noted that the Kiethley Picoammeter (Model 4145) has an input voltage drop of less than 10 mV for full scale deflection, so that the presence of the meter does not significantly affect the calibration of the spectrometer. Generally a number of adjustments are required to the spectrometer input lens voltages and to the position of the specimen to obtain an optimum signal. The potential difference across the hemispheres is always set at 1.67 volts for the correct calibration of the emitter Fermi level to apply as discussed in Chapter 4.

In order to measure the effect of the gap field on a spectrum, the voltage applied to the anode is varied. This normally necessitates refocusing of the input lenses at each field value, although occasionally the signal is quite insensitive to focusing, presumably indicating an electron beam which is near to the axis of the electron-optical system. The determination of the current drawn from an individual site at a given field whilst recording its associated energy spectrum is not straightforward; however, two complementary techniques have been employed. Firstly, the I-V characteristic of each site can be determined using the circuit of Fig.5.1(a) from which it is clear that the I-V relationship for the whole gap may also be concurrently measured by the picoammeter connected to the anode. This latter I-V relationship may be expected to be the same as that obtained using the circuit of Fig.5.1(b), i.e. when taking spectra. However, Fig.5.1(b) which compares the voltage applied to the cathode in the circuit of Fig. 5.1(a)

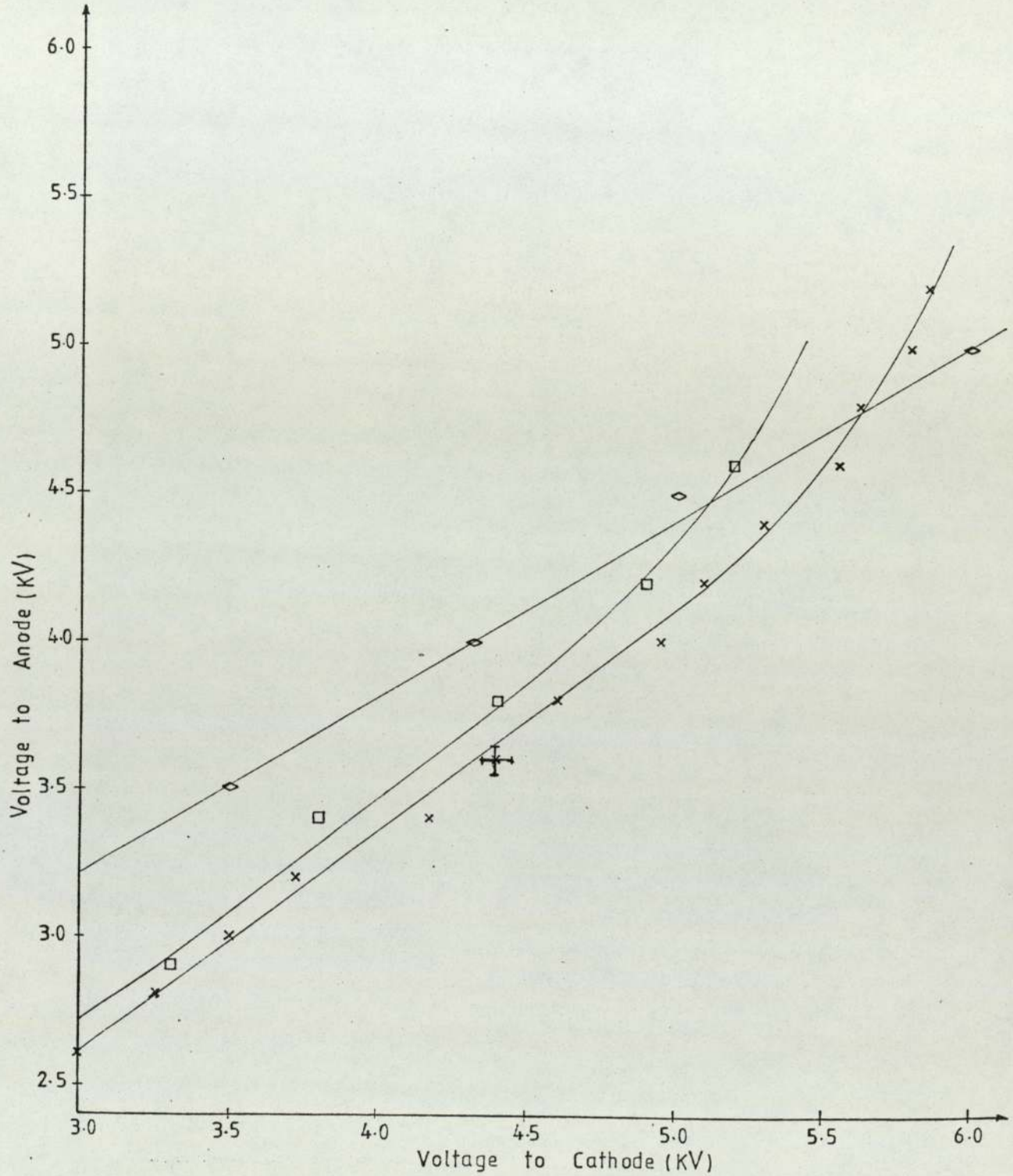

Fig. 5.3 Voltage applied to anode versus voltage applied to cathode to obtain the same gap current. Calibration curves for three different specimen gaps are presented.

with that applied to the anode in the circuit of Fig. 5.1(b) in order to draw an equivalent current, shows that in general these two voltages are not the same. Such an effect has been discussed by Beukema,[102] who attributed it to the influence of the earthed walls of the vacuum chamber: other factors to be taken into consideration include non-collection of electrons by the anode and leakage currents. To allow for this polarity effect the determination of the individual site current at each field value becomes a two stage process: firstly, employing a calibration such as Fig. 5.3 to discover the appropriate field in the high voltage cathode configuration, and then reading off the current from the site's I-V relationship obtained as in Fig. 5.1(a).

However, it was found necessary to develop an alternative and complementary approach to determine the site current for a particular spectral measurement. This was because, as discussed in Chapter 2, a characteristic of the prebreakdown currents is their temporal instability, so that during the procedure for obtaining a spectrum it is not unusual for the current to suddenly vary. Therefore, the second current monitoring technique involves calibrating the gain of the spectrometer signal amplification system, so that any variation in the magnitude of this signal can be directly related to variation in site current. However, since the fraction of the site current which enters the analysing head of the spectrometer will, in general, be different for each site, this method on its own will only reveal relative magnitudes of current. Thus whilst it is possible to estimate the actual current by making an aver-

aged comparison with the first method, it has to be said in conclusion that the absolute magnitude of the site current corresponding to any given spectrum is not an accurately determined parameter.

5.3 Spectra from Different Materials

In collaboration with Allen & Latham [92] FEED measurements were made on the emission sites found on mechanically polished specimens of titanium and stainless steel at current levels $\lesssim 10^{-8}$A where the associated spectra are shown in Fig. 5.4(a) and (c). After 18 hours under U.H.V. the spectrum from the titanium alloy changed to that shown in Fig. 5.4(b), and which can most probably be interpreted as a change in the relative magnitude of the two peaks which are contained in these distributions.

Next, an attempt was made to obtain a spectrum from a mechanically polished aluminium specimen. Although a number of microdischarges were observed no continuous emission could be achieved with the maximum available field of $2.5 \times 10^{-7} Vm^{-1}$. It appeared reasonable to suppose that the extremely continuous $\sim$ 3nm thick insulating oxide film, which covers aluminium surfaces at room temperature, may in some way be inhibiting continuous electron emission. Therefore it was decided to cover the aluminium specimen with an evaporated gold film, of a thickness estimated to be $\sim$ 100nm. This new sample, which would have negligible oxide coverage, was very emissive; its energy distribution and F-N plot are presented in Figs. 5.4(d) and 5.5 respectively.

Since the variation among the distributions from a range of materials was not significantly greater than from

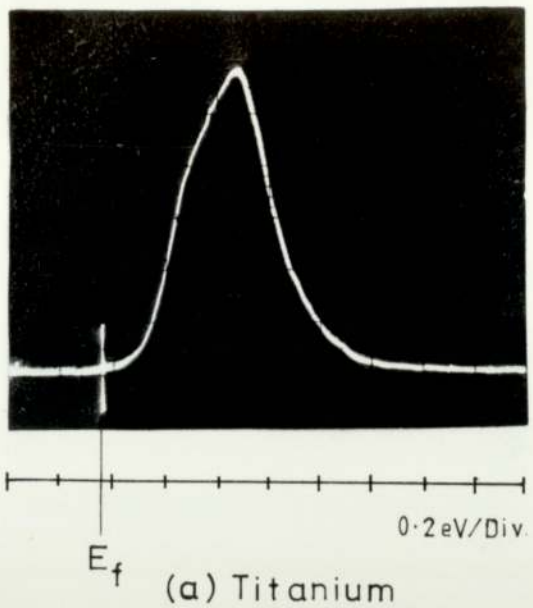

(a) Titanium

Field= 6·3Mvm^{-1}

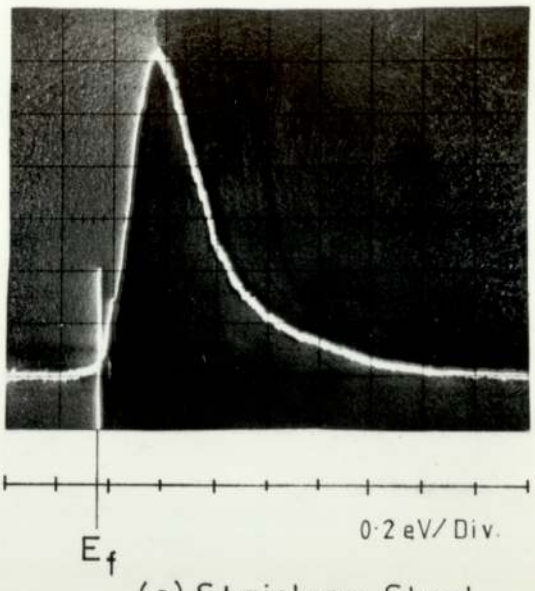

(c) Stainless Steel

Field = 7·5Mvm^{-1}

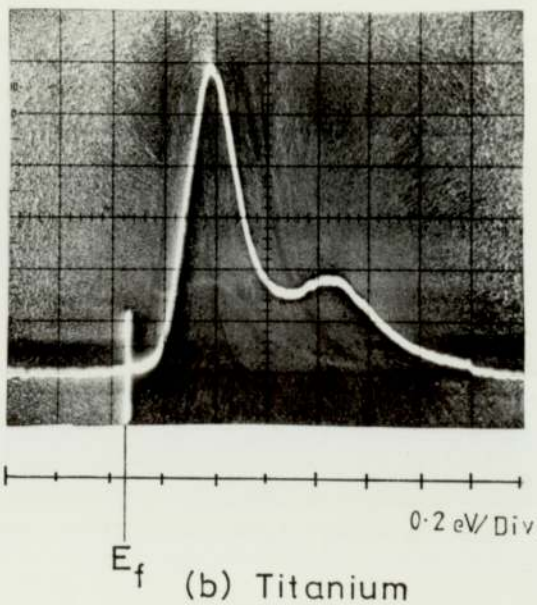

(b) Titanium

Field = 4·4Mvm^{-1}

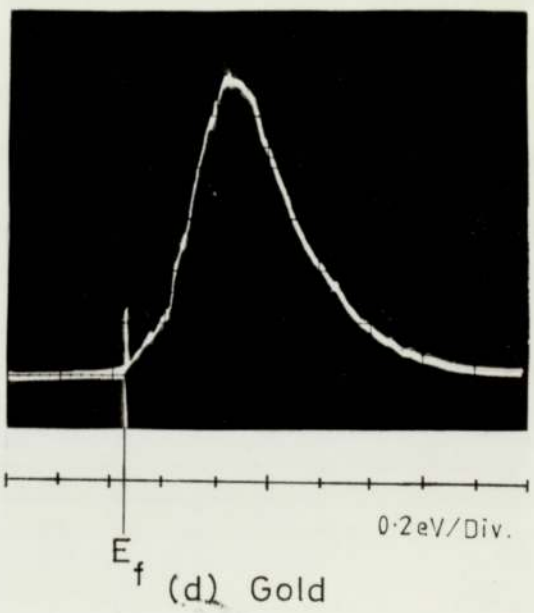

(d) Gold

Field = 9·1Mvm^{-1}

DECREASING ENERGY →

Fig. 5.4 Spectra obtained from different materials at low currents. The position of the emitter Fermi energy is marked. Energy decreasing from left to right is X-axis. Electron current per unit energy (arbitrarily normalised) is Y-axis.

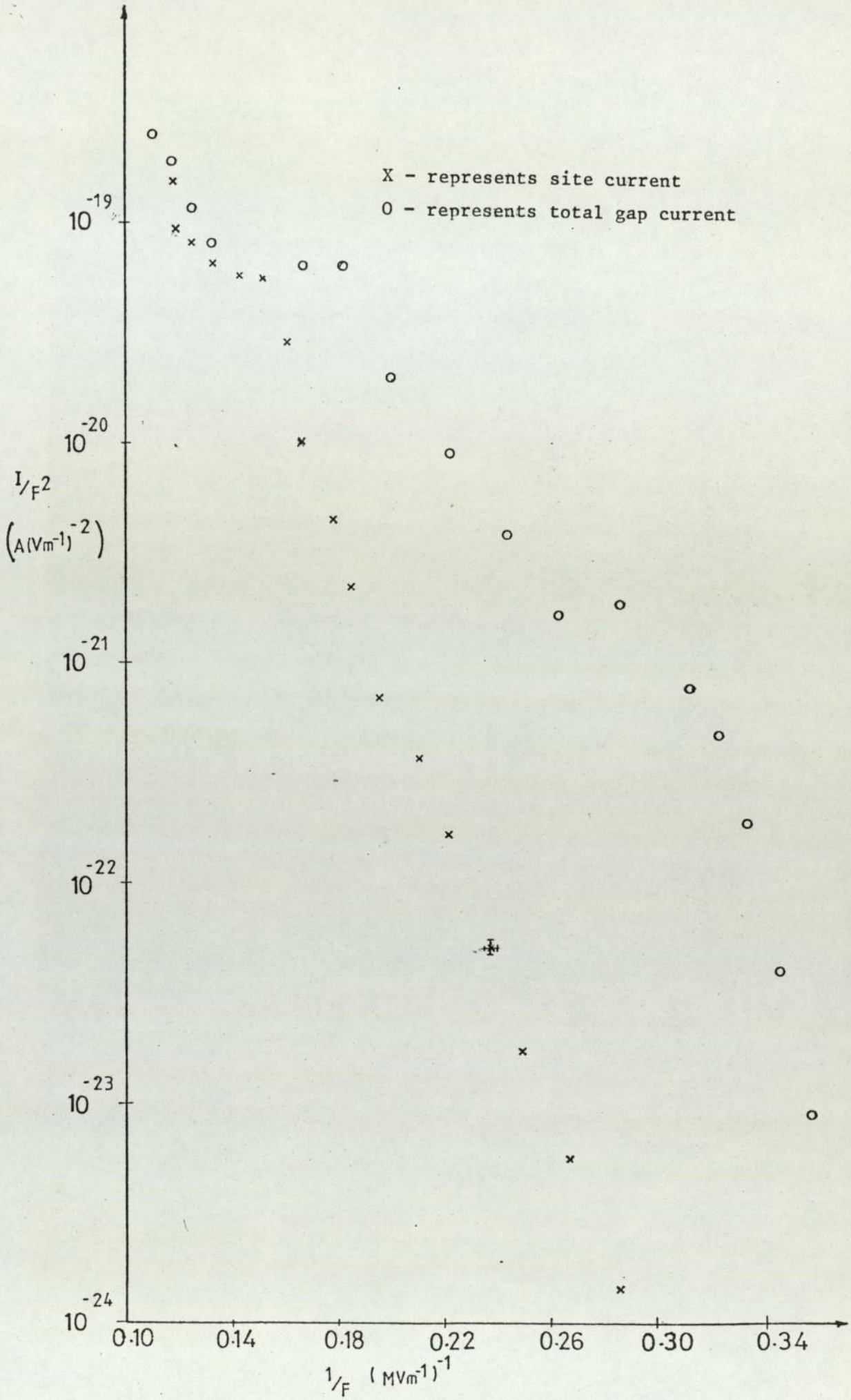

Fig. 5.5 Fowler-Nordheim plots for the evaporated gold specimen.

the range obtained from sites on a given material, it was decided to pursue more extensive measurements using only one material. For this investigation, copper was chosen because it invariably provides emission in a field range that is convenient for this instrument. In addition micro-discharges, which frequently occur with stainless steel, aluminium or titanium electrodes, are rare on copper.

5.4 The Effect of the Gap Field on the Electron Spectra

Three different types of copper specimen were studied in detail, viz mechanically polished and lathe-turned OFHC (Oxygen Free High Conductivity) copper, and a high purity single crystal copper specimen grown from the melt in a (111) orientation. The emitting sites located on each specimen are collated in Table 5.1.

Specimen Type	Surface Finish	Specimen No.	Site Numbers
OFHC	Mech. Polished	1	1A, 1B, 1C
OFHC	Mech. Polished	2	2A, after micro-discharge 2B, 2C, 2D
OFHC	Machined	3	3A, 3B
Single Crystal	From melt	4	4A, 4B, 4C, after microdischarge 4D, 4E

5.1 Table of Specimens and Sites

Before taking spectral measurements, each site has to be located, and a series of adjustments made both to its position and the focusing of the input lenses of the spectrometer. Also the I-V relationship for the site is usually measured at this stage. Therefore, the electrode gap is inevitably "current conditioned" before an electron energy

distribution is determined. Nevertheless, occasionally the electron spectra obtained are still so unstable that a measurement of the field effect would not be very meaningful, e.g. Sites 2A, 4A and 4E fell in this category. However, for the remainder it was possible, with sufficient patience, to obtain a series of measurements during which no sudden changes had occurred in the shape of the spectrum. Whilst these spectra are exactly reproducible for several hours at low current levels, the instabilities increase with site current such that at $\gtrsim 10^{-6}$A small variations often occur within a minute. The range of measurements then extends from $\sim 10^{-9}$A site current, limited by the sensitivity of the spectrometer, to $\sim 10^{-6}$A, limited by the increasing instability of the spectrum.

A majority of the sites provided single peaked spectra, with an occasional shoulder or secondary peak appearing during the course of a series of measurements. However, a number of sites displayed a multi-peaked structure throughout. In the ensuing sections these two types of result are considered separately.

a) Single Peaked Spectra

Fig. 5.6 shows two typical spectra recorded from site 1B at different gap fields, and clearly illustrates how this parameter influences their shape and position with respect to the Fermi level of the specimen cathode. For this investigation such spectra have been characterised in terms of two parameters: (i) the shift of the maximum of the distribution below the Fermi level of the specimen, and (ii) the spectral full-width at half-maximum (FWHM). These

parameters are plotted against the macroscopic gap field, taken as $E = \frac{V}{d}$, where V is the potential difference between the electrodes and d is their separation. The variation of the spectra can also be interpreted as a current effect by plotting these same parameters against site current. Fowler-Nordheim plots for the emission from several sites are also reported to enable comparison to be made with metallic micro-protusion theories.

Sites 1A and 1B were sufficiently stable to enable a large number of measurements to be taken, and which are summarised in Figs. 5.7 and 5.8. Both sites exhibit a non-linear variation of parameters (i) and (ii) with field. There is only a small, although significant, field effect until fields of 9 to 10 MVm^{-1}, corresponding to currents $\lesssim 10^{-7}$A in these cases when in particular the shift below the Fermi level increases quite dramatically. Owing to inherent instabilities, only limited measurements were obtained from sites 1C, 2B, 4B, 4C and 4D, whose field dependencies are presented respectively in Figs. 5.9, 5.10, 5.11, 5.12 and 5.13. These findings serve to emphasise that the trends detailed for sites 1A and 1B are fairly general with single peaked spectra, although it was often not found possible to take reproducible measurements in the field range where the shift from the Fermi-level increases rapidly. Further measurements of the field effect are illustrated in Figs. 5.32 and 5.34 in section 5.6.

b) Multi-peaked Spectra

Sites 2B, 3A and 3B displayed multi-peaked spectra throughout the course of measurements of the field effect.

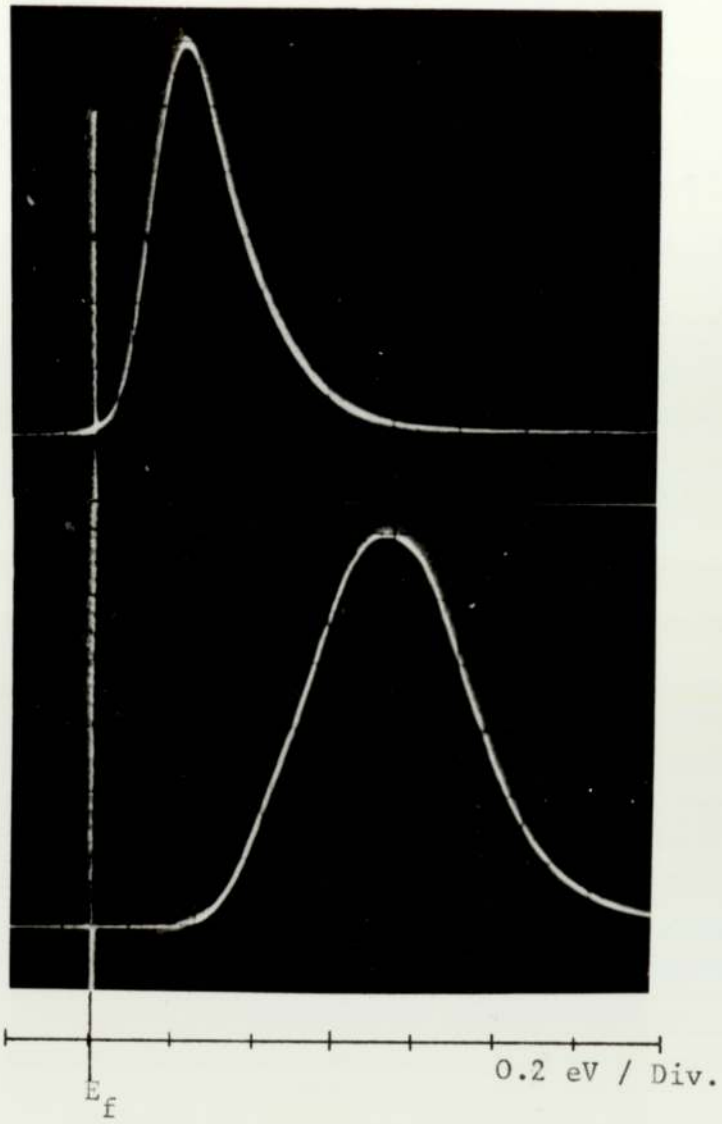

Fig. 5.6 Typical electron energy spectra (from Site 1B) under low and high field conditions, showing 2eV scans, with energy decreasing to the right. The vertical line represents the Fermi level.
Top - gap field = 8 MVm^{-1} ; site current = 1.6 X 10^{-7} A.
Bottom - gap field = 10 MVm^{-1} ; site current = 9 X 10^{-7} A.

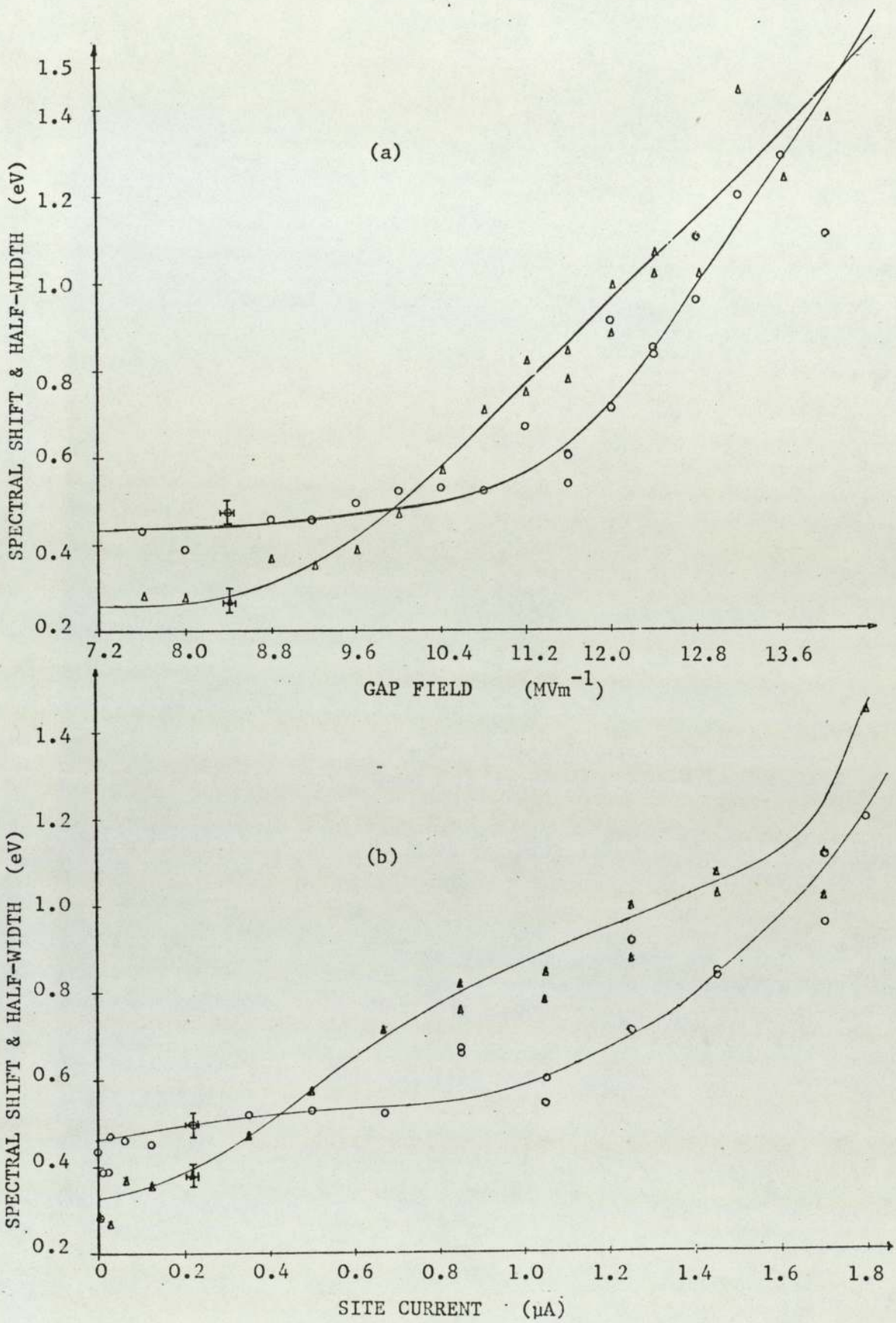

Fig. 5.7 Variation of the spectral shift and half-width with (a) applied field and (b) site current for site 1A. Δ represents the shift of the maximum of the energy distribution below the substrate Fermi level. o represents the FWHM of the energy distribution.

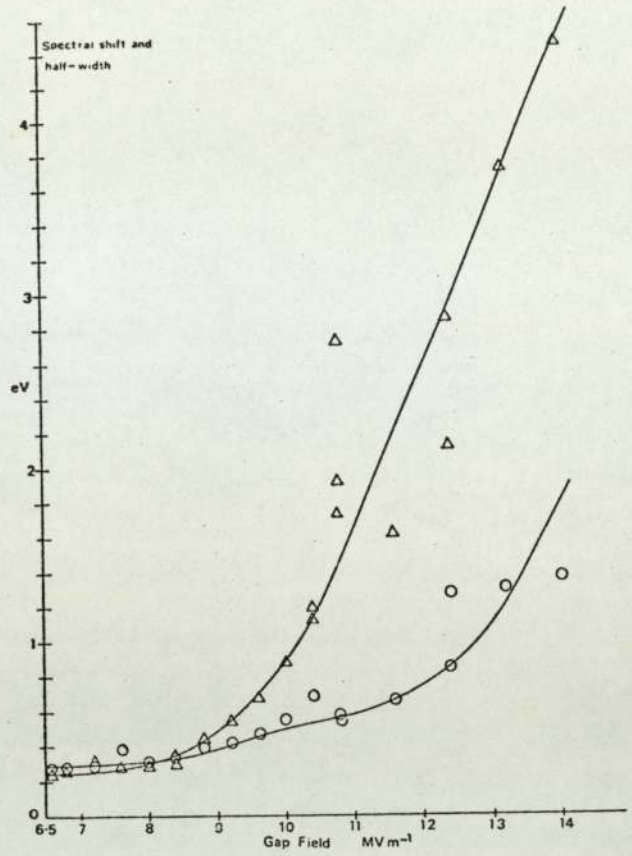

(a) Variation of the spectral shift and half-width (FWHM) with applied field. △ represents the shift of the maximum of the energy distribution from the substrate Fermi level. ○ represents the half-width (FWHM) of the energy distribution.

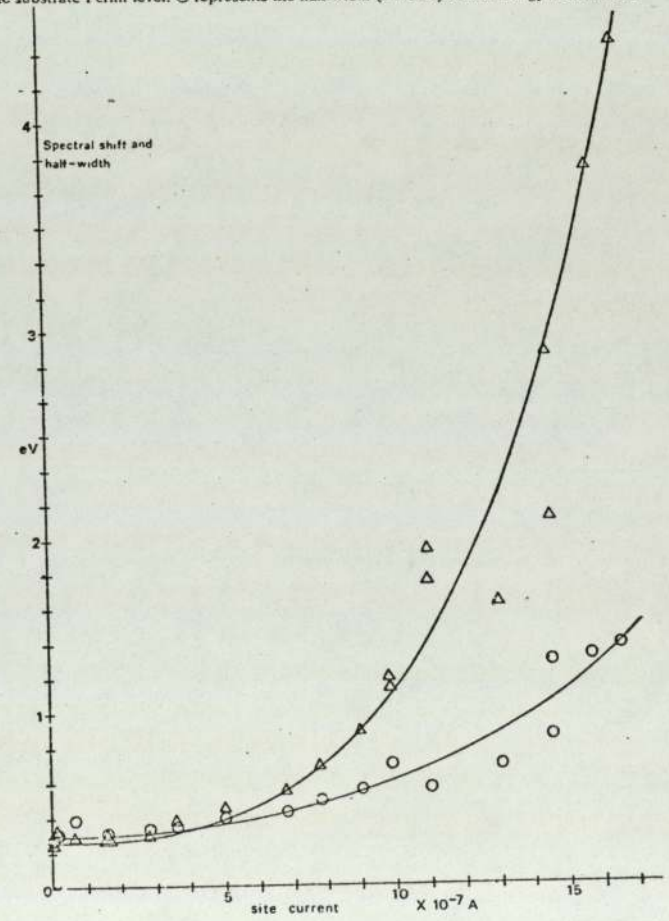

(b) Variation of the spectral shift and half-width (FWHM) with site current. △ represents the shift of the maximum of the energy distribution from the substrate Fermi level. ○ represents the half-width (FWHM) of the energy distribution.

Fig .5.8 Site 1B

Fig 5.9 Variation of the spectral shift and half- width with applied field for site 1C.

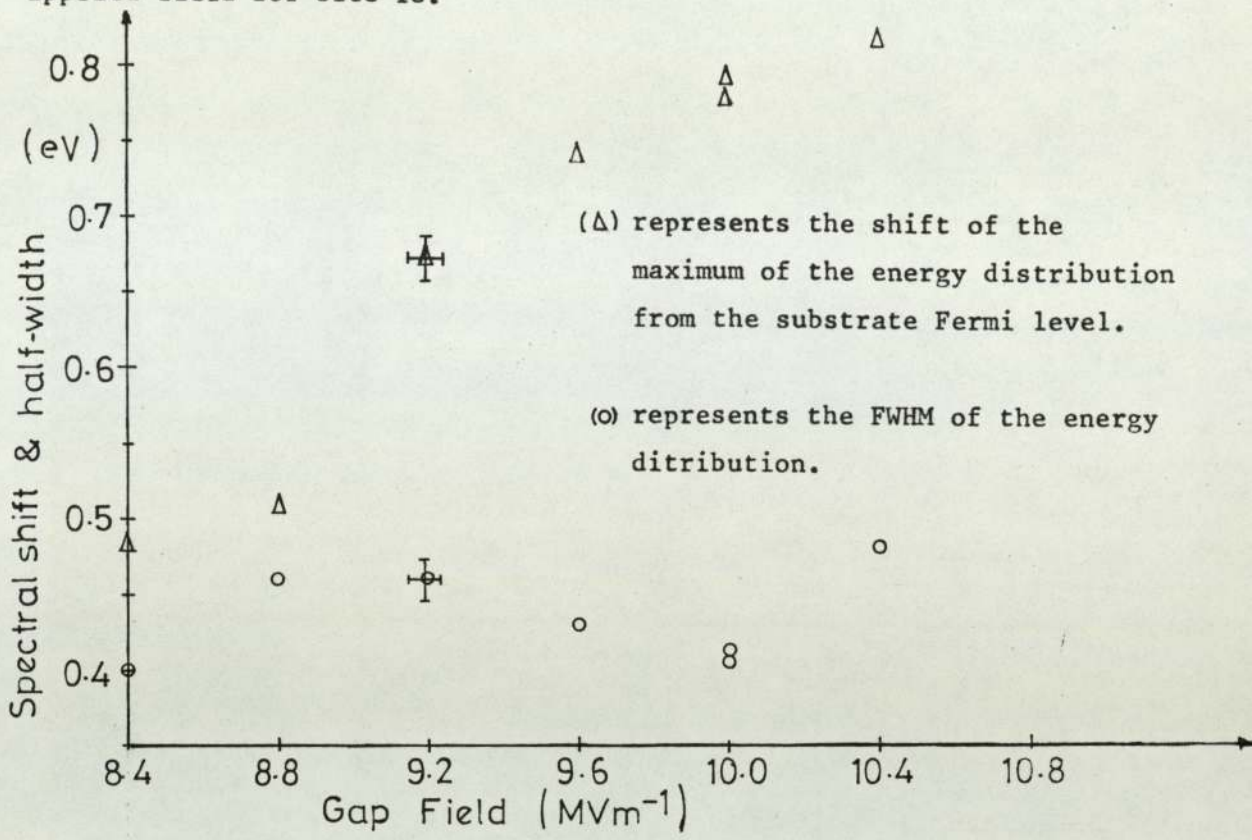

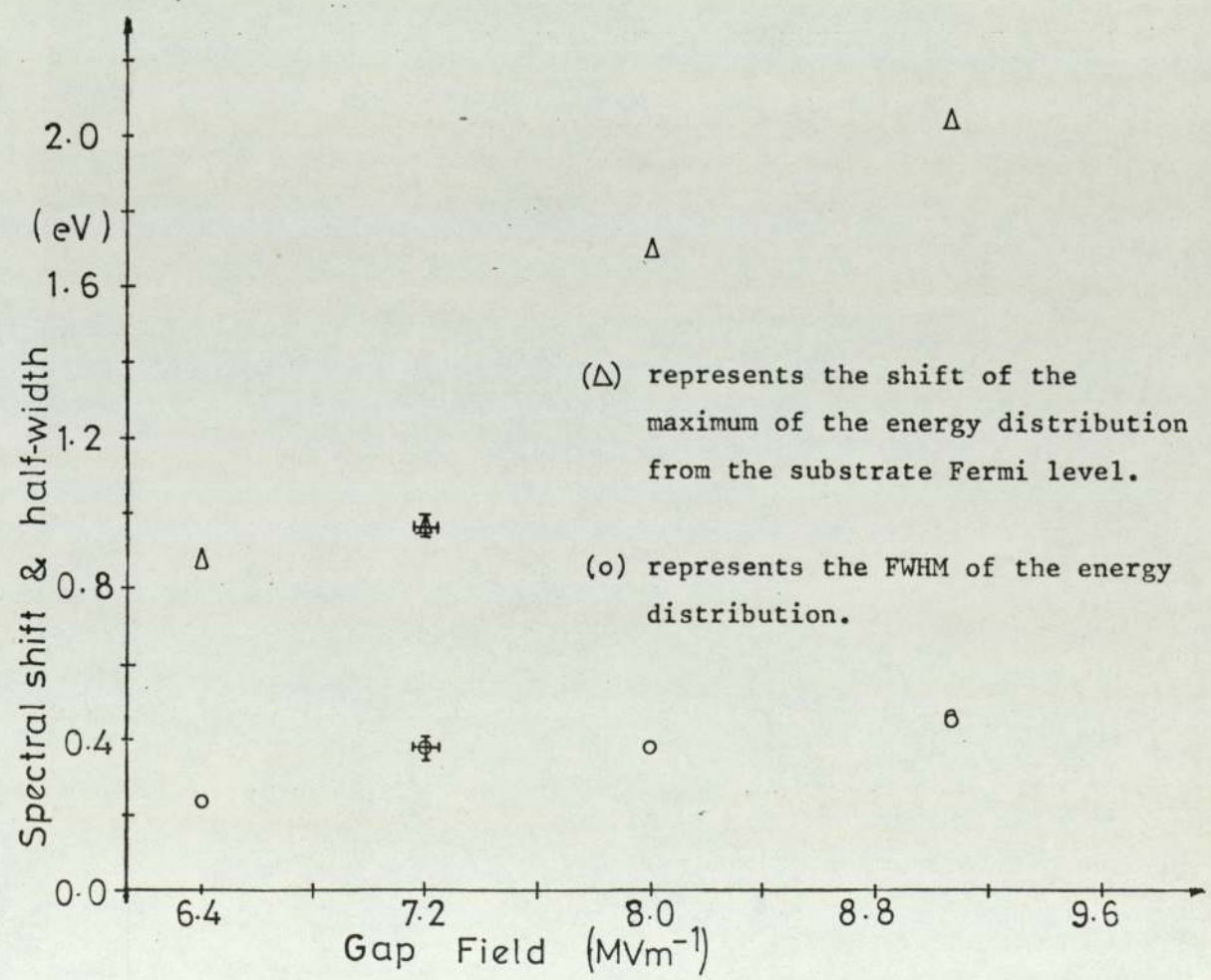

Fig. 5.10 Variation of the spectral shift and half-width with applied field for site 4B.

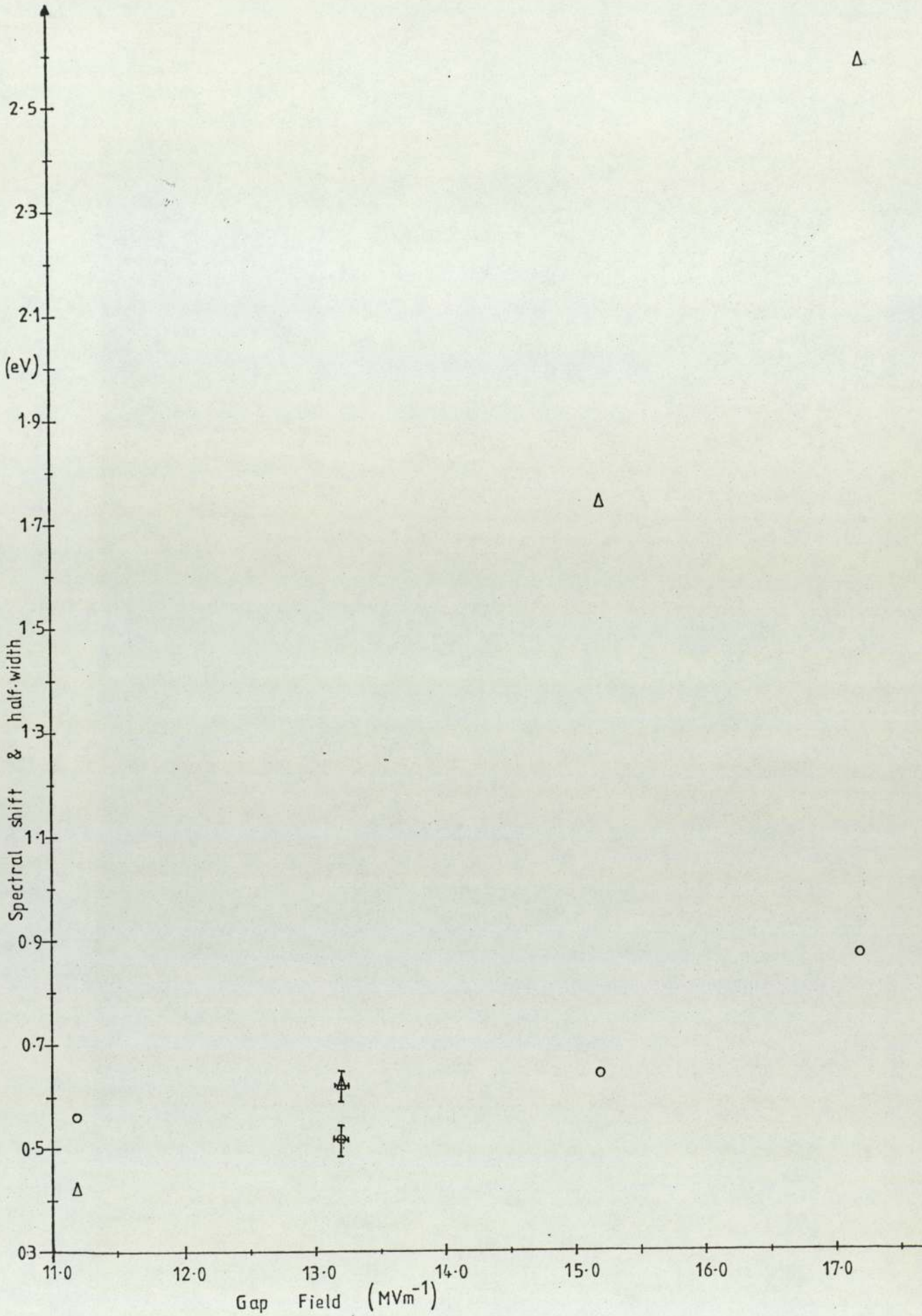

Fig.5.11 Variation of the spectral shift and half-width with applied field for site 4C. Δ represents the shift of the maximum of the energy distribution below the Fermi level; o represents the FWHM of the energy distribution.

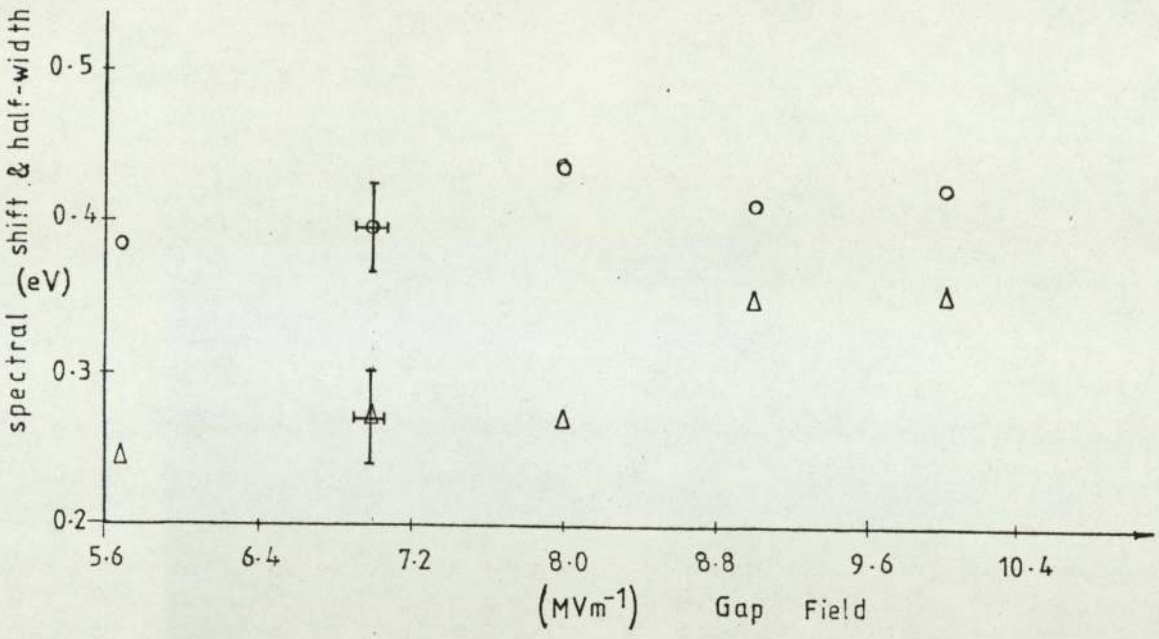

Fig. 5.12 Variation of the spectral shift and half-width with applied field for site 4D. Δ represents the shift of the maximum of the energy distribution below the substrate Fermi level. o reprsents the FWHM of the energy distribution.

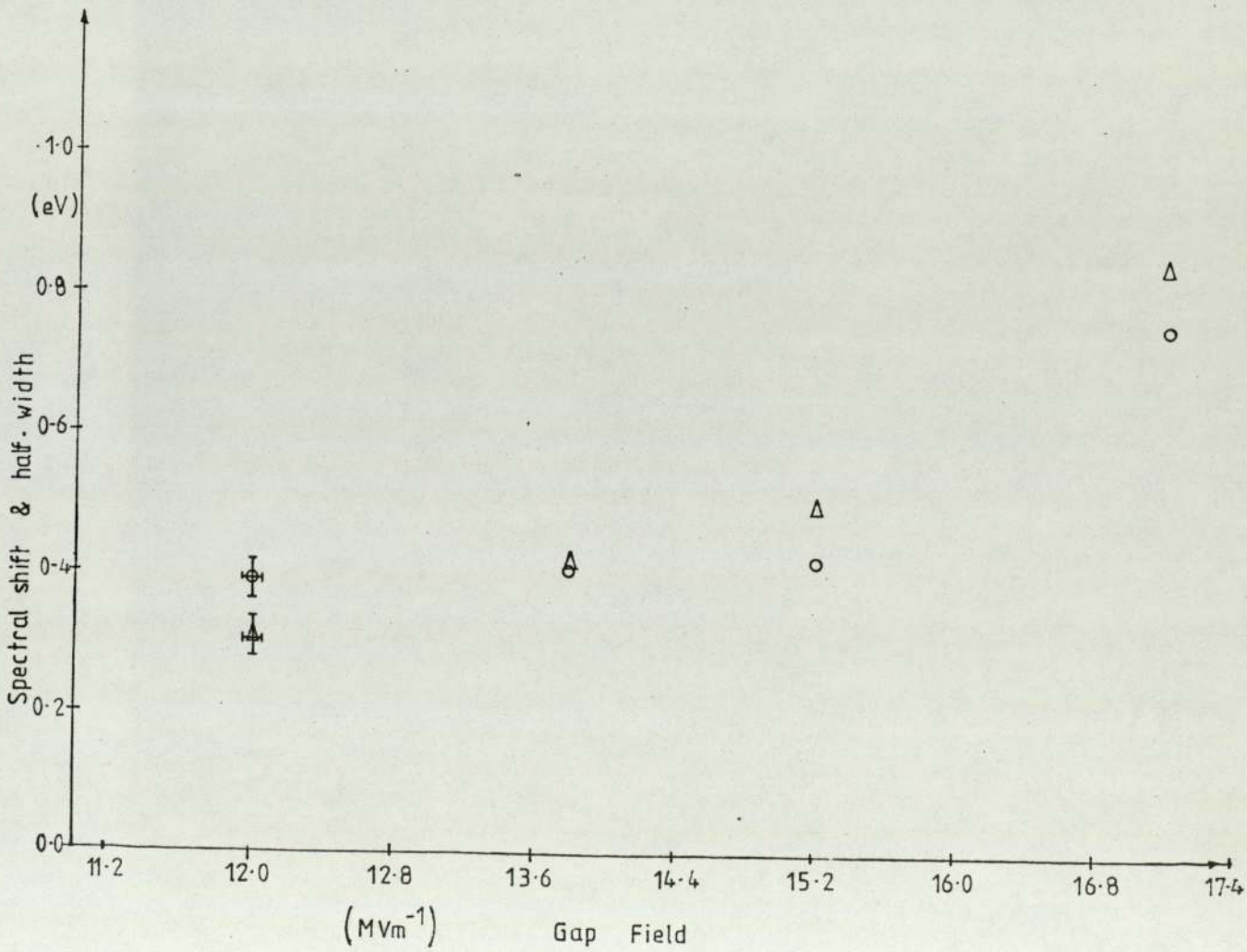

Fig.5.13 Variation of the spectral shift and half-width with applied field for site 4E. Δ and o represent the shift of the maximum of the energy distribution below the Fermi level and its FWHM respectively.

Figs. 5.14 and 5.15 which show respectively a series of spectra from sites 2B and 3A, reveal that, as the gap field increases, peaks appear and grow in relative magnitude on the high energy side of the distribution, i.e. closer to the Fermi level. Concurrently all the peaks are observed to be shifting away from the Fermi level. Thus, in the series of Fig. 5.14, the small peak in (a) grows as in (b), until in (c) it is so large that the original large peak is almost insignificant. In (d) a new peak is seen to appear on the high energy side. Alternatively, the series of Fig. 5.15 (a), (b) and (c) show how peak (ii) begins to dominate the distribution until in (d) a new peak (iii) appears on the high energy edge: this peak then grows to dominate the distribution in (g), until a further peak (iv) appears in (h) and predominates in (i). Similar effects have been observed for a further two sites (see Fig. 5.35) during the course of an investigation into the effects of etching reported in section 5.6.

The series of spectra obtained from site 3B are presented in Fig. 5.16. The behaviour of these spectra differs from those discussed above, in that the relative magnitude of the three peaks which are believed to be superimposed in each distribution does not vary excessively. Therefore, an attempt has been made to identify the shape and position of the individual peaks. To do this it was firstly necessary to determine the geometrical character of a typical distribution obtained from a broad area emission site. This was done by inspecting a large number of single-peaked spectra, obtained from four different sites, a procedure which revealed that the shape of a typical distribut-

ion can be expressed in terms of the parameters shown in Fig. 5.17. Then assuming that one side or edge of the measured spectrum is produced by only one of the peaks, the remainder of this peak may be constructed such that its shape accords to the rules of Fig. 5.17. Finally, the shape of other peaks may be estimated by a trial and error process of subtraction from the measured spectrum, followed by construction; thus the peaks contained in the spectra of Fig. 5.16 (e, f, g and h) are found to be those of Fig. 5.18.

From constructions, such as Fig. 5.18, it is possible to determine the relative current (proportional to the area), the half-width and the shift of the Fermi level for each sub-distribution. Thus the variation of the latter two parameters with field is shown in Fig. 5.19(a). The graph reveals that, whilst no significant trends can be observed in the FWHM data, due to the large uncertainty in this measurement, the shift from the Fermi level of peaks (i) and (ii) increases in an almost parallel manner, i.e. the peak separation remains constant. The variation of the shifts has also been plotted in Fig. 5.19(b) against the logarithm of the current contained in each peak which again demonstrates the constancy of the peak separation which is estimated to be 0.27 ± 0.03eV. It is not possible however, to decide if the small peak (iii) is also at a constant separation due to the large percentage error in its construction. Finally FN plots relating to the current contained in each peak are presented in Fig. 5.19(c).

Fig. 5.20 presents the results from a similar field

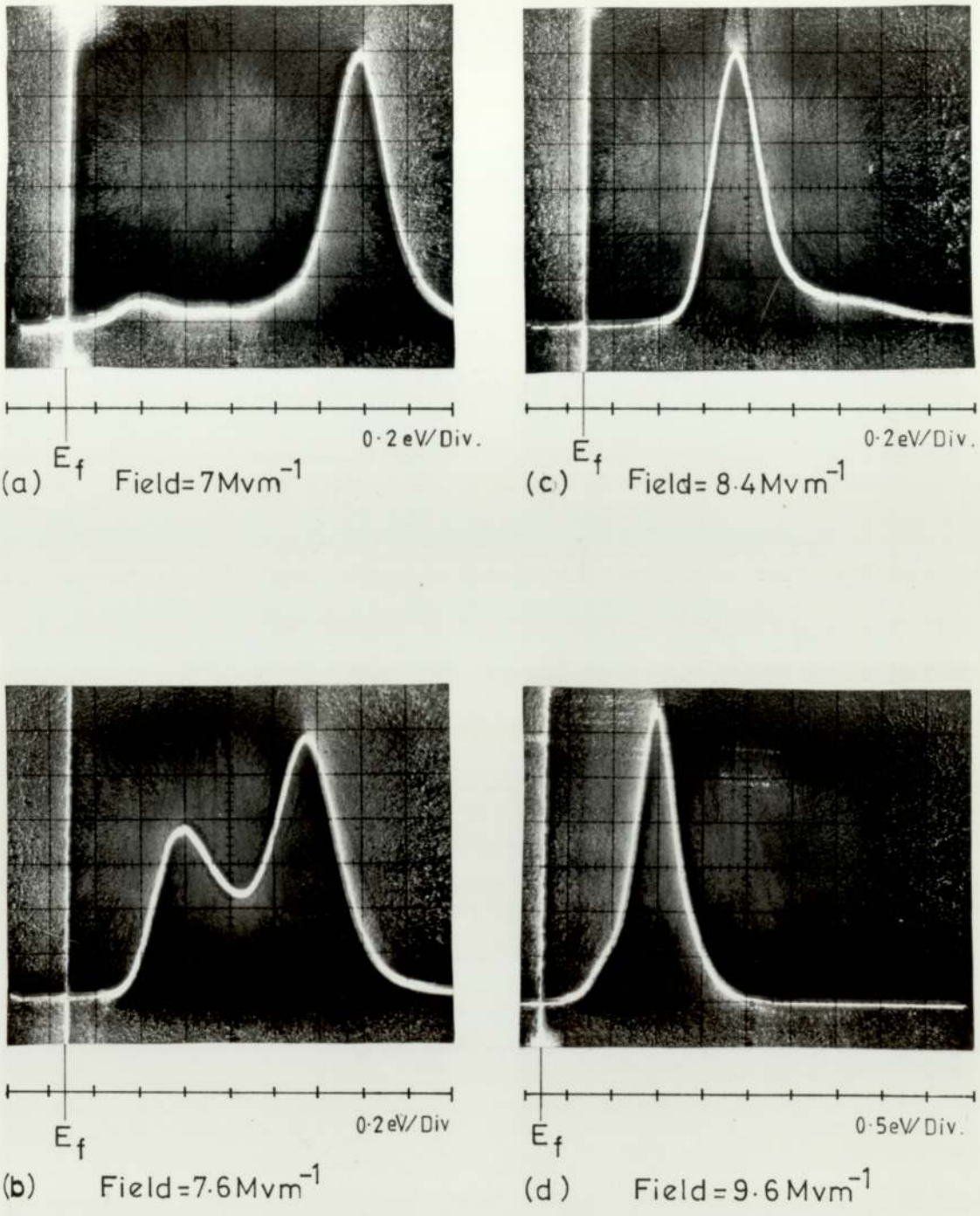

Fig. 5.14 Series of spectra with increasing field for site 2 B. The position of emitter Fermi level is shown. Electron energy decreasing from left to right is X-axis. Electron current per unit energy (arbitrarily normalised) is Y-axis. (Note change of scale in (d).)

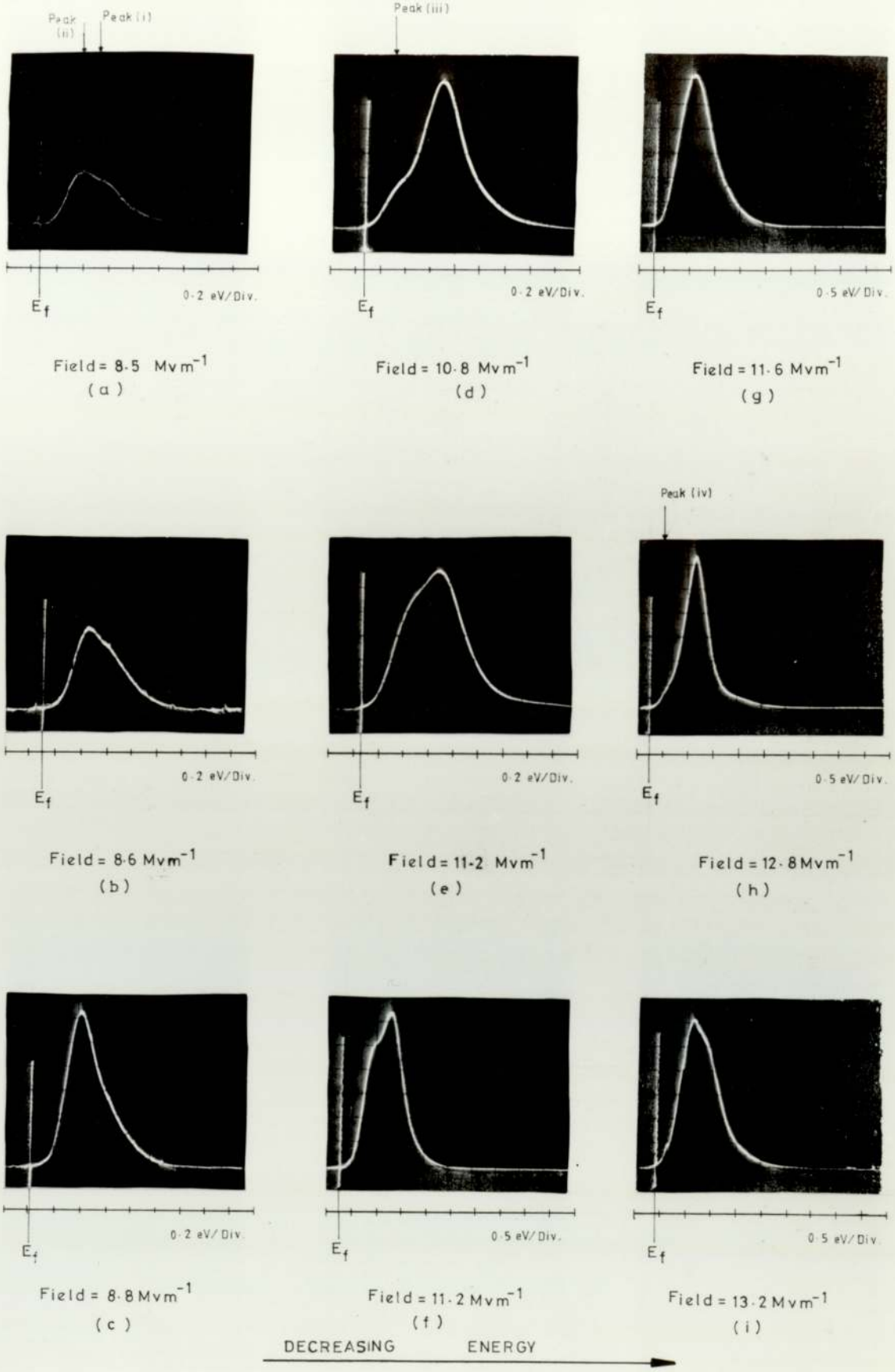

Fig. 5. 15 Series of spectra with increasing field for site 3A. The position of the emitter Fermi level is shown. Electron energy decreasing from left to right is X-axis. Electron current per unit energy (arbitrarily normalised) is Y-axis. (Note change of scale from (f) onwards.)

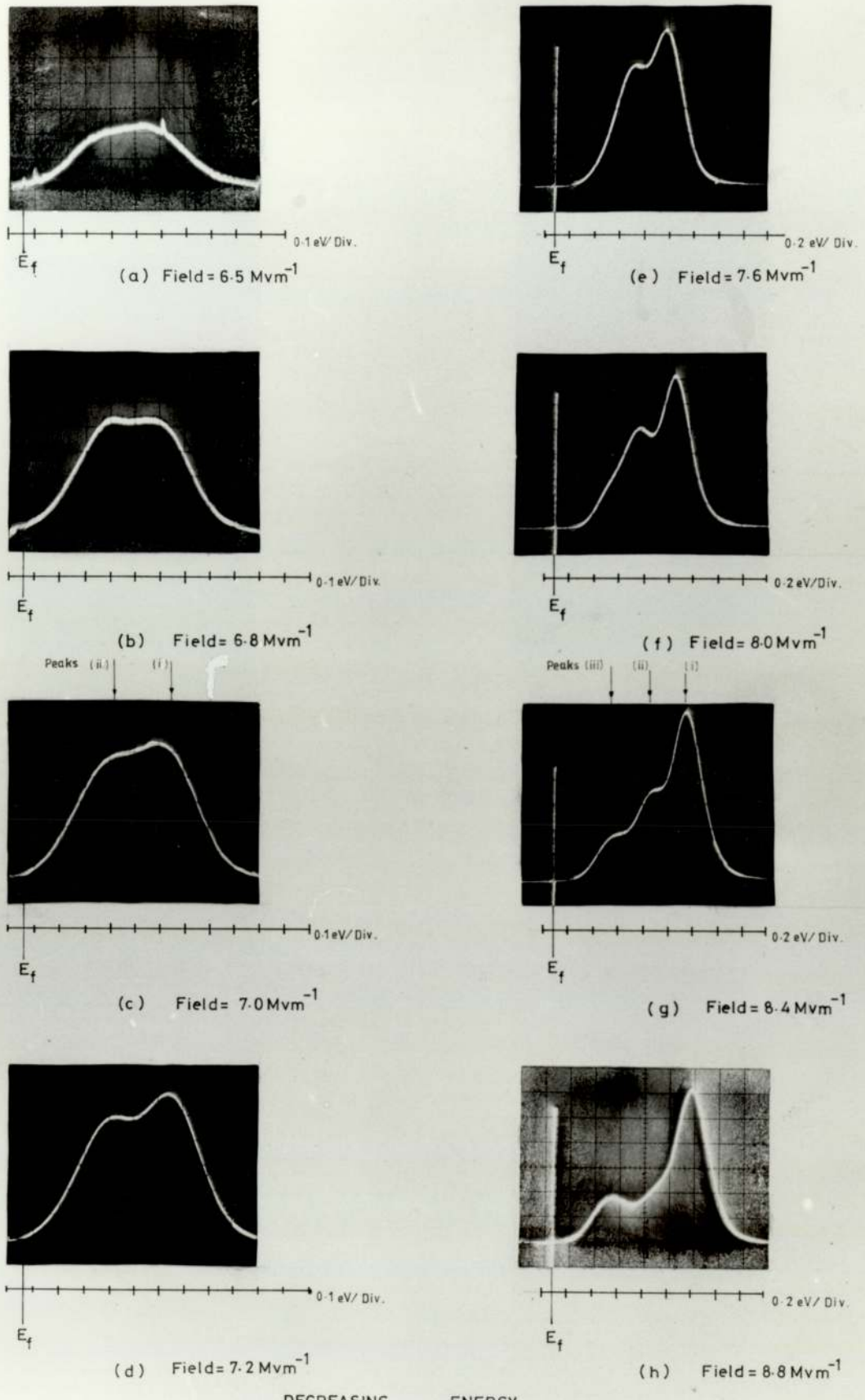

Fig. 5.16 Series of spectra with increasing field for site 3 B. The position of the emitter Fermi level is shown. Electron energy decreasing from left to right is X-axis. Electron current per unit energy (arbitrarily normalised) is Y-axis. (Note the change of scale from (e) onwards.)

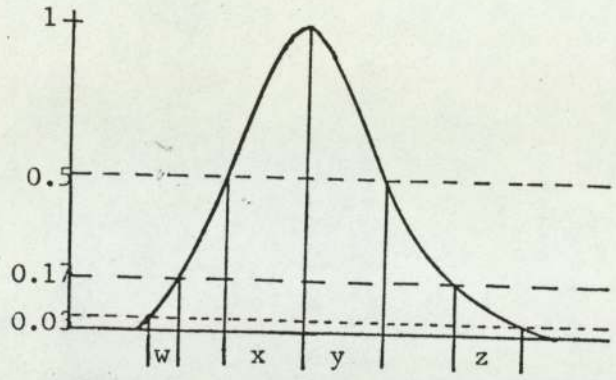

$\frac{w}{z} = 0.39 \pm 0.12$

$\frac{x}{y} = 0.88 \pm 0.11$

Fig. 5.17 The geometrical character of the typical electron energy distribution from broad area emission sites.

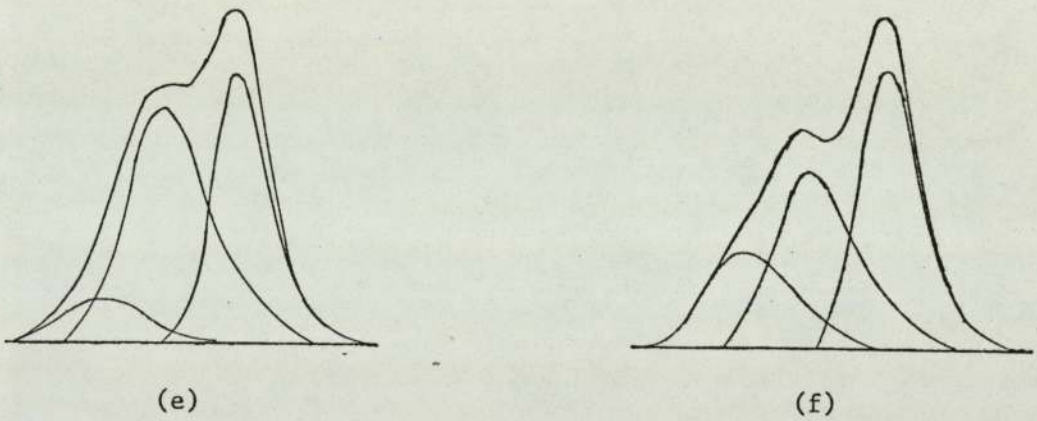

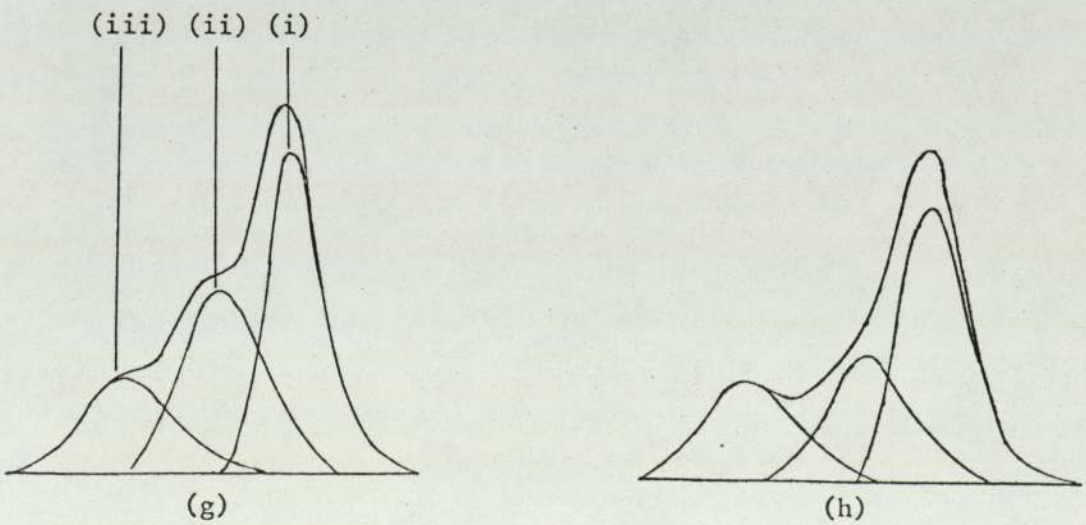

Fig. 5.18 The estimated character of the individual peaks contained in the spectra from site 3B as presented in Fig. 5.16.

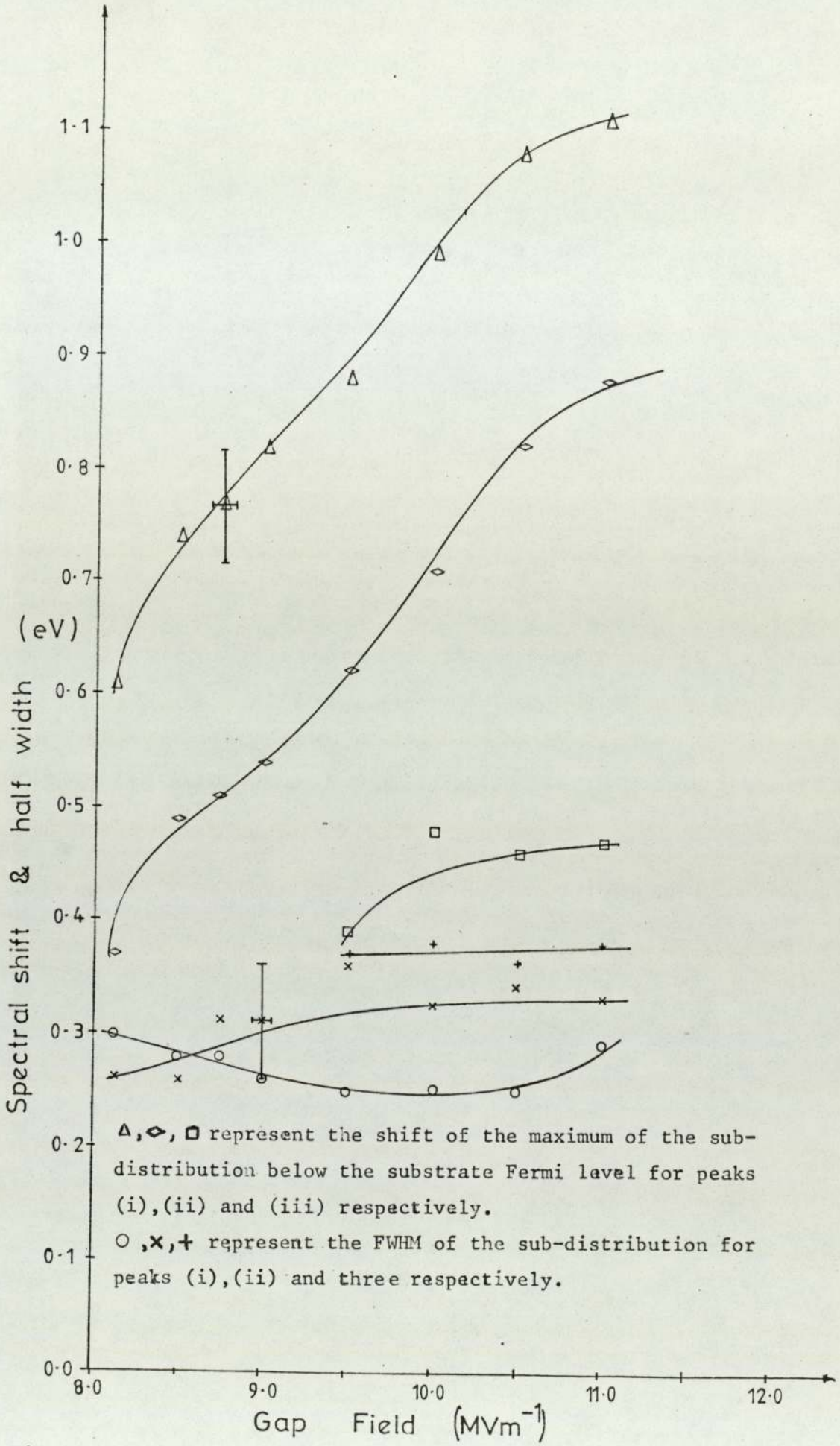

Fig. 5.19(a) Variation of the spectral shift and half-width with applied field for the individual sub-distributions contained in the electron spectra from site 3B.

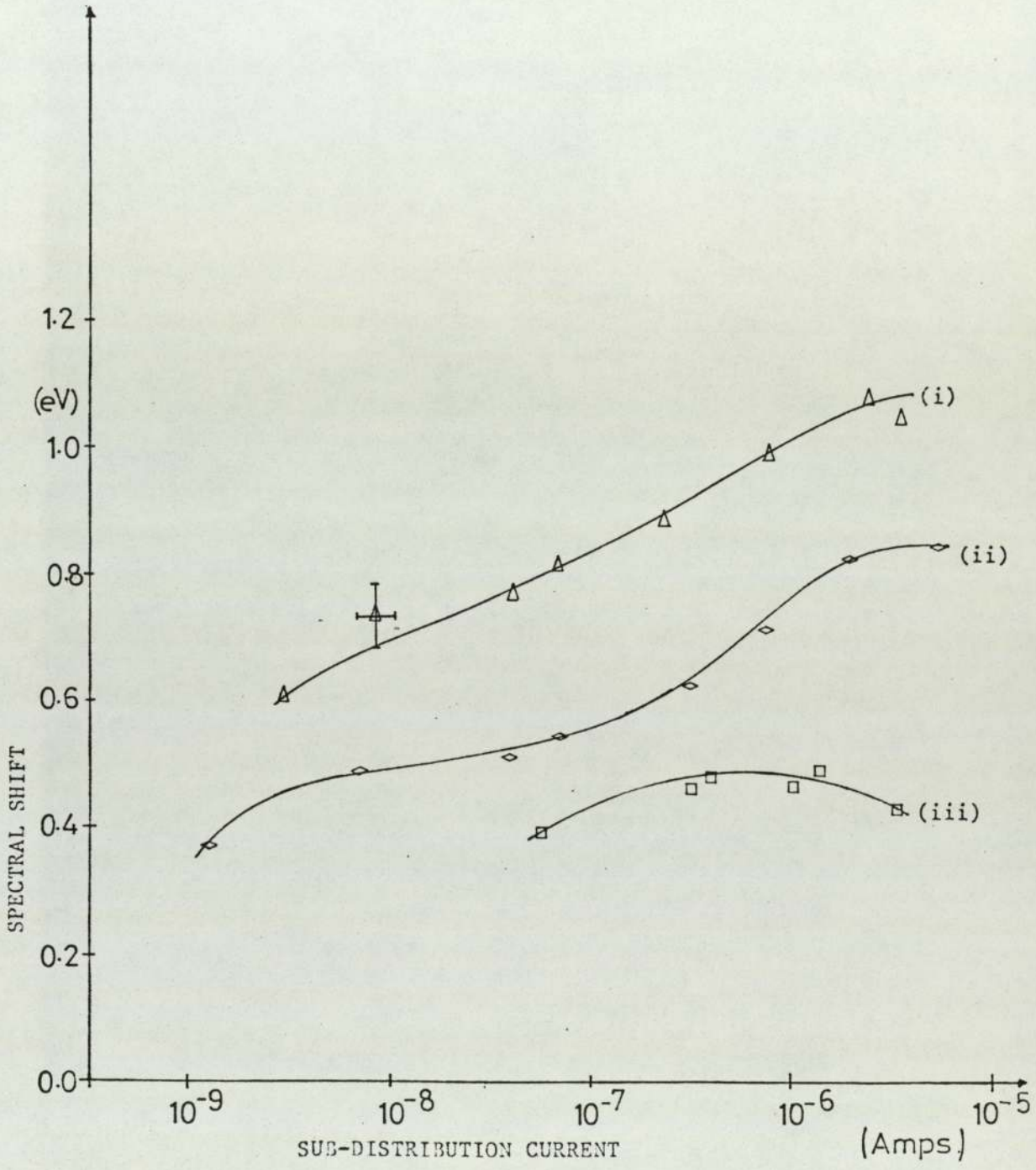

Fig. 5.19(b) Variation of the spectral shift with the current carried in each peak contained in the energy distribution for site 3B.
Δ ,◇, □ represent the shift of the maximum of the sub-distribution below the substrate Fermi level for peaks (i), (ii) and (iii) respectively.

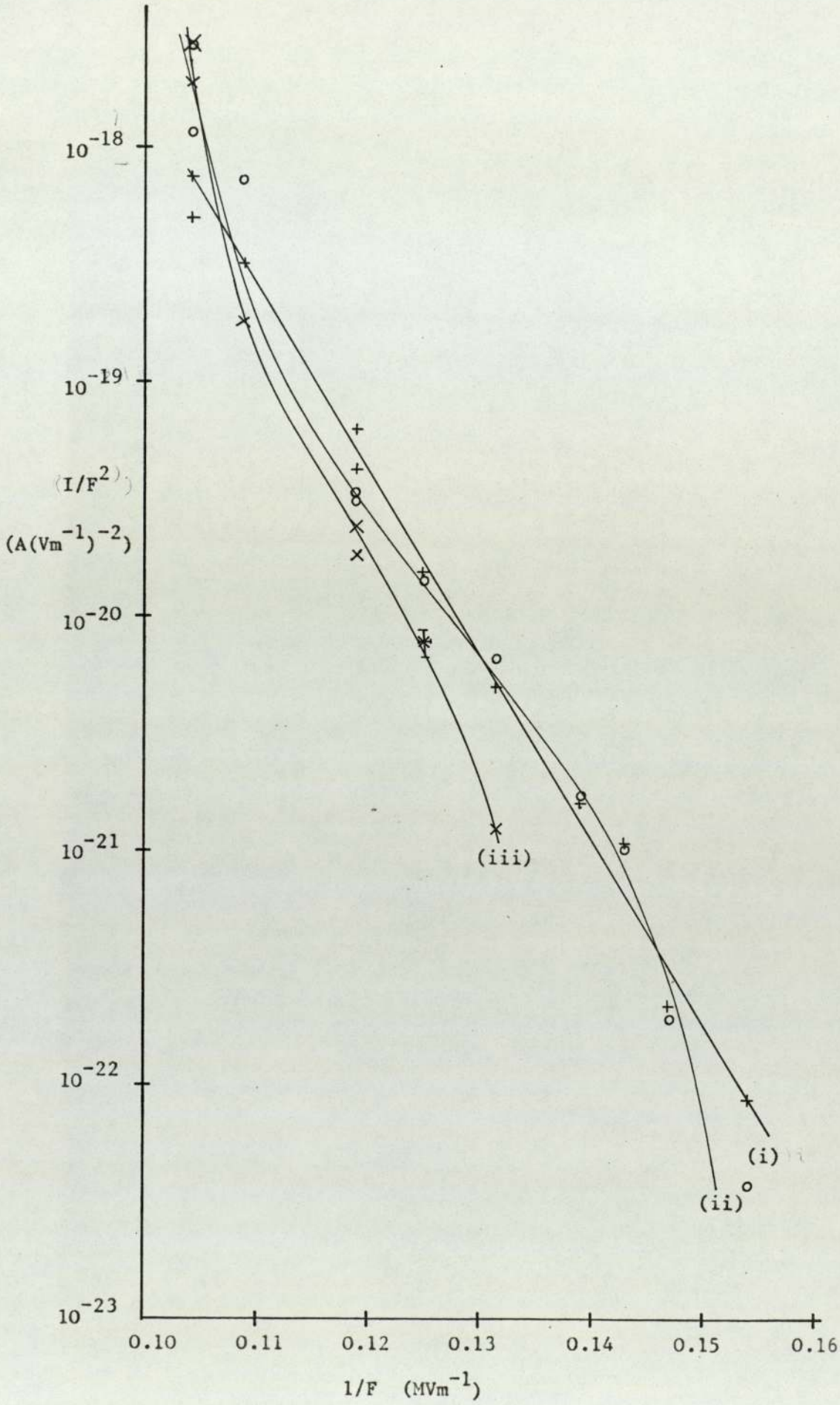

Fig. 5.19(c) The FN plots relating to the current estimated to be contained in each peak in the energy spectra from site 3B. +,o and X represent peaks (i), (ii) and (iii) respectively.

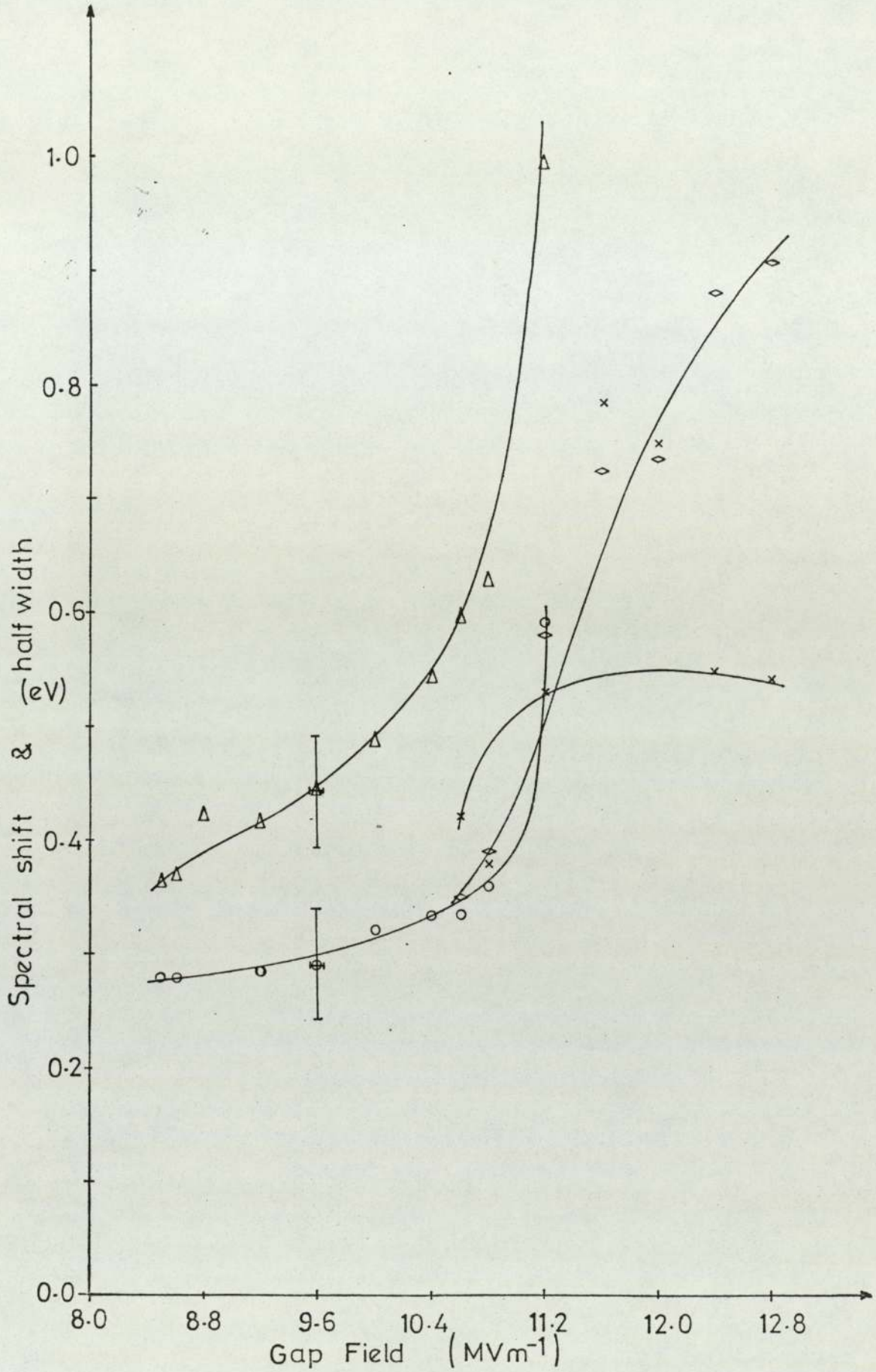

Fig. 5.20: Variation of the spectral shift and half-width with applied field for peaks (ii) and (iii) in the electron spectra from site 3A. Δ and ◇ represent the shift of the maximum of the sub-distribution below the substrate Fermi level for peaks (ii) and (iii) respectively. O and X represent the FWHM of the sub-distribution for peaks (ii) and (iii) respectively.

effect analysis that was performed for peaks (ii) and (iii) in the series of spectra from site 3A (Fig. 5.15). Unfortunately, due to the rapidly changing relative magnitudes of the two peaks, there is only a small range of overlap from which a separation of 0.30 ± 0.07eV has been deduced. However, this exercise does serve to illustrate that the variation with field of the individual peaks in multi-peaked distributions is quite similar to that of single-peaked distributions.

5.5 Other Phenomena Observed During Spectral Measurements

a) The "Switch-on" effect

This phenomenon is observed when a gradually increasing field is applied to the surface of a specimen that has not previously been exposed to high fields. It is found that the first emission does not begin at the lowest measurable current of 10^{-11}A but at a value which is often several orders of magnitude higher. Thus for specimen 1 when the field reached 24MVm^{-1} the current suddenly increased from less than 10^{-11}A to a value between 10^{-4} and 10^{-3}A, i.e. only limited by the external series resistor of 2M In contrast, as the field was decreased, continuous currents could be obtained at field values as low as 10MVm^{-1}. For specimen 2, the first current was registered at a value of 10^{-9}A for a field of 16MVm^{-1}, whilst for specimen 4 no current was recorded until the field reached a value of 18MVm^{-1} when a current of 1.4 x 10^{-6}A was suddenly obtained. When the field was subsequently reduced a current of 5 x 10^{-10}A could be obtained at 10MVm^{-1}.

b) Microdischarges

During the course of the examination of specimens 2

and 4, small breakdown events or microdischarges occurred, following which the emission from these specimen became greatly enhanced. Thus for specimen 2, 10^{-7}A could now be obtained at the much reduced field of 8MVm^{-1} compared to 20MVm^{-1} initially. Three new sites, 2B, 2C and 2D were identified, the original site 2A presumably being too faint to register any current at this low field. The three initial sites on specimen 4 together emitted 10^{-7}A at a field of 12.5MVm^{-1}, but after a microdischarge this same current was provided by two new closely spaced sites, 4D and 4E, at a field of only 7.5MVm^{-1}. It was not possible to ascertain if the original sites had been extinguished since they would not have provided significant currents at the lower field in any case.

c) Emission mode switching

During the course of studying site 1B its spectrum was seen to exhibit an unusual property whereby it switched between two well defined states with a non-uniform lifetime of a few seconds in each state. The distributions in the two states are shown in Fig. 5.21(a) for the field value of 9.6MVm^{-1}. Careful checks were made to eliminate instrumental effects, and it was also noted that micro-adjustments to the position of the specimen relative to the anode probe hole did not affect the switching behaviour, i.e. suggesting that the phenomenon was unlikely to be the result of the superposition of emission from two nearby sites. In further support of this contention, it was found that the site current for a given field during each state was different, and complete FN plots for the individual states are presented in Fig. 5.22 by the curves (1) and (2). Here it can

also be seen that the well defined two-state switching gives way to switching between several more rapidly changing current levels when the site current is greater than 5×10^{-7}A. Finally, as the field is decreased, the two-state switching disappears (curve (3) of Fig. 5.22) although instabilities are still present at high currents. The slight hysterisis in the total current from the specimen, shown in curves (4) (increasing field) and (5) (decreasing field) is fairly general for the specimens studied in this investigation. Following this sequence the switching effect was no longer produced, and the variation of the spectra with field for this site was measured to be that of Fig. 5.8.

The disappearance of the switching phenomenon seemed to be due to a conditioning effect caused either by the passage of a high current or the presence of a high electric field. Therefore, a deconditioning procedure was attempted, by applying a high positive field to the specimen surface, i.e. by reversing the polarity of the specimen gap. Thus, whilst a positive field of $9MVm^{-1}$ applied for a period of 1 minute did not appreciably affect the subsequently obtained spectrum, it was found that a higher field of $12MVm^{-1}$ applied for 5 minutes led to the recovering of a switching behaviour. At this stage a number of spectral states were observed, which were reproducible over times ranging from seconds to many minutes, and produced traces such as shown in Fig. 5.21(b), where continuous energy scans each of 10 seconds duration are superimposed for 3 minutes. The switching time between states has also been determined. A typical result is shown by the oscillo-

gram of Fig. 5.21(c) for switching between current levels of 5×10^{-8}A and 1.8×10^{-7}A, where it is apparent that the switching risetime is 0.2ms, which was checked to be independent of circuit components. If a current of $> 10^{-6}$A is drawn from the site (corresponding to a total specimen current of $> 5 \times 10^{-5}$A) the switching behaviour is eliminated, but it could always be regained by the deconditioning procedure described above.

d) Anomalous Spectra

The unusual spectrum of Fig. 5.23(a) was recorded from site 1A at the maximum gain of the signal measuring system for a gap field of $6.8 MVm^{-1}$ and a site current of 4.3×10^{-10}A. The spectrum which is abnormally close to the Fermi level and displays several peaks and shoulders was exactly reproducible over a period of several hours on the day. As the field was increased the distribution gradually smoothed out as shown in Fig. 5.23(b) for a field of $7.4 MVm^{-1}$ (site current 3×10^{-9}A). However when the measurement was repeated after a lapse of two days the multi-humped spectrum could not be reproduced, and the single peaked spectra whose characteristics have been plotted in Fig. 5.7 were obtained.

Site 4A also presented an anomalous spectrum, whose shape varied as the position of the site was changed with respect to the anode probe hole. Such a manipulation normally only changes the magnitude of the signal, but in this case a displacement of 0.28mm caused the double peaked spectrum of Fig.5.24(a) to vary continuously into the single peak of Fig. 5.24(b); the latter is obtained by increasing the signal gain by a factor of 7. This effect was

Fig. 5.21 Emission Mode Switching Behaviour.

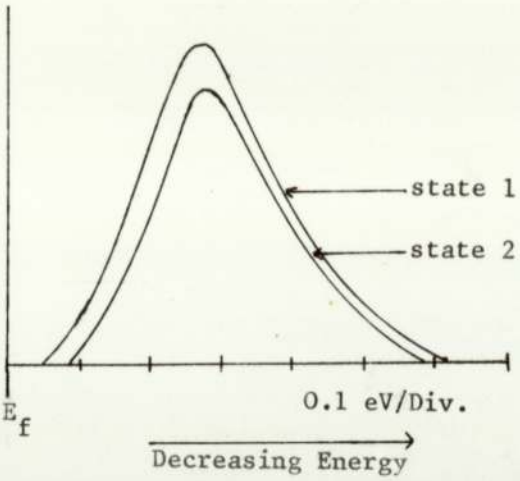

(a) Spectra of emission mode switching between two regular states at a gap field of 9.6 MVm^{-1}.

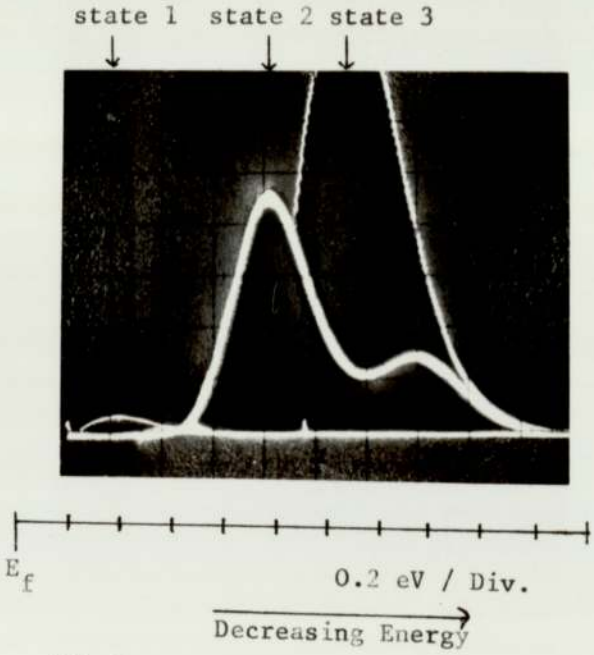

(b) Spectra of switching states at a gap field of 9.9 MVm^{-1} after deconditioning. Lifetimes: state 1 - 20 s , state 2 - 90 s , state 3 - 5 s .

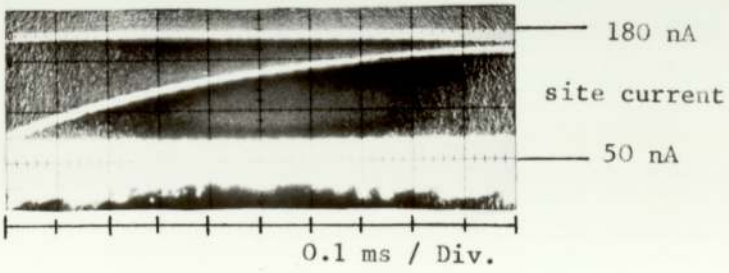

(c) Oscillogram showing switching transient.

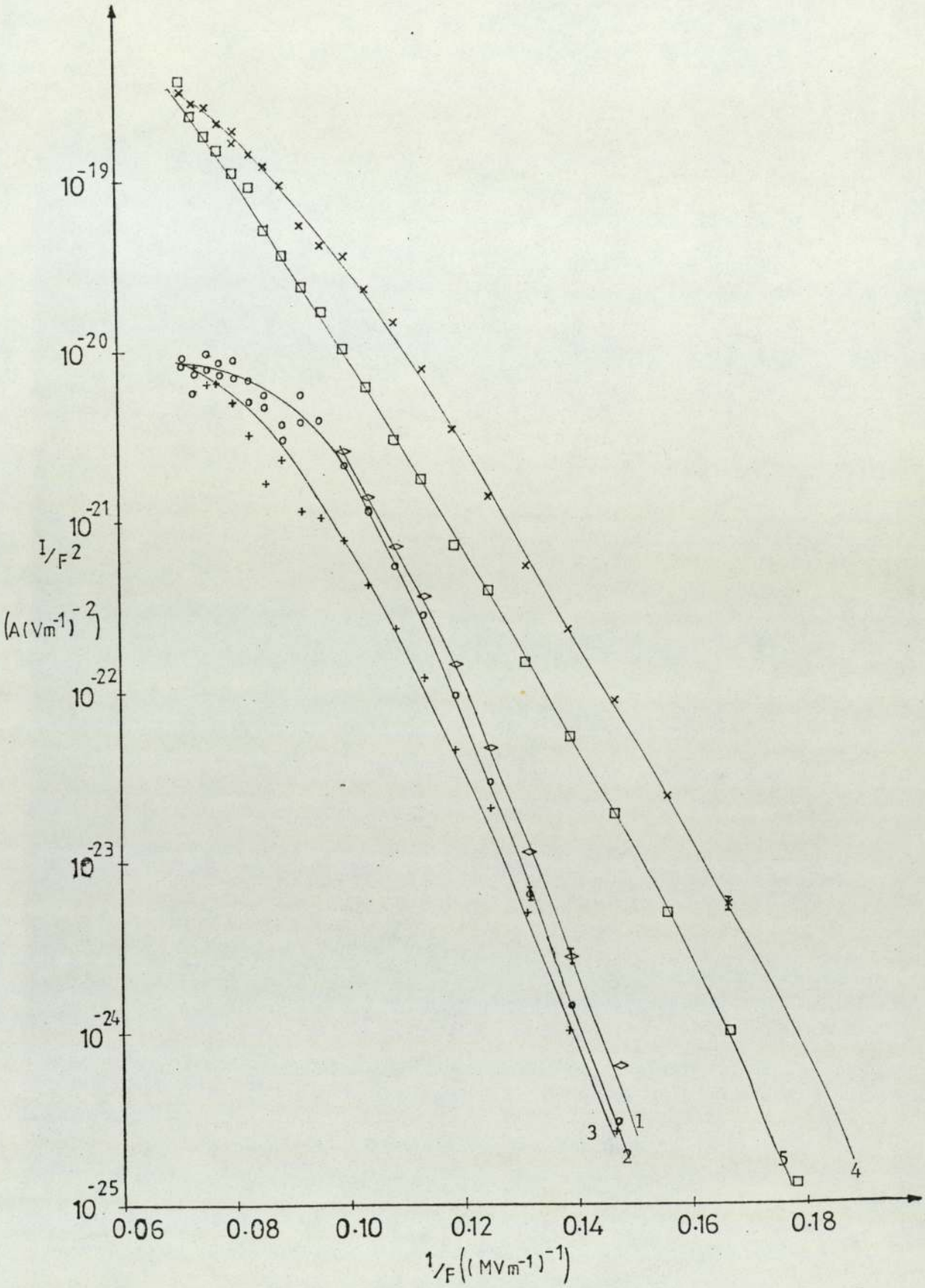

Fig. 5.22: Fowler Nordheim plots for site 1B and concurrently for the total current from specimen 1: ◇ (1) and O (2) - the two switching states of site 1B, +(3) - non-switching state of site 1B obtained after passing a high current; x (4) and □ (5) - total current charactertistics from specimen 1 for increasing and decreasing fields respectively.

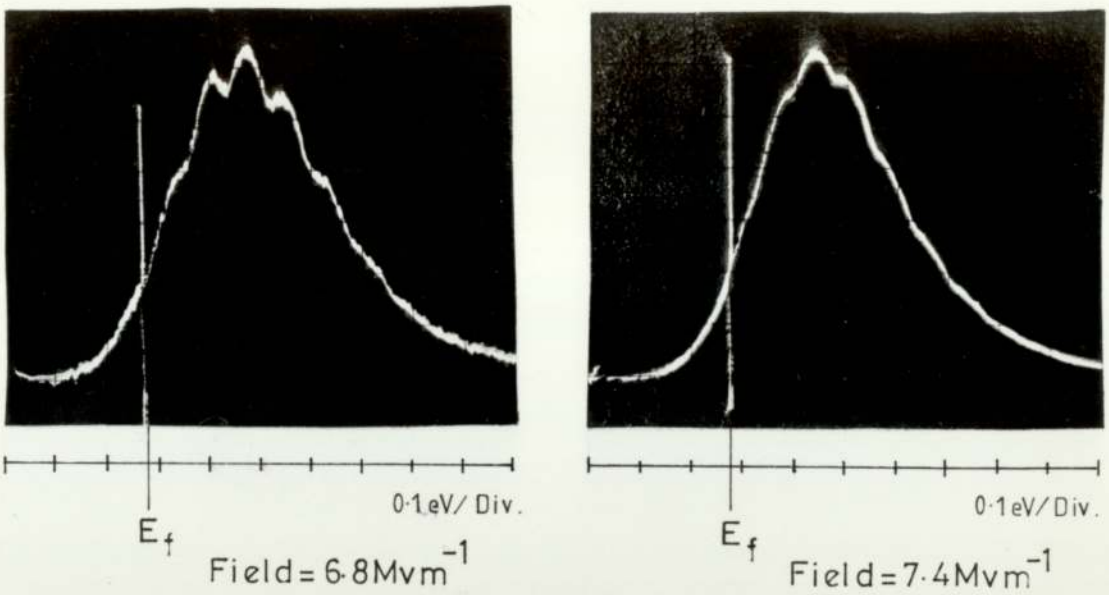

Fig. 5.23 Anomalous spectra for site 1A

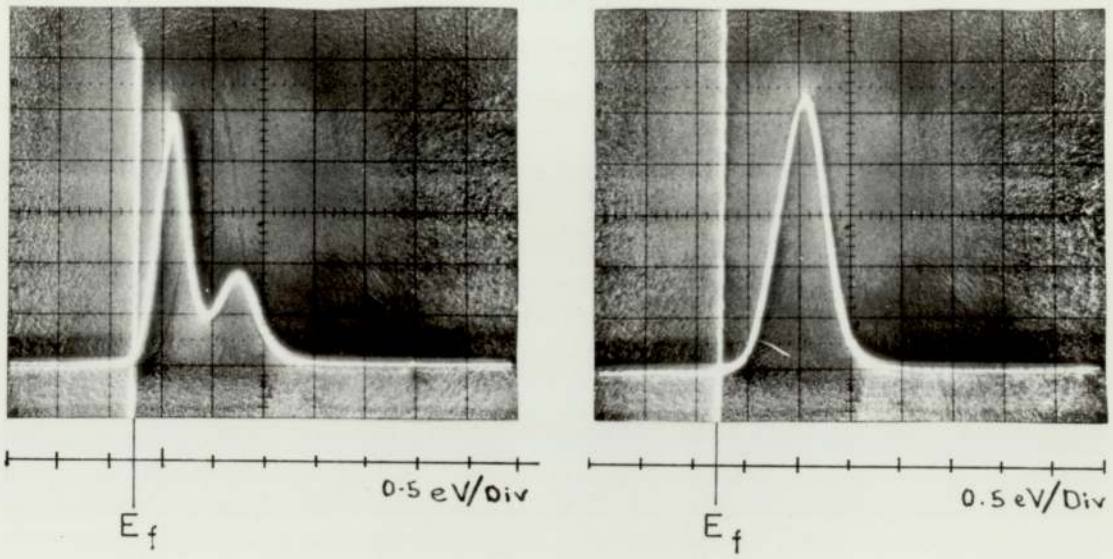

Fig. 5.24 Spectra for site 4A at a field of 13Mvm^{-1}, showing the effect of translating the specimen by 0·28 mm in front of the anode probe hole.

In both figs. 5.23 & 5.24 the position of the emitter Fermi level is marked.

also observed at one stage (see Fig. 5.31) during the etching experiments discussed in section 5.6(a).

e) F N plots

A summary of the plots associated with the various sites and electrode gaps already discussed are presented in Figs. 5.5, 5.22, 5.25, 5.26, 5.33 and 5.36 where the last two are for ion bombarded gaps (see section 5.6). They are generally remarkable for their non-linearity; most curves being only slightly convex at lower currents ($\lesssim 10^{-7}$A), but the individual site current curves especially depart strongly from the Fowler Nordheim Law at higher currents. These effects are due to the current not increasing with field as rapidly as predicted by the Fowler Nordheim equation. By drawing best fit straight lines through the points before the onset of marked departure, geometrical field enhancement facts, β, are calculated to be between 200 and 500.

5.6 Surface Treatment

Two facilities have been incorporated within the specimen chamber for the in situ surface treatment of specimens; namely a) electron bombardment for heating and outgassing and b) ion bombardment for etching.

a) Electron Bombardment

This is achieved by means of a tungsten filament situated behind the specimen assembly, as illustrated in Fig. 5.27, and has been used routinely for outgassing the specimen. This procedure involves applying a positive voltage of $\sim$ 1kV on the specimen so that electrons which are thermionically emitted from the filament will bombard the back of the specimen and its holder. Typically, with

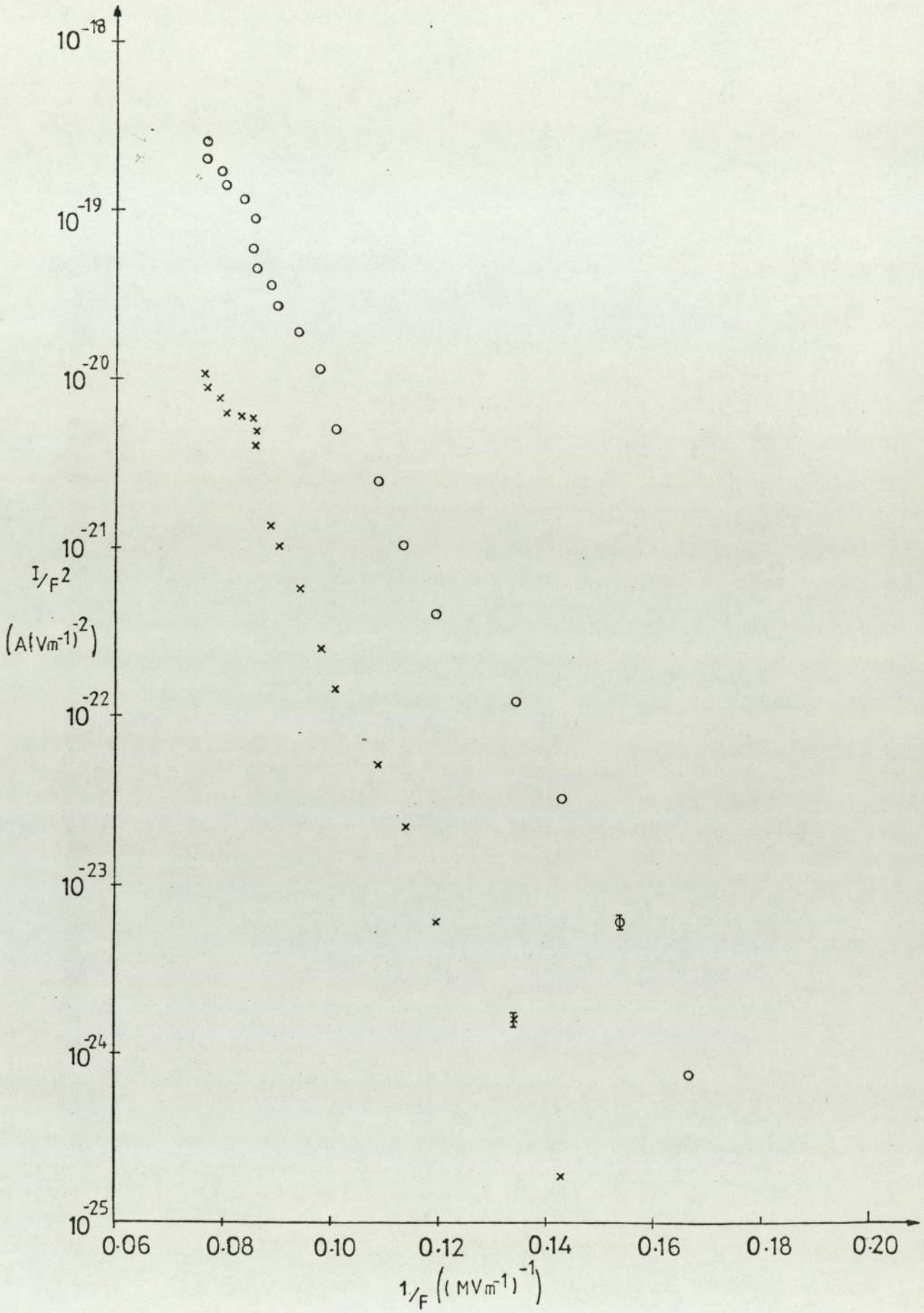

Fig. 5.25: Fowler Nordheim plots for site 1A(X) and concurrently for the total current from specimen 1(O).

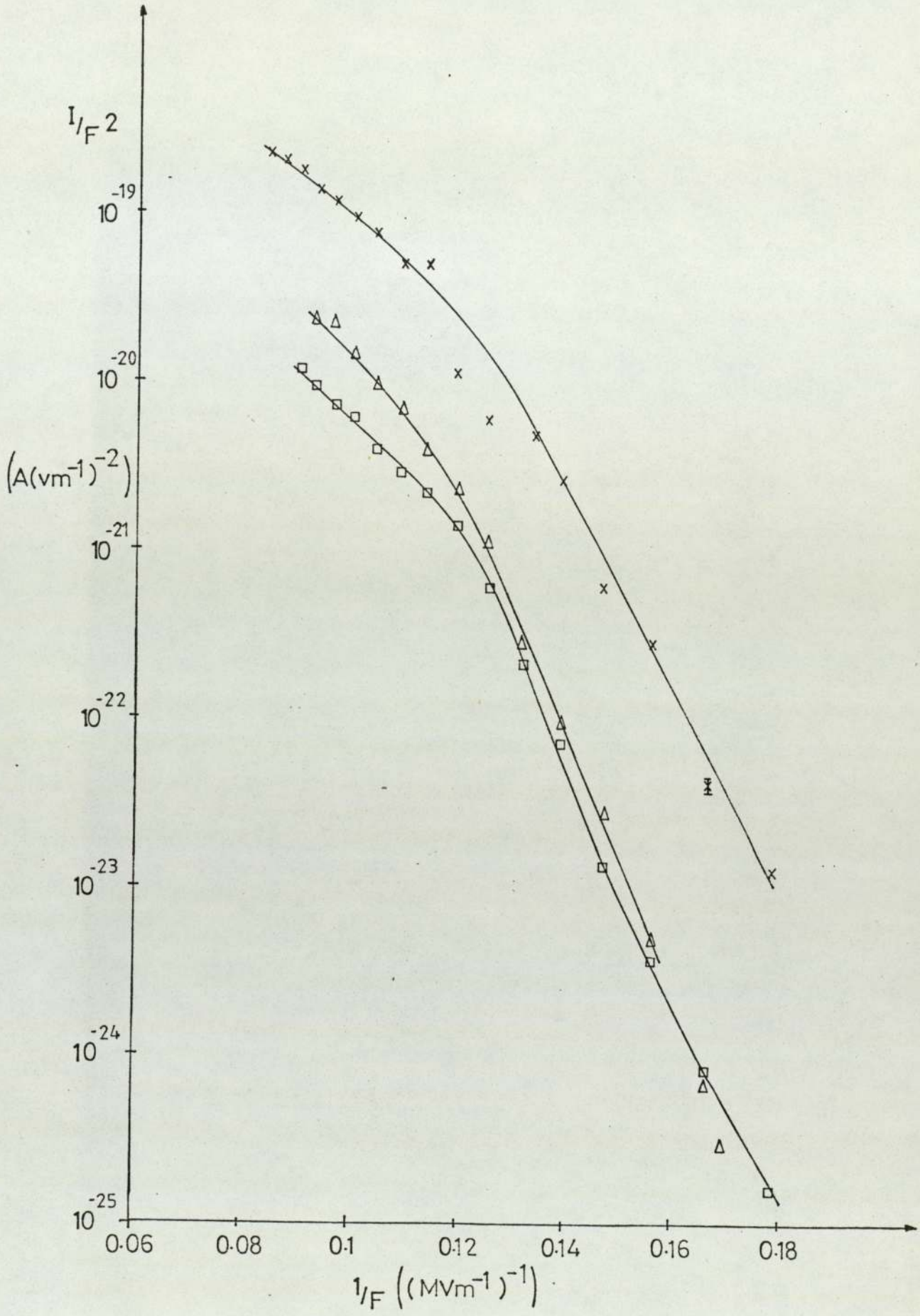

Fig. 5.26: Fowler Nordheim plots for sites 4D (□), 4E (Δ) and the total current from specimen 4 (X).

an electron beam current of 50mA, i.e. 5W of power, the specimen is heated to dull red heat in two minutes. Outgassing of the specimen has also been employed with a measure of success as a means of increasing the stability of the electron emission, both as reflected in the current and the spectra. However, comparisons of electrons spectra before and after outgassing do not show consistent characteristics. Sometimes secondary peaks are removed by outgassing, (e.g. Fig. 5.30) whilst on another specimen an additional peak may appear after the same treatment. Often no dramatic change in the spectrum is observed after such a treatment.

b) Ion Bombardment

A spherical saddle-field ion source, as described by Franks,[102] has been positioned within the spectrometer vacuum system, such that the emerging beam will bombard the specimen when it is rotated to be at right angles to the anode, as in Fig. 5.27. A gas inlet system, see Fig. 5.28, comprising a leak valve and ancillary vacuum system capable of maintaining a pressure of $\sim 10^{-3}$ torr has been set up. By these means it is possible to ensure that the bombarding gas is substantially free from contamination by air, and also to enable particularly low leak rates to be maintained. The characteristics of the ion source have been measured and found to be typically as described by Franks and Ghander[103]. It is noted that sensitive control of the gas pressure and energy of the ions will achieve a wide range of etching rates.

The spread and intensity of the ion beam at the position of the specimen has been measured by replacing the specimen

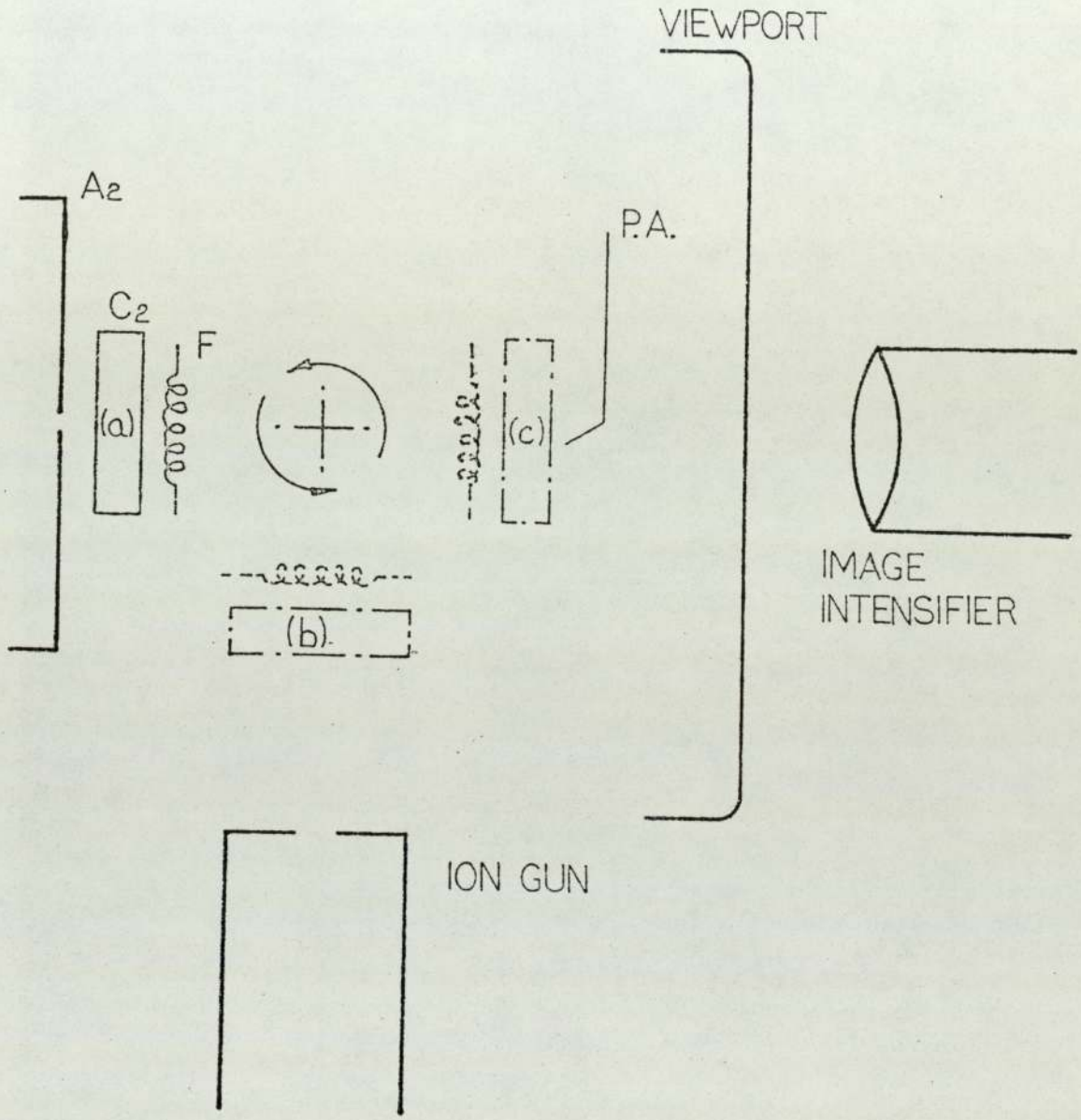

Fig. 5.27: The positions of the specimen and filament for (a) obtaining electron spectra, (b) surface treatment and (c) obtaining optical spectra.

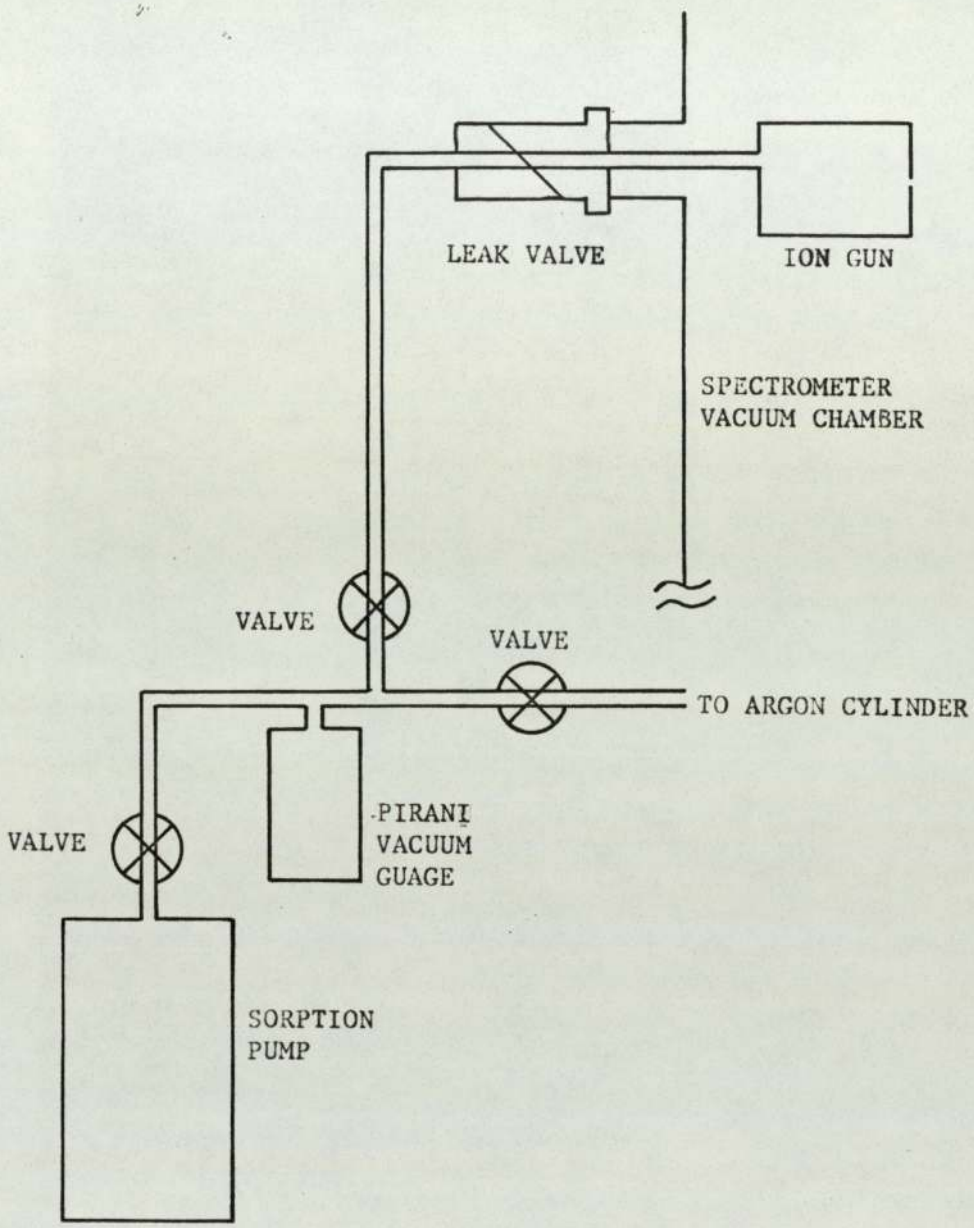

Fig. 5.28 The gas inlet system for the ion gun.

Fig. 5.29: A - original specimen holder. B - specimen holder for ion etching.

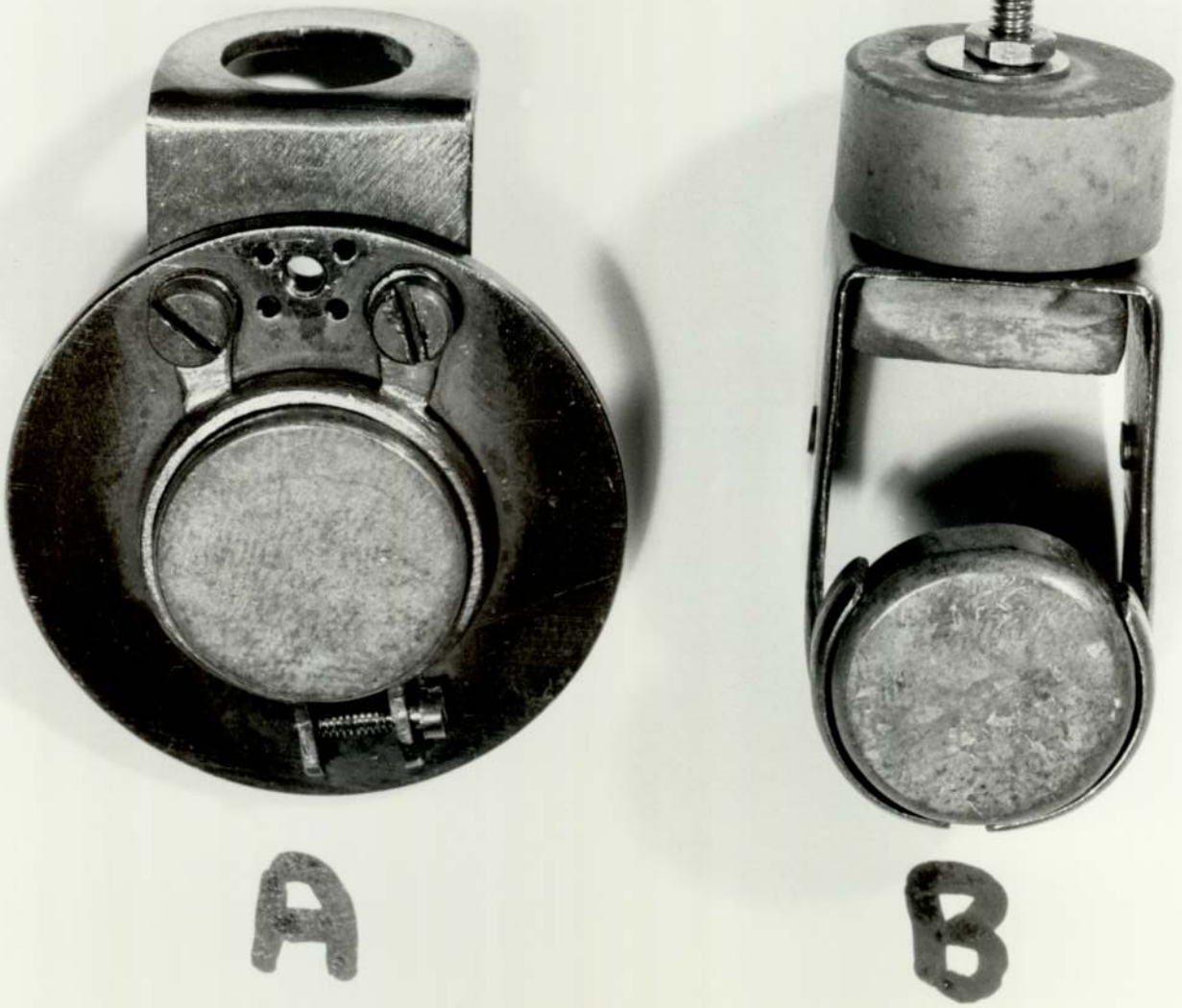
A
B

by a small (1 mm square) probe, which can be moved around in the beam. This technique has verified that a fairly uniform (< 50% variation) beam intensity will strike the 14 mm diameter specimen when it is correctly centralised, i.e. the position where it obtains maximum current. However, it proved difficult to centralise the specimen and measure the current falling on it when using the original holder (see Fig. 5.29(a)), since a large proporation of the ion current can be expected to be collected on the holder. Accordingly a new holder (Fig. 5.29(b)) has been designed such that only a minimal area was displayed to the ion beam.

The etching rate of the ion beam may be calculated from the value of the sputtering yield which is approximately 5 atoms per ion for copper bombarded by argon ions in the energy interval of 2 to 5 keV,[104] such as has been employed in this investigation. Calculation then shows that for a beam of 1μA striking the specimen surface (area 150 mm^2) 100nm of copper are etched per hour. However this value must be treated with caution because the current measured on the specimen is not an accurate indicator of the number of high energy gas particles (ions and neutral atoms) reaching the surface. In fact Fitch et.al.[105] have shown that the beam from an electrostatic spherical ion source contains significant proportions of neutrals, and multiply charged ions, in addition, other effects may also occur such as ion reflection without loss of charge and emission of secondary electrons. A further point to bear in mind is that the initial etching will have to remove the ambient oxide film.

If it is assumed that an electron emitting site is associated with an insulator type impurity, then the etching rate for the impurity will in general be different from that of the metal. Sputtering yields for insulators have been measured by Davidse and Maissel[106] for 2 to 3 keV argon ions and are found to be 0.1 molecules per ion for aluminium oxide and between 0.3 and 0.5 molecules per ion for glass. These values were measured for extended area surfaces and using an r.f. ion source which produces a beam containing less than 2% of neutrals. Therefore, when considering the high percentage of neutrals (20 to 70% depending on precise operating conditions) present in the beam from an electrostatic spherical ion source, etching of insulators may be expected to be enhanced. Further, since the actual compositions of an electron emitting impurity is, in general, unknown, it appears reasonable to assume an etching rate for the impurity to be 1/5 of that for copper, i.e. 1μA sputters 20nm per hour.

A preliminary experiment on the effects of etching was carried out on a polished OFHC copper specimen which had previously been shown to contain one emitting site having a typical electron spectrum. The specimen was subsequently bombarded with a 4keV argon ion beam at a current of 15mA for 40 minutes, i.e. corresponding to an etching depth of around 0.1μm in copper and possibly 200nm in an insulator. Following this treatment the emission in the gap was slightly reduced such that a current of 1μA now required a field of $14MVm^{-1}$ as opposed to $12MVm^{-1}$ before etching. Subsequent location of the emitting sites revealed that the original site had disappeared, whilst a new one was found well away

from it.

A more extensive study was carried out on a new polished specimen. One site 5A was originally found on this specimen and its energy distribution is shown in Fig. 5.30(a). It was noted that the shape of the distribution, and in particular the relative magnitudes of the two peaks did not change when small adjustments were made to the position of the specimen with respect to the probe hole in the anode. The specimen was outgassed as described in section (a), and then the energy distribution was found to have changed to that shown in Fig. 5.30(b), i.e. the secondary peak had been removed. The specimen was then bombarded with argon ions at 500eV and a current of 0.2μA for 10 minutes, i.e. an etching depth in copper of a few angstroms. No new sites were created but the energy distribution from the original site became substantially more unstable, with secondary peaks of a transitory nature appearing on either or both sides of the main distribution. In this case, during periods of stability, the relative magnitude of the various peaks depended on the position of the specimen with respect to the anode probe hole, see Fig. 5.31. After leaving the specimen in ultra-high vacuum for five days, the energy distribution was found to have become more stable and the influence of the applied field on the spectrum was measured as outlined in section 5.2 and is presented in Fig. 5.32 where the different peaks which dominated the spectrum as the field was increased are indicated. In this case it was noted that the focussing of the input lenses of the spectrometer was not critical; indeed all the spectra were obtained without need to adjust the lens settings. F-N plots for

this site and the total gap are presented in Fig. 5.33 by the curves (a) and (b).

The same specimen was further treated with a 2 keV argon beam, supplying a specimen current of 5μA for 10 minutes, i.e. a theoretical etching depth of approximately 100nm in copper. The original site (5A) was found to be still emitting, although requiring a higher field but now two new emitting sites were identified. The variation of the spectrum with field was again measured for site 5A and is shown in Fig. 5.34(a). It was now found that the magnitude of the distribution was very sensitive to the focussing of the spectrometer input lenses. However, when the character of the spectrum was checked the following day this sensitivity had disappeared. Spectral measurements were therefore taken over a greater range of field, and are presented in Fig. 5.34(b), whilst the corresponding F N plots are shown by curves (c) and (d) in Fig. 5.33. The two new sites (5B and 5C) exhibited a spectral behaviour similar to that of sites 2B and 3A discussed in section 5.4(b), where new peaks appeared on the high energy side and grew to dominate the spectrum as the field was increased. Three spectra from each site are presented in Fig. 5.35 and the respective FN plots in Fig. 5.36.

A further etching experiment was carried out on the single-crystal copper specimen, which was in the state discussed in section 5.5, i.e. containing the two closely spaced sites 4D and 4E that appeared after a microdischarge. This specimen was bombarded with a 4keV argon beam giving 14μA of current for 90 minutes, i.e. realising a theoretical etching depth of around 0.2 μm in copper. It was found that whilst

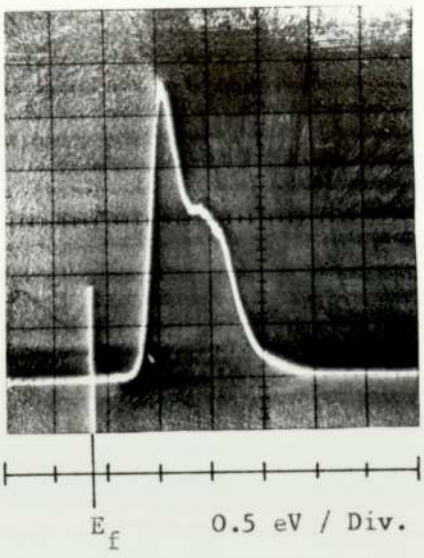

(a) No Treatment

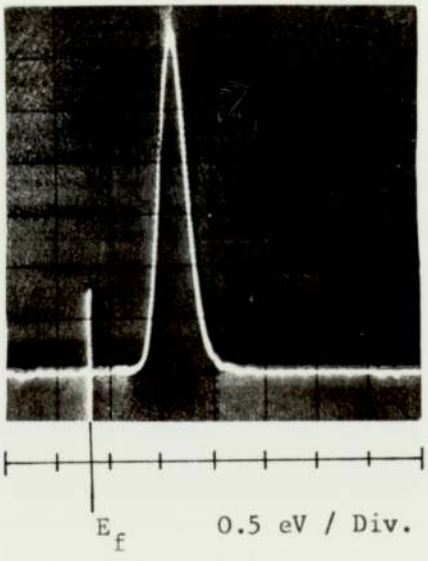

(b) After Outgassing

Fig.5.30 Spectra from site 5A showing the effect of outgassing.

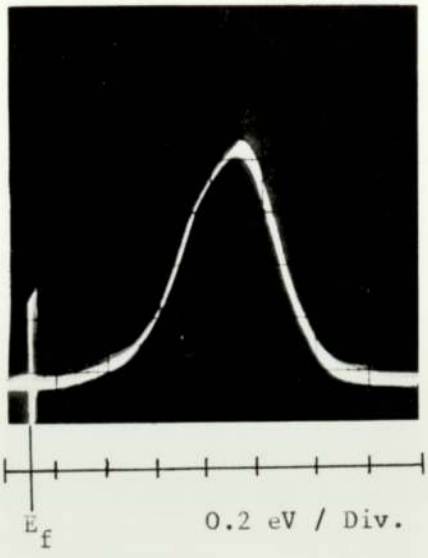

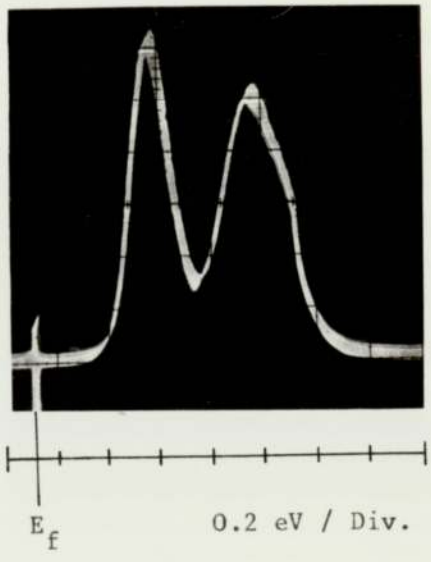

Fig.5.31 Spectra from site 5A after first ion etching treatment showing the effect of translating the specimen by 0.11 mm with respect to the anode probe hole.

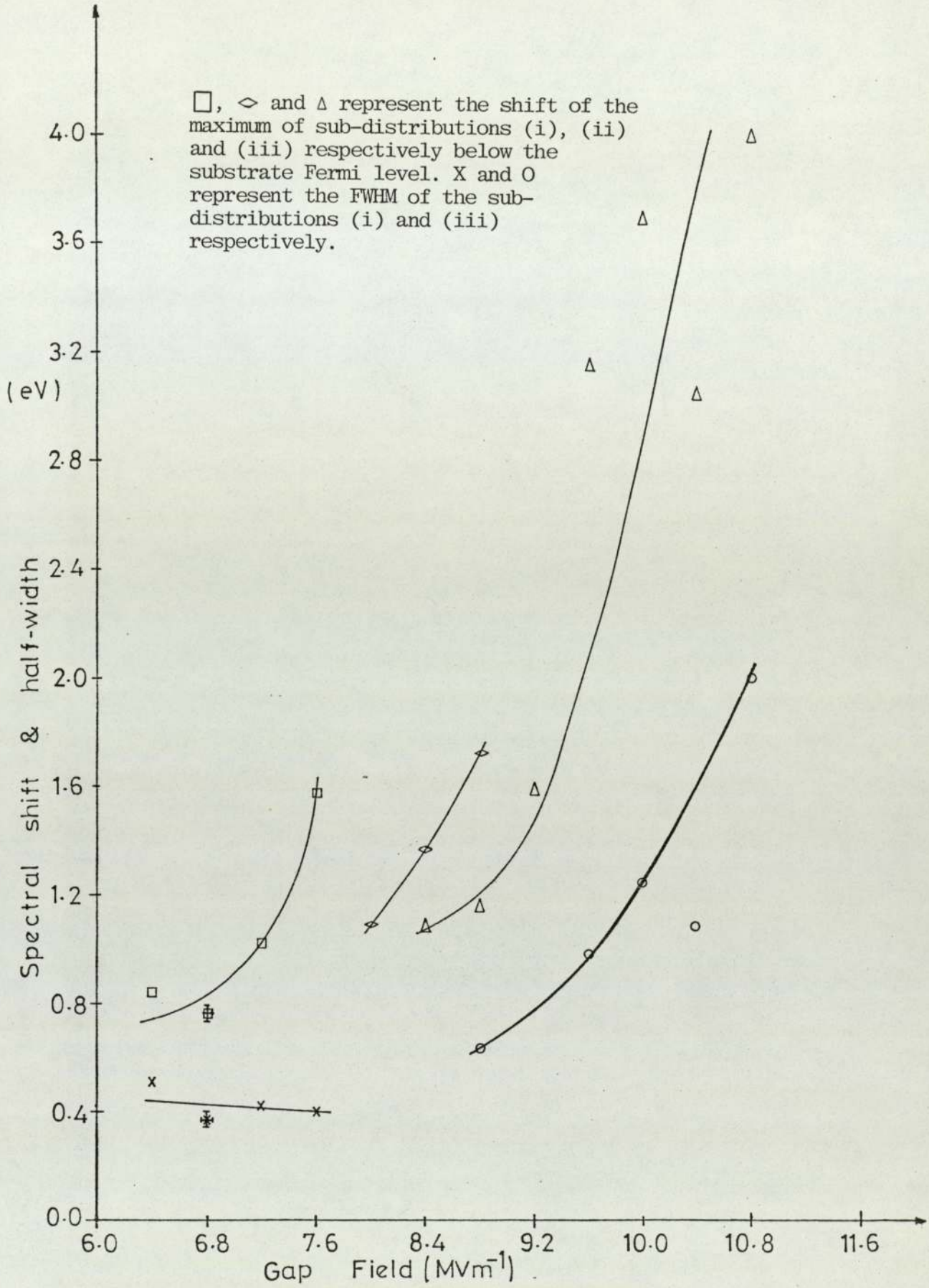

Fig. 5.32: Variation of the spectral shift and half-width with the applied field for the dominant peaks in the energy distribution for site 5A after bombardment with argon ions at 500 eV and a current of 0.2 μA for 10 minutes.

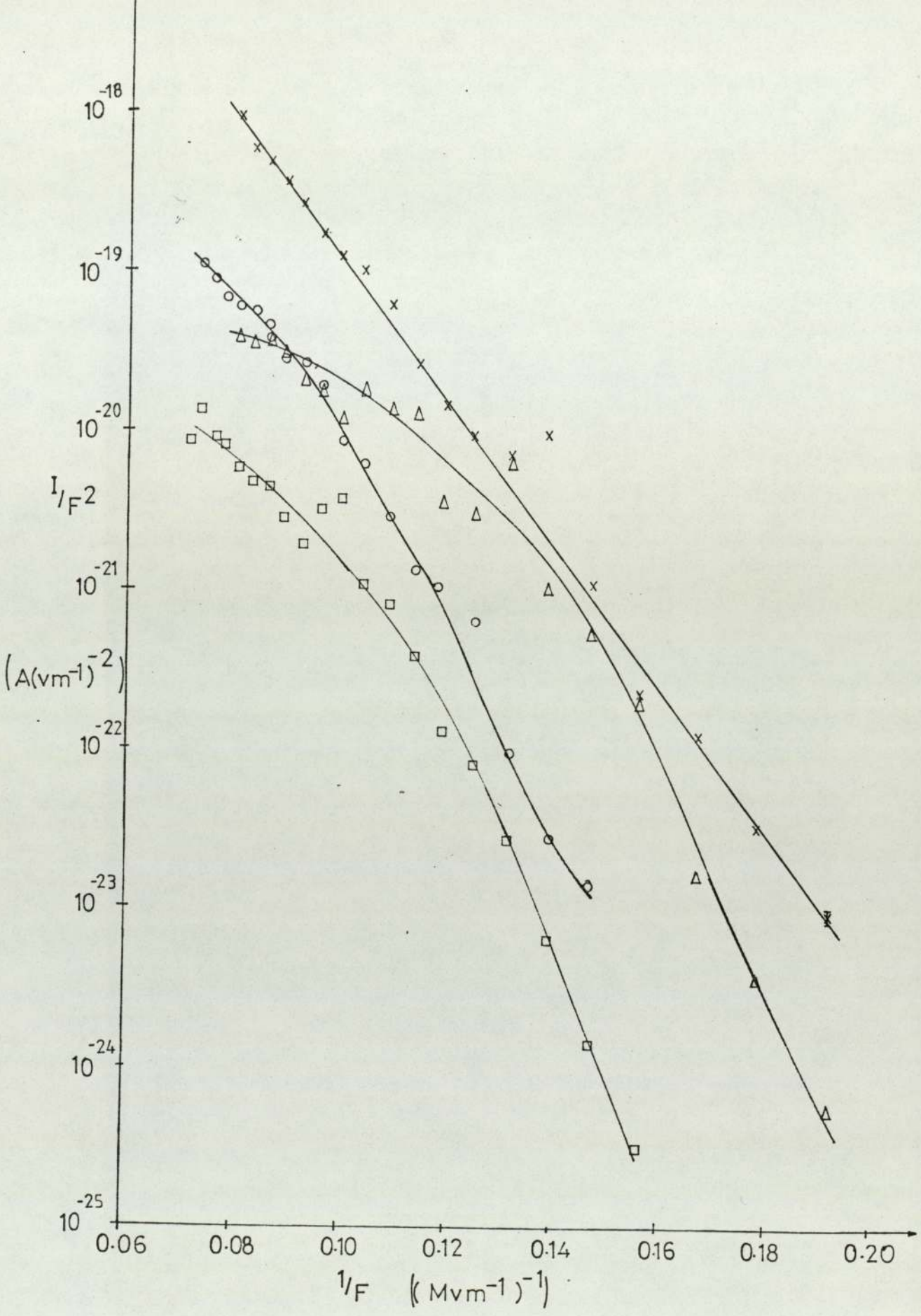

Fig. 5.33: Fowler Nordheim plots from site 5A. Δ and X represent the currents from the site and the whole specimen respectively after argon ion bombardment at 500 eV and 0.2 μA for 10 minutes. □ and O represent the currents from the site and the whole speciment respectively after further argon ion bombardment at 2 keV and 5 μA for 10 minutes.

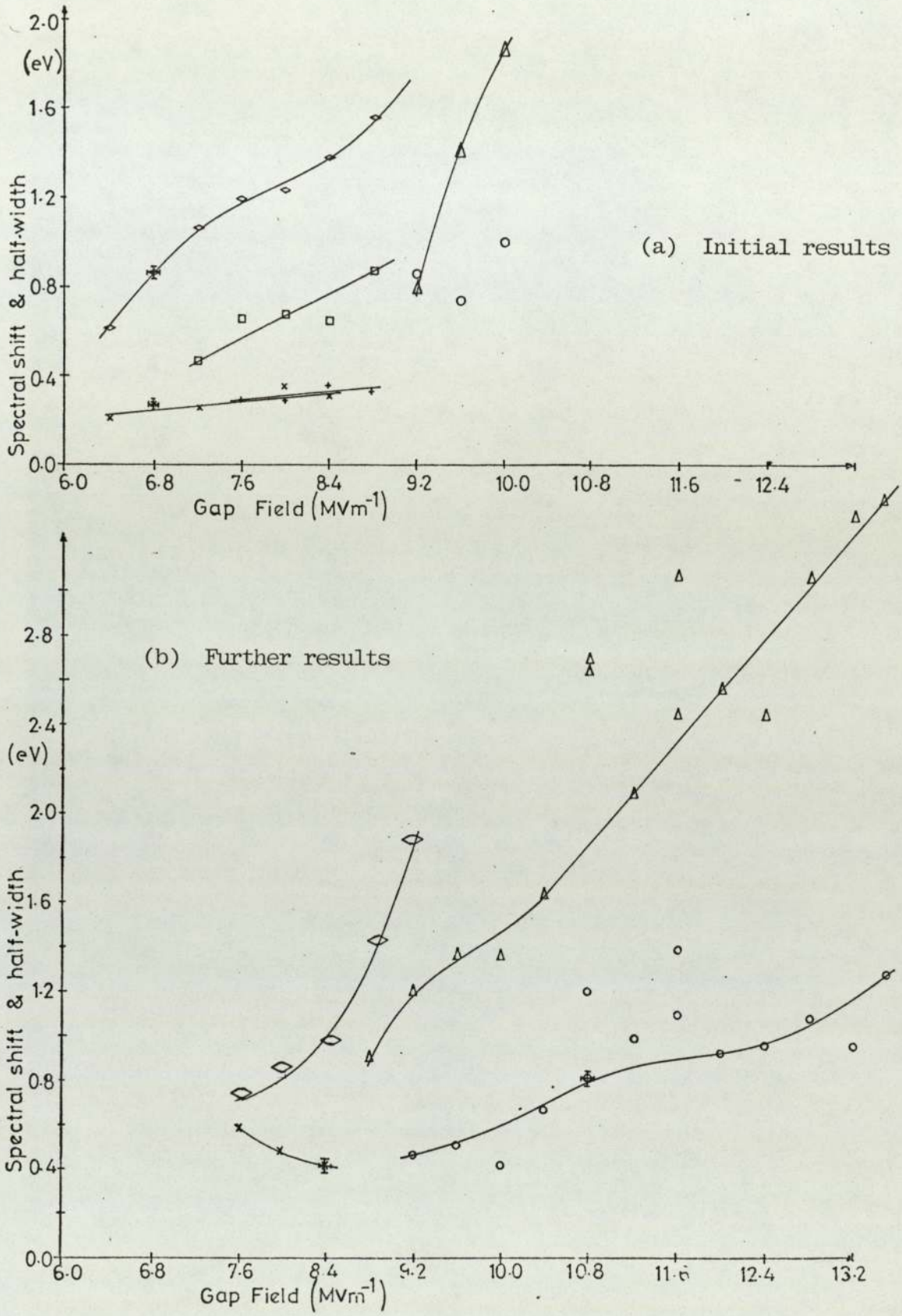

Fig. 5.34: Variation of the spectral shift and half-width with applied field for the dominant peaks in the energy distribution from site 5A after further argon ion bombardment at 2 keV and 5 μA for 10 minutes. ◇, □ and △ represent the shift of sub-distributions (i), (ii) and (iii) respectively below the substrate Fermi level. X, + and O represent the FWHM of sub-distributions (i), (ii) and (iii) respectively.

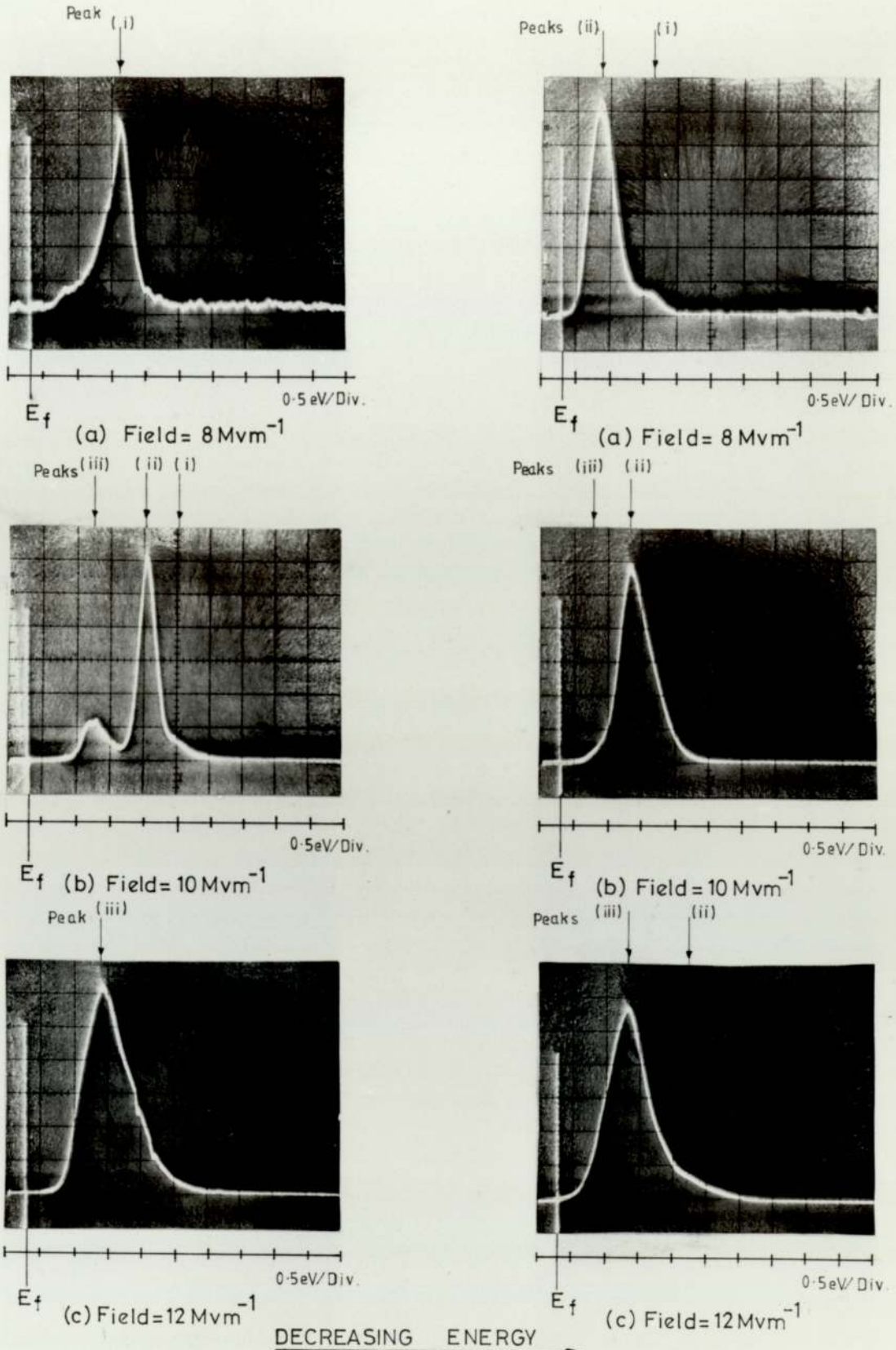

Fig. 5.35 Series of spectra with increasing field for sites 5B & 5C. The position of emitter Fermi level is shown. Electron energy decreasing from left to right is X-axis. Electron current per unit energy (arbitrarily normalised) is Y-axis.

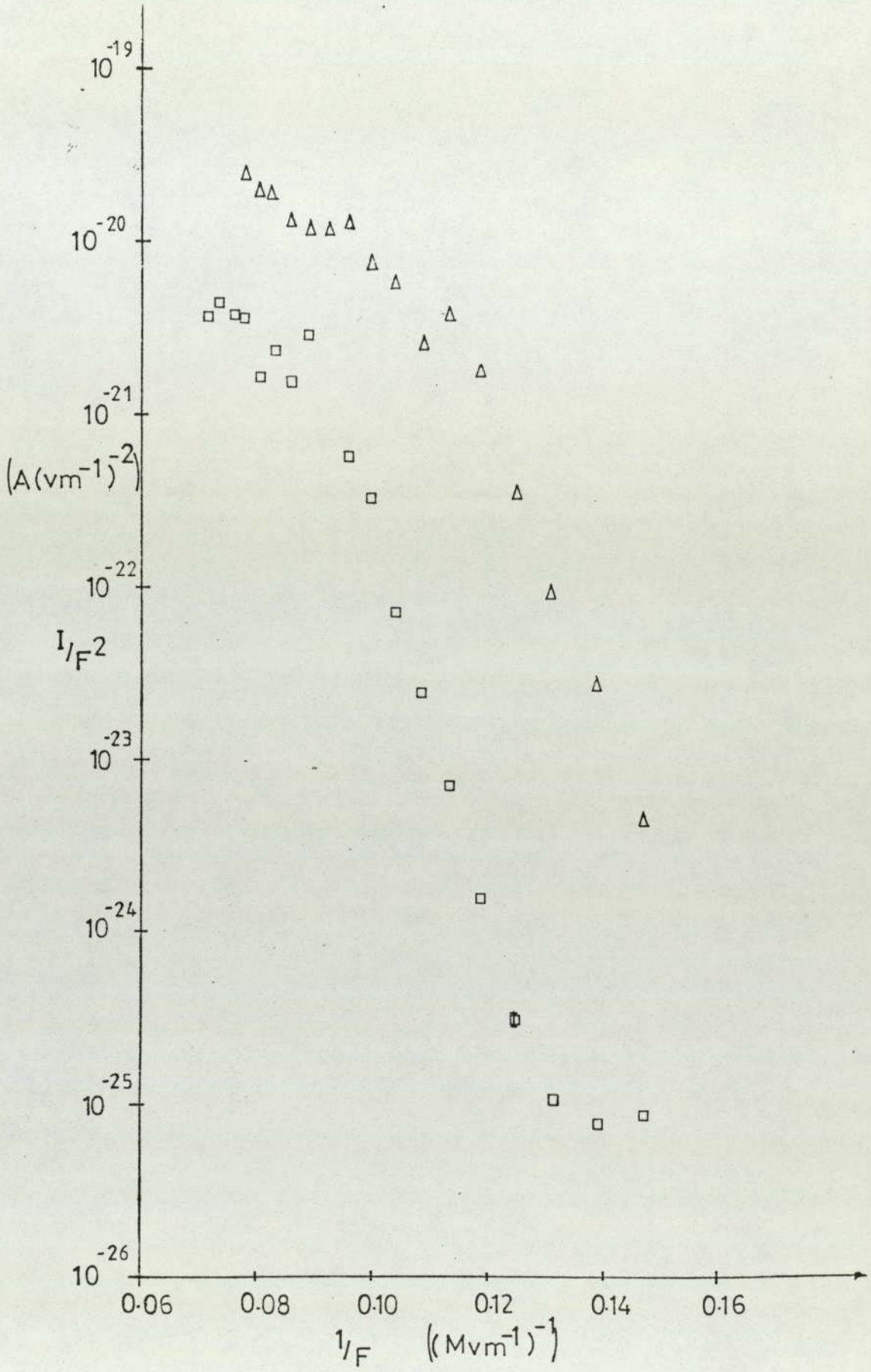

Fig. 5.36: Fowler-Nordheim plots for sites 5B (□) and 5C (△).

site E disappeared site D was left unaffected with emission characteristics that were substantially unchanged. It should, however, be borne in mind that this site was believed to be right on the edge and possible on the side of the specimen where the etching rate may reasonably be expected to be diminished.

5.7 The Effects of Heating and Illumination

a) Heating

The specimen was heated either by electron bombardment (see section 5.6a) or a high-wattage focussed projector lamp through a lens and viewport so that its image fell completely on the back of the specimen holder. The former method allowed the highest temperatures to be reached ($\sim 700^{o}C$) whilst the latter method enabled the heating to be better controlled. Then, by setting the scan speed at 30 seconds, successive spectra could be obtained whilst the specimen cooled, see Fig. 5.37. An extensive number of measurements of this type were taken, but the interpretation of the results was confused by expansion effects, which not only lead to a reduction of the interelectrode gap, and hence an increase in the field, but also a displacement of the emitting site away from its optimum position with respect ot the anode probe hole. Clearly the latter displacement is a linear function of the distance of the site from the centre of the specimen. Working back from the displacement, the temperature of the specimen and the change in the interelectrode gap may be estimated. Calculations of this nature and consideration of the variation of the spectra with field have led to the conclusion that the electron energy spectrum is independent of temperature in the range of 300 to 800K, within an uncertainty of $\sim$80meV.

b) Illumination

Since illumination of the whole chamber could cause heating and expansion of the specimen, a mirror was positioned in the vacuum chamber so that a fine beam of light from a projector lamp or a laser could be reflected into the gap. Even when light was directed onto a site which was right on the edge of the specimen, no complementary effect was recorded in the electron spectrum which was being concurrently recorded. The surface flux of radiation on this site has been calculated to be $\sim 10^{5} Wm^{-2}$, and it is concluded that the electron energy spectrum is independent of illumination below this value.

5.8 Optical Measurements.

Hurley and co-workers [42, 48, 107] have demonstrated that light is also emitted from electron emission sites on broad area electrodes. Furthermore they have identified this light as being due to an electroluminescence phenomenon, and then optical spectra measurements provide an additional means of characterising the emission sites. Accordingly, it would clearly be desirable to obtain complementary measurements of the optical and electron spectra from a particular site since such information should lead to a fuller understanding of its nature. Therefore as a first approach, a copper specimen was specially designed so that it could be transferred on a collaborative basis between the Hurley optical spectrometer and the Aston electron spectrometer. However, due to problems of contamination in transit and fitting, and the difficulty in defining precise fiducial reference points, it was decided that a more convenient method would be to establish the optical experiment in situ in the vacuum system of the Aston

spectrometer. Accordingly, the system of Fig.5.39 was set up, and is closely analogous to that described by Hurley[48], with the exception that the specimen is scanned in front of a stationary anode probe, rather than vice versa. This optical analysis technique was originally developed by Young[108] for studying anode spots.

Referring to Figs. 5.27 and 5.39 the experimental procedure is as follows. After obtaining the electron spectra of a site, the specimen is moved back from the planar anode and rotated through 180° to face a pointed tungsten anode probe of tip radius $\sim$ 20 μm. Then to allow scanning at a constant electrode separation, the specimen is aligned into the scanning plane by carrying out adjustments to its mechanically manipulated stage as described in Chapter 4. The alignment is checked and the electrode gap determined by allowing the two electrodes to touch gently near the ends of the central vertical and horizontal scans respectively. Since the approximate location of the emission sites was already known from the procedure to obtain electron spectra it was usually only necessary to scan these regions at an electrode separation of 0.4mm until the site is located as indicated by a current of 10^{-9} to 10^{-6} A on the electrometer.

Whenever a site is found two spots of light may be observed through the image intensifier, e.g. see Fig.5.38. One is due to electrons striking the anode[108], and the other somewhat fainter spot (called K-spot) to electroluminescence at the electron emitting site. The image intensifier (Mullard CV62401) is mounted on a manipulator stage allowing movement in the horizontal and vertical planes, so that the image of the K-spot can be positioned in the centre of the P5 phosphor

output screen as referenced by a thin cross-wire. A mask with a 0.5mm diameter central hole is placed over the screen allowing only the light from the K-spot to be measured by the photomultiplier (EMI type 60948). It is then possible to measure the light intensity as a function of the applied field and current by varying the voltage applied to the anode probe and noting the photomultiplier and gap current. Finally, the spectrum of the light may be taken by interposing sharp cut-off high-pass filters between the telescopic lens of the image intensifier and the viewport.

Complementary optical data has been obtained from site 2C on the polished copper specimen discussed in section 5.4. The photograph of Fig. 5.38 taken from the image intensifier screen shows the light emitted from the cathode (marked K) and from the anode probe (marked A). The light from the two spots is well distinguished by their respective spectra shown in Fig. 5.40; the K-spot showing peaks at 620 and 710nm close to those previously reported by Hurley and Doorley [42] on copper electrodes, whilst the anode spot displays the typical broad spectrum reported by Young [108]. The intensity of the K-spot emission has also been measured and is seen in Fig. 5.41 to obey the Alfrey-Taylor [47] relationship characteristic of electroluminescence.

It was not found possible, using the present experimental set-up, to measure the variation of the optical spectrum with field. At low fields, the signal to noise rate was too low after transmission of the light through the filters, and at high fields there was excessive interference from the light of the anode spot. Accordingly the measurement reported in Fig. 5.40 was taken at a suitable intermediate value.

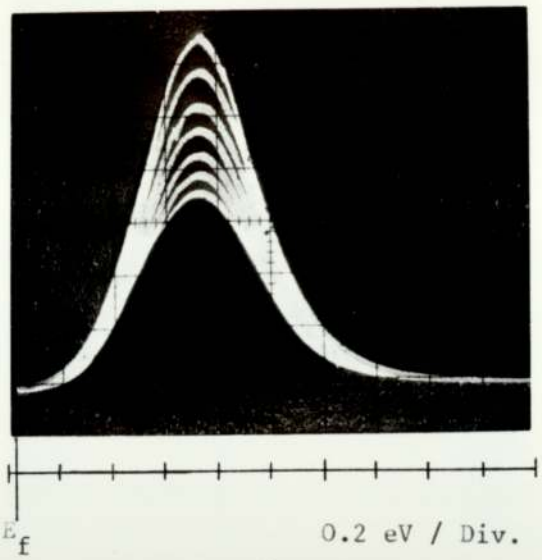

Fig. 5.37 Successive spectra obtained from a copper specimen whilst it cooled showing the decrease in current as the electrode gap increases due to contraction of the specimen. Each scan lasts for 30 s, i.e. total scanning time = 210 s .

(a)

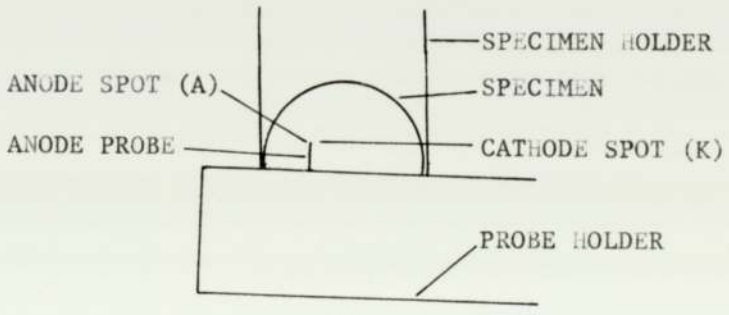

(b)

Fig.5.38 (a) Photograph taken from the image intensifier screen showing the cathode spot (K) and the anode spot (B) .
(b) A "tracing" of (a) pointing out the relevant features.

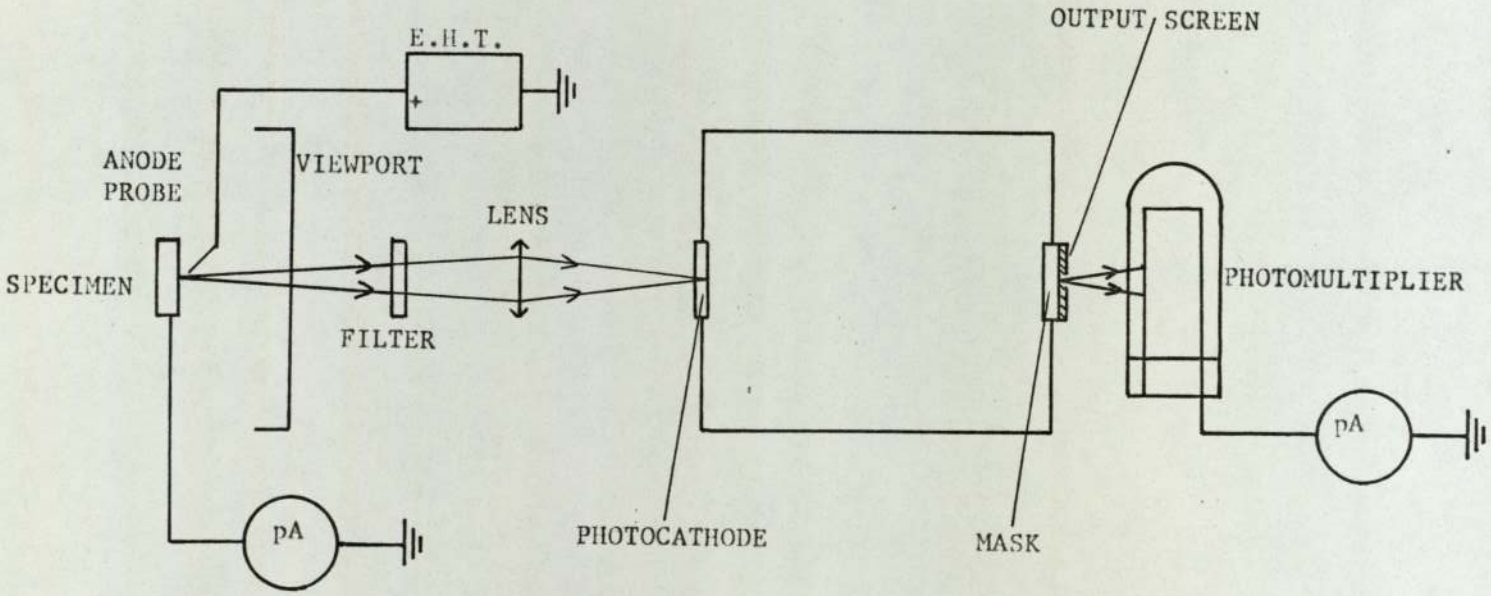

Fig. 5.39 The experimental technique for optical spectrometry of electron emitting sites.

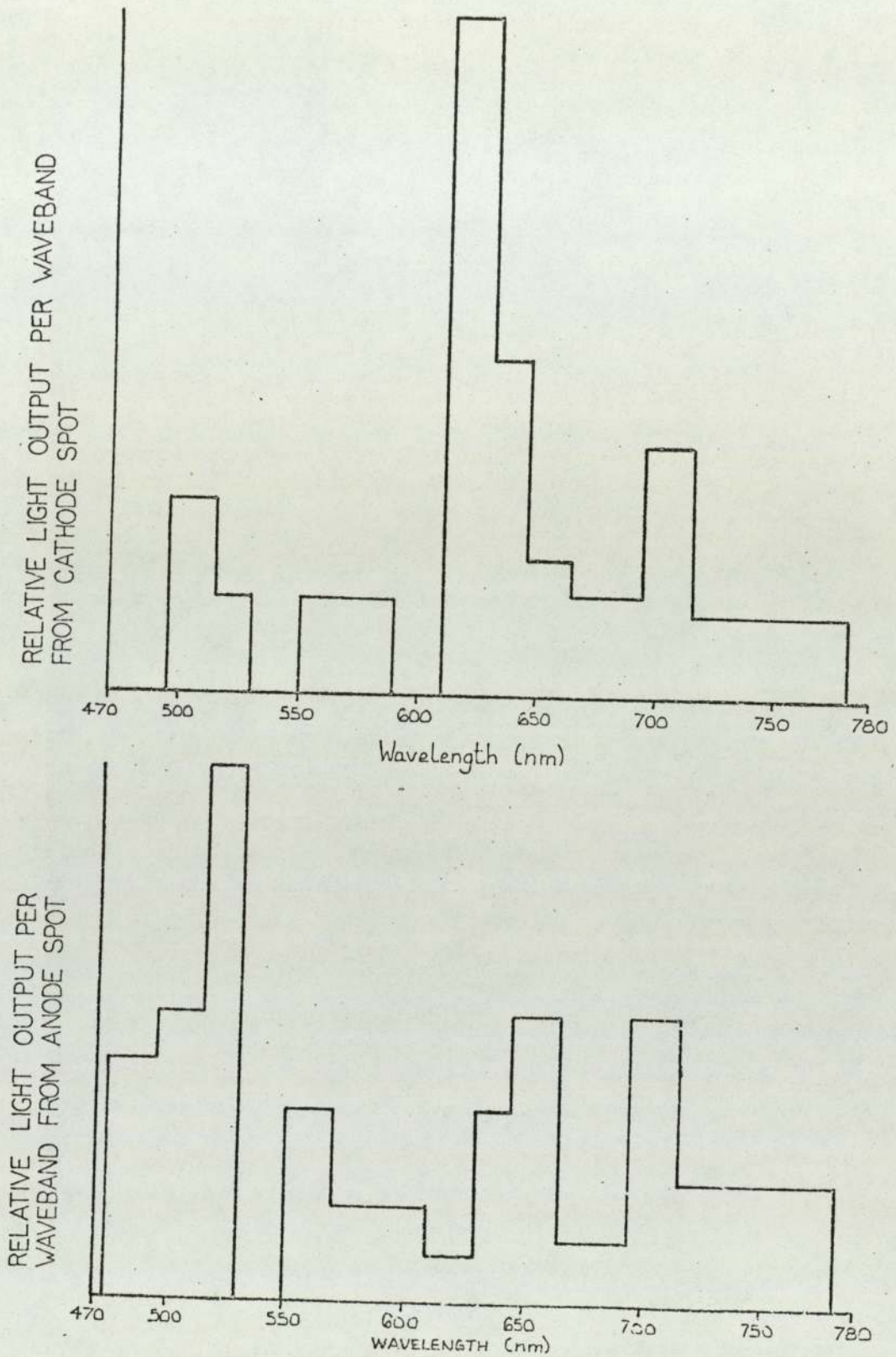

Fig. 5.40: (a) Spectrum of the radiation from the cathode spot (K) of Fig. 5.38. (b) Spectrum of the radiation from the anode spot (A) of Fig. 5.38.

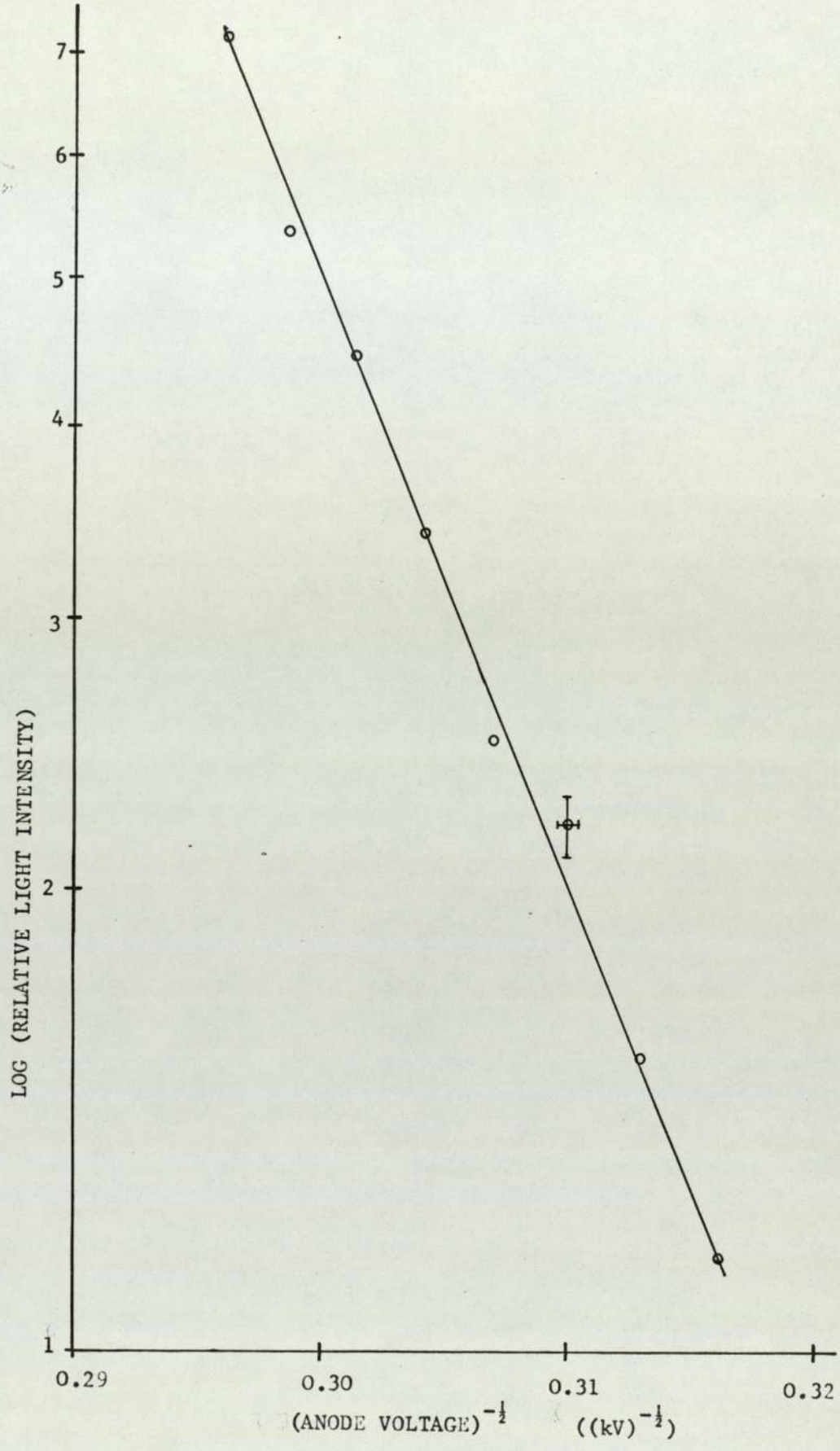

Fig. 5.41 Alfrey-Taylor plot for light output from the K-spot.

CHAPTER 6

A SCANNING ELECTRON MICROSCOPY TECHNIQUE, FOR IDENTIFYING EMISSION SITES

6.1 Introduction

The earliest electron microscopy studies of electrode surfaces,[17, 18, 19] reviewed in Chapter 2, apparently provided *indirect* evidence for the microprotusion hypothesis for electron emission, in so far as that protusions were observed on electrodes which had previously been subjected to high electric fields. However, no attempt was made to correlate the position of these protusions with actual emitting sites, until the *direct* electron optical technique of Cox,[41] who showed that the localised region of the electrode surface containing a site rarely included the anticipated sharp microprotusion. Instead insulating type particles and grain boundaries were often observed in these areas, with one report [93] providing strong although circumstantial evidence for an emission site on a copper-chromium alloy to be associated with an impurity including the elements aluminium and iron. Unfortunately the resolution of Cox's anode probe hole technique was limited to $\sim \pm$ 10 μm, so that it was not possible to identify the individual topographical feature responsible for the emission. In an attempt to obtain this information, the alternative anode micropoint probe technique described in this chapter was developed which, in principle, has a higher resolution. It also offerred the possibility of locating other emission processes such as the so-called "b" sites[28] which usually appear at fields when a normal test gap would have broken down. Furthermore an energy-dispersive x-ray spectrometer

is available for use directly in conjunction with the S.E.M. in order to investigate the elemental composition of any microscopic area of the specimen.

6.2 Instrumental Details

The principle of the experimental technique, which is incorporated in the specimen chamber of a Cambridge 2A Stereoscan scanning electron microscope (S.E.M.) capable of realizing a vacuum of 10^{-5}torr, is illustrated schematically in Fig. 6.1. The specimen cathode, in the form of a standard 15mm diameter disc which is orientated normally to the anode probe and at 45^{o} to the S.E.M. axis, is mounted on the goniometer stage of the instrument such that its surface can be mechanically scanned in front of the fixed high voltage probe. By arranging for the specimen to be electrically insulated from the earthed mechanical stage, it is possible to use a series picoammeter (electrometer) to monitor any emission current drawn from the specimen.

In the original design a conducting rod, carrying a *single* electrolytically etched tungsten microtip, was suitably shaped so that it could reach over the goniometer stage to position the tip under the S.E.M. axis in the restricted space directly above the specimen. However, this single-tip technique proved to be impractical for reasons which may be understood by considering the electrostatic field on the specimen cathode due to the point-plane configuration shown in Fig. 6.2(a) which has been analysed by Coelho and Debeau.[109] The results of these authors (Fig. 6.2(b)) show that for a gap separation of 0.5mm, which is the minimum for the initial location of sites due to variations in the gap during scanning (typically 0.1 to 0.2mm), and typical

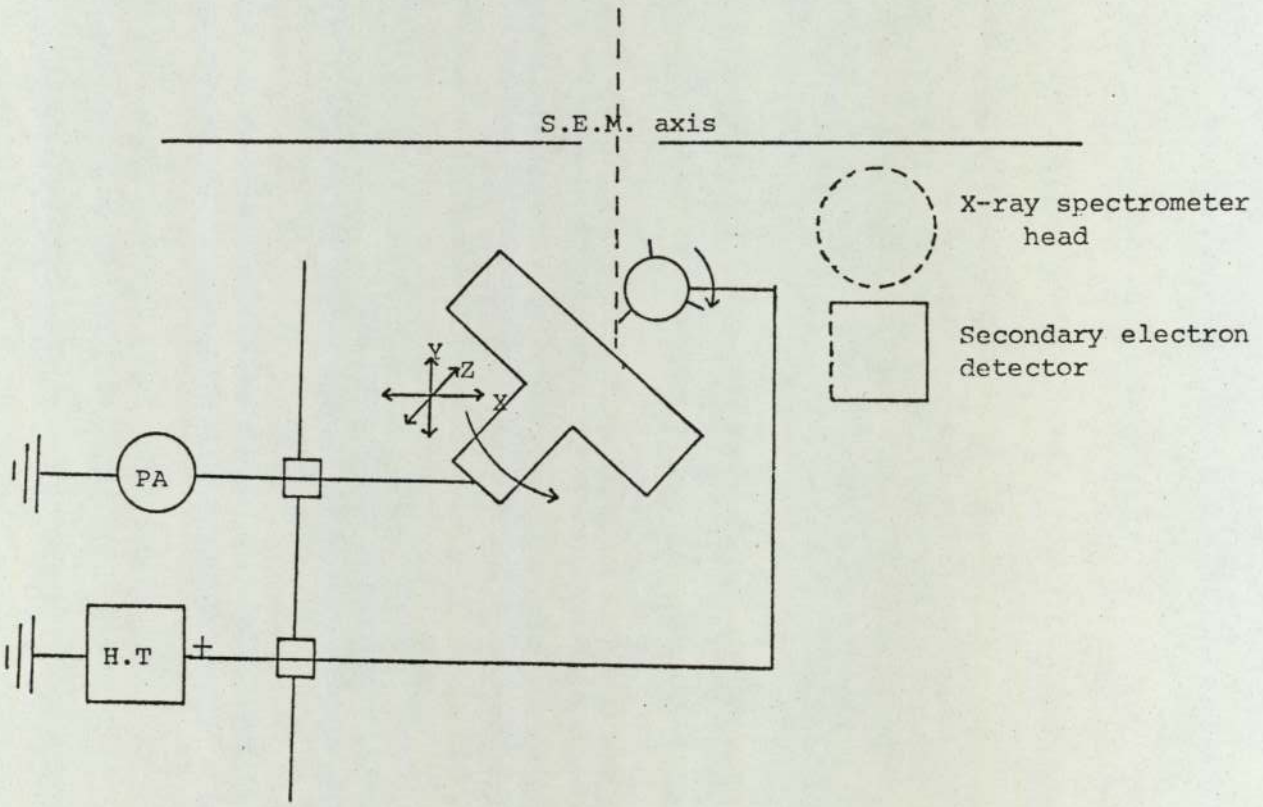

Fig. 6.1: Schematic representation of specimen and anode probe assembly as mounted in the scanning electron microscope.

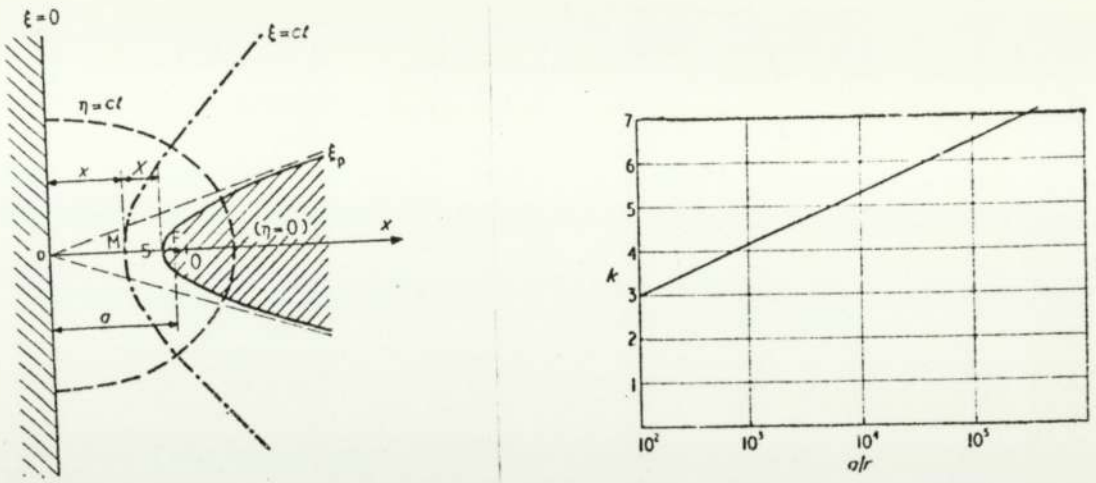

a) Representation of a point-plane configuration.

b) Representation of k against a/r

where: $k = \frac{\text{Field at plane for parallel plates with gap a}}{\text{Field at plane below tip of radius r with gap a}}$

Fig. 6.2 From Coelho & Debeau[109]

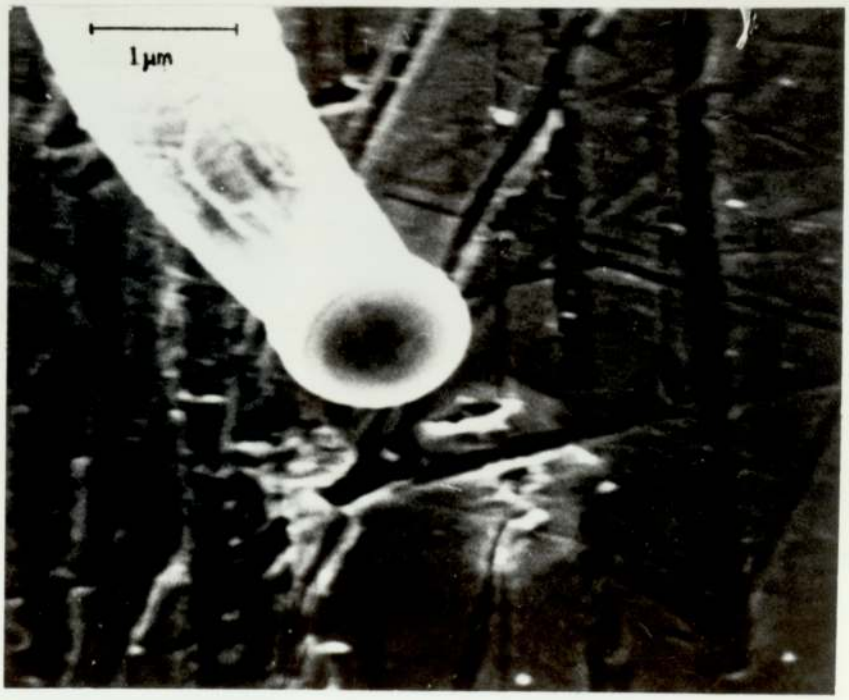

Fig. 6.3 Micrograph of a tip that has undergone melting above a machined copper surface .

tip radii (0:1 to 0.5μm) the axial field on the cathode is a factor of 4 to 5 lower than for broad area electrodes at the same separation. Accordingly a potential of at least 30keV is required on the tip to realize sufficient field on the cathode for electron emission. Once a site has been located by this method high energy electrons will strike the microtip causing it to melt and take up the characteristic shape shown in the photographs of Fig. 6.3. One attempt to overcome the melting problem was to use a probe made by etching a standard 7 μm diameter carbon fibre. However the fibres were mechanically unstable under the high electric fields, and this approach was abandoned. Another problem with the single tip technique was that the gap separation could not be accurately determined, since touching would grossly deform the tip and estimating the separation from the focusing of the S.E.M. is only possible to ∿ 0.1μm because of the large depth of view which is a characteristic of this instrument.

Therefore it was concluded that using a single anode probe is unsuitable for a high resolution identification of an emitting site. Accordingly the apparatus was redesigned involving a system using three probes of diminishing tip diameter, namely rounded copper and tungsten wries of tip diameters (a) 0.7mm and (b) 0.1mm, and (c) a standard electrolytically etched tungsten microtip having a diameter varying between 0.2 and 1μm from tip to tip. The probes are mounted radially and may be located in turn precisely on the axis of the S.E.M., as shown in Fig. 6.1, this being achieved by the combination of translatory manipulation via a bellows-operated, pivot-adjustable mounting, and rotation by a system

of gears connected to a rotational feedthrough. The added complexity of the system (see Fig. 6.4) requires an independent electrical feedthrough with the probe holder being insulated from the manipulating stage.

The first stage of the experimental procedure is to roughly locate the position of the sites by systematically scanning the specimen in a spiral fashion under the large probe (a) with an electrode gap of $\sim$ 0.5mm and a probe potential of 10kV. Once a site is located as indicated by a current of $\geq 10^{-9}$A, the probe holder is rotated and the site more finely located under the probe (b). Finally the tungsten microtip (c) is appropriately positioned and a gap of 0.1 to 0.2mm established by means of the focus of the S.E.M. At this stage a current limiting resistor of value 5×10^{9} Ω is inserted in the high voltage line to prevent melting of the tip due to excessive electron bombardment. The small identified area is now finely scanned to obtain a current of 5×10^{-8}A, and then the gap and potential gradually reduced keeping the current constant: at this current level the fluctuations are typically about $\pm$ 2×10^{-8}A. From a plot of this potential versus the gap co-ordinate the actual separation, which may be $\sim$ 10μm for the closest approach, can be deduced by extrapolation.

The micrometers on the goniometer specimen stage limit the precision of the manipulation to $\sim$2-3μm. In order to improve on this precision a simple heat translator, see Fig. 6.5, was made to sit just below the specimen, such that when a current is passed through the heating coil the aluminium cylinder of the translator will expand and enable very fine movement of the specimen towards the tip.

Fig. 6.4: Photograph of the S.E.M. compatible manipulation and electrical stage carrying the anode probes.

Unfortunately this instrument has not been found to be particularly useful in this experiment, because the limited room on top of the goniometer stage only allows the use of thin insulators between the translator and the specimen. Consequently the specimen itself has heated up and expanded: leading to the problem of lateral displacement of the emitting site as discussed in Chapter 5.7.

6.3 Resolution of the Technique

In order to interpret the results from micrographs such as Fig. 6.10 & 6.11 it is firstly necessary to consider briefly the image formation of the S.E.M. for the particular geometry employed in this experiment. Fig. 6.6 illustrates how the image of a vertical plane through the axis of the anode probe is produced on the image screen for unity magnification. Then it is clear that the predicted position of the emitting site on a micrograph will be a distance of $M \times a/\sqrt{2}$ below the end of the probe, where M is the magnification and "a" is the normal separation of the electrodes. Therefore in order to determine the position of the emitting site on the S.E.M. image it is important to measure the separation "a" as accurately as possible. As mentioned earlier it is not possible to make this measurement by touching the electrodes together, since this would destroy the microtip. An attempt was made to measure the gap by reversing the polarity and using the tip as a standard electron emitter. However, drawing a field emission current under these poor vacuum conditions invariably led to melting of the tip, into a shape similar to that in the micrograph of Fig. 6.3, an effect which has also been reported by

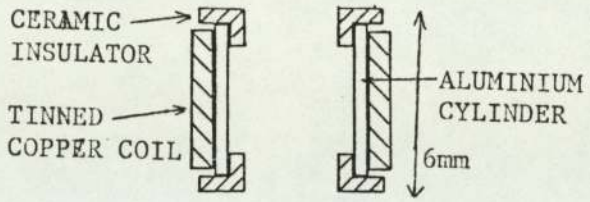

Fig. 6.5: A simple heat translator which may be positioned between the specimen and the S.E.M. goniometer stage.

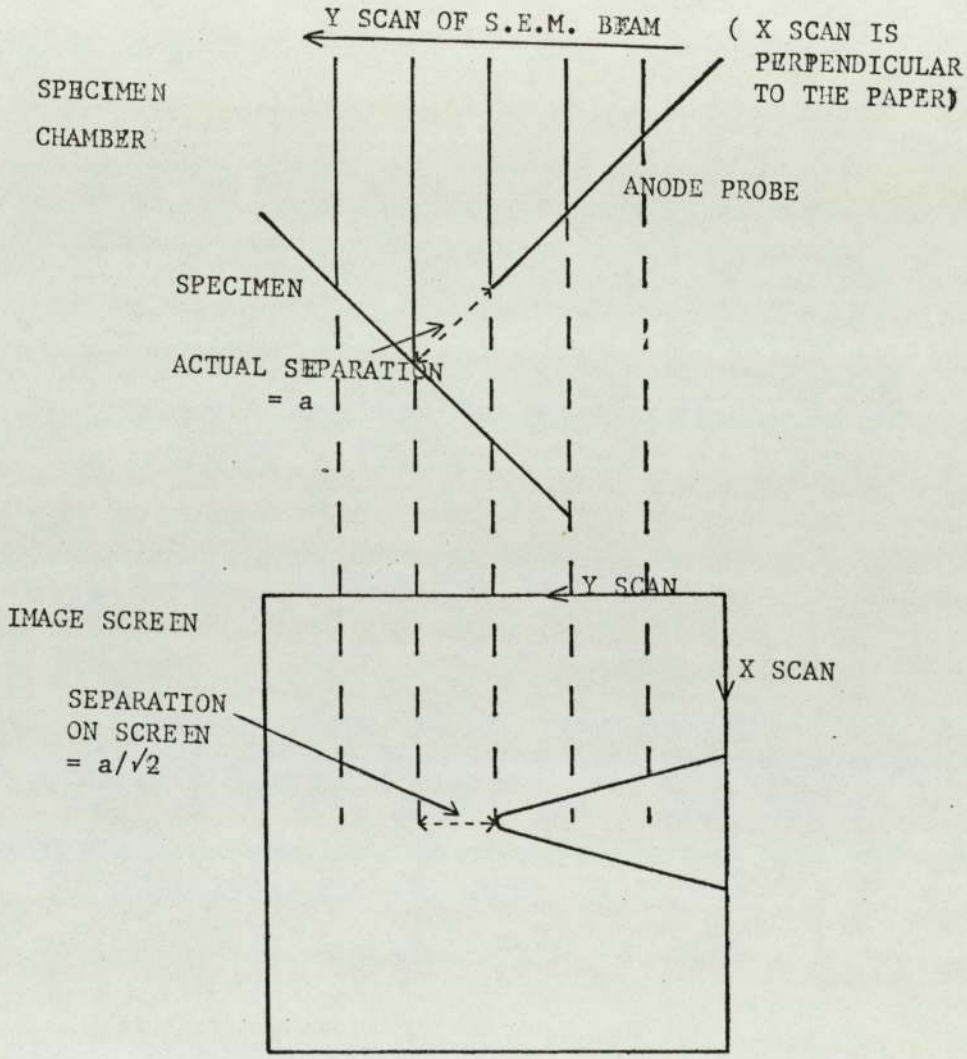

Fig. 6.6: A schematic representation of the image formation in the S.E.M. for the experimental geometry.

Young[110] in similar vacuum conditions.

The experimental procedure actually adopted for determining the gap has been discussed earlier, i.e. decreasing the potential of the tip and the gap separation to maintain a constant current. A typical plot of potential versus gap is presented in Fig. 6.7, and may be compared with the plot using the theory of Coelho and Debeau,[109] who have used the approximation of a hyperboloid tip to derive an expression for the field on the plane directly below the tip

$$Ep = \frac{V}{a \ln (2 (a/r)^{\frac{1}{2}})}$$

where a is the gap, r is the radius of curvature of the hyperbola (0.3μm for the example of Fig. 6.7) and a >> r. It is clear that the curvature of the experimental plot is opposite to the theoretical expectations. In fact the apparent decrease of emission with gap is well known; often presented in the literature as a decrease in the field enhancement factor (β) for diminishing electrode separations [15,16] and has been reviewed in Chapter 2. The value of "a" used to locate the emitting area on the S.E.M. image has been determined by extrapolating plots such as Fig. 6.7 to zero voltage. This procedure has been verified to be correct to ∿ 4μm by allowing the tip to touch the specimen in a few trial cases.

Another approach to calculating the electrostatic field for the configuration of this experiment has been made by Cox,[111] using a field plotting programme, which requires the electrode surfaces to be radially symmetric and definable by straight line segments. In this case the tip has been approximated by a spheroid on a cone, see Fig. 6.8 The

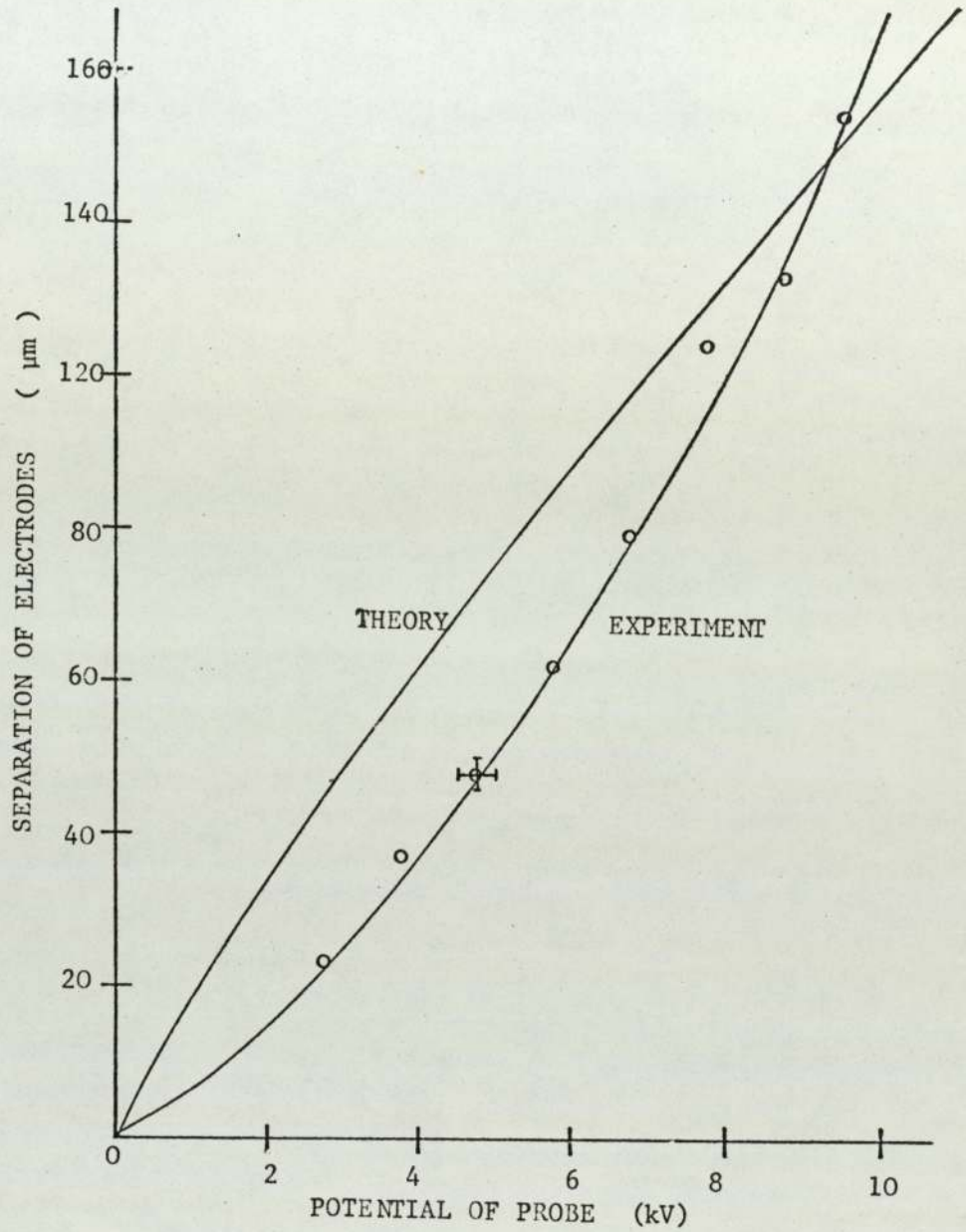

Fig. 6.7: A comparison of theory and experiment for the potential applied to the anode probe to maintain a constant emission current versus the separation of the electrodes.

field in the plane of the specimen has been calculated for a tip of radius 50nm, with gap separations of 10, 15 and 20 μm. A 5% drop in the field will typically produce a halving of the current drawn from an emission site, and would thus be clearly resolved. Using this criterion the circle of confusion of the emission has been calculated by Cox to vary from a diameter of 7μm for a 10μm gap, to 18μm for a 20μm gap. Geometrically, a 50nm radius tip at 20μm is equivalent to a 25nm radius tip at 10μm, hence the latter would have a resolution of 9μm. Thus one obtains the somewhat surprising result that a sharper tip leads to a reduction in resolution (when $a >> r$). In practice the tips used in these experiments varied in radius between 0.1 and 0.5μm, and thus for gaps in the region of 10 to 20μm may be expected to give a resolution of the order of 2-3μm. In fact this was the experimentally observed resolution, and is also the limit of the goniometer specimen stage.

Cox has carried out further calculations to determine the effect of surface features on the distribution of the field on the plane. Computations have been carried for regimes such as illustrated in Fig. 6.9, and reveal that there is a very sharp maximum in the field on the projection, such that distances of less than a micron can be satisfactorily resolved. It is found that the resolution depends most critically on the shape of the projection, i.e. the resolution increases with the height to width ratio of the projection.

6.4 Results of Site Locations

Experiments on copper electrodes at the present spatial resolution of emission site location of 2-4μm confirm the

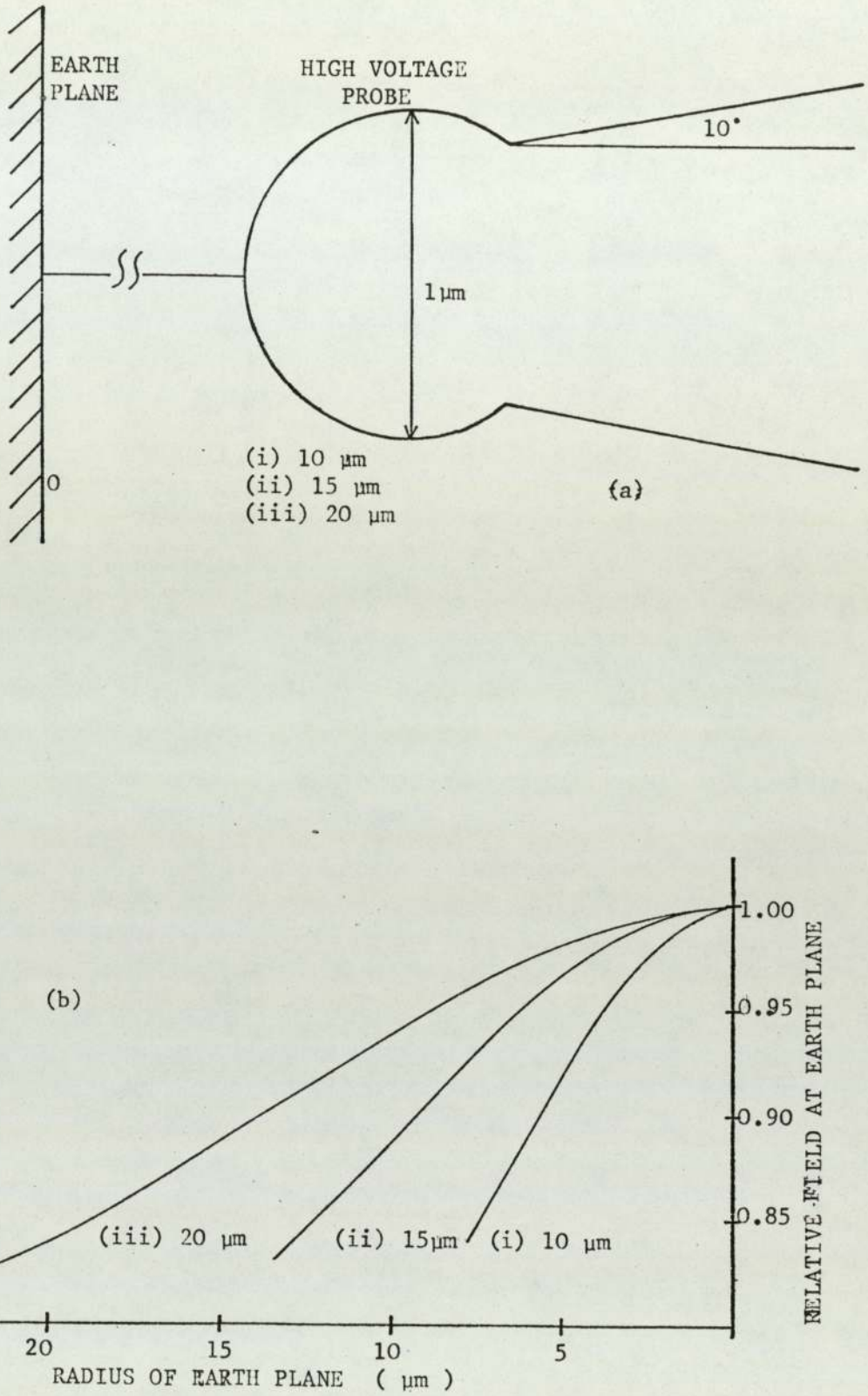

Fig. 6.8: (a) Electrode geometry for the initial field calculations of Cox[111], and (b) the calculated distribution of the field on the specimen surface for this geometry.

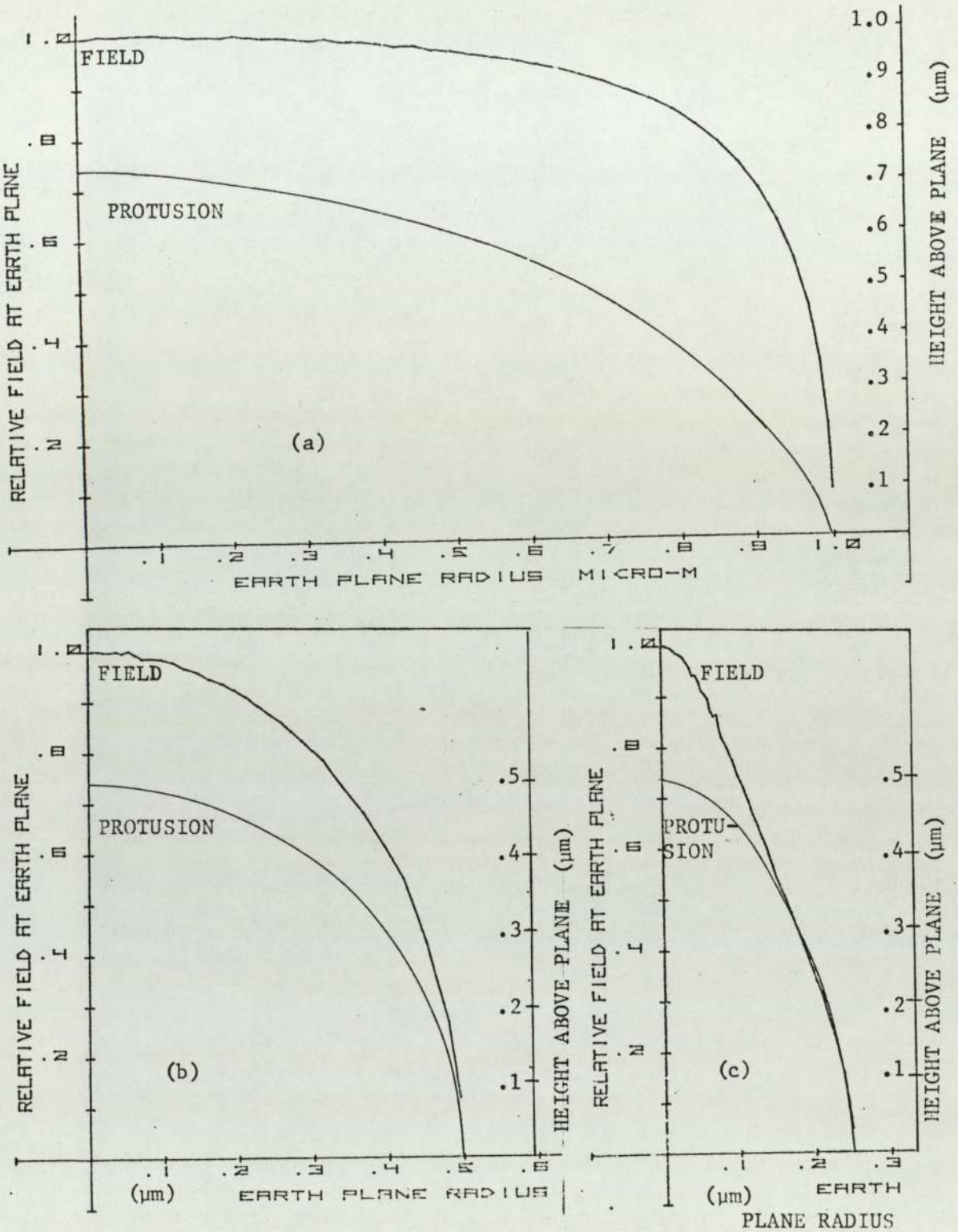

Fig. 6.9: The calculated distribution of relative field on protusions on a panar surface below a tip; from Cox[111]: (a) oblate hemisphere, (b) hemisphere, (c) prolate hemisphere.

findings of Cox, viz. that there are no conical or whisker-like field enhancing projections having the type of geometry required by the conventional field emitting model based on the "metallic" FN theory. Instead the localised area of $\sim (3\mu m)^2$ containing the site typically includes one or possibly two micron or sub-micron particles, having an insulating character (i.e. they appear charged in the S.E.M. image) and which are assumed to be responsible for the measured emission.

Fig. 6.10(a)and(b) show micrographs of emission site locations on two different specimens of polished OFHC copper, with the superimposed anode probe. In these cases, as in several of the observations, an x-ray spectrometer (Kevex) analysis of each of the insulating particles within the predicted area did not reveal any anomalous elements. It must however be realized that the Kevex is incapable of identifying elements of atomic number less than 8, so that elements such as oxygen, carbon and nitrogen would not be detected if present in the particles. For this reason it was assumed that the identified particles were either copper oxide or carbon from the diamond polishing compound.

An interesting example of a site location which positively revealed an impurity element on an unpolished OFHC copper specimen is shown firstly under the medium probe (b), Fig. 6.11(a), then under the fine probe, Fig. 6.12(b), and at higher magnification, Fig. 6.11(c). The Kevex spectrum see Fig. 6.12, in this case revealed an impurity of silver that is present in an insulating form, most likely as an oxide since a compound involving an element having an atomic number greater than 8 would have revealed an additional peak.

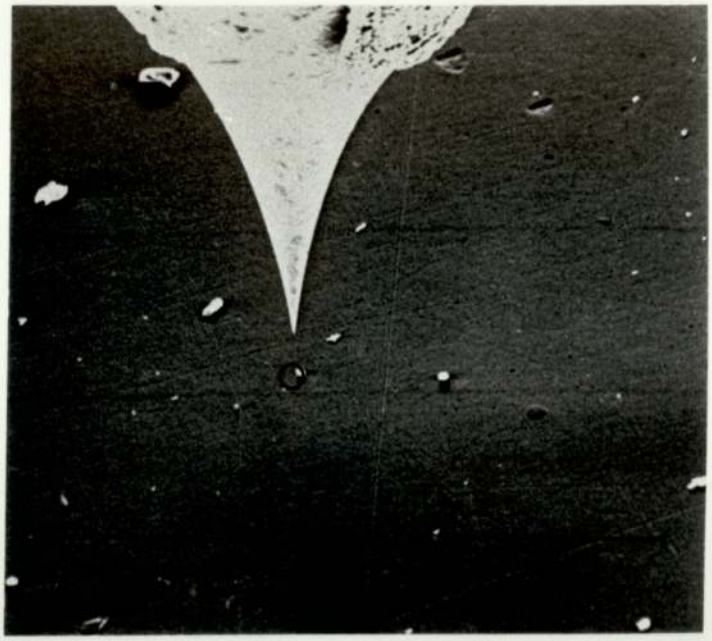

(a)

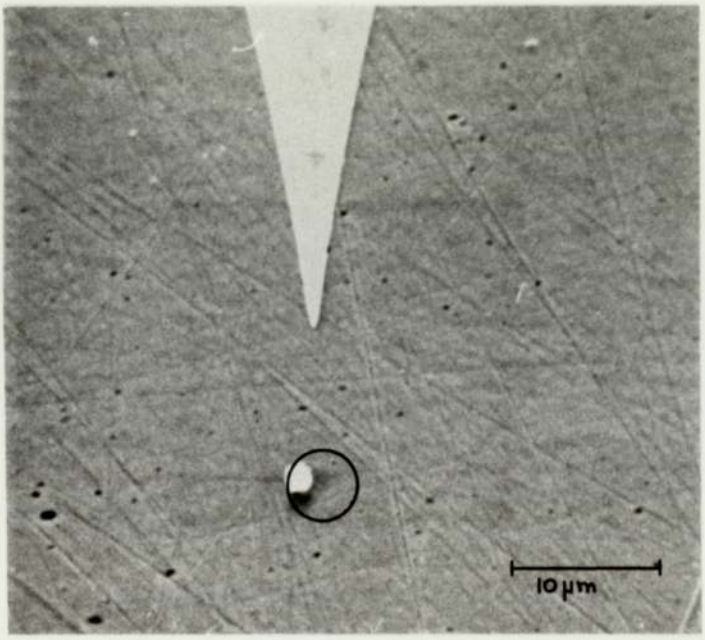

(b)

Fig. 6.10 Scanning electron micrographs showing the tip of the anode probe immediately above regions (circled), on polished copper surfaces, identified as containing an emmision site.

a) Site below the medium probe.

b) Site below the fine probe at low magnification.

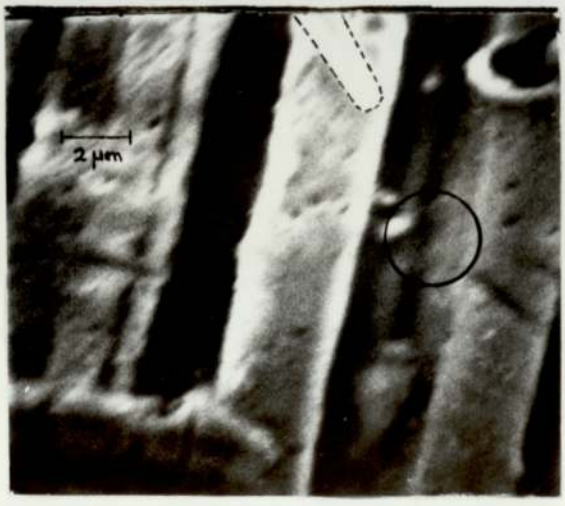

c) High magnification image of the same regime as in (b). The electron emission site is predicted to occur within the marked circle; the profile of the probe is also shown.

Fig. 6.11 Scanning electron micrographs of an emission site location on a machined copper specimen.

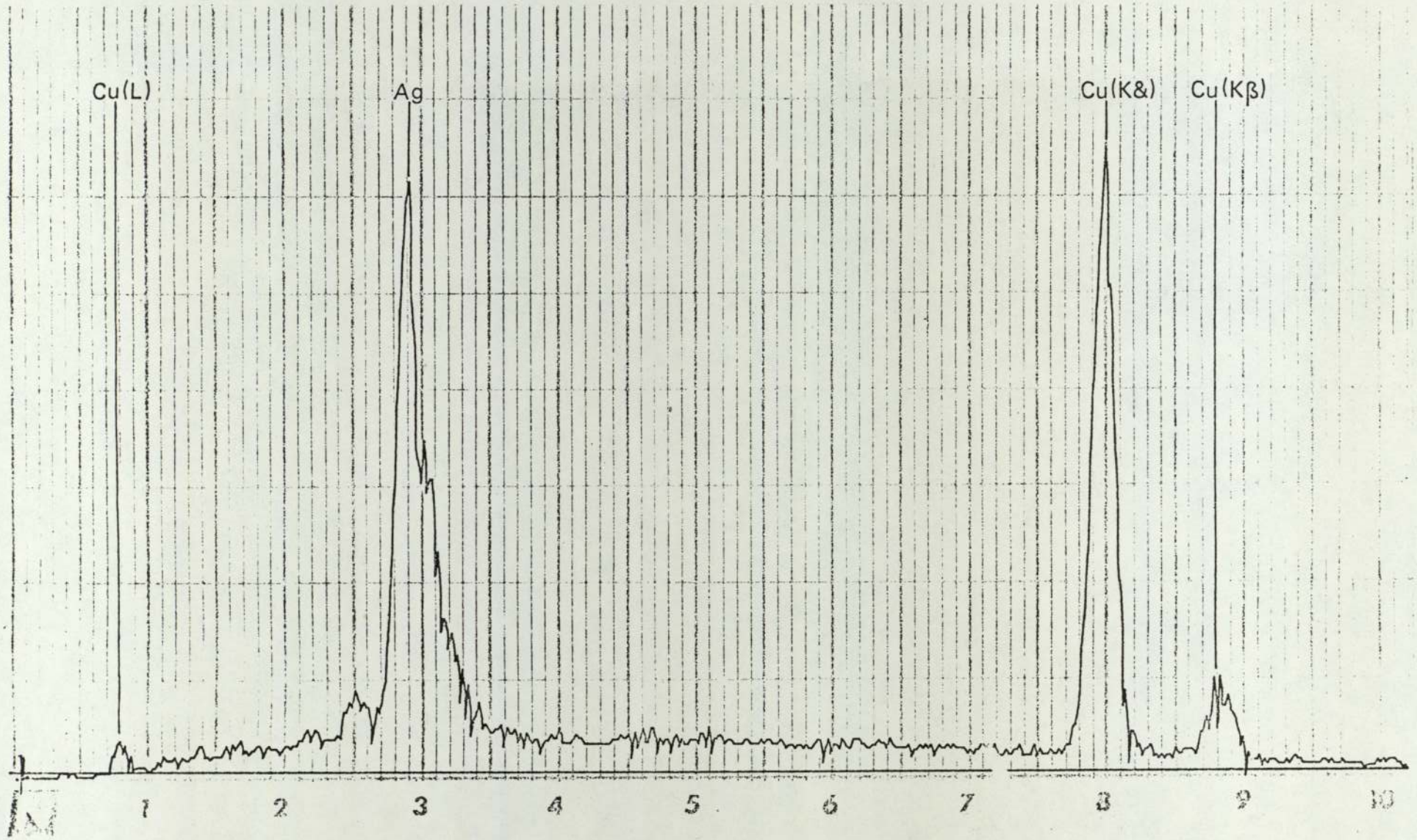

Fig. 6.12: X-ray spectrum obtained from the insulating particle within the marked circle of Fig. 6.11 (c).

The irregular gouge marks crossing the turning grooves on the specimen was caused by a microtip scratching the surface in an earlier attempt to locate this site. It is of particular interest to note that this drastic event led to no additional emitting sites, thus serving to re-emphasize the point that electron emission on extended area cathodes rarely originates from field enhancing features.

6.5 Conclusions

The findings of this experiment further reinforces the conclusion that an insulating or semi-conducting regime exists at the source of the field electron emission from broad area electrodes. The present resolution is estimated at between 2 and 4μm, however theoretical computations[111] suggest that if surface irregularities are present at the emitting site the technique is capable of a sub-micron resolution. In order to realize such precision, the experiment must firstly be performed in an ultra high vacuum system, at the vacuum of 10^{-5}torr currently available the emission current is highly unstable; secondly, a more precise goniometer stage is required, possibly with piezoelectric translators for the final location of the site.

CHAPTER 7

DISCUSSION OF RESULTS

7.1 Summary of Results

The most important findings reported in this thesis may be summarised as follows.

1) A switch-on phenomenon has been observed such that when a high field is slowly applied to a virgin electrode there is no emission until a certain value is reached when the current suddenly switches on to a fairly high value $\geq 10^{-7}$A. If the field is then lowered, a continuous emission is obtained to a much lower field, and subsequent cycling of the field gives smooth I-V characteristics.

2) In general the Fowler-Nordheim plots of the current-voltage charateristics have been found to be only approximately linear at current levels $\leq 10^{-7}$A, with a marked deviation at higher currents. However, if the Fowler-Nordheim theory is applied at lower currents it predicts field enhancement factors β of several hundreds.

3) Electron spectra obtained from a variety of metals, namely copper, stainless steel, titanium and gold, have all shown similar characteristics. However, it is noted that copper and in particular gold provide more emission at a given field than stainless steel, titanium or aluminium, with less likelihood of microdischarge occurrences.

4) The electron energy spectra from sites on broad area electrodes have departed markedly from those expected for a metallic emitter. In particular the FWHM and the shift of the maximum of the distribution below the Fermi level have both displayed a non-linear increase with field and current.

5) Many spectra have displayed a multi-peaked structure. It has been shown that additional peaks invariably appear on the high energy side of the spectrum as the field is increased. In one case, the sub-distributions contained in the spectrum have been estimated, and it has then been possible to show that the separation between two of these distributions remains constant as the field is increased.

6) Several anomalous spectra have been observed. In this classification are included instabilities, switching between current and spectral states, a spectrum displaying unusual structure, and spectra whose shape altered dramatically with micro-adjustment in the position of the specimen at constant field.

7) Electron emitting sites have been demonstrated to exhibit electroluminescence with optical spectra typically in the range of 1.5 to 2.5eV.

8) Insulating particles of $\sim$ micron dimensions are found to be present within the areas predicted to contain electron emitting sites.

9) Outgassing of the specimen has been found to increase the stability of the electron spectra.

10) Ion etching to depths that are estimated to be $\sim$ 0.1μm in copper and possibly $\sim$ 20nm for an insulating impurity is capable of removing emission sites, although other sites may become activated. Etching to depths of $\sim$ 10nm in copper or $\sim$ 2nm in an insulator lead to instabilities in the spectra.

7.2 Comparison of Results with Traditional Models

It is worthwhile to consider the microprotusion hypothesis in the light of these results. The switch-on

phenomenon (1) may be related in this model to the growth or erection of a whisker under the action of the electric field. On this premise attempts can be made to explain some of the other results by assuming the protrusion to be covered by adsorbates. Accordingly instabilities and departures of the current/voltage characteristics from Fowler-Nordheim theory may be discussed as outlined by Powell and Chatterton[25] and reviewed in Chapter 2.3. Similarly electron spectra may be interpreted using the theory of Duke and Alferieff[74] for resonance tunnelling through adsorbed atoms, which has been reviewed in Chapter 3.3.

In such a model the observed spectra could apparently arise due to a metallic adsorbate, in which case current enhancements of several orders of magnitude are possible. (However it is to be noted that this current enhancement will not be reflected by a comparable field enhancement as measured by the factor β. The exponential nature of the tunnelling probability implies that the contribution to β from this source will be of the order of one to ten). Then it also follows from the model that the observed spectrum will be characteristic of the energy levels of the adsorbed atom, and may be broadened and shifted below the Fermi level. Further it would also be expected that as the field increases the spectrum will move linearly towards low energies. In practice, however, the observed shift for sites on broad area electrodes is certainly not linear; equally there is no apparent explanation in this model for the increase in the FWHM with field.

Although the theory of Duke and Alferieff is fairly idealised and considers only monolayer coverage by the ad-

sorbate, Swanson and Crouser[77] have carried out an experimental investigation of the electron spectra obtained from emission through large molecular adsorbates, as discussed in Chapter 3.3. Many of their results are qualitatively similar to those obtained from broad area electron emission sites, although again they only report linear shifts of the energy distribution with field. Whilst purely from the spectral measurements the development of a model based on the regime of a "dirty tip" may appear promising, it was not considered to be justified since other results indicated that such a mechanism is unlikely. Thus, outgassing and in particular ion bombardment will remove adsorbates and should therefore lead to the observation of purely metallic type spectra, i.e. contrary to results 9 and 10. Furthermore electroluminescence is totally inconsistent with such a model, and there has been a failure to directly identify field enhancing features within the area predicted to contain field emission sites.

On the basis of the above reasoning the traditional microprotusion model for electron emission from broad area electrodes has been rejected; meanwhile observations in the scanning electron microscope (result 8) and other work reviewed in sections 2.4 and 2.5 suggests that electron emission is, in fact, associated with microscopic insulator-type impurities. Thus two new theories involving such impurities have recently been reported.

7.3 Band Theory Interpretation

The model originally proposed by Latham and his co-workers[92, 93] was developed from the electron spectrometry measurements described in Chapter 3.5 and is based on the

physical regime of a semiconducting/insulating micro-impurity that is in intimate contact with the substrate metallic cathode, i.e. perhaps partially embedded as illustrated in Fig. 7.1. Very little is known about the composition of such impurities, although the results of the electron microscope experiment suggest that they are often either oxides of the substrate metal or possibly carbon from the polishing material. In several cases elements that are alien to the substrate electrode have been identified, e.g. silver and aluminium, both probably in their insulating oxide forms.

The model has been developed for an insulating or semiconducting impurity such that in the absence of an applied field, the idealised energy band representation of the regime of Fig. 7.1 would appear as shown in Fig. 7.2(a) where the band bending at the metal/insulator and insulator/vacuum interfaces is an effect arising from work function differences and the presence of surface states as discussed in Chapter 3.4. When a high field is applied to this surface it can be assumed that there will be some field penetration, so that the band structure and surface potential barrier of Fig. 7.2(a) would become modified to that shown in Fig. 7.2(b). Under these circumstances it is possible to envisage a three-stage electron emission mechanism:

(i) an initial tunnelling of electrons from the metal substrate to the bottom of the conduction band of the insulator;
(ii) the subsequent "heating" of these electrons by 2-3eV as a result of their acceleration in the penetrating field;
and (iii) a final enhanced tunnelling of the heated electrons into the vacuum through the top of the surface potential barrier.

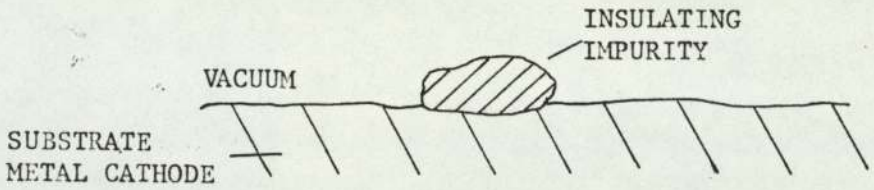

Fig. 7.1: The microregime proposed as being responsible for electron emission on broad-area electrodes.

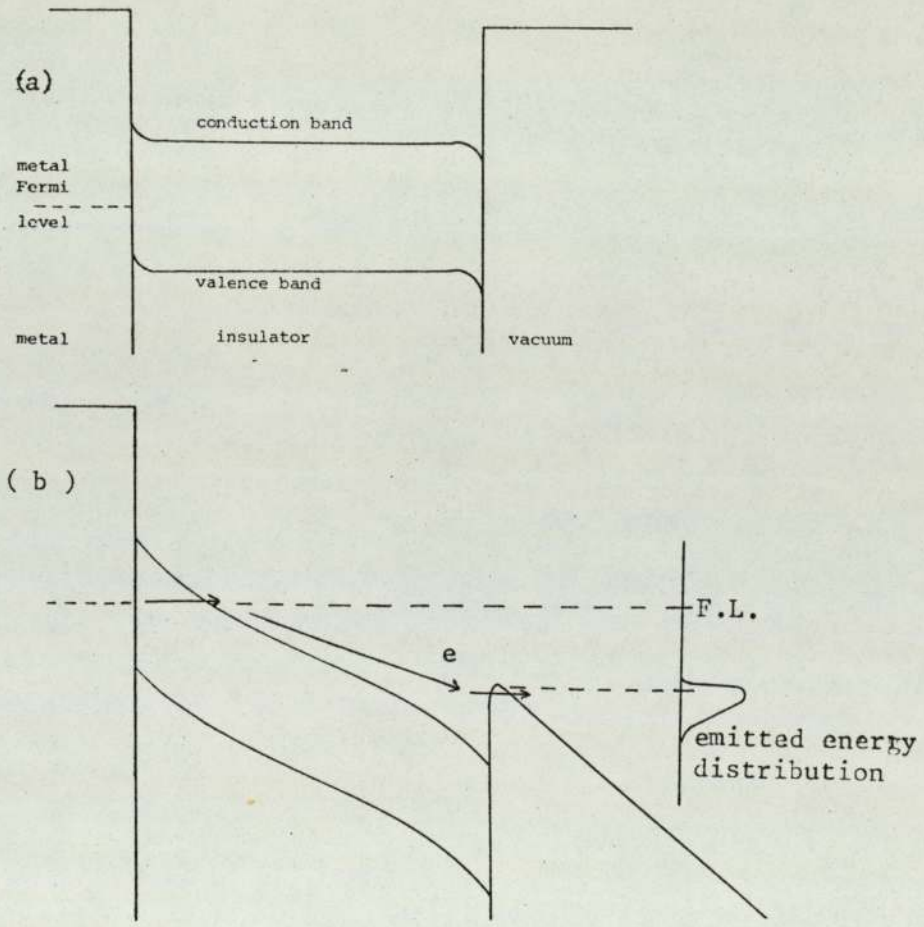

Fig. 7.2: Energy band and surface barrier configurations of the metal-insulator microregime, (a) at zero field and (b) at high field for the electron emission mechanism according to Allen et al[92,93].

This model has a number of favourable features. Firstly, whilst still maintaining a Fowler-Nordheim type of current-voltage characteristic, it is not necessary to postulate field enhancement since the "hot" electrons will effectively see a much reduced barrier at the surface. Secondly, the electron spectra, being a convolution of the hot electron energy distribution with the reduced surface barrier, will clearly be shifted below the substrate Fermi-level, as observed experimentally. Also, in strong support of their proposed mechanism Allen et.al.[93] noted that the hot electrons could give rise to the type of excitation processes that lead to electroluminescence. Indeed the electro-luminescent spectra measured in this investigation and previously by Hurley and Dooley[42] clearly indicate the existence of excitation processes involving at least 2-3eV, i.e. the order of electron heating required to produce the enhanced tunnelling described above.

As an early approach to explaining the second low-energy peak that is sometimes present in the spectra of these sites Latham and his co-workers[92, 93] attributed it to an unstable surface effect, and suggested that the model of Fig. 7.2(b) could be modified to take account of the possibility of ad-atom resonance tunnelling as described by the model of Duke and Alferieff[74]. Thus referring to Fig. 7.3 it is assumed that under certain conditions, an ad-atom can provide a favourable resonance tunnelling state relative to the population of hot electrons so that those within the appropriate narrow energy band will have a high probability of escaping to the vacuum by this additional mechanism. In the early discussion of the basic model of Fig. 7.2(b),

consideration was also given to the possible role played by inter-band impurity states. This followed from the recognition that the least plausible aspect of the model was the requirement that there should be sufficient band bending to allow the initial tunnelling of electrons from the Fermi level in the metal into the bottom of the conduction band of the insulator. To alleviate this difficulty, it was suggested that the model could be further modified as shown in Fig. 7.3 to include a level of inter-band impurity states near the bottom of the conduction band in the insulator that would provide an intermediate "resting place" for an electron undergoing a two-stage tunnelling process (i) + (ii).

7.4 Filamentary interpretation

In a recent detailed discussion of the cathode or k-spot electro-luminescent measurements, Hurley[107] has proposed an alternative explanation of the electron emission that can stem from the type of microregime illustrated in Fig. 7.1. This is based on a well known phenomenon exhibited by nanometer to micron thick films of certain semiconducting and insulating materials, particularly oxides, nitrides, fluorides and amorphous semiconducting glasses, whereby the application of a high electric field (10-100 $MV.m^{-1}$) via surface electrodes can lead to the device "switching" from a non-conducting "off" state to a conducting "on" state in which the externally measured conducitivity of the film can be increased by as much as a factor of 10^8. Such a switching event is also accompanied by the simultaneous appearance of two further "external" phenomena that are of particular significance to the present discussion, viz. microscopically localised electro-

luminescent and electron emission processes.

An important feature of the switching phenomenon is that if the field is applied for sufficient lengths of time a conducting filament becomes "electroformed" through the dielectric by the permanent or semi-permanent re-arrangement of atoms or molecules; electroforming times are typically in the millisecond to second range, whereas switching times are generally < 1μs. Estimates of the cross-sectional diameter of these filaments show that they depend on the film thickness, varying from 1nm to 50μm for 40nm to 500μm thick films.[112, 113] For a full discussion of the early work on the switching and associated properties of these devices, the reader is referred to the review article of Dearnaley et.al.[113]

According to the model of Hurley[107] impurity inclusions, such as illustrated in Fig. 7.1 are distributed at random throughout the surface. A few of these occur in regions where the field is locally intensified at cracks and grain boundaries by a factor β above average values. The field throughout the impurity is given, to a good approximation, by $\beta E/\varepsilon_r$ where E is the average field, so that if both β and ε_r are of the order of 5 to 10, the electroforming of filaments is possible when $E \simeq 10^7 V/m$. This situation will be as illustrated in Fig. 7.4 from which it follows that such a filament will behave as a metallic-like whisker and hence give rise to a local field enhancement that could be sufficient to promote field electron emission at its intersection with the vacuum interface. Extending the analogy with the Dearnaley filamentary model,[114] it can also be assumed there are likely to be high resistance spots in the electroformed filament where the enhanced

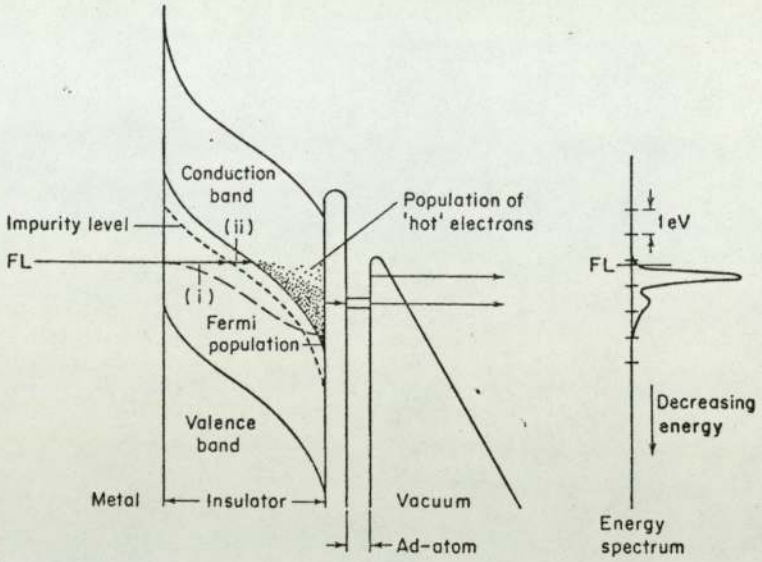

Fig. 7.3 The high-field electron emission regime of Fig.7.2(b) as it is modified by the presence of interband impurity levels and ad-atom surface states. (From Allen, Cox and Latham (93) with permission).

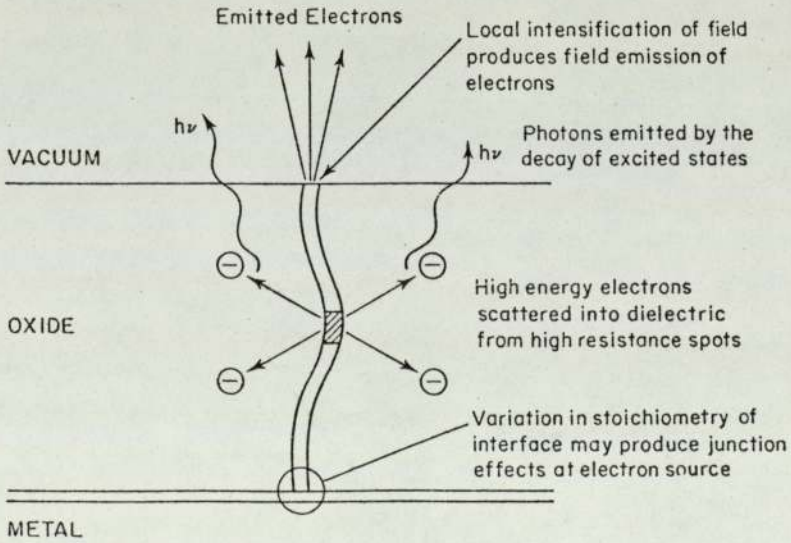

Fig. 7.4 The simultaneous production of electroluminescence and electron emission from an electroformed conducting filament in an oxide microimpurity.
From Hurley (107).

electric field will give rise to a population of "hot" carriers that will subsequently be scattered by the surrounding oxide to give rise to electroluminescence effects through some form of impact ionisation or recombination process such as discussed by Hickmott.[115] The injection of electrons from the metal substrate into the filament is assumed to arise from complex semiconductor/metal junction effects.

Several important phenomena can be explained on the basis of this type of model. Firstly, it offers a plausible interpretation for the experiments of Juttner et.al.[116,117] who demonstrated that electron emission is selectively suppressed by such "active" gases as oxygen, carbon monoxide and nitrogen, and also the more recent observation of Hurley [107] that the associated electroluminescence is also suppressed by increasing the ambient pressure. Thus, these effects can now be attributed to the "poisoning" mechanism discussed by Dearnaley,[114] in which absorbed gases such as oxygen or nitrogen will fill up the oxygen vacancies that are thought to characterise a conducting filament. Secondly, discontinuities in the current voltage characteristics and deviations from the Fowler-Nordheim theory can be attributed to either the thermal rupture and possible reforming of the filaments that are contributing to the total emission, or to the forming of new filaments as the gap field is raised. In particular, the thermal rupture of filaments suggests a mechanism for breakdown of the impurity, possibly initiating electrical breakdown of the gap. Hurley[107] envisaged a breakdown mechanism for the filamentary regime based on the thermal instability model of Cook[113] whereby at a certain current level the conducting

filament becomes thermally unstable and "explodes" so that a molten impurity particle is ejected from the electrode surface. Vivid evidence for such a process has been reported by Hurley and Dooley.[49] and reviewed in Chapter 2.5.

Finally, by considering filaments that only partly penetrate the impurity, Hurley[28] has suggested an explanation for the b sites reviewed in Chapter 2.3. Thus, the conducting filament may either grow from the insulator/vacuum interface and terminate in the insulator near the metal/insulator junction, or grow from this junction and terminate just below the surface of the insulator. In each case emission is believed to be controlled at a metal/insulator boundary, i.e. the termination of the filament in the insulator, which may take the form of a reverse-biased rectifier junction and exhibit a negative resistance characteristic if the bias voltage is increased beyond a certain point.[180]

7.5 Insulator "Switching" Model

Although each of the emission models described so far have many attractive features, they also have evident limitations. For example, the energy band model of Fig. 7.2.(b) does not readily explain how a significant number of the hot electrons will be able to cross the micron-dimension impurity without losing most or all of their energy through phonon scattering processes; neither is it clear that a sufficient field exists for tunnelling from the metal into the insulator conduction band. Equally, the filament model offers no explanation for the electron spectrometry results, and it is not clear that sufficient field intensification will occur at the end of the filaments. In an attempt to over-

come these arguments and explain the various results obtained in this investigation the following revised model has been evolved which incorporates the essential features of both of the earlier versions.

This new model is chiefly based on the phenomenon of "Ovshinsky switching"[119, 120] whereby an amorphous insulator switches from a low conducitivity ($< 10^{-7}$ (Ω cm)$^{-1}$) to a high conductivity (> 10 (Ω cm)$^{-1}$) state. This behaviour has been widely studied using thin films (0.1μm to 10μm) of insulating material sandwiched between metal electrodes. With such devices a potential difference of 1 to 10 volts is typically required to produce the switching. The most commonly investigated materials have been various chalcogenide glasses, which have device applications both as threshold switches, where the switching is completely reversible, and memory switches which lock into the high conductivity state. However, switching has been demonstrated to occur in a very large number of amorphous insulators,[121] the chalcogenide glasses being exceptional from the point of view of their stability. In fact it is quite likely that switching is a prerequisite of the "forming" discussed earlier in Hurley's model; Ovshinsky switching being a very fast process, with a risetime $\leq$ nanoseconds, although there may sometimes be an associated delay time of the order of microseconds at low voltages.

Although the insulating impurity of Fig. 7.1 is now assumed to be generally amorphous and hence band theory will not strictly apply, the band structure of Fig. 7.2 is still acceptable if it is tacitly assumed that a multiplicity of localised interband states are also present.[122] Then

applying the concepts of switching as discussed by Adler, Henisch and Mott[123] it is envisaged that the energy band regime of Fig. 7.2(b) may be rapidly altered to that of Fig. 7.5. This highly distorted shape is the result of the superposition of the electrostatic potentials due to space charges just within each interface and the potential of the penetrating field. (Fig. 7.6.)

The details of the switching phenomenon and the "on" state will be considered presently, but accepting the band configuration of Fig. 7.5 as a working hypothesis, electron emission may be realised basically as follows. Due to the positive space charge in region 1 the barrier at the metal/insulator boundary will be thin enough to allow appreciable tunnelling of electrons from the metal Fermi level into the conduction band of the insulator. These electrons will be rapidly thermalised and hence be able to cross the extended low field region in the bottom of the conduction band where their lifetime can be $\sim 10^{-8}$s.[124] They, then, enter the second high field region, where they are heated, i.e. accelerated, to energies great enough for the electrons to escape into the vacuum over the top of the work-function barrier; in terms of an energy band model this escape process is very similar to that assumed for negative affinity photo-emission devices.[125] Hence this regime is capable of overcoming the chief weaknesses of the original energy band model,[92, 93] i.e. the injection of electrons into the impurity and their transport throughout it.

We now return to discuss the details of this model, beginning with the switching event. This is believed to be initiated by the appearance of single electron in the con-

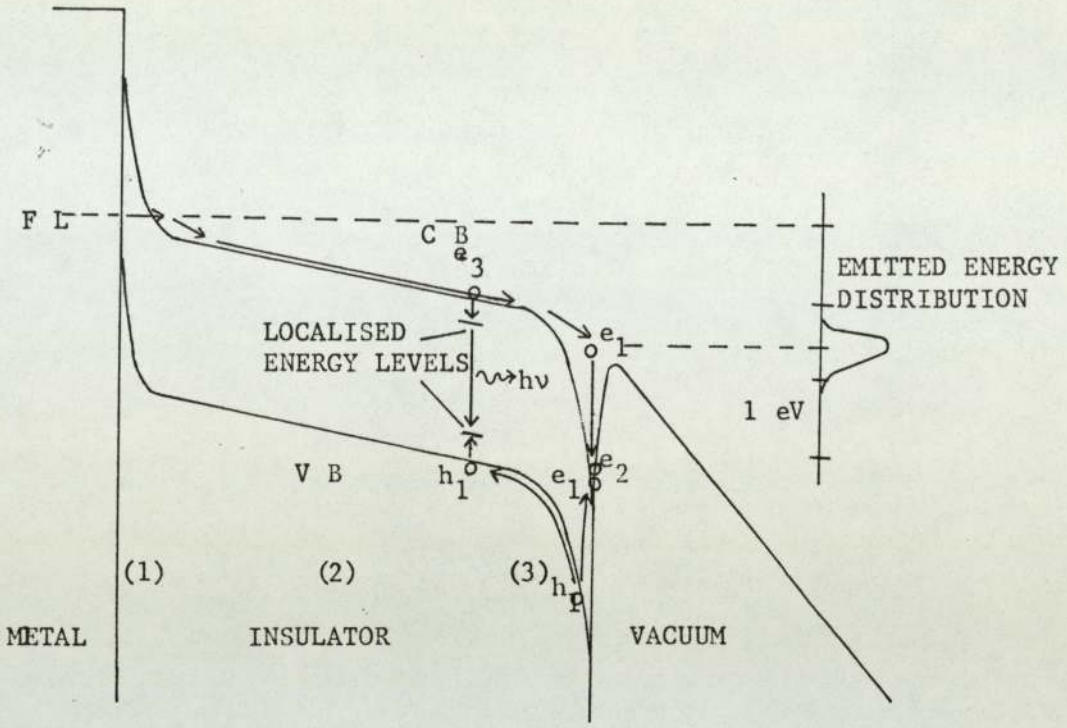

Fig. 7.5: Energy band configuration of the "on" state of an electron and photon emitting composite microregime.

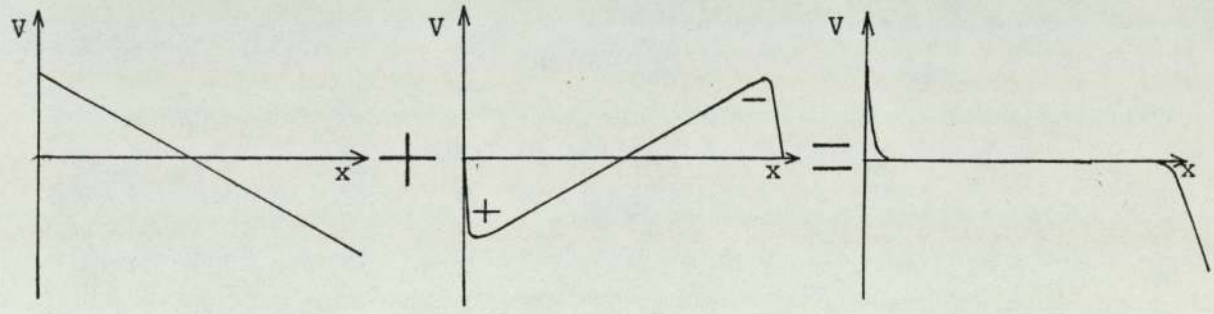

Fig. 7.6: The addition of electrostatic potentials within the insulator to form the potential diagram of Fig. 7.5.

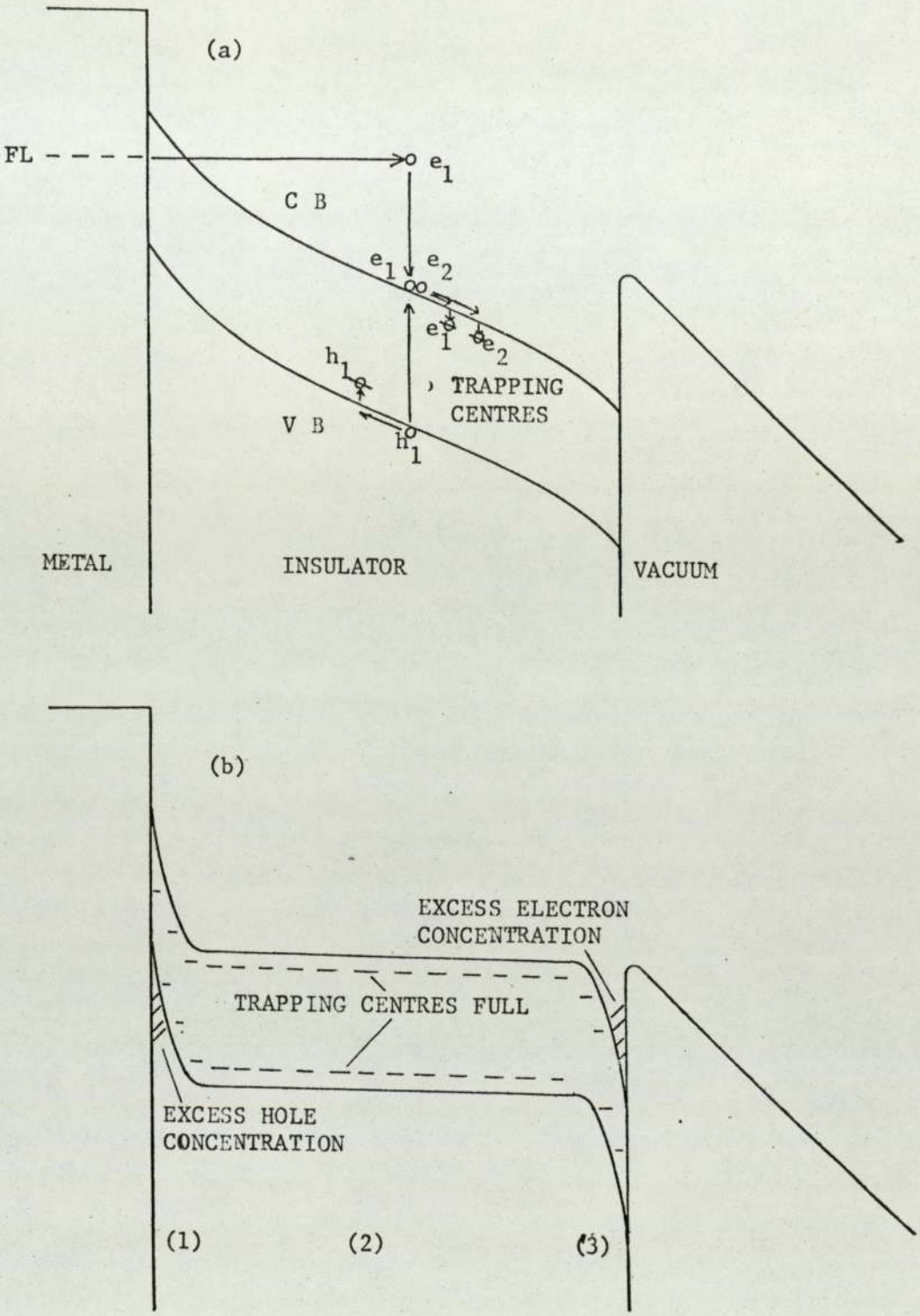

Fig. 7.7: The proposed initiating mechanism for switching.

duction band of the insulator which is experiencing a high penetrating field as illustrated in Fig. 7.2(b). The most likely mechanism for the production of this electron is tunnelling from the metal. Then if the field is high enough the electron can cause an avalanche process by impact ionisation. The resultant electrons will migrate towards the vacuum interface and the holes towards the metal interface. However, due to the presence of the large number of localised interband states many of these carriers will be trapped and the situation of Fig. 7.7(a) will ensue from which it is clear that the tunnelling probability of electrons into the impurity will become enhanced. Thus the process may repeat itself until the situation of Fig. 7.7(b) is realised when all the interband states are full. There are good reasons to believe that for most amorphous materials the number of electron and hole traps are equal,[126] and therefore charge neutrality may exist in the bulk. However, the presence of excess carriers will cause the space charges to build up in the vicinity of the two interfaces until they are large enough to cause firstly appreciable tunnelling of electrons into the insulator and secondly heating of electrons into the vacuum.

Next we shall discuss the maintenance of the space charges once electron flow and emission is established. Firstly consider the insulator/vacuum boundary since it is believed that the holes required for the space charge at the metal/insulator junction will originate here. When electrons arrive in region 3 they can experience a number of possible processes:

1) Although unlikely they might not suffer any energy loss

scattering mechanism, but be merely accelerated over the work function barrier.

2) Most electrons can be expected to undergo scattering by phonons where typical Debye energies for semiconductors are $\lesssim$ 0.1 eV and the mean free path of electrons is $\sim$ 10nm.

3) At higher current densities electrons may exchange energy by scattering against each other.

4) Electrons can cause impact ionisation of the insulator.

The final process is of especial interest since it can give rise to electroluminescence by the sequence of events illustrated in Fig. 7.5. Firstly, a hot electron creates an electron-hole pair; the latter of which migrates towards the metal but soon relinquishes its energy to excite a luminescent centre; finally there is a recombination process with a conduction electron via a trap state in which an optical photon $h\nu$ is emitted. It should also be noted that there is another mechanism that may also contribute to the observed electroluminescence which involves the production of an electron-hole pair by the field ionisation of a luminescent centre in one of the high field regions. An estimate of the relative number of radiactive recombinations can be obtained from the measurement of the total light energy output per solid angle made by Hurley and Dooley.[42] Thus integrating over all angles and taking the value for an average photon energy from their spectral measurements, it is found that the ratio of the number of photons emitted to the number of electrons present in the emission current is of the order of 1 to 10^3. However, since only a small proportion of carriers are expected to recombine radiatively,

the number of impact ionisation processes, which is equivalent to holes created, may be considerably greater. Unfortunately, in general, there appears to be no direct means of determining this factor

It is clear that in each impact ionisation process two low energy electrons will result. In addition there will exist a density of electrons which have lost so much energy by phonon scattering that they arrive at the vacuum boundary with an energy less than the height of the work function barrier. Thus electrons from these two sources will be reflected at the barrier, and it is postulated they give rise to the space charge in this region. However, if electrons accumulate indefinitely the emission mechanism will collapse, therefore an equilibrium situation must be realised where the number of electrons accumulating is balanced by the number which gain energy from collisions with higher energy electrons. For this condition to be satisfied the accelerating potential in this region must significantly exceed the electron affinity of the insulator.

From the above considerations it is likely that the number of holes created will only be a small fraction of the number of electrons crossing the insulator. Some of these holes will also be lost in recombination processes, such as those giving rise to electroluminescence. Therefore if the holes and electrons travel at the same speed through the bulk of the insulator a negative space charge will result. However, this is unlikely since in general the mobility is higher in the conduction band than in the valence band.[126] Then, in order to maintain a relatively low field in the bulk of the insulator, the ratio of the carrier concentrations would have

to be nearly equal to the inverse of the mobilities. However, near the metal junction the electrons which have just tunnelled through the barrier will have an enhanced mobility before thermalising into the bottom of the conduction band. Furthermore Mott[126] has argued that the mobility of the holes may be expected to decrease in this region. Therefore the space charges due to the two sets of carriers will not balance. In fact it has been shown[126] that the positive space charge can be large enough to maintain the tunnelling of electrons through the barrier, which is normally $\sim$ 0.5eV, i.e. sufficient to create a field of $\sim 2 \times 10^{8} Vm^{-1}$.

A further requirement of this model is that the current density must be high enough to keep the interband states fully occupied otherwise electrons will be continually trapped by these states and recombination will occur with holes, leading to a great reduction in the conductivity. Mott[126] has also shown that the dynamic space charge regime at the metal/insulator junction leads to a requirement for a constant current density. Therefore he postulated that for the current to increase the cross-sectional area of the conducting channel must also increase. However, from Fig. 7.8 it is clear that if the cross-sectional width w of the channel is less than the film thickness d, the current density in the bulk will be appreciable smaller than at the boundaries and it may become too low to satisfy the condition for the minimum current density that can prevent significant trapping and recombination. Therefore, in general, it is necessary for $w \geq d$ and this, in conjunction with the requirement for a minimum current density (j_m), leads to a minimum holding current condition, where

$i_m = j_m d^2$. These predictions have been verified experimentally by Petersen and Adler[124] who have determined the minimum current density to be $\sim 10^8$ Am^{-2}.

The model as presented at this stage can explain a number of experimental observations. In particular the switch-on phenomenon for virgin electrodes and the electroluminescent effects are integral in its development. Furthermore the high current and b sites[27, 28] discussed in Chapter 2.3 can be seen to be clear manifestations of the above current-controlled model. In larger gaps the sudden switch on could initiate the commonly observed microdischarges. However, in most cases it is thought that a further development occurs in this model such that once current flow is established the insulator undergoes atomic rearrangement or "forming". The current density that is required in the threshold switching model is so high that it can cause disintegration of the solid, unless the material has a particularly stable character, as is the case for chalcogenide glasses where the valence electrons do not take any part in the bonding. In addition when considering micron sized impurities on the surface of the electrode, it is quite plausible that the cross-section of the conducting channel may become restricted by the diameter of the impurity, hence leading to an increase in current density and heating of the channel. Accordingly, the source of the aforementioned high current and b sites may lie in particularly stable or large impurities, possibly occurring at grain boundaries.

The interpretation that is put on the forming process in the insulator switching model differs from that in

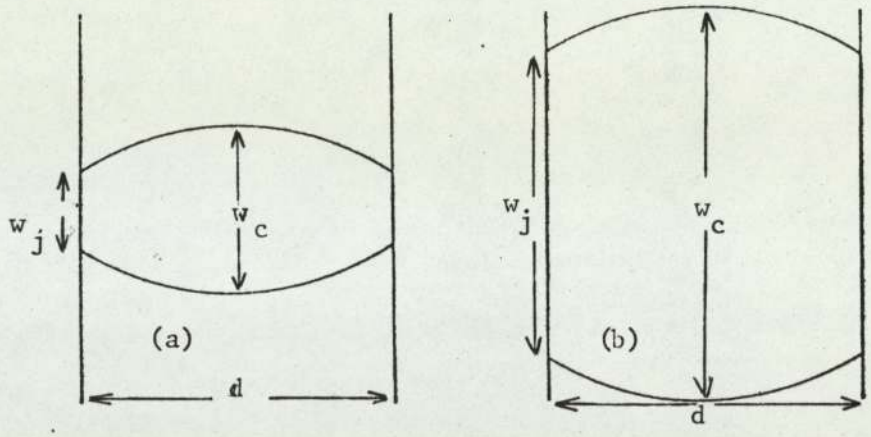

Fig. 7.8: The condition for the cross-sectional width of the conducting channel ; from Mott[126].
For (a) $w_j < d$ leads to $w_c > w_j$; whilst for (b) $w_j \simeq d$ leads to $w_c \simeq w_j$.

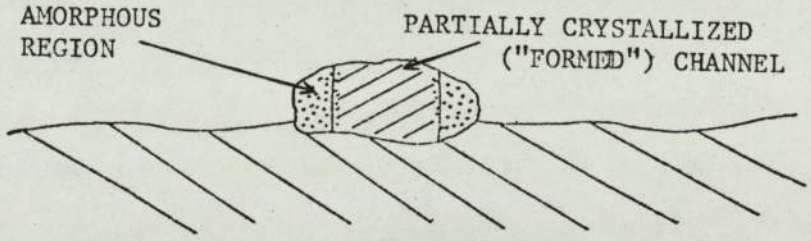

Fig. 7.9: The crystalline nature of an emitting impurity after "switching" and "forming".

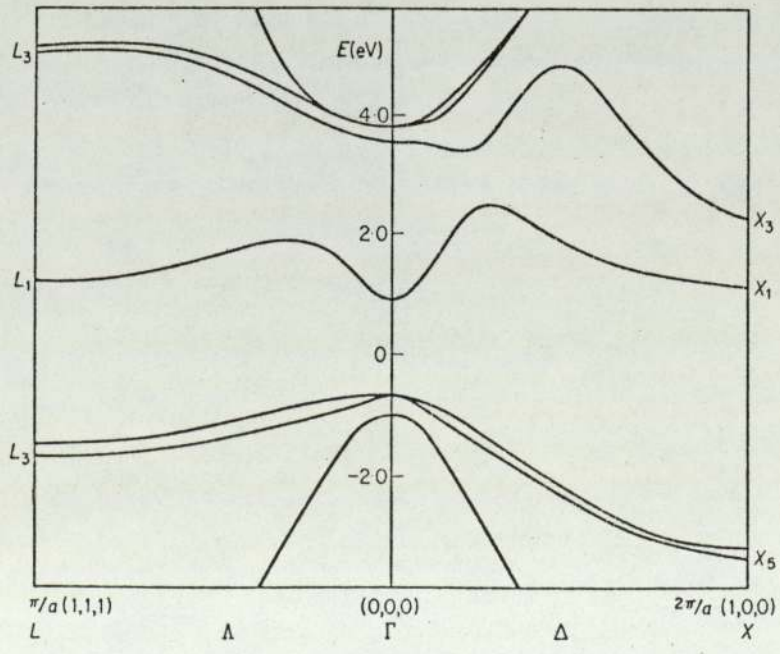

Fig .7.10 Band structure of GaAs, showing only lowest conduction bands and highest valence bands. Note the three close minima in the conduction band at Γ, X and L. The spin orbit splitting of the valence band is larger than in Si. (After M. Pollak *et al., Physics of Semiconductors,* p. 23. Kyoto, (1966).[128])

Hurley's model where it was assumed that a metallic whisker grew threw the impurity. Rather it is now envisaged that atomic rearrangement occurs within the conducting channel, such that it becomes more crystalline to give the emitting regime illustrated in Fig. 7.9. The concept of this amorphous-to-crystalline transition is strongly supported by the x-ray diffraction measurements made by Moridi and Hogarth[127] on switches which had become locked into the on-state. However, in general, other atomic rearrangement phenomena may also occur, depending on the explicit properties of the substrate metal and the insulating impurity. One interesting possibility is the diffusion of metal atoms into the insulator changing the discrete metal/insulator junction into a more gradual one. Another possible mechanism is solid state electrolysis where negative ions migrate towards the metal and positive ions towards the vacuum boundary.

7.6 Comparison of the Insulator Switching Model with the Experimental Results

We shall now proceed to compare the predictions of the above model with the experimental results, following the same listing as in section 7.1. It must, however, be stated at the outset that this discussion is necessarily of a generalised nature since the actual impurity which may be involved at a particular emission site is not known. However, it is possible to draw attention to the points that would have to be considered if this information was available.

1. The switch-on effect for virgin electrodes has already been considered in the development of the model, and the sub-

sequent continuous emission at a reduced field is believed to be a consequence of the forming process. Once a channel has been crystallised it will contain substantially fewer interband trapping states and hence the minimum current density condition will be relaxed, allowing emission at very low current levels. In addition, a lower external field may be required to initiate the electron emission by introducing electrons into the conduction band of the insulator if a gradual metal/insulator boundary exists, or there is an internal field due to solid-state electrolysis.

2. The current-voltage characteristics of vacuum gaps have often been reported, for example[16, 18, 23], to show excellent fits to the Fowler-Nordheim theory for field emission if a geometrical field enhancement factor is assumed. However, in the present investigation the experimental data for individual sites has only shown an approximate fit to F-N theory at low and intermediate currents ($\lesssim 10^{-7}$A), with quite a strong divergence at higher currents. This discrepancy may be understood when it is realised that the former reports usually referred to gaps which had been conditioned until stable and reproducible I-V results could be obtained. Various conditioning procedures have been used by these workers such as passing high currents for long periods or more usually sparking or striking arcs. However, where the electrodes are not thoroughly conditioned anomalous I-V relationships have been reported[25, 26] and are discussed in Chapter 2.3.

Consider now the form of the I-V characteristic to be expected from the model proposed in Fig. 7.5. From this it follows that if the current is controlled by the rate of

electrons tunnelling into the insulator conduction band the I-V relationship should be of the F-N type, and then the enhancement factor β would be of $\sim \frac{x}{d}$. However, once forming has occurred it seems likely that this junction will not be dominant, but rather that the emission will be controlled by the rate of escape of electrons in region 3. Here the situation is somewhat analagous to thermionic emission, where the "temperature" of the electrons is a function of the accelerating field. Thus whilst the supply function may be complex, and dictated by the scattering mechanisms in this region, the escape probaility will be exactly that of the thermionic form. A possible explanation for the tendency of the current to saturate at high values is that at these levels the electron flow may no longer be confined to the formed channel but also pass through the outer regions of the impurity which are expected to be still of a disordered nature.

The various anomalous phenomena, reported by Powell and Chatterton,[25] and discussed in Chapter 2.3 can now be attributed to the effects of "forming". Thus rectangular pulse conduction is attributed to the unstable nature of a partially formed channel. The passage of high currents or ageing leads to complete forming, whilst deageing is believed to be relaxation away from the formed state possibly due to the absorption of "active" gases into the channel.

3. Since the emission spectrum is almost entirely a property of the surface impurity, it is not surprising that no general differences are distinguishable in the energy distributions from sites on different metals. It has also been noted that metals which have particularly continuous

and/or thick (∿ several nanometres) ambient oxide films are less emissive; a fact which may be attributed to the complicated metal-oxide-insulator situation that will generally exist at the junction of the impurity with the substrate. When such a site eventually switches on the current and field conditions may have become sufficiently critical to initiate a microdischarge.

4. The origin of the shift of the energy distribution below the Fermi-level of the substrate metal can be understood by referring to Fig. 7.5. From this the shift is clearly seen to be the sum of three components: (i) the energy lost in thermalising into the conduction band minimum in region 1; (ii) the ohmic energy loss in low field region 2; and (iii) the energy lost due to scattering in region 3. Electrons which have thermalised in a parabolic conduction band minimum will have a FWHM of ∿ 1.5kT (0.04eV at room temperature) before entering region 3. Hence the FWHM of the emitted distribution will be almost exclusively due to scattering of "hot electrons" in this region. Each of the energy loss mechanisms may be expected to increase with increasing field and current, so that referring to Fig. 5.7 and 5.8, which illustrate two of the more complete range of measurements, it may be observed that at high fields both the FWHM and the shifts are increasing rapidly. Therefore, it must be concluded that at current levels > 10^{-7}A, energy losses in region 3 predominate; an effect which can be attributed to the increasing cross-sections for impact ionisation and electron-electron scattering at high fields and currents. In the low field range there is very little variation of FWHM and shift suggesting that the ohmic losses

are not significant until the current exceeds $\sim 10^{-8}$A.

5. In the original band theory model[92] the multi-peaked spectra were attributed to resonances in the tunnelling probability due to adsorbed atoms. Clearly such an explanation is inappropriate in the present model, since the energy levels of adsorbed atoms will not have any significant effect on electrons which are transmitted over the work function barrier, although changes in the height of barrier due to adsorption may be important for the total current. An alternative explanation for the multi-peaked spectra is that they are due to electrons which have travelled through the insulator in more than one conduction band minimum. The energy-momentum relationship of a typical semiconductor are shown in Fig. 7.10 where several conduction band minima may be observed, differing in energy by $\sim$ tenths of eVs. Under these circumstances the above concept fits the experimental observations in the following manner: (i) the separation of the observed peaks are also of order of tenths of eVs and have in one case been demonstrated to remain fairly constant with field; (ii) the behaviour of the individual peaks appears to be reasonably independent and similar to that of single peaked distributions; (iii) as the field is increased more electrons will either tunnel directly into higher conduction bands or be scattered into these explaining why new peaks always appear and grow on the high energy side.

6. The proposed model, which involves dynamic space charges and a partially crystallised impurity, is inherently unstable. In addition it has already been suggested that adsorbed atoms may effect the emission by changing the height of the

work function barrier, although the suppression of electron emission by some "active" gases may also be understood in a manner very similar to that used in Hurley's model and discussed in section 7.3. Now it is assumed that these gases are absorbed into the conducting channel, creating trapping states and hence reducing the current flow.

Tentative explanations are now forwarded for some of the anomalous spectral effects observed during this investigation. Thus, it is suggested that the many shouldered spectrum of Fig. 5.23 contains a number of sub-distributions each of which have suffered a discrete number of phonon scattering events. This assertion is supported by the facts that the distribution was obtained at an unusually low current and the separation of the sub-distributions is approximately constant and equal to 0.07 eV, e.g. typical of the Debye energy for semiconductors and insulators. The spectrum of Fig. 5.24 which is found to vary as the specimen is displaced in front of the anode probe is attributed to two closely spaced sites or possibly the existence of two independent conducting channels having formed in a largish impurity. The unusually stable two-state switching behaviour of the site illustrated in Fig. 5.21 could be the result of an incomplete conditioning or forming of the conducting channel, since the effect is, on the one hand, eliminated by the passage of a high current and, on the other, can be recovered in a slightly different form by reversing the polarity of the gap for a few minutes. In this respect the transition time between different states has been measured to be $\sim$ 1ms and this also suggests that the switching is not a totally electronic process but probably

involves stoichometric changes in the conducting channel. One possible explanation for the two-state switching is that the insulator is able to exist in two easily reversible crystalline states.

7. Electroluminescence has already been discussed in terms of an amorphous channel during the development of the model. However, even after forming, the crystallised channel is still expected to contain many interband states, in addition, electrons may be scattered into the disordered region that surrounds the channel. The complex nature of the interband luminescent and recombination energy levels is reflected in the broad optical spectrum which ranges in energy from < 1.5 to 2.5eV, where the higher figure represents a minimum value for the insulator band gap.

8. Electrons within the emitting impurity must have energies $\gtrsim$ 2.5eV in order to excite the transitions which lead to electroluminescence. A similar condition also arises for the electrons to have an energy greater than the electron affinity of the insulator in order to escape over the barrier into the vacuum, when energy losses inside the impurity are still low. Hence, if it is assumed that the insulating material has the most favourable dielectric properties for supporting the maximum internal field, viz, that it should have a low dielectric constant $\varepsilon_r \to 1$, the necessary thickness for such an impurity to drop 2.5eV in a field of $\sim 10^7 Vm^{-1}$ is $\sim$ 0.25 m. This figure agrees well with the dimensions (typically $\sim$ μm) of the insulating impurities that have been directly identified as being responsible for the localised emission sites.

9. Outgassing of the specimen at high temperatures has been

found to stabilise the emission current and the associated spectra. This clearly appears to be due to an annealing effect such that the conducting channel becomes more completely formed or crystalline.

10. The effects of ion bombardment can be considered in two stages. Firstly, when the etching is slight ($\sim$ nm for the insulator) the major effect of the bombardment may be deconditioning of the channel by disturbance of the crystallinity either by causing dislocations or by penetration of the ions into the impurity. Such effects lead directly to instabilities in the electron spectrum. When etching is carried to greater depths, the dimensions of the impurity may become the critical factor. If an impurity becomes too thin it may no longer be able to effect a sufficient electrostatic potential drop within itself. However, if it is too thick electron transport through the impurity becomes more difficult. Thus the original emission site may be extinguished after etching, whilst another begins to emit. Another possibility for the activation of an emitting site is the exposure of a favourable impurity which was previously totally included inside the metal.

The interpretation of the experimental results as discussed above is very generalised and is open to criticism, however it does have the merit of offering qualitative explanations for most of the observed phenomena.

CHAPTER 8

CONCLUSIONS

This thesis describes a wide ranging investigation into the nature of electron emitting sites on broad area electrodes. In the major experimental method a purposefully modified high resolution (< 300 meV) electron spectrometer has been employed to determine the energy distribution of the electrons arising from such sites. Early measurements immediately revealed that the general form of the observed spectra was basically different from that expected for electrons which had been emitted according to the traditional theories of field emission: the maximum of the distribution was always shifted 200 - 500 meV below the Fermi energy of the substrate metal and it had an half-width of 300 - 500 meV and which may be compared with 500 meV and 230 meV respectively for electrons that have quantum-mechanically tunnelled through a metallic work-function barrier at room temperature. Subsequent experiments have concentrated on determining the influence of various parameters on the form of the electron spectra.

Thus:

1) Spectra from four different metals, namely copper, stainless steel, titanium and gold, were all found to have the same general form as outlined above; hence further investigations were confined to copper specimens.
2) Three different types of surface finish, viz. machined, mechanically polished and grown from the melt, for copper specimens again revealed no significant differences in the nature of the electron spectra.
3) As the applied field was increased the observed spectra changed such that both the shift of the distribution below the metallic Fermi level and its half-width

increased in a non-linear fashion. Several sites provided multi-peaked spectra in which case new peaks appeared and grew in relative magnitude on the high energy side of the distribution as the field was increased.

4) The effects of two types of in situ surface treatment have been studied. Outgassing of the specimen at 700°C for two minutes has been found to increase the stability of the electron spectra. However ion-etching of the surface to a depth of $\sim$ 10nm in copper causes the spectrum to become very unstable and irregular, whilst etching to depths of $\sim$ 100nm can eliminate some sites and possibly activate others.

5) Preliminary studies have revealed that the electron spectra are independent of illumination ($< 10^5$ Wm^{-2}) and temperature in the range of 300K to 800K; although the latter result suffers from an estimated resolution of 80 meV, in the electron spectra.

Further experimental observations have been made which are not directly related to electron spectrometry. Thus the current from virgin electrodes is found to switch on suddenly once a certain field value is reached, following which the field may be reduced and continuous emission currents still obtained. Fowler-Nordheim plots of the subsequent current-voltage data have generally been found to be non-linear. A technique has also been established to obtain complementary optical spectra measurements from a specimen without removing it from the vacuum chamber that includes the electron spectrometer. With this facility it has been possible to characterise an individual emitting site both in terms of its electron spectrum and its optical spectrum. Finally an important

subsidiary facility has been developed to directly locate electron emitting sites in situ in a scanning electron microscope. This technique has realized a resolution of 2-4 μm and has shown that microscopic (∿ μm) insulator type impurities are to be found within the areas predicted to contain electron emitting sites.

The traditional explanation for the prebreakdown currents from broad area electrodes assumed that the electrons arose from surface features, such as protusions or whiskers, where the field is sufficiently enhanced to induce tunnelling of electrons through the modified work function barrier of the metal. However the results obtained in this investigation are clearly not consistent with this hypothesis; instead it appears that the emission is associated with microscopic insulator-type surface impurities. Two models have recently been proposed to explain the emission of electrons through an insulating impurity that is being subjected to an high electric field. The concepts inherent is these models have been used to evolve a new model which is believed to be theoretically more realistic. The basis of this hypothesis is that the external electric field penetrates through the insulator, and as this field is increased it becomes high enough to cause the insulator to switch into a conducting state. Then space charges come into existence within the impurity which favour both the injection of electrons from the metallic substrate into the impurity and their subsequent emission over the work function barrier into the vacuum. The initial emission is though to be followed by atomic rearrangement or "forming" within the impurity such that subsequently continuous emission currents may be obtained at reduced fields. This model is

shown to be capable of accounting for most of the experimental observations, e.g. the shift of the energy distribution below the Fermi-level is related to energy losses within the impurity. However these explanations are at present invariably qualitative and sometimes tentative, since the actual physical and chemical nature of the impurity assumed to be part of the emission regime is not generally known.

Suggestions for future work that arise from the present investigations can be conveniently divided into two categories. Firstly further studies of the emission properties of broad area electrodes, and secondly studies involving simulation of hypothetical emission regimes. The following fall in the former category:

1) There is considerable scope for further measurements of the effects of temperature on the electron spectra; in particular the provision of a cold stage for low temperature studies.
2) The effects of the various conditioning procedures need to be investigated, and spectra should be obtained from electrodes which have been conditioned to produce linear and reproducible Fowler-Nordheim plots.
3) More extensive spectral measurements could be made on materials other than copper.
4) Further studies could be made of in situ surface treatments which may prduce impurity-free surfaces, e.g. ion plating.
5) There is scope for the improvement of the optical spectra facility in terms of resolution, sensitivity and flexibility.
6) Fast pulse experiments could be carried out to discover

more information about the switch-on phenomenon.

In the second category the proposed emission regime could be simulated by either depositing thin films of appropiate insulators onto metallic substrates or embedding single insulating particles onto a well conditioned electrode using a microparticle gun. Then if it was verified that an electron emission site can be created in this manner, the possibility exists for the development of novel high current density cold cathodes. Furthermore by obtaining electron emission spectra from a known insulator it should be possible to deduce many of its electronic properties.

REFERENCES

1. R H Fowler & L Nordheim, Proc. Roy. Soc., Ser. A119, 173-181 (1928).

2. L Nordheim, Proc. Roy. Soc., Ser. A121, 626-639 (1928)

3. R H Good & E W Muller, Handbuch der Physik (Springer-Verlag, Berlin), 21, 176-231 (1956)

4. A G J Van Oostrom, Philips Res. Reports Supplements, No. 1, (1966).

5. H C Miller, J.Franklin Inst., 282, 382-388 (1966)

6. H C Miller, J.Franklin Inst., 289, 347-351 (1969)

7. H E Tomasche & D Alpert, J. Appl. Phys., 38, 881-883 (1967)

8. R Haefer, Z.Physik. 116, 604-622 (1940)

9. W P Dyke, J K Trolan, W W Dolan & G Barnes, J. Appl. Phys. 24, 570-576 (1953)

10. W P Dyke, J K Trolan, E E Martin & J P Barbour, Phys. Rev., 91, 1043-1054 (1953)

11. R A Millikan & R A Sawyer, Phys. Rev., 12, 167-170 (1918)

12. R A Millikan & B E Shackeford, Phys. Rev., 15, 239-240 (1920)

13. R A Millikan & C F Eyring, Phys. Rev., 27, 51-67 (1926).

14. R A Millikan & C C Lawitsen, Proc. Natl. Acad. Sci. (U.S.A.), 14, 45-49.

15. W S Boyle, P Kisliuk & L H Germer, J. Appl. Phys. 26, 720-725 (1955)

16. D Alpert, D A Lee, E M Lyman & H E Tomaschke, J. Vac. Sci. Tech., 1, 35-50 (1964)

17. R P Little & S T Smith, J. App. Phys., 36, 1502-1504 (1965)

18. H E Tomaschke & D Alpert, J. Vac. Sci. Tech., 4, 192-198 (1967)

19. R P Little & W T Whitney, J. App. Phys., 34, 2430-2432 (1963)

20. I Brodie, J. Appl. Phys., 35, 2324-2332 (1964)

21. I Brodie, J. Vac. Sci. Tech., 2, 249-256 (1965)

22. R Gomer, J. Chem. Phys., 21, 293-303 (1953)

23. D K Davies & M A Biondi, J. App. Phys., 37, 2969-2977 (1966)

24. D K Davies & M A Biondi, J. App. Phys., 39, 2979-2990 (1968)

25. H P S Powell & P A Chatterton, Vacuum, 20, 419-429 (1971)

26. R Hackam & S K Salman, Proc. IEE, 119, 377-384 (1972)

27. B M Cox, CEGB Laboratory Note, R/M/N1021 (1979)

28. R E Hurley, J. Phys. D: Appl. Phys., 13, 1121-1128 (1980)

29. R Hawley & A A Zaky, Progressin Dielectrics, 7, 115 - 215 (1967)

30. L I Pivovar & V I Gordienko, Sov. Phys.: Tech. Phys., 3, 2101-2105 (1958)

31. L I Pivovar & V I Gordienko, Sov. Phys.: Tech. Phys., 7, 908-912 (1963)

32. P C L Pfeil & J Griffiths, J. Nucl. Mater., 3, 244-248 (1966)

33. R. Hancox, Brit. J. Appl. Phys., 11, 468-471 (1960)

34. J T Maskrey & R A Dugdale, Brit. J. Appl. Phys., 17, 1023-1034 (1966)

35. J T Maskrey & R A Dugdale, J. Sci. Instrum., 42, 284-286, (1966)

36. E E Donaldson & M Rabinowitz, J. Appl. Phys., 34, 319-322 (1963)

37. A S Pokrovskaya-Soboleva, V V Kraft, T S Borisova & L K Mazurova, Proc. 5th Int. Symp. Discharges and Elect. Ins. in Vac., Poznan, Poland, 105-109 (1972)

38. G A Farrall & M Owens, J. Appl. Phys., 43, 938-943 (1972)

39. G A Garrall, M Owens & F G Hudda, J. Appl. Phys., 46, 610-617 (1975)

40. G A Farrall, F G Hudda & R H Johnston, J. Appl. Phys., 50, 3608-3614 (1979)

41. B M Cox, J. Phys. D : Appl. Phys., 8, 2065-2073 (1975)

42. R E Hurley & P J Dooley, J. Phys.D: Appl. Phys, 10, L 195 - L 201 (1977)

43. N K Allen & R V Latham, J. Phys.D: Appl. Phys., 11, L 55 - L 57, (1978)

44. B M Cox & D E J Wort, Vacuum, 22, 453-455 (1972)

45. B M Cox & W T Williams, J. Phys.D: Appl. Phys, 10, L5 - L9 ((1977)

46. B N Klyarfel'd & A S Pokrovskaya-Sobole a, Sov. Phys.: Tech. Phys., 15, 149-152 (1970)

47. G F Alfrey & J B Taylor, Brit. J. Appl. Phys., 6, Suppl. 4, S44-S49 (1955)

48 R E Hurley, J. Phys.D: Appl. Phys., 12, 2247-2252 (1979)

49. R E Hurley & P J Dooley, Vacuum, 28, 147-149 (1978)

50. J E Henderson & R E Badgley, Phys. Rev., 38, 590 (1931)

51. J E Henderson & R K Dahlstron, Phys. Rev., 55, 473-481 (1939)

52. E W Muller, Z. Physik. 102, 734-761 (1936)

53. E W Muller, Z. Physik. 120, 261-269 (1943)

54. E W Muller & K Bahadur, Phys. Rev., 102, 624-631, (1956)

55. R D Young & E W Muller, Phys. Rev., 113, 115-120 (1959)

56. J W Gadzuk & E W Plummer, Rev. Mod. Phys., 45, 487-548, (1973)

57. R D Young, Phys. Rev., 113, 110-114 (1959)

58. L W Swanson & L C Crouser, Phys. Rev., 163, 622-641 (1967)

59. E W Plummer & A E Bell, J. Vac. Sci. Tech., 9, 583-590 (1972)

60. N Nicolaou & A Modinos, Phys. Rev., B 11, 3687-3696 (1975)

61. A Modinos & N Nicolaou, Phys. Rev., B 13, 1536-1547 (1976)

62. A Modinos, Surf. Sci., 70, 52-91 (1978)

63. R D B Whitcutt & B H Blott, Phys. Rev. Lett., 23, 639-640 (1969)

64. N Kar & P Soven, Solid State Comm., 19, 1041-1043, (1976)

65. J P Jones & E W Roberts, Surf. Sci., 64, 355-381, (1977)

66. L W Swanson & L C Crouser, Phys. Rev. Lett., 19. 1179-1181 (1967)

67. N J Dionne & T N Rhodin, Phys. Rev., B14, 322-340 (1976)

68. N Rihon, Phys. Stat. Sol., A49, 697-703 (1978)

69. C Lea & R Gomer, Phys. Rev. Lett., 25, 804-806 (1970)

70. J W Gadzuk & E W Plummer, Phys. Rev. Lett., 26, 92-95 (1971)

71. J J Czyzewvski, Surf. Sci., 39, 1-20 (1973)

72. J W Gadzuk & A A Lucas, Phys. Rev., B7, 4770-4775 (1973)

73. A E Bell & L W Swanson, Phys. Rev., B19, 3353-3364 (1979)

74. C B Duke & H E Alferieff, J. Chem, Phys., 46, 923-937 (1967)

75. E Merzebacher, Quantum Mechanics, (Wiley, New York) 121-130 (1961)

76. E W Plummer & R D Young, Phys. Rev., B1, 2088-2109 (1970)

77. L W Swanson & L C Crouser, Surf. Sci., 23, 1-29 (1970)

78. R Stratton, Proc. Roy. Soc., B68, 746-757 (1955)

79. R Stratton, Phys. Rev., 125, 67-82 (1962)

80. R Stratton, Phys. Rev., 135, A794-A805 (1964)

81. J Bardeen, Phys. Rev., 71, 717-727 (1947)

82. L M Baskin, O I Lvov & G N Fursey, Phys. Stat. Sol., B47, 49-62 (1971)

83. J R Arthur Jr., J. Appl: Phys., 36, 3221-3227 (1965)

84. O H Hughes & P M White, Phys. Stat. Sol., 33, 309-316 (1969)

85. L T J Salman & E Braun, Phys. Stat. Sol., A16, 527-532 (1973)

86. B F Lewis & T E Fischer, Surf. Sci., 41, 371-376 (1974)

87. A Modinos, Surf. Sci., 42, 205-227 (1973)

88. P Handler, J. Phys. Chem. Solids., 44, 1-8, (1960)

89. W B Shepherd & W T Peria, Surf. Sci., 38, 461-498 (1973)

90. D E Sykes & E Braun, Phys. Stat. Sol., B69, K137-K140 (1975)

91. N Rihon, Surf. Sci., 70, 92-100 (1978)

92. N K Allen & R V Latham, Proc. 8th Int. Symp. Disch. & Elec. Ins. in Vac., Alburquerque, B3, 1-13 (1978)

93. N K Allen, B M Cox & R V Latham, J. Phys. D: Appl. Phys., 12, 969-977 (1979)

94. A G J Van Oostrom, Philips Research Reports Supplements, 1, 1-102 (1966)

95. C E Kuyatt & E W Plummer, Rev. Sci. Inst., 43, 108-111 (1972)

96. E.Braun, R G Forbes, J Pearson, J M Pelmore & R V Latham, J. Phys. E: Sci. Inst., 11, 222-228 (1978)

97. E M Purcell, Phys. Rev., 54, 818-826 (1938)

98. J H Parker Jr. & R W Warren, Rev. Sci. Inst., 33, 948-950 (1962)

99. J Pearson, Private Communication

100. D W O Heddle, R G W Keesing & J M Kurega, Proc. Roy. Soc. A334, 135-147 (1973)

101. R D Young & C E Kuyatt, Rev. Sci. Inst., 39, 1477-1480 (1968)

102. G P Beukema, J. Phys. D: Appl. Phys., 6, 1455-1466 (1973)

103. J Franks, British Patent No. 44718/73 (1973).

104. J Franks and A M Ghander, Vacuum, 24, 489-491 (1974)

105. R K Fitch, M Khorassany and T N Mawlood, Proc. 7th Int. Vac. Congr. and 3rd Int. Conf. on Solid Surfaces, Vienna, 285-288 (1977)

106. P D Davidse and L I Maissel, J. Vac. Sci. Tech., 4, 33-36(1967).

107. R E Hurley, J. Phys. D:Appl. Phys. 12, 2229-2245 (1979)

108. R W Young, Vacuum, 24, 167-172 (1973)

109. R Coelho and J Debeau, J. Phys. D:Appl. Phys. 4, 1266-1280 (1971)

110. R Young, J Ward and F Scire, Rev. Sci. Instrum., 43, 999-1011 (1972)

111. B M Cox, Private Communication (1980)

112. E L Cook, J. Appl. Phys., 41, 551-554 (1970)

113. G Dearnaley, A M Stoneham and D V Morgan, Rep. Prog. Phys., 33, 1129-1191 (1970)

114. G Dearnaley, Thin Solid Films, 3, 161-174, (1969)

115. T W Hickmott, J. Appl. Phys., 37, 4380-4388 (1966)

116. B Juttner, W Rohrbech and H Wolff, Proc. 5th Int. Symp. Disch. and Elec. Ins. Vac., 65-69 (1972).

117. B Juttner, H Wolff and B Altrichter, Phys. Stat. Sol., 27 403-412 (1975)

118. S Benzer, J. Appl. Phys., 20, 804-815 (1949)

119. S R Ovshinsky, Phys. Rev. Lett., 21, 1450-1453 (1968)

120. D Adler, M S Shur, M Silver and S R Ovshinsky, J. Appl. Phys., 51, 3289-3309 (1980).

121. K Homma, H K Henisch and S R Ovshinsky,J. Non-Cryst. Solids, 35 and 36, 1105-1110 (1980)

122. D Adler, Amorphous Semiconductors, (Butterworths, London, 1972)

123. D Adler, H K Henisch and N F Mott, Rev. Mod. Phys., 50, 209-220 (1978)

124. K E Petersen and D Adler, J. Appl. Phys., 47, 256-263 (1976)

125. L W James and J L Moll, Phys. Rev., 183, 740 - 753 (1969).

126. N F Mott, Philos. Mag., 32, 159-171 (1975)

127 G R Moridi and C A Hogarth, Int. J. Electron., 44, 297-304 (1978)

128. M Pollak et al., Physics of Semiconductors, p. 23, Kyoto (1966).

ACKNOWLEDGEMENTS

The work described in this thesis was carried out during the tenure of a Science Research Council grant.

I would like to thank my Supervisor Dr. R.V. Latham, for many useful discussions, advice and encouragement throughout the course of the work.

Physica 104C (1981) 46–49

A MICROPOINT PROBE TECHNIQUE FOR IDENTIFYING FIELD-EMITTING SITES OF BROAD-AREA HIGH VOLTAGE ELECTRODES

C.S. ATHWAL and R.V. LATHAM

Physics Department, University of Aston in Birmingham, Birmingham B4 7ET, U.K.

A technique has been developed that uses a microtip anode probe for locating and observing field-emitting sites on broad-area high voltage electrodes in situ in a conventional scanning electron microscope. Results obtained with the present version of the technique, where the resolution is ≈2–4 μm, have not only confirmed earlier findings that emission sites are not generally associated with the presence of sharp field enhancing microfeatures, but also established that micron and sub-micron sized impurity particles are commonly observed at emission site locations.

1. Introduction

It is well established that electrical breakdown in vacuum is often associated with electrons emitted from microscopic sites on the surface of broad-area high voltage electrodes. Prior to the work of Cox [1, 2] the popular conception of these sites was of metallic microprotrusions at which the field was sufficiently enhanced to give rise to a Fowler–Nordheim type of free electron field emission process: this view was based principally on the *indirect* electron optical evidence of such features on the surface of arced electrodes [3, 4] and the fact that the F–N current–voltage characteristic of a vacuum gap is generally linear over a wide range of fields. However, this model was questioned by the findings of the *direct* electron optical technique of Cox [1, 2] which showed that the localised region of the electrode surface containing a site rarely included the anticipated sharp microprotrusion. The resolution of his anode probe hole technique was unfortunately limited to ≈10 μm, so that it was not possible to identify the individual topographical feature responsible for the emission. In an attempt to obtain this information, the alternative anode micropoint probe technique described in this paper was developed which, in principle, has a higher resolution. It also offered the possibility of locating other emission processes such as the so-called *b*-sites [5] which usually appear at fields when a normal test gap would have broken down. Furthermore, an energy-dispersive X-ray spectrometer is available for use directly in conjunction with the SEM in order to investigate the elemental composition of any microscopic area on the specimen.

2. Experimental

We follow Hurley [6] and use a pointed anode probe to detect the electron emitting sites. In practice, this involves employing a technique that uses three probes of diminishing tip diameter, namely rounded copper and tungsten wires of respective tip diameters (a) 0.7 mm and (b) 0.1 mm, and (c) a standard electrolytically etched tungsten microtip having a diameter of ≈100 nm. Referring to fig. 1, the probes are mounted radially on an insulated electrical feedthrough, and can be located in turn precisely on the axis of the SEM by the combination of translatory manipulation via a bellows-operated, pivot-adjustable mounting, and rotation by a system of gears. The specimen cathode, which is oriented normally to the probe and at 45° to the SEM axis, is mounted on the goniometer stage of the instrument such that its surface can be scanned in a spiral pattern in front of the fixed probe. By arranging for the specimen to be electrically insulated from the earthed mechanical stage, it is

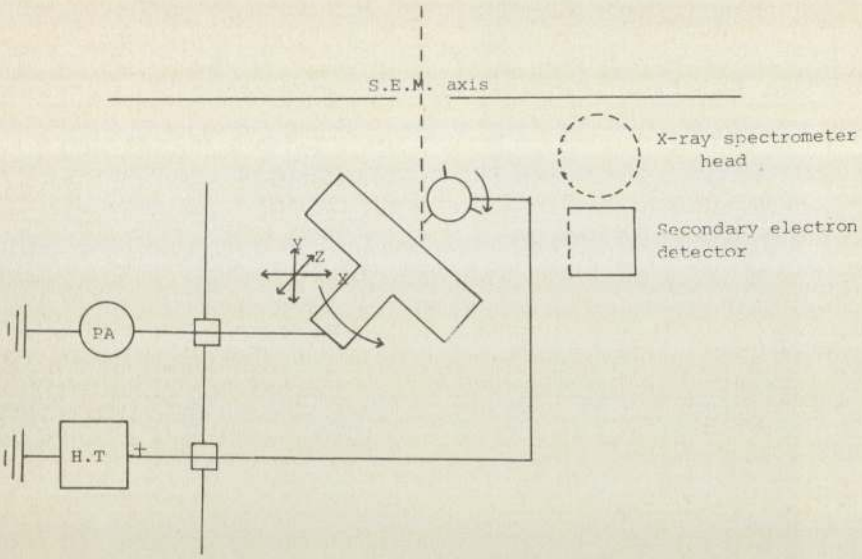

Fig. 1. Schematic representation of specimen and anode probe assembly as mounted in the scanning electron microscope.

possible to use a series picoammeter (electrometer) to monitor any emission current drawn from the specimen. Since the experiment was performed in a conventional SEM, the working pressure was only $\approx 10^{-3}$ Pa.

The experimental procedure is first systematically to scan the specimen under the large probe (a) with an electrode gap of ≈ 0.4 mm and a probe potential of ≈ 10 kV. Once a site has been found as indicated by a current of $\geq 10^{-8}$ A, the probe holder is rotated and the site more finely located under the probe (b). Finally, the tungsten microtip (c) is appropriately positioned and a gap of 0.1–0.2 mm established by means of the focus of the SEM. At this stage a current-limiting resistor of value $5 \times 10^9\ \Omega$ is inserted in the high voltage line to prevent melting of the tip due to excessive electron bombardment. The small area identified is now finely scanned to obtain a current of 5×10^{-8} A, and then the gap and potential gradually reduced keeping the current constant: at this current level the fluctuations are typically about $\pm 2 \times 10^{-8}$ A. From a plot of this potential versus the gap co-ordinate, and using the theoretical considerations of Coelho and Debeau [7] for the electrostatic field of this electrode configuration, the actual separation may be deduced. For the closest approach this may be $\sim 10\ \mu$m.

3. Results

Experiments on copper electrodes at the present spatial resolution of emission site location of 2–4 μm confirm the findings of Cox [2] that there are no conical or whisker-like field enhancing projections having the type of geometry required by the conventional field emitting model based on the Fowler–Nordheim theory. Instead, the isolated area of $\approx (3\ \mu\text{m})^2$ containing the site typically includes one or possibly two micron or sub-micron particles, having an insulating character (i.e. they appear charged in the SEM image), and which are assumed to be responsible for the measured emission. An example of an emission site location with the superimposed probe is shown in the micrograph of fig. 2. In this case an X-ray spectrometer (Kevex) analysis of each of the insulating-type particles did not reveal any anomalous elements, so it was assumed that they were probably copper oxide; it must however be recognised that the Kevex is incapable of identifying elements of atomic number less than 8, so that such elements

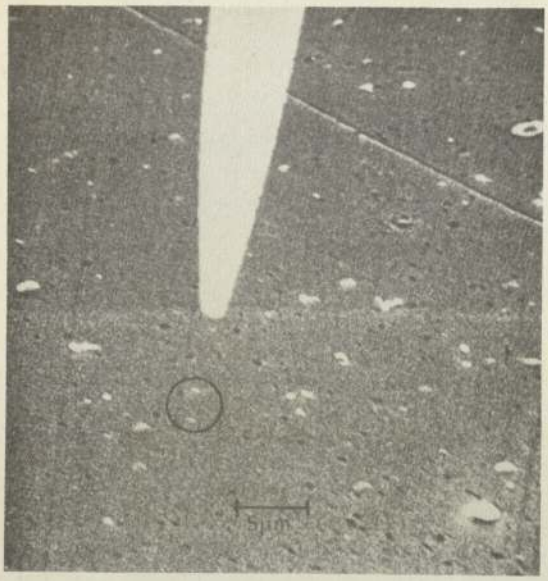

Fig. 2. Electron micrograph of a tungsten micropoint anode immediately above an electron emission site on a polished copper surface. The site is predicted to occur within the marked circle.

as oxygen, carbon and nitrogen would not be detected if present in the particles. For the example shown in fig. 3 and at higher magnification in fig. 4, which is an unpolished surface showing the circular machine marks, the Kevex spectrum (fig. 5) revealed an impurity of

Fig. 3. A low magnification electron micrograph of a tungsten micropoint immediately above an electron emitting site on a turned and damaged copper surface.

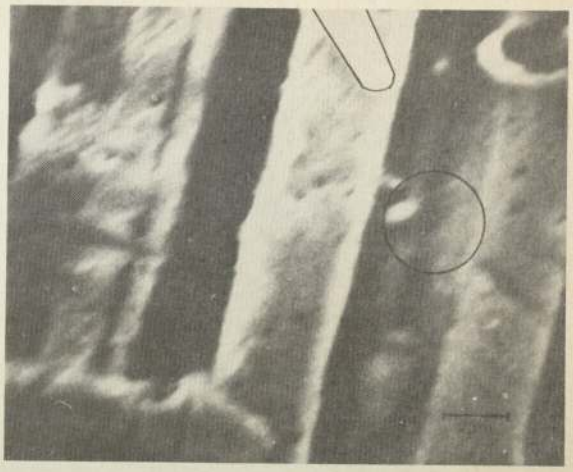

Fig. 4. High magnification electron micrograph of the same emission regime as shown in fig. 3. The electron emission site is predicted to occur within the marked circle: the profile of the probe is also shown.

silver that is present in an insulating form, most likely an oxide since a compound involving an element having an atomic number greater than 8 would have revealed an additional peak. The irregular gouge mark crossing the turning grooves on the specimen was caused by one of the other microtips scratching the surface in an earlier attempt to precisely locate this site. It is of particular interest to note that this drastic event in fact led to no additional emitting sites, thus serving to re-emphasize the point that electron emission on extended area cathodes rarely originates from field enhancing features.

4. Conclusion

The findings of this investigation further reinforce the conclusion drawn from measurements of the electron spectra of the emitted electrons [8, 9] and their associated electroluminescence [10, 11], that an insulating or semiconducting regime exists at the source of this emission phenomena. It should also be added that the present technique could be substantially improved in two respects: first, by employing an ultra-high vacuum microscope, since the poor vacuum of $\approx 10^{-3}$ Pa of a conventional SEM

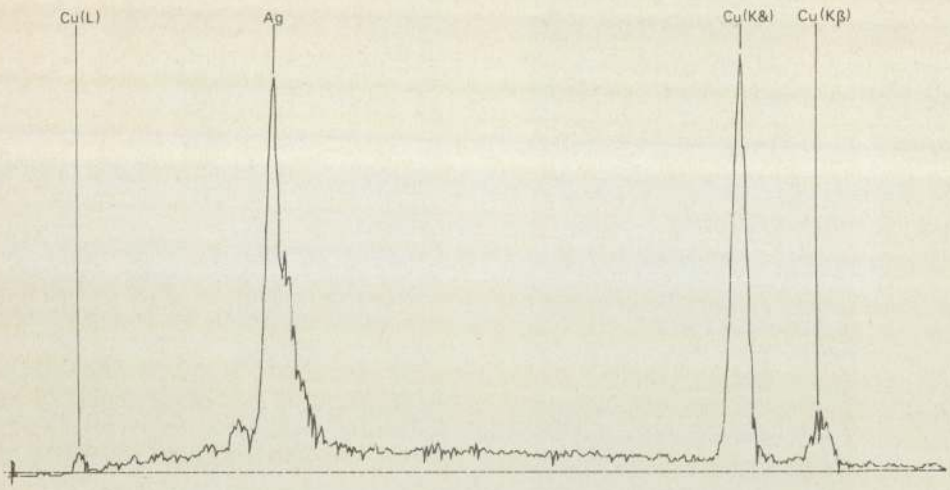

Fig. 5. X-ray spectrum obtained from the insulating particle within the marked circle of fig. 4.

causes the observed emission to be particularly unstable, and secondly, by using a more precise goniometer stage, possibly with piezoelectric translators for the final location of the site.

Acknowledgment

The authors wish to thank the Science Research Council for its support of this work.

References

[1] B.M. Cox, J. Phys. D: Appl. Phys. 8 (1975) 2065.
[2] B.M. Cox, Proc. 6th Int. Symp. on Discharges and Elect. Ins. in Vacuum, Swansea, U.K. (1974) pp. 135.
[3] R.P. Little and W.T. Whitney, J. Appl. Phys. 34 (1963) 2430.
[4] R.V. Latham and E. Braun, J. Phys. D: Appl. Phys. 1 (1968) 1731.
[5] R.E. Hurley, J. Phys. D: Appl. Phys. (1980).
[6] R.E. Hurley, J. Phys. D: Appl. Phys. 12 (1979) 2246.
[7] R. Coelho and J. Debeau, J. Phys. D: Appl. Phys. 4 (1971) 1266.
[8] N.K. Allen and R.V. Latham, J. Phys. D: Appl. Phys. 11 (1978) L55.
[9] N.K. Allen, B.M. Cox and R.V. Latham, J. Phys.D: Appl. Phys. 12 (1979) 969.
[10] R.E. Hurley and P.J. Dooley, J. Phys. D: Appl. Phys. 10 (1977) L195.
[11] R.E. Hurley, J. Phys. D: Appl. Phys. 12 (1979) 2229.

Physica 104C (1981) 189–195

THE EFFECT OF THE APPLIED FIELD ON THE ENERGY SPECTRA OF ELECTRONS FIELD EMITTED FROM MICROSCOPIC SITES ON BROAD-AREA COPPER ELECTRODES

C.S. ATHWAL and R.V. LATHAM

Department of Physics, University of Aston in Birmingham, Birmingham B4 7ET, UK

From detailed measurements of the energy spectra of electrons emitted from microscopic sites on broad-area copper electrodes, it has been established that both the displacement of the maximum of the distribution below the substrate copper Fermi level, and its full width at half maximum, increase in a non-linear manner with the applied field and emission current. These results are interpreted in terms of a model based on the physical regime of an insulating microimpurity that is in intimate contact with the substrate metallic cathode. It is proposed that field penetration in the insulator causes it to "switch" to a high-conductivity state, and that this switching is a prerequisite for electron emission.

1. Introduction

It is well known that electrical breakdown in vacuum can be initiated by electrons field emitted from localised sites on high-voltage electrodes. To gain more insight into the physical basis of this emission mechanism, a sophisticated electron spectrometry technique was established in this laboratory for studying the energy spectra of these electrons. In previous reports [1–3] describing the early findings from this facility, it was established that there are three important differences between the electrons emitted from these sites and those field emitted from metallic microtips: (i) the electrons are emitted from states that are well below the metallic Fermi level; (ii) the half-width of the distribution is appreciably broader; and (iii) the shape of the distribution is more symmetrical.

These findings and the discovery by Hurley [4] of an associated cathodic electroluminescence phenomenon led independently to the conclusion that a semiconducting or insulating micro regime must exist at the source of the electron emission. However, differing models were proposed to explain its origin. That of the present authors' group [2, 3, 5] was based on the concept of the internal heating of electrons as a result of field penetration, whilst that of Hurley [6] introduced the concept of a conducting filament, within the microimpurity, that provided the necessary geometrical field enhancement, i.e. eliminating the need for an "external whisker". Both of these early models were based on restricted experimental data and in consequence were fairly rudimentary so that it is not surprising that they were each open to criticism. The present paper reports on more detailed studies of how the electron energy spectrum is influenced by the applied field and the site emission current. As a result it has been possible to develop a revised model that not only takes into account this new information but also the electroluminescence data of Hurley.

2. Experimental

Full details of the experimental technique and measuring procedure that has been developed for obtaining the energy spectra of these emission processes has been reported elsewhere [1, 5]. In short, the experimental arrangement consists of a high-voltage 0.5-mm "test" gap interfaced with a high resolution electrostatic deflection electron energy analyser, which is fully described by Braun et al. [7]. The specimen cathode is set exactly parallel to the anode by an optical method, and it is then mechanically scanned in a raster pattern in front of a probe hole in the anode in order to locate the emitting

sites. By measuring the current passing through the probe hole, the current–voltage characteristics of each site may be determined. In order to obtain the energy spectrum, the electrons passing through the probe hole are focused by an interfacing lens into the entrance aperture of the input lenses of the hemispherical energy analyser. Those that are transmitted by the analyser are detected by an electron multiplier, and the resulting signal is amplified and displayed on a storage oscilloscope.

For studying the influence of the applied field on the emission spectra, it was found more convenient to vary the anode potential rather than the gap, despite the fact that this involved the additional operation of periodically refocusing the input lenses of the spectrometer to obtain the maximum signal. Spectra at the various field values were recorded, using a slow (30-s) energy scan, by photographing directly from the storage oscilloscope. The current from a given site at each field value is known from the initial current–voltage calibration; but a check on the relative value of this current was also made by noting the gain of the signal amplification system.

3. Results

Energy spectra were measured for sites on broad-area (15-mm diameter) specimens of lathe-turned OFHC copper, highly polished OFHC copper and a high purity copper crystal grown from the melt in a (111) orientation, where generally, any specimen would have up to five sites within the available field range up to $2\times 10^{7}\,\mathrm{Vm^{-1}}$. Fig. 1 shows two typical spectra recorded from a given site at different gap fields, and clearly illustrates how this parameter influences their shape and position with respect to the Fermi level of the cathode substrate. For this investigation such spectra have been characterised in terms of (i) the shift of the maximum of the distribution from the Fermi level of the copper substrate, and (ii) the full width at half maximum (FWHM). Although no two sites produced the same quantitative results, and even the characteristics obtained from a given site could not always be precisely reproduced from day to day, they exhibited the same qualitative trends, despite the widely differing material specifications of the specimens. A related effect was the frequent observation of double or multi-peaked spectra, but in the present work we limit our analysis to the simpler case when reproducible single peaked distributions were obtained. Thus, the variation of parameters (i) and (ii) with applied field and site current for a typical site on OFHC copper is shown in figs. 2 and 3, respectively.

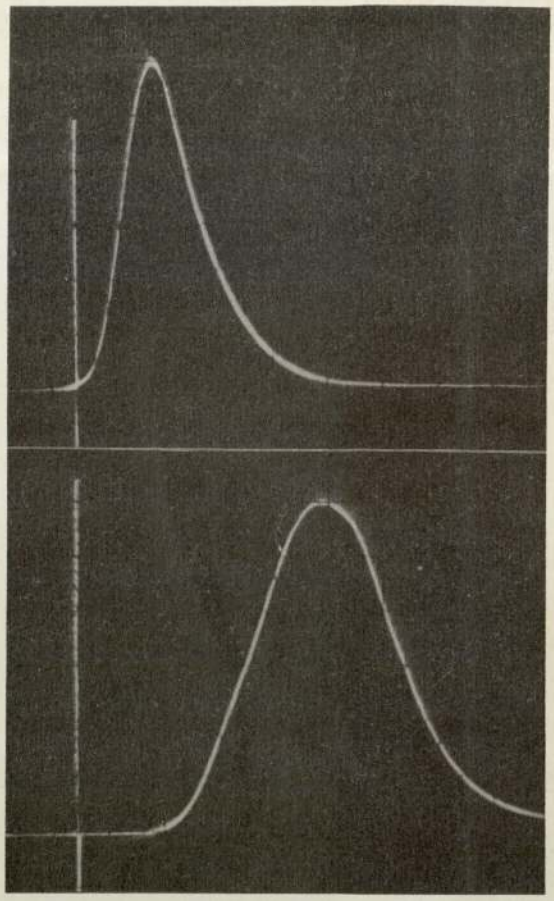

Fig. 1. Typical electron energy spectra under low and high field conditions, showing 2 eV scans, with energy decreasing to the right. The vertical lines represent the Fermi level. Top – gap field = $8\,\mathrm{MV\,m^{-1}}$; site current = 1.6×10^{-7} A. Bottom – gap field = $10\,\mathrm{MV\,m^{-1}}$; site current = 9×10^{-7} A.

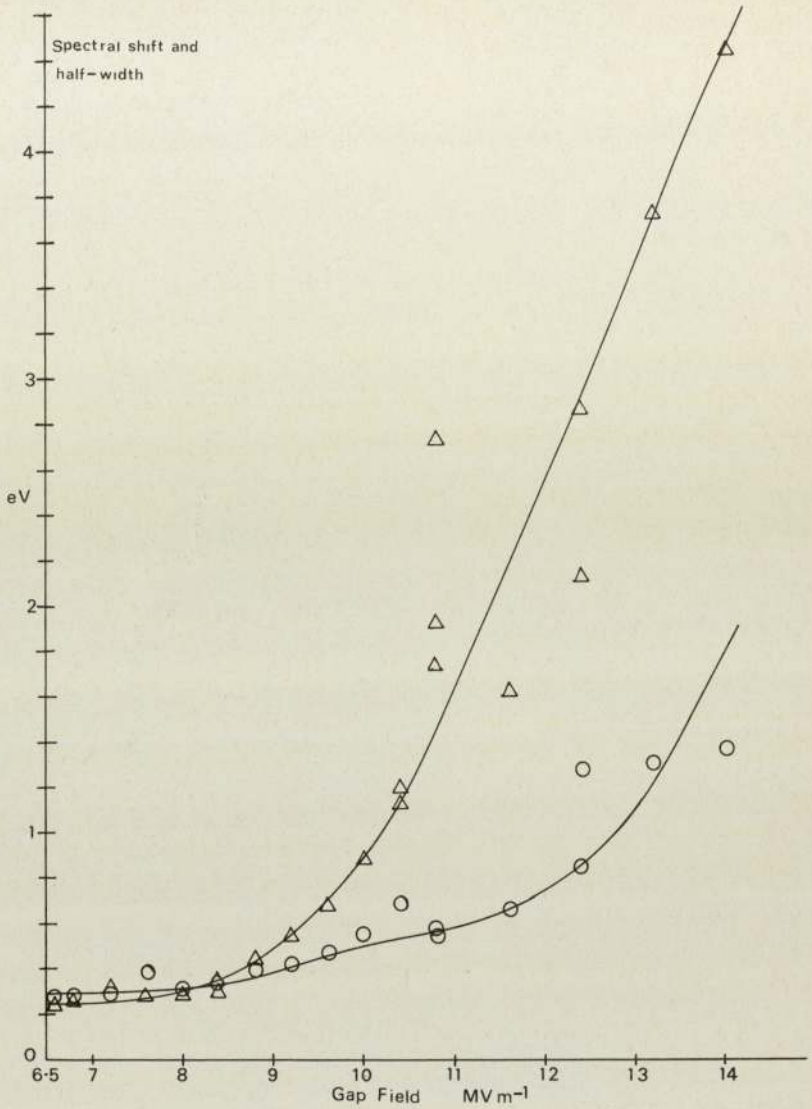

Fig. 2. Variation of the spectral shift and half-width (FWHM) with applied field. △ represents the shift of the maximum of the energy distribution from the substrate Fermi level. ○ represents the half-width (FWHM) of the energy distribution.

4. Discussion

We interpret our results in terms of a model based on the physical regime of an insulating microimpurity that is in intimate contact with the substrate metallic cathode. As indicated in the Introduction, two models have been proposed to explain the emission of electrons from such a regime, both models having many attractive features, but also being recognised to have evident limitations. For example, the energy band model [2, 3, 5] does not readily explain how a significant number of the hot electrons will be able to cross the micron-dimension impurity without losing most or all of their energy through phonon scattering processes, whilst the simple filament model [6] does not correctly predict the behaviour of the energy spectra with field and

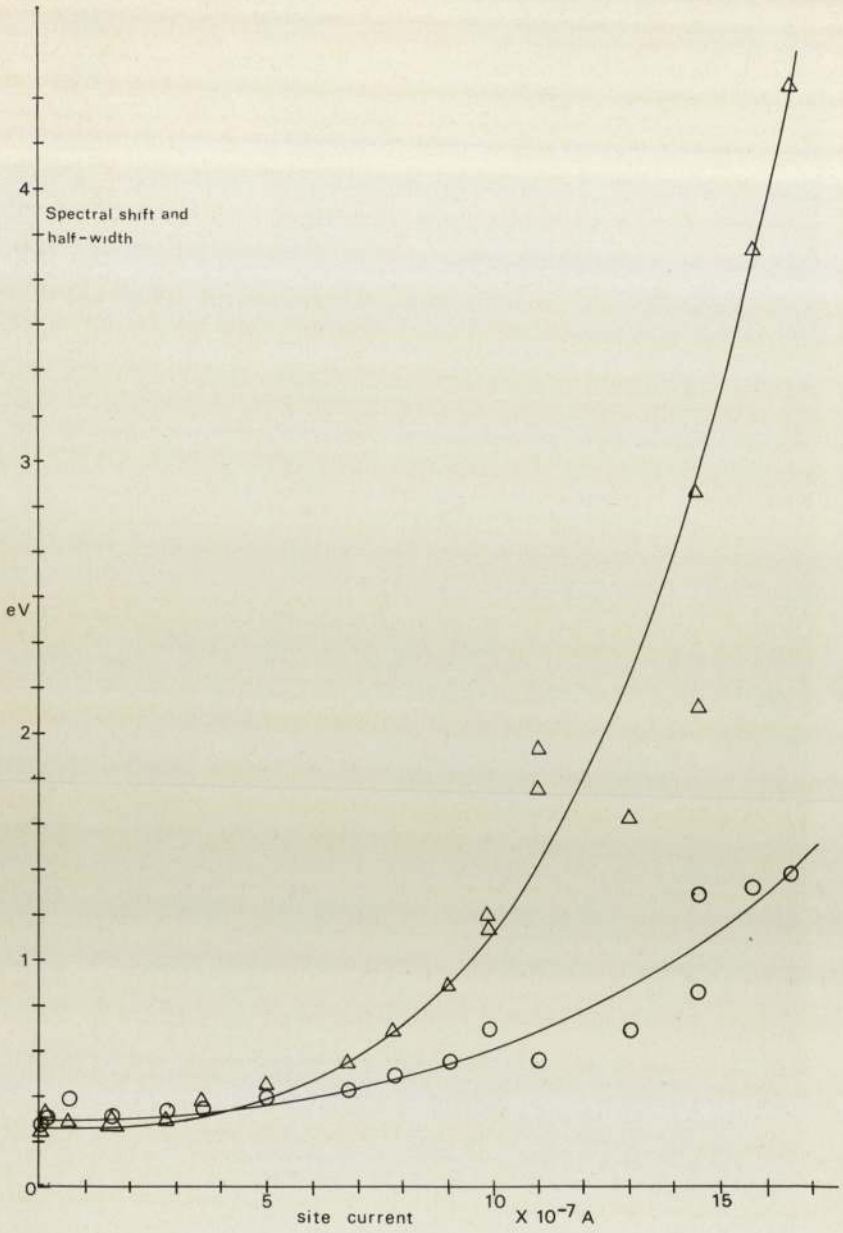

Fig. 3. Variation of the spectral shift and half-width (FWHM) with site current. △ represents the shift of the maximum of the energy distribution from the substrate Fermi level. ○ represents the half-width (FWHM) of the energy distribution.

current: both models are also equally vague about the precise mechanism whereby electrons tunnel from the metal into the impurity. In an attempt to overcome these arguments and also explain the spectral field effect outlined earlier, the following revised model has been evolved which incorporates the essential features of both of the earlier versions.

Before the application of any field, the energy band configuration of a metal–insulator–vacuum system is typically as shown in fig. 4(i). For the insulator we may deduce the band-gap to be

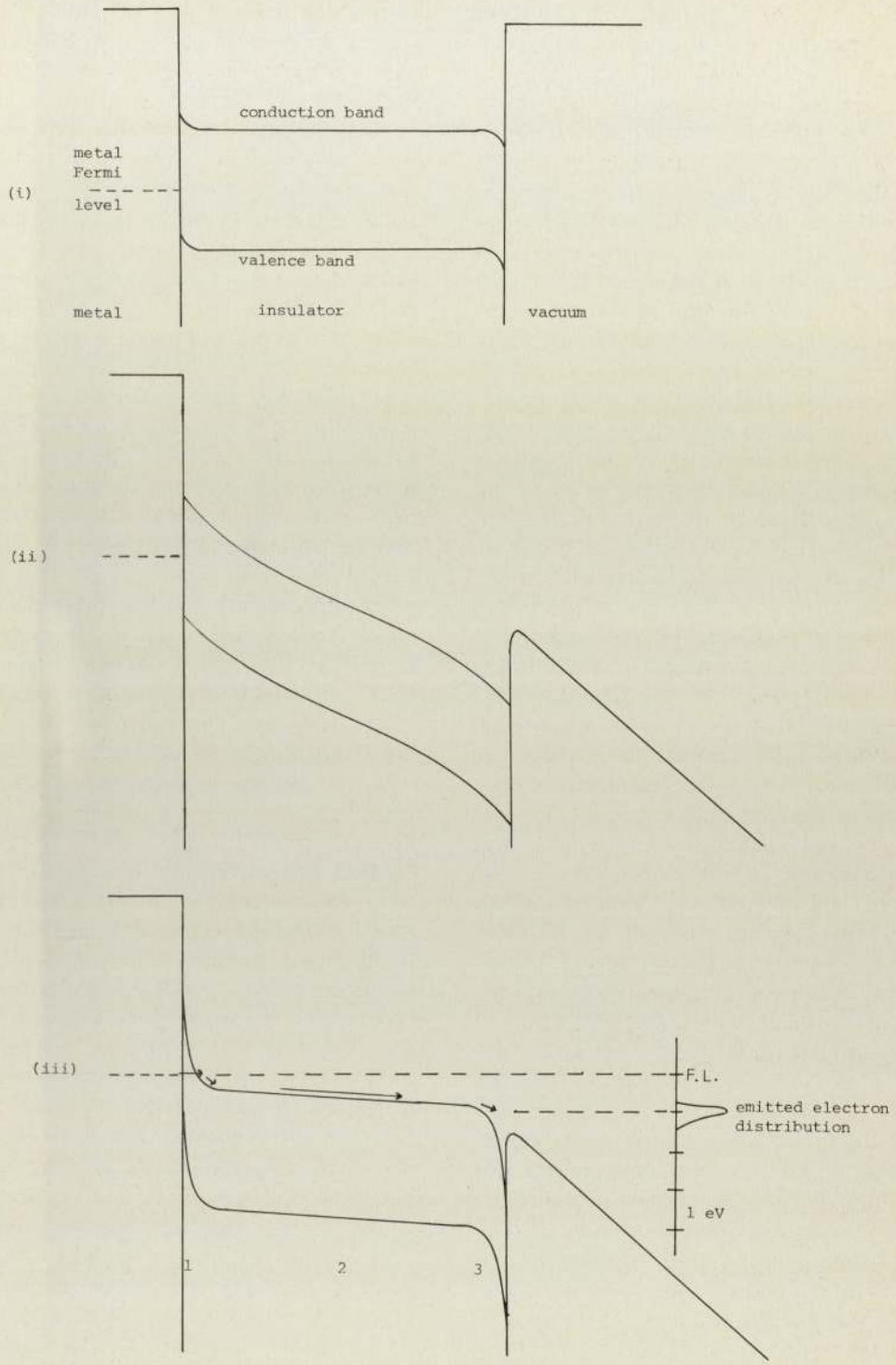

Fig. 4. Energy band and surface barrier configurations of the metal–insulator micro-emitting regime under varying field conditions: (i) zero field; (ii) high field prior to switching and electron emission; (iii) high field stable electron emission regime.

greater than 2.5 eV from the electroluminescent spectra of Hurley [6], and we assume the typical work function of 4.5 eV. The small band bending at the two interfaces is determined by the surface energy barriers which in turn are due to work function differences and the presence of surface states. As the field is increased to a value just below the onset of emission, the bands will bend in the manner shown in fig. 4(ii) due to field penetration. It is now envisaged that the insulator is capable of "switching" or "forming" to a high conductivity state, as is observed for many insulators, e.g. amorphous oxides and chalcogenide glasses, at fields of this order [8, 9]. The character of the emitted electron spectra can then be best explained if it is assumed that on switching there is a rapid re-arrangement of the energy band configuration, illustrated in fig. 4(ii), to that in fig. 4(iii), which is indeed of the type postulated to occur in metal–chalcogenide glass–metal systems [10]. Now the regime is characterised by two very narrow high-field regions at the metal–insulator and insulator–vacuum interfaces, with an extended intermediate low field region. There has been much speculation as to the precise physical mechanism responsible for this transition, but it could be attributed to the simultaneous production of positive and negative charge carriers, such as electron–hole pairs from impact ionisation by the hot electrons. On this basis the high field regions may result from the trapping of appropriate carriers in localised states near the two interfaces. However, at this stage we cannot discount the possibility of (a) the build up of a "dynamic" space charge in region 1 due to the differing mobilities of electrons and holes there [11], the holes having arisen from the same processes which initiate electroluminescence; and (b) the space charge in both regions being due to a solid-state electrolysis process involving the migration of positive ions towards region 1 and negative ions to region 3. The actual situation may well consist of contributions from all three sources: the dynamic effect dominating near the metal junction, trapping in localised states being most important near the vacuum interface, and the electrolysis leading to irreversible electroforming.

In order to maintain electron transport in the conduction band of an amorphous material containing a profusion of trapping levels in the band gap, a current density of the order of 10^8 Am^{-2} is necessary [12]. Since this is much higher than the current density from known emitting sites, especially at very low current levels, the channels involved may consist of relatively trap-free crystalline regions. In this respect it may be noted that in a measurement made on a virgin copper electrode (i.e. not previously exposed to high electric fields) there was no emission (i.e. $<10^{-10}$ A), as the field was slowly increased to a value of 1.8×10^7 Vm^{-1}, at which point the current suddenly increased to 1.4×10^{-6} A. Subsequently the field could be lowered and the site exhibited the normal Fowler–Nordheim type behaviour. Such a switch-on phenomena has also been observed in about 1% of tests on commercial contact switches by Cox [13]. This small percentage of observations can be understood when it is remembered that these electrodes had already undergone arcing. It must also be recognised that such a phenomenon could result from a non-metallic emission site being created "instantaneously" from the impact of an insulating clump launched from the anode. So far as the switch-on process is concerned, it is believed that after the first switching, the conducting channel fills the whole of the particle, leading to increased current density, heating and an irreversible electro-forming (memory switching) to a more crystalline state [14], in which case the requirement for high current density will no longer be strictly applicable. The so-called *b*-sites reported by Hurley [15] and Cox [13], which pass high currents and exhibit a current-controlled $I-V$ characteristic, may also be relevant to this discussion. It is tentatively suggested that in this case the irreversible crystallisation does not occur, possibly due to the impurity being large enough to accommodate the conducting channel whose cross-section may increase to maintain a constant current density, in which case significant heating will not occur. Accordingly the *b*-sites may be likely to be associated with grain boundaries or large impurities ($\geq$ few microns).

Whatever the origin of the equilibroum on-state of fig. 4(iii), it is assumed that electrons tunnelling from the metal will be rapidly ther-

malised and hence be able to cross the extended low field region in the bottom of the conduction band where their lifetime can be $\sim 10^{-8}$ s [10]. They then enter the second narrow high field region of ~10 nm thick where they are heated through the 2–3 eV necessary to escape over the depressed barrier, and for exciting the electron transitions required for producing the typical optical spectra. Then referring to fig. 4(iii), the shift of the maximum of the energy distribution from the Fermi level will be the sum of three components: (i) energy lost in thermalising into the conduction band minimum in region 1; (ii) ohmic energy loss in low field region 2; and (iii) energy lost due to phonon scattering in region 3. Each of these losses may be expected to increase with increasing field and current, though the ohmic losses should only be significant at current levels of $\geq 10^{-8}$ A. Electrons which have thermalised in a parabolic conduction band minimum will have a FWHM of ~1.5 kT (0.04 eV at room temperature) before entering region 3. Hence, assuming that the electrons escape over the work function barrier, the FWHM of the emitted distribution will be due in the most part to the phonon scattering of hot electrons. The increase in FWHM with field may be attributed to: (a) an increase in the length of the high field region 3; (b) an increase in phonon scattering cross-section with the energy of the electrons; and (c) an introduction of carrier–carrier scattering.

The instabilities in the spectra which are commonly observed may reflect inherent instabilities in the space charges in regions 1 and 2. The appearance of double and multi-peaked spectra need to be studied in greater detail. They may be due to the presence of more than one conducting channel through a particular impurity, or alternatively they may be attributed to a more complicated band structure in the insulator, with electrons able to travel in other conduction band minima or a continuum of interband states. However, it is believed that the typical Fowler–Nordheim type current voltage characteristics obtained from these sites may in all cases be attributed to the electrons tunnelling in region 1.

5. Conclusion

The reported measurements of the field and current dependence of the energy spectra of electrons emitted from sites on broad area high voltage electrodes have been shown to be in good qualitative agreement with the assumption that they are derived from an emission regime involving an insulating microimpurity embedded in the metallic substrate. However, to explain these findings, together with the associated electroluminescent effects and certain switching phenomena, it has been necessary to develop a revised model of the emission mechanism that is based on the concepts that are used to explain the switching phenomena that occur in metal–insulator–metal devices.

Acknowledgement

The authors wish to thank the Science Research Council for its support of this work.

References

[1] N.K. Allen and R.V. Latham, J. Phys. D: Appl. Phys. 11 (1978) L55.
[2] N.K. Allen and R.V. Latham, Proc. VIII Int. Symp. on Discharges and Electrical Insulation in Vacuum (1978), B3, 1.
[3] N.K. Allen, B.M. Cox and R.V. Latham, J. Phys. D: Appl. Phys. 12 (1979) 969.
[4] Hurley, R.E. and Dooley, P.J., J. Phys. D: Appl. Phys. 10 (1977) L5.
[5] N.K. Allen, Ph.D. Thesis, University of Aston in Birmingham (1979).
[6] Hurley, R.E., J. Phys. D: Appl. Phys. 12 (1979) 2229.
[7] E. Braun, R.G. Forbes, J. Pearson, J.M. Pelmore and R.V. Latham, J. Phys. E: Sci. Instrum. 11 (1978) 1.
[8] K.W. Boer and S.R. Ovshinsky, J. Appl. Phys. 41 (1970) 2675.
[9] G. Dearnaley, A.M. Stoneham and D.V. Morgan, Rep. Progr. Phys. 33 (1970) 1129.
[10] D. Adler, H.K. Henisch and S.N. Mott, Rev. Mod. Phys. 50 (1978) 209.
[11] S.H. Lee, Appl. Phys. Lett. 21 (1972) 544.
[12] K.E. Petersen and D. Adler, J. Appl. Phys. 47 (1976) 256.
[13] B.M. Cox, C.E.G.B. Report R/M/N1021 (1979).
[14] J. Feinleib, J. de Neufville, S.C. Moss and S.R. Ovshinsky, Appl. Phys. Lett. 18 (1971) 254.
[15] R.E. Hurley, J. Phys. D: Appl. Phys. 13 (1980).